

Dissertation

submitted to the
Combined Faculty of Natural Sciences and Mathematics
of the Ruperto Carola University Heidelberg, Germany
for the degree of
Doctor of Natural Sciences

Presented by
Mira Stadler, M.Sc.
born in: Vienna, Austria
Oral examination: 5th of October 2020

Inflammatory cytokines influence fatty acid metabolism in hepatocytes

Referees:
Prof. Dr. Peter Angel
Prof. Dr. Mathias Heikenwalder

Table of Contents

1. Summary.....	11
1. Zusammenfassung.....	12
2. Introduction	14
2.1. Metabolic energy storage.....	14
2.2. The liver as central organ of metabolism.....	15
2.2.1. Hepatocyte lipid metabolism.....	15
2.2.2. Fatty acid uptake and transport	17
2.2.3. Fatty acid <i>de novo</i> synthesis	17
2.2.4. Fatty acid storage.....	18
2.2.5. Lipid droplet metabolism.....	19
2.2.6. Mitochondrial fatty acid oxidation.....	21
2.2.7. Mitochondrial energy production.....	24
2.2.8. Glucose metabolism	25
2.2.9. Glucose and fatty acid catabolism	25
2.3. Acute and chronic liver inflammation.....	26
2.3.1 NF- κ B pathway.....	27
2.4. Metabolism control and the NF- κ B signalling pathway	29
2.5. Non-alcoholic fatty liver disease, NAFLD, and non-alcoholic steatohepatitis, NASH ..	30
2.5.1. Lipotoxicity.....	32
2.5.2 Mitochondria during NAFLD	33
2.6. Hypothesis and Aims of the Thesis	34
3. Material and Methods.....	35
3.1. Material.....	35
3.2. Methods.....	39
4. Results	52
4.1. Fatty acid metabolism in hepatocytes	52
4.1.1. <i>In vitro</i> experimental set-up to study the influence of inflammatory mediators on hepatic fatty acid metabolism	52
4.1.2. <i>Fatty acid storage into neutral lipids is intensified by NASH-derived inflammatory cytokines</i>	53
4.1.3. <i>Inflammation promotes fatty acid storage in form of triglycerides</i>	55
4.1.4. <i>Catabolic deficiencies induced by inflammatory mediators promote aberrant lipid storage</i>	58
4.1.5. <i>Inflammation rapidly affects fatty acid metabolism in hepatocytes</i>	59
4.1.6. <i>NF-κB-driven inflammation affects lipid metabolism in dHepaRG cells</i>	60
4.1.7. <i>Activation of the canonical- and non-canonical NF-κB pathway drives neutral lipid accumulation in hepatocytes</i>	62
4.2. Cellular stress response to inflammation and lipids.....	63

4.2.1. Mitochondrial morphology is affected by inflammation in a lipid-rich environment	63
4.2.2. Inflammatory cytokines interfere with mitochondrial polarization and function	64
4.2.3. Mitochondrial dysfunction is induced by specific inflammatory cytokines	68
4.2.4. Inflammatory cytokines affect mitochondrial function via NF- κ B signalling	69
4.2.5. Fatty acids and inflammatory cytokines increase reactive oxygen species production, induce cell- apoptosis, proliferation and trigger replication stress and DNA damage	70
4.3. NF- κ B signalling – PPAR- α signalling	73
4.3.1. Inflammatory cytokines affect gene and protein levels of PDK4	73
4.3.2. PPAR- α and PDK4 are not involved in inflammation-triggered elevated lipid accumulation	75
4.4. Transcriptome profiling by RNA sequencing	76
4.4.1. Inflammatory cytokines are the major regulators of overall gene expression in a lipid-rich environment in human dHepaRG cells	76
4.4.2. Fatty acid stimulation promotes upregulation of genes involved in lipid metabolic processes and proliferation	78
4.4.3. Lymphotoxin β receptor signalling activators affect the expression of genes essential for the regulation of inflammation, proliferation, apoptosis, and metabolic processes	80
4.4.4. IL-17A stimulation elevates the expression of genes involved in the regulation of inflammation and immune response and reduces expression of genes essential for metabolic regulations, NF- κ B signalling prevents gene regulations induced by IL-17A	85
4.4.5. The pro-inflammatory cytokine TNF- α regulates gene expression of various genes critical for inflammation, anti-viral response, and metabolic processes	88
4.4.6. Inflammatory mediators affect expression levels of genes essential for cellular inflammatory response, proliferation, apoptosis, and regulations of major metabolic processes	91
4.4.7. The overall gene expression is primarily regulated by absence or presence of an inflammatory mediator	94
4.5. Proteomics analysis	95
4.5.1. Inflammatory cytokines affect abundance of proteins implicated in the regulation of inflammation induced cellular stress response and metabolic processes	95
4.5.2. Fatty acid stimulation leads to elevated levels of proteins implicated in lipid metabolism and proliferation	96
4.5.3. Exposure to the inflammatory mediators BS1 and LIGHT affects levels of proteins essential for the regulation of inflammation, proliferation, and metabolic processes	98
4.5.4. IL-17A stimulation affects abundance of proteins essential for the regulation of inflammation, proliferation, and metabolic processes	102
4.5.5. TNF- α stimulation increases abundance of proteins critical for the regulation of inflammation and anti-viral response and decreases proteins levels implicated in metabolic processes	104
4.6. Phosphoproteomics analysis	106

4.6.1. Inflammation affects phosphorylation of proteins involved in the regulation in programmed cell death and DNA damage response	106
4.7. Proteome based complex analysis.....	108
4.7.1. Inflammatory cytokines downregulate and destabilize proteins that regulate carbohydrate metabolism	108
5. Discussion.....	118
6. References.....	127
7. Acknowledgements	135
I. Appendix	136
I.I. Inflammation induced increased lipid storage is independent of PPAR- α	136
I.II. Inflammation driven aberrant lipid accumulation is not regulated by PPAR- α activation.....	136

Abbreviations

ATP	adenosine triphosphate
TG	triglyceride
FA	fatty acid
LD	lipid droplet
CE	cholesterol ester
WAT	white adipose tissue
FFA	free fatty acid
LSEC	sinusoidal endothelial cell
HSC	hepatic stellate cells
FAO	Fatty acid oxidation
SCFA	Short-chain fatty acid
MCFA	medium-chain fatty acid
LCFA	long-chain fatty acid
VLCFA	very long chain fatty acid
FABP	fatty acid binding protein
PL	phospholipid
FATP	fatty acid transport protein
FABP _{pm}	plasma membrane (pm) located FA binding protein
PPAR- α	peroxisome proliferator-activated receptor alpha
HSL	hormone sensitive lipase
GLUT	glucose transporter
GK	glucokinase
G6P	glucose-6-phosphate
PDH	pyruvate dehydrogenase
ACC	acetyl-CoA-carboxylase
FAS	FA synthase
SREBP1c	sterol regulatory element binding protein 1c
ChREBP	carbohydrate response element binding protein
PI3K	phosphoinositide-3 kinase
PKB	protein kinase B
LXR	Liver X receptor
GLUT2	glucose transporter 2
HMGR	HMG-CoA reductase
LDLR	LDL receptor
ACS	acyl-CoA synthase
G3P	glycerol-3-phosphate
GPL	glycerophospholipids
GPAT	glycerophosphate-O-acyltransferases
LPA	lysophosphatidic acid
ER	endoplasmic reticulum
AGPAT	1-acylglycerol-3-phosphate
PA	phosphatidic acid
PAP	phosphatidic acid phosphohydrolases
DG	diglycerides
PC	phosphatidylcholine
PE	phosphatidylethanolamine
DGAT	diglycerol acyl transferase
VLDL	very low-density lipoprotein
ATGL	adipose triglyceride lipase
MGL	monoglyceride lipase

TCA	tricarboxylic acid
FAD	flavin adenine dinucleotide
NAD	nicotinamide adenine dinucleotide nicotinamide adenine dinucleotide
CPT	carnitine palmitoyl transferase
CACT	carnitine acylcarnitine translocase
OCTN2	organic cation transporter
VLCD	very long chain acyl-CoA dehydrogenase
LCAD	long-chain acyl-CoA dehydrogenase
MCAD	medium-chain acyl-CoA dehydrogenase
SCAD	short-chain dehydrogenase
RXR	retinoid X receptor
PPRE	peroxisome proliferator response element
HNF4- α	hepatocyte nuclear factor 4 alpha
MCD	malonyl-CoA decarboxylase
AMPK	AMP-activated protein kinase
AMP	adenosine monophosphate
mtDNA	mitochondrial DNA
SLC2A2	solute carrier family 2, member A2
HKVI	Hexokinase IV
UDP	uridine diphosphate
PDH	pyruvate dehydrogenase
PDK	pyruvate dehydrogenase kinase
LDL	low-density lipoprotein
HDL	high-density lipoprotein
SAA	serum amyloid A
CRP	C-reactive protein
Hp	haptoglobin
NF- κ B	Nuclear factor kappa-light-chain-enhancer of activated B cells
TNF- α	tumour necrosis factor α
IL-1 β	Interleukin β
ROS	reactive oxygen species
UV	ultraviolet
LPS	lipopolysaccharide
RHD	Rel homology domain
IKK	I κ B kinase
NEMO	NF- κ B essential modulator
PRR	pattern recognition receptors
TNFR	tumour necrosis factor-receptors
TLR	Toll-like receptor
TCR	T-cell receptor
BCR	B-cell receptor
LT β R	lymphotoxin β receptor
BAFFR	B-cell activating factor receptor
CD40	cluster of differentiation 40
RANK	receptor activator of nuclear factor κ B
NIK	NF- κ B inducing kinase
HCC	hepatocellular carcinoma
GSH	glutathione
C/EBP- β	CCAAT-box/enhancer-binding protein- β
LTB $_4$	dihydroxy leukotriene B $_4$
PGC-1a	peroxisome proliferator activated receptor coactivator 1a
IL-17	Interleukin-17

ACT1	NF- κ B activator 1
TRAF6	TNFR associated factor 6
IR	insulin resistance
NAFLD	non-alcoholic fatty liver disease
AFLD	alcohol fatty liver disease
NAFL	hepatic steatosis
NASH	non-alcoholic steatohepatitis
T2DM	type 2 diabetes mellitus
FXR	farnesoid X receptor
TNFSF14	tumour necrosis factor superfamily member 14
LIGHT	lymphotoxin-like inducible protein that competes with glycoprotein D for herpesvirus entry on T cells
ACAD1	acyl-CoA dehydrogenase family, member 10
ABCA1	ATP-binding cassette transporter
LPL	lipoprotein lipase
NKT	natural killer T
URI	unconventional prefoldin RPB5 interactor
Th17	T helper 17
FC	free cholesterol
AP-1	activator protein 1
Nrf2	nuclear factor erythroid 2-related factor 2

1. Summary

The metabolic syndrome and obesity are currently reaching pandemic dimensions worldwide. The hepatic consequence is an imbalance in fatty acid (FA) homeostasis, which results in hepatic lipid accumulation, a critical characteristic of non-alcoholic fatty liver disease (NAFLD), the most common chronic liver disease. NAFLD is a highly heterogeneous liver disease that ranges from simple steatosis (non-alcoholic fatty liver, NAFL), to non-alcoholic steatohepatitis (NASH), which is associated with inflammation and liver injury, and can ultimately lead to NASH-driven hepatocellular carcinoma (HCC). Pro-inflammatory cytokines, derived from activated immune cells, strongly affect hepatic FA metabolism, and are implicated in NASH and NASH-derived HCC. However, underlying molecular mechanisms and signalling pathways are not known in detail yet.

To investigate the influence of NASH-derived inflammatory cytokines on hepatic FA metabolism and to study molecular mechanisms as well as involved signalling pathways, I established an *in vitro* NASH model to recapitulate the transition from steatosis to steatohepatitis in mouse and human hepatocytes. I used several *in vitro* and *ex vivo* experimental set-ups including fluorescence and radioactive labelling of lipids, to study changes in FA- uptake, *de novo* synthesis, storage, oxidation, and secretion. In addition, I performed fluorescence-based assays to focus on regulations affecting mitochondrial function, cell viability, proliferation and associated replication stress, and DNA damage. By using CRISPR-Cas based knock out cell models and si-RNA mediated knock downs in hepatocytes, as well as treatment of cells with different inhibitors, antagonists, and agonists, I studied involved inflammatory and metabolic pathways. To disentangle molecular mechanisms induced by FAs and pro-inflammatory cytokines, I performed a multi omics approach including lipidome, transcriptome, proteome, phosphoproteome, and thermal proteome profiling.

I demonstrated that inflammatory cytokines increase FA storage in a NF- κ B dependent manner by interference with catabolic processes. Exacerbated lipid accumulation in hepatocytes subsequently promoted mitochondrial dysfunction, apoptotic cell death and compensatory proliferation. In addition, inflammatory cytokines induced an inflammatory stress response, replication stress, and DNA damage. Importantly, the exposure to inflammatory cytokines alone and in combination with FAs lead to the downregulation of genes and proteins involved in essential metabolic processes in hepatocytes, not only specific for FA metabolism.

The understanding of the effect of inflammatory cytokines on metabolic dysregulation and transcriptional control of metabolic genes in hepatocytes will help to find possible treatment options for NAFLD / NASH.

1. Zusammenfassung

Fettleibigkeit und das metabolische Syndrom, erreichen derzeit weltweit pandemische Dimensionen. Die hepatische Manifestation ist ein Ungleichgewicht in der Lipid Homöostase welche zu einer Ansammlung von Neutrallipiden in Lipidtröpfchen führt, und ein Hauptmerkmal der am häufigsten vorkommende chronischen Lebererkrankung, der nichtalkoholischen Fettlebererkrankung (engl.: non-alcoholic fatty liver disease, NAFLD) ist. NAFLD ist eine heterogene Lebererkrankung, die von einfacher Steatose bis zu einer Steatohepatitis, (engl.: non-alcoholic fatty liver disease, NASH) reicht, die mit Entzündungen und Leberschäden verbunden ist und letztendlich zur Entstehung des NASH-induzierten hepatozellulärem Karzinoms führen kann. Proinflammatorische Zytokine, die von aktivierten Immunzellen stammen, beeinflussen den Fettsäure Metabolismus in Hepatozyten und sind an der Entstehung und der Progression zu NASH und NASH-induzierten HCC beteiligt. Die diesen Pathologien zugrunde liegenden molekularen Mechanismen und Signalwege, als auch als auch die zellulären Grundlagen sind jedoch noch nicht im Detail bekannt.

Um den Einfluss von entzündlichen Zytokinen auf den Fettsäure Metabolismus in der Leber zu untersuchen und molekulare Mechanismen und Signalwege, die daran beteiligt sind, zu identifizieren, habe ich ein *in-vitro* NASH-Modell etabliert, um den Fortschritt von einer Steatose zu einer Steatohepatitis in Maus und Humanen Hepatozyten zu rekapitulieren. Ich habe verschiedene *in-vitro*- und *ex-vivo*-Versuche darunter Fluoreszenz- und radioaktive Markierung von Lipiden, um Änderungen in der Fettsäure Aufnahme, der *de-novo*-Synthese, der Speicherung, der Oxidation und der Sekretion zu untersuchen, durchgeführt. Zusätzlich führte ich fluoreszenzbasierte Experimente durch, um Regulationen zu untersuchen, die die Mitochondrien Funktion, die Lebensfähigkeit der Zellen, die Proliferation und den damit verbundenen Replikationsstress sowie die DNA-Schädigung beeinflussen. Unter Verwendung von CRISPR-Cas-basierten knock-out-Zellmodellen und si-RNA-basierten Knock-downs sowie durch Behandlung der Zellen mit verschiedenen Inhibitoren, Antagonisten und Agonisten, untersuchte ich die Beteiligung von verschiedenen Entzündungs- und Stoffwechselwegen. Um die durch Fettsäure und proinflammatorische Zytokin-induzierten molekularen Mechanismen zu untersuchen, führte ich einen Multi-Omics-Ansatz durch, der das Lipidom, das Transkriptom, das Proteom, das Phosphoproteom und das thermische Proteom-Profilum umfasste.

In der hier vorgelegten Doktorarbeit konnte ich zeigen, dass entzündliche Zytokine die Fettsäurespeicherung in NF- κ B-abhängiger Weise erhöhen indem sie katabolische Prozesse wie die Oxidation von Fettsäuren inhibierten. Eine verstärkte Lipidakkumulation in Hepatozyten induzierte eine mitochondriale Dysfunktion, apoptotischen Zelltod und eine kompensatorische Proliferation. Darüber hinaus aktivierten entzündliche Zytokine eine

Entzündungsstressreaktion, Replikationsstress und DNA-Schäden. Entzündliche Zytokine allein und in Kombination mit Fettsäuren führte zu einer herab Regulierung von Genen und Proteinen, die an essenziellen Stoffwechselprozessen in Hepatozyten beteiligt sind, und welche nicht nur spezifisch für den Fettsäuremetabolismus sind.

Die Untersuchung der Wirkung von entzündlichen Zytokinen auf die metabolische Dysregulation und Transkriptionskontrolle von metabolischen Genen in Hepatozyten, trägt dazu beimögliche Behandlungsoptionen für NAFLD / NASH zu finden.

2. Introduction

2.1. Metabolic energy storage

Energy metabolism is the conversion of nutrients into energy, such as adenosine triphosphate (ATP), and is essential for virtually all processes related to life and biological systems. Changes in energy availability impel organisms to generate storage depots. In times of energy excess these storage depots are filled up and are decomposed during times of energy demand ^{1,2}. The most common used molecules for metabolic energy storage are triglycerides (TGs), consisting of fatty acids (FAs) and glycerol ³. Almost all cells can synthesise and store TGs in lipid droplets (LDs) within their cytosol ⁴. LDs are lipid-rich organelles involved in various cellular processes including lipid (TGs and sterols/cholesterol esters (CE)) storage, transport, hydrolysis, as well as membrane trafficking and signalling ^{5,6}. Mammals have specialized tissues (white adipose tissue (WAT)) and cells (adipocytes) (**Figure 1I**) for long-term lipid storage ¹. In times of excess FA availability (**Figure 1II**), adipocytes store them by esterification in form of TGs in LDs. Sustained FA excess leads to increased TG storage resulting in adipocyte hypertrophy and thereby to an extension of the storage and fat depot (**Figure 1III**). TG catabolic processes are tightly controlled by adipocyte regulated lipolysis and insulin signalling ⁷. Insulin is a peptide hormone that regulates carbohydrate, fat, and protein metabolism by facilitating the uptake and absorption of glucose from blood to adipocytes, hepatocytes, and muscle cells. Under homeostatic conditions, insulin inhibits lipolysis in WAT. During starvation or energy demand, TGs are destructed leading to free fatty acid (FFA) release into the blood stream (**Figure 1IV**). FFAs in the blood are delivered to peripheral organs such as the liver where they can be used as energy source (**Figure 1V**) ⁸⁻¹⁰.

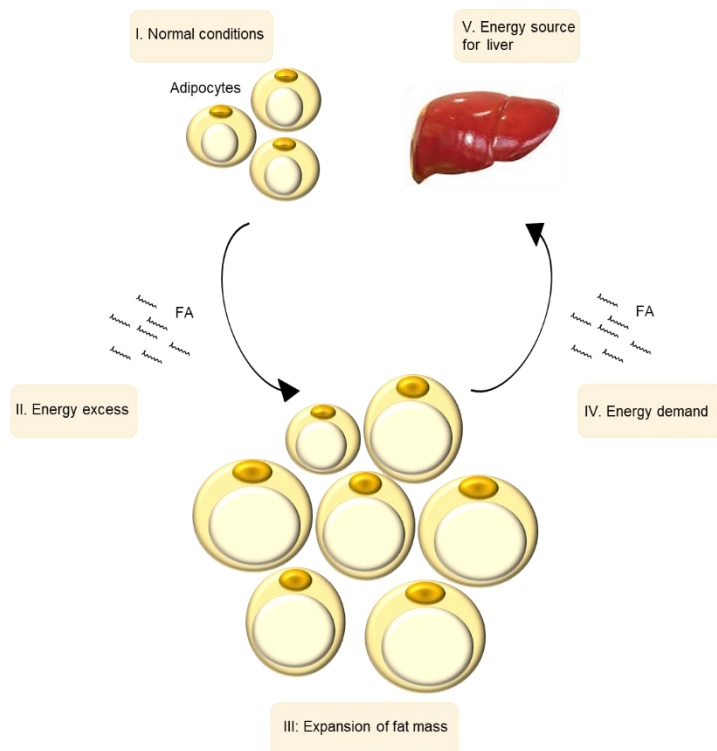


Figure 1: Illustration of energy metabolism

(I) FAs are stored in adipocytes in TGs for long-term storage. (II) Sustained energy excess promotes increased storage and leads to the (III) expansion of the fat mass. (VI) In times of energy demand TGs are destructed which results in FA release into the bloodstream, and delivery to peripheral organs such as the (V) liver where they are used as energy source.

2.2. The liver as central organ of metabolism

The liver is a central metabolic organ that regulates whole body energy and metabolically connects several tissues including adipose tissue and skeletal muscle. Main functions of the liver include detoxification of metabolites, bile acid production, and the regulation of lipid-, carbohydrate-, and protein metabolism. The metabolic activity and function of the liver is tightly controlled by nutrients, hormones, and neuronal signals ¹¹³. The liver is composed of parenchymal cells, hepatocytes, and non-parenchymal cells including hepatic stellate cells (HSCs), liver sinusoidal endothelial cells (LSECs), biliary cells (cholangiocytes), and immune cells such as Kupffer cells (liver resident macrophages) and intrahepatic lymphocytes ¹².

2.2.1. Hepatocyte lipid metabolism

Hepatocytes constitute about 60% of the whole cell mass of in the liver and control critical processes such as FA metabolism ¹². FAs are essential energy sources, can act as signalling molecules and are critical structural components of cellular membranes ^{4,13,14}. They consist of a carboxyl group (R-COOH) (**Figure 2I**) at one end, with an aliphatic chain (hydrocarbons, C-

H) in between and a methyl group (-CH₃) (**Figure 2II**) at the other end. The carbon atoms of the aliphatic chains following the carboxyl group are labelled according to the Greek alphabet, e.g. the first carbon of the aliphatic chain is the α carbon and the second is the β carbon (**Figure 2I**). Fatty acid oxidation (FAO) is also known as β-oxidation due to the oxidative processes taking place at the β carbon. The last carbon is labelled as ω carbon independent on the length of the aliphatic chain (**Figure 2II**). FAs can be either saturated (contain exclusively C-C bonds) (**Figure 2A**) or unsaturated (contain at least one C=C double bond) (**Figure 2B**)⁹. FAs are categorized by their length. Short-chain fatty acids (SCFA) have aliphatic chains of 6 or less carbons, medium-chain fatty acids (MCFA) contain aliphatic chains of 7 to 12 carbons, long-chain fatty acids (LCFA) consists of aliphatic chains of 13 to 21 carbons and very long chain fatty acids (VLCFA) have aliphatic chains of 22 or more carbons¹⁵. Number and position of carbon bonds can affect the biological activity of FAs¹⁶. The most common saturated fatty acid is the LCFA palmitic acid (C16:0) (**Figure 2A**) which is the first FA generated by *de novo* synthesis and can be used as precursor for synthesis of other FAs^{16,17}. Palmitic acid makes up about 20-30% of the fat depot in humans and is a major component of TGs in palm oil. It is also found in soap, cosmetics, and in food including meat and dairy products¹⁷. Oleic acid (C18:1) (**Figure 2B**) is the most common naturally occurring monounsaturated FA and the main component of TGs in olive oil. Oleic acid is primarily found in vegetable oils and fats^{18,19}.

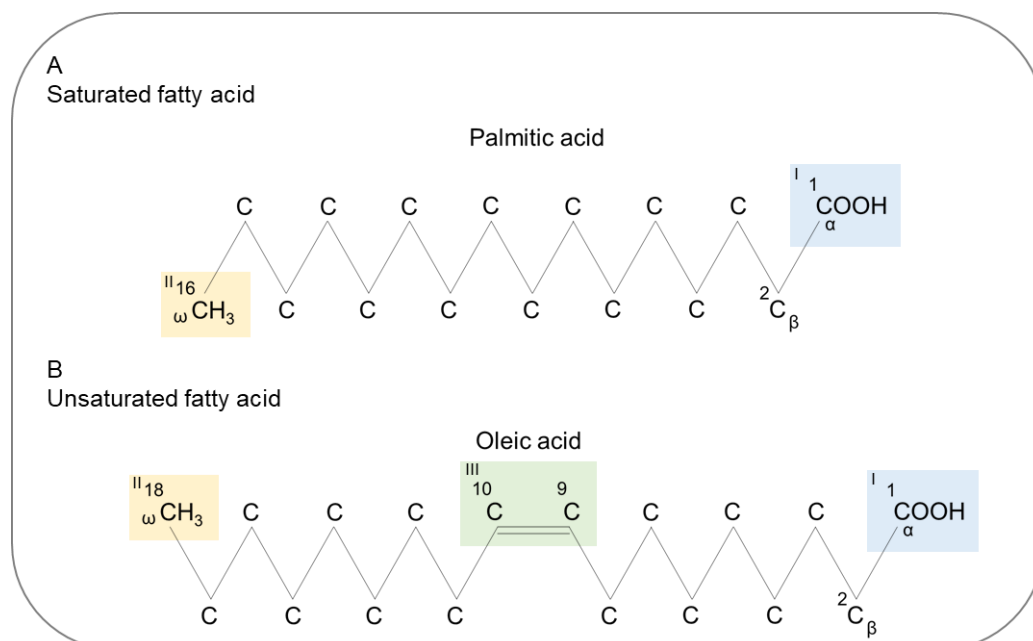


Figure 2: Illustration of saturated and unsaturated fatty acids

FAs are composed of a (I) carboxyl group (R-COOH) and a (II) methyl group (-CH₃) at each end of an aliphatic chain of hydrocarbons, C-H. The carbon atoms of the aliphatic chain are labelled with numbers displaying the length of FAs and according to the Greek alphabet, the first carbon of the aliphatic chain is the α carbon, the second is the β carbon and the last is the ω carbon. (A) Saturated FA, palmitic acid contains exclusively C-C bonds and is a LCFA that with 16 C atoms, C16:0 (16 is the number of carbon atoms and the 0 is indicating without double bonds). (B) unsaturated FA, oleic acid contains (III) one C=C double bond within the aliphatic chain and is also a LCFA with 18C atoms, C18:1 (18 is the number of carbon atoms and 1 is indicating one double bond).

Hepatocytes can take up FAs from the circulation (e.g. derived from adipose tissue or dietary sources) or can generate them by FA *de novo* synthesis²⁰. Once in the cell, FAs are either stored, most commonly in form of TGs in LDs but also in phospholipids (PLs) and CEs, or are used as energy source and catabolized by mitochondrial FAO (β -oxidation)^{21,22}.

2.2.2. Fatty acid uptake and transport

FAs are lipophilic molecules and can potentially diffuse passively through plasma membranes, however, this mechanism is concentration dependent, slow, and not efficient. Thus, FA uptake is mediated by specific transmembrane proteins e.g. by the scavenger receptor CD36²³, fatty acid transport proteins (FATPs), and by plasma membrane (pm) located FA binding proteins (FABPpm) (**Figure 3I**)^{24,25}. Intracellular FAs are bound by transport proteins including FABPs (**Figure 3I**)²⁵. FABPs can influence whole lipid metabolism by shuttling FAs between membranes, organelles, and other proteins and enzymes. FABPs can regulate FA binding to nuclear receptors such as peroxisome proliferator-activated receptor alpha (PPAR- α) leading to its activation. In adipocytes they can also interact with hormone sensitive lipase (HSL), involved in TG catabolism, to remove and channel released FAs from TGs¹⁴.

2.2.3. Fatty acid *de novo* synthesis

FA *de novo* synthesis is dependent on the nutritional status of the cell, substrate availability, and is primarily regulated by transcription²⁶. Acetyl-coenzyme A (acetyl-CoA) generated by glucose catabolism (glycolysis) is the main substrate used for lipogenesis (**Figure 3**)¹⁶. The uptake of glucose is mediated by glucose transporters (GLUT). Once in the cell, glucose is phosphorylated by glucokinase (GK) to form glucose-6-phosphate (G6P), and through glycolysis, pyruvate is generated (**Figure 3II, III**). In the mitochondria pyruvate is converted to acetyl-CoA by pyruvate dehydrogenase (PDH). Acetyl-CoA is then shuttled into the cytoplasm where malonyl-CoA is generated by the acetyl-CoA-carboxylase (ACC). Malonyl-CoA is the substrate for FA synthase (FAS) to generate new FAs (**Figure 3IV**). To adapt to nutrient and energy availability, lipid metabolic pathways are tightly regulated, e.g. malonyl-CoA promotes lipogenesis and at the same time inhibits FA catabolic processes such as mitochondrial FA uptake and oxidation. Palmitic acid can inhibit ACC function and thereby FA *de novo* synthesis^{13,27,27}.

FA *de novo* synthesis is transcriptionally regulated by glucose and insulin which can act synergistically to induce gene expression of lipogenic enzymes²⁶. The expression of enzymes necessary for FA *de novo* synthesis is controlled by the two transcription factors, carbohydrate response element binding protein (ChREBP) and sterol regulatory element binding protein 1c (SREBP1c). The transcription factor ChREBP is activated by intermediate and final products

of glycolysis, thus induced by elevated glucose levels. ChREBP target genes include ACC, FAS, and GLUT^{26,28}. SREBP1c target genes include FAS and also cholesterol synthesis associated genes including HMG-CoA reductase (HMGR) and LDL receptor (LDLR)²⁹. Insulin signalling regulates the activity of SREBP1c²⁹. SREBP1c activation is dependent on insulin receptor signalling induced phosphoinositide-3 kinase (PI3K) and protein kinase B (PKB) pathway³⁰, or by Liver X receptor (LXR) pathway^{31,32}.

FAs need to be activated by conversion into acyl-CoA esters by FA activating enzymes to enable FA metabolic processes such as TG synthesis and FAO (**Figure 3V**). FA activating enzymes include acyl-CoA synthase (ACS) proteins and FATPs³³

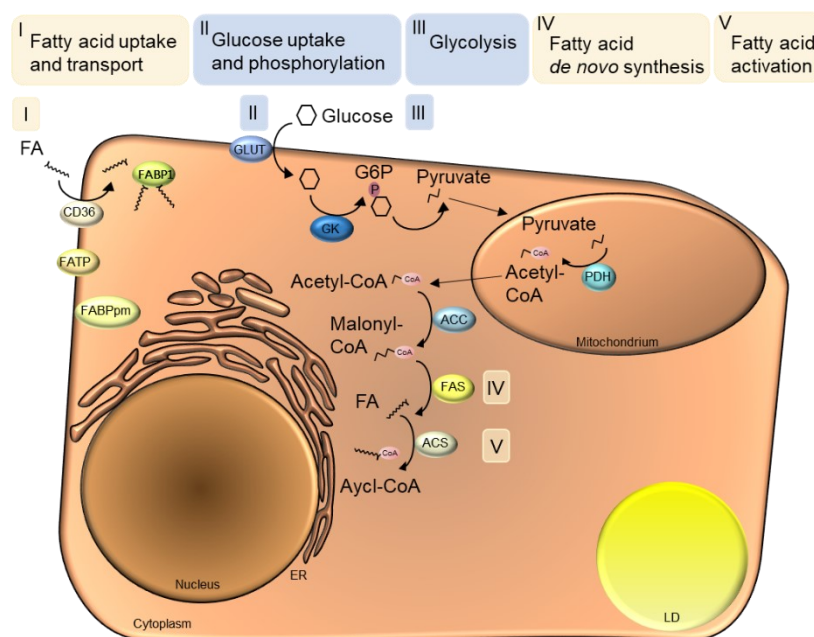


Figure 3: Fatty acid- uptake, transport, *de novo* synthesis, and activation

(I) FA uptake by transmembrane proteins, scavenger receptor CD36, FATPs or FABPpm. Within the cell, FAs are bound and shuttled by FABPs. (II) Glucose uptake is facilitated by GLUTs. GK phosphorylates (P) glucose to generate G6P. (III) By glycolysis pyruvate is generated, transferred into the mitochondria, and converted into acetyl-CoA by PDH. Acetyl-CoA is transported into the cytoplasm where ACC synthesizes malonyl-CoA the substrate for (IV) FAS. (V) FAs are activated by ACS proteins to generate acyl-CoAs.

2.2.4. Fatty acid storage

Activated FAs can be stored in form of TGs by the glycerol-3-phosphate pathway (**Figure 4**).

The glycerol-3-phosphate pathway uses glycerol-3-phosphate (G3P) from glycolysis to generate either TGs or glycerophospholipids (GPLs) by addition of acyl-CoA^{34,35}.

Intermediate substrates that are generated during FA storage can serve as second messengers or can be used for phospholipid synthesis to build up cellular membranes^{20,34,36}.

The initial step in TG synthesis is catalysed by glycerophosphate-O-acyltransferases (GPATs) in which lysophosphatidic acid (LPA) is formed by acetylation of G3P (**Figure 4**).

There are four GPAT isoforms known in mammals. GPAT1 and GPAT2 are highly expressed in the liver and localized at the mitochondrial membrane^{4,34}. Subsequently, 1-acylglycerol-3-

phosphate (AGPAT) which is located at the ER converts LPA into phosphatidic acid (PA) by addition of acyl-CoA. PA can serve as second messenger or as substrate for phospholipid synthesis to generate phosphatidylinositol, phosphatidylglycerol, and cardiolipin. PA is dephosphorylated by phosphatidic acid phosphohydrolases (PAPs also known as Lipins) to generate diglyceride (DG)^{34,36}. DG can be used as substrate for phospholipid synthesis for e.g. phosphatidylcholine (PC), phosphatidylethanolamine (PE), and phosphatidylserine or can be used as second messenger³⁴. In the final step diglycerol acyl transferase (DGAT) catalyses the condensation of a DG with a FA acyl-CoA to form a TG (**Figure 4I**). In mammals, two DGAT isoforms are known, DGAT1 is localized at the outer ER membrane. DGAT2 is localised at the ER membrane and at LDs^{4,37,38}. Synthesised TGs are either stored in form of LDs in the cytoplasm of hepatocytes or they are packed into very low-density lipoproteins (VLDLs) and exported into the bloodstream and can be subsequently stored in adipose tissue²⁰.

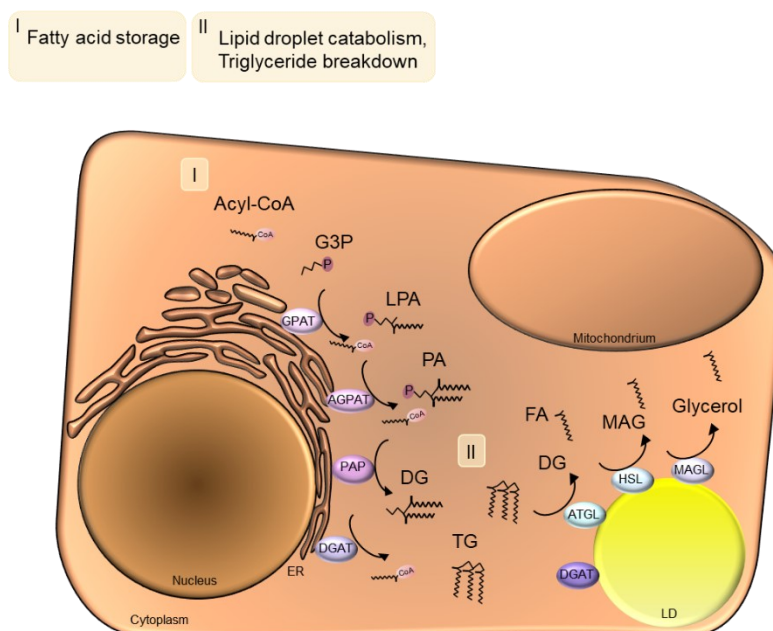


Figure 4: Triglyceride metabolism

(I) For FA storage in form of TGs, GPAT adds an acyl-CoA to glycerol-3-phosphat to generate LPA. Then AGPAT adds an acyl-CoA to LPA to synthesizes PA which is subsequently dephosphorylated by PAP to generate DG. DGAT adds another acyl-CoA to DG for TG synthesis. (II) TGs are catabolized by lipolysis, facilitated by ATGL, HSL, and MGL, that subsequently remove the three FAs from the glycerol backbone.

2.2.5. Lipid droplet metabolism

LDs are composed of TGs and CEs that form the neutral lipid core which is coated by a PL monolayer (**Figure 5**)⁵. The PL monolayer contains specific LD proteins such as perilipin proteins and adipose triglyceride lipase (ATGL) with critical metabolic functions during LD formation, lipolysis, endo-, and exocytosis^{4,20,39}. The LD size and composition, including lipid

species and proteins, greatly varies also within one cell ¹. The size of LDs is dependent on the cell type. In hepatocytes LD size can range from 0.1µm to 5µm, in adipocytes LDs can range from 20µm to 100µm and can constitute most of the cell ⁵. FFA availability can induce LD formation within hours and some LDs can increase their volume up to 3-fold ⁴⁰. TGs are generated at the ER where most enzymes required for synthesis are located. Due to the close vicinity of LDs to the ER, the most prominent model for LD biosynthesis describes LD formation by budding off the ER ⁴¹. LD growth is mediated by LD fusion or LDs can grow by addition of TGs to the LD core and PLs to the monolayer ^{4,40,42,43}.

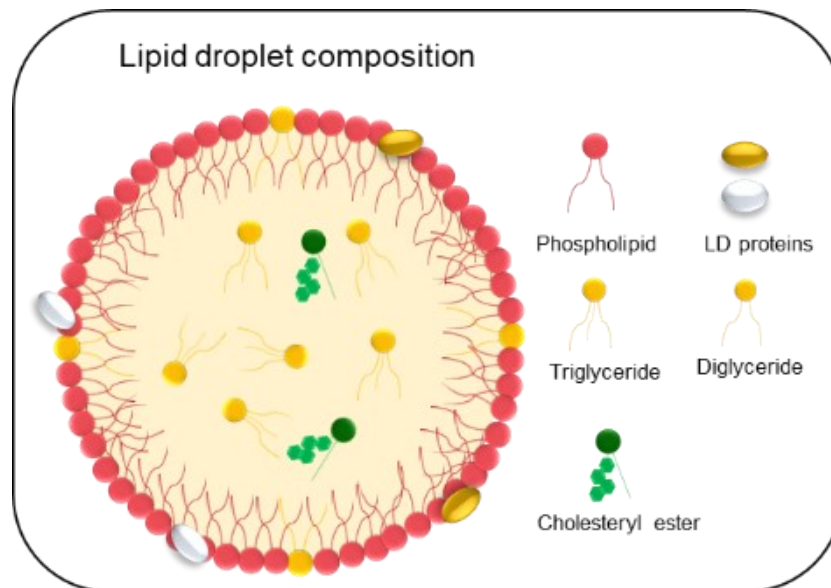


Figure 5: Lipid droplet composition

LDs consists of a neutral lipid core containing TGs, DGs, and CEs surrounded by a monolayer of PLs with LD proteins embedded.

LD catabolism is regulated by two distinct mechanism, lipolysis and lipophagy ⁴⁴. Lipolysis is mediated by specific lipases located in the cytoplasm or at the LD surface including ATGL, HSL, and monoglyceride lipase (MGL), that consecutively catalyse the removal of all three FAs from the TG (**Figure 4II**) ^{5,45,46}. FFAs can then serve as energy source by mitochondrial FAO or as signalling molecules involved in several cellular processes ^{47,48}. Lipophagy is a specific autophagic mechanism used to mobilize and catabolize LDs. Various proteins tightly regulate autophagic processes to transport and sequester intracellular components into autophagosomes that are composed of double membraned layers. During lipophagy, the autophagosome containing LD fuses with the lysosome, leading to the generation of an autolysosome where acid lipases facilitate LD breakdown. The rate-limiting lipase ATGL commonly catabolises large LDs, whereas small LD are preferably catabolized by lipophagy ^{44,49}.

2.2.6. Mitochondrial fatty acid oxidation

During energy demand FAs can be used as energy source by mitochondrial or peroxisomal β -oxidation that differ in substrate specificity, transport, energy production, and final products ³. Mitochondrial FAO is the most common pathway for LCFA breakdown ⁵⁰. FAO products such as acetyl-CoA fuel the tricarboxylic acid (TCA) cycle and ketogenesis ⁵¹. Oxidative phosphorylation is fuelled by energetic molecules via reduction of nicotinamide adenine dinucleotide (NAD) to NADH and flavin adenine dinucleotide (FAD) to FADH₂ which drives ATP synthesis ⁵⁰.

Mitochondrial FAO requires the import of acyl-CoA into the mitochondria which is accomplished by the carnitine palmitoyl transferase (CPT) system (**Figure 6**). The mitochondrial membrane consists of an outer and an inner membrane with an intermembrane space surrounding the mitochondrial matrix. The CPT system comprises the acyltransferases, CPT1 and CPT2, the carnitine acylcarnitine translocase (CACT also known as SLC25A20) and requires L-carnitine (**Figure 6I**). CPT1 is located at the outer mitochondrial membrane and by transesterification catalyses the conversion of acyl-CoA to acylcarnitine. Acylcarnitine is then transported by CACT across the inner mitochondrial membrane by substitution of free carnitine from the mitochondria. CPT2 is located at the inner mitochondrial membrane and reconverts acylcarnitine to acyl-CoA ^{9,50} which can be oxidized by β -oxidation (**Figure 6II**). Carnitine can be generated by carnitine biosynthesis in hepatocytes or can derive from dietary sources such as meat and dairy products and is transported by organic cation transporter (OCTN2 also known as SLC22A5) across the plasma membrane ^{2,52}.

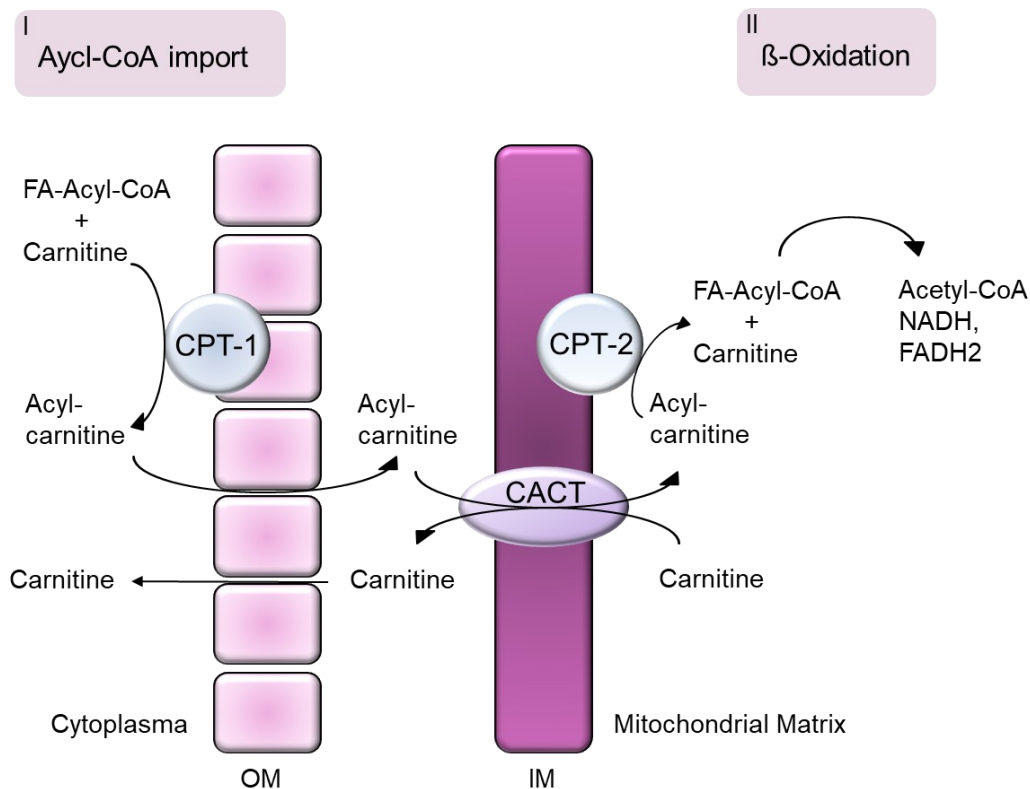


Figure 6: Mitochondrial fatty acid oxidation, fatty acid (Acyl-CoA) import into the mitochondrial matrix

(I) CPT1, located at the mitochondrial outer membrane (OM), converts activated fatty acids (FA-Acyl-CoA) to acyl-carnitine by transesterification. CACT shuttles acyl-carnitine across the inner mitochondrial membrane (IM) into the mitochondrial matrix by carnitine exchange. CPT2 reconverts acyl-carnitine into acyl-CoA the substrate for (II) β-oxidation where acetyl-CoA, NADH and FADH₂ is generated.

2.2.6.1 Mitochondrial β-Oxidation

FA acyl-CoA is degraded by β-oxidation inside the mitochondria in four enzymatic reactions (**Figure 7**). The initial step is catalysed by acyl-CoA dehydrogenase converting acyl-CoA to trans-2-enoyl-CoA. Subsequent enoyl-CoA hydratase is generating (S)-3-hydroxyacyl-CoA by hydration. Then (S)-3-hydroxyacyl-CoA dehydrogenase converts (S)-3-hydroxyacyl-CoA to 3-ketoacyl-CoA which is cleaved by the enzyme thiolase into acetyl-CoA and two acyl-CoAs with shortened carbon chains (**Figure 7I-V**). FA degradation requires specific enzymes for distinct chain-length. Three Acyl-CoA dehydrogenases regulate the catabolism of long- to medium- to short-chain acyl-CoAs including very long chain acyl-CoA dehydrogenase (VLCD), long-chain acyl-CoA dehydrogenase (LCAD), medium-chain acyl-CoA dehydrogenase (MCAD), and short-chain dehydrogenase (SCAD)^{9,50}. Deficiencies in the CPT system interferes with FAO, reduces the generation of acetyl-CoA and mitochondrial energy production⁵¹. Mitochondrial FAO is a key metabolic pathway in mammalian organisms for aerobic ATP generation. Several

nutrient and energy sensing factors including PPAR transcription factors control mitochondrial FAO⁵³.

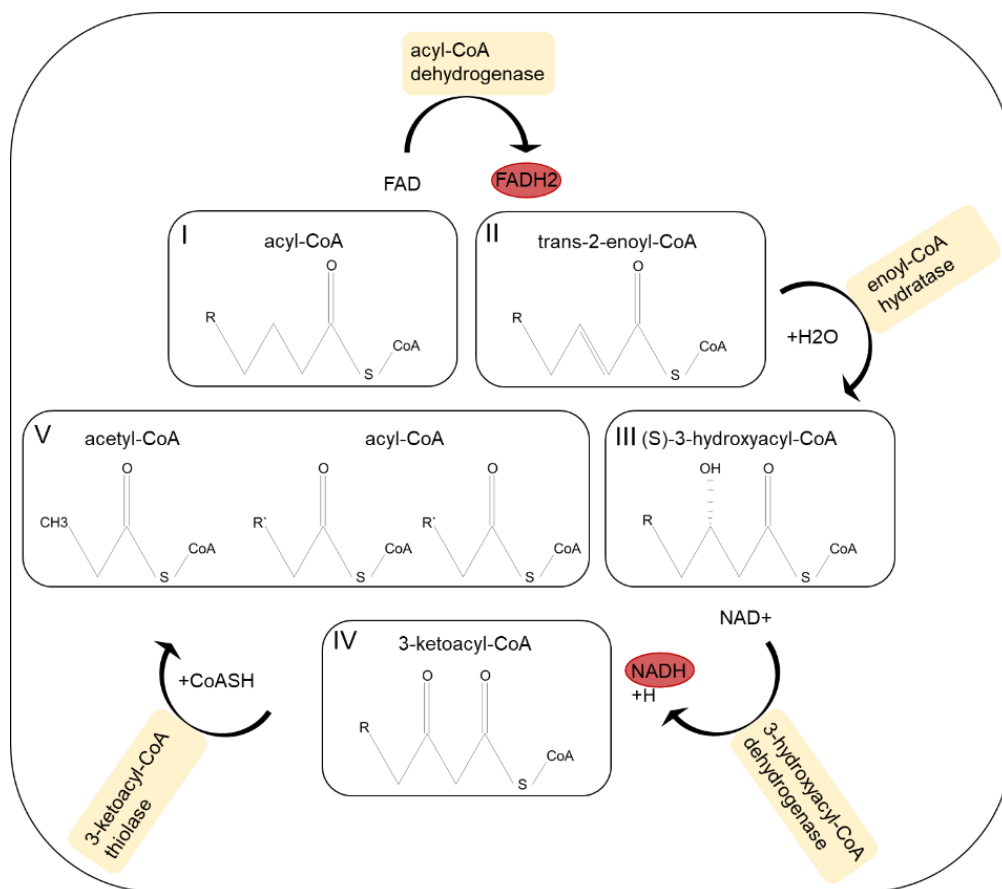


Figure 7: Mitochondrial fatty acid oxidation, β -oxidation

(I) Acyl-CoA within the mitochondria is oxidized by acyl-CoA dehydrogenase to (II) trans-2-enoyl-CoA. FAD is reduced to FADH₂ which is used by mitochondrial respiratory chain for ATP production. Then enoyl-CoA hydratase is catalysing the conversion of trans-2-enoyl-CoA to (III) (S)-3-hydroxyacyl-CoA which is subsequently converted to (IV) 3-ketoacyl-CoA by (S)-3-hydroxyacyl-CoA dehydrogenase. NAD⁺ is reduced to NADH that fuels the mitochondrial respiratory chain. The enzyme thiolase cleaves 3-ketoacyl-CoA into acetyl-CoA and two acyl-CoAs with shortened carbon chains that can enter the next β -oxidation cycle.

FAO is primarily regulated by transcriptional and posttranscriptional mechanisms. PPARs are essential transcriptional regulators of metabolic pathways to maintain energy homeostasis^{50,54}. PPARs are nuclear receptors that are activated in response to fasting, by FAs and their derivatives. The activation of PPARs leads to nuclear translocation and heterodimer formation with the retinoid X receptor (RXR), which allows for binding to peroxisome proliferator response elements (PPREs); located in the promoter sites of target genes leading to PPAR-target gene transcription. PPARs consist of three family members, PPAR- α (NR1C1), PPAR- β/δ (NR1C2), and PPAR- γ (NR1C3)⁵⁵. Their expression is heterogeneous and tissue dependent. PPAR- α is mainly expressed in tissues with FAO capability including the liver, skeletal muscle, and heart. In the liver, PPAR α is an essential regulator of mitochondrial, peroxisomal, and microsomal FAO^{56–58}. Overall, lipid metabolic processes in hepatocytes are primarily regulated by PPAR α ⁵⁸. The expression of genes involved in FA- uptake, transport, oxidation, and

ketogenesis are regulated by PPAR- α activity^{59–61}. PPAR- α is primarily activated by direct ligand binding including FAs, FA derived derivatives, and synthetic ligands such as fibrates (compounds to treat hyperlipidaemia)⁶¹. PPAR- α target gene transcription is regulated by transcription factor hepatocyte nuclear factor 4 alpha (HNF4- α) binding to the PPAR α promoter in human hepatocytes^{62–64}. PPAR γ is highly expressed in adipose tissues and regulates key functions in adipocytes such as cell differentiation and energy storage⁶⁵. In skeletal muscle, adipose tissue and the heart FAO is controlled by PPAR α and PPAR β/δ . In skeletal muscle PPAR β/δ is involved in the response to exercise^{50,66}.

An essential post transcriptional regulation of FAO is the inhibition of CPT1A (mainly expressed in the liver) and CPT1B (expressed in the muscle and the heart) by cellular malonyl-CoA levels^{2,67}. Malonyl-CoA concentration is dependent on the synthesis induced by ACC and degradation regulated by malonyl-CoA decarboxylase (MCD). PPAR activation induces MCD transcription, thus promoting FAO by reducing malonyl-CoA levels. AMP-activated protein kinase (AMPK) is activated by elevated adenosine monophosphate (AMP) levels, to restore decreased ATP levels. Activated AMPK inhibits ACC enzymatic activity by phosphorylation and is thereby also stimulating FAO⁵⁰.

2.2.7. Mitochondrial energy production

Mitochondria are essential for energy production in form of ATP by aerobic respiration, biosynthesis of phospholipids, and regulation of calcium signalling, cell growth, proliferation, and apoptotic cell death⁶⁸. Mitochondria are double membraned bound organelles originated by engulfment of an α -proteobacterium by a precursor of an eukaryotic cell⁶⁹. Thus, they comprise a residual genome, mitochondrial DNA (mtDNA), encoding for proteins involved in the regulation of the respiratory chain. An essential function of mitochondria is the oxidation of lipids, carbohydrates, and proteins for ATP synthesis⁶⁸. Acetyl-CoA generated from pyruvate (derived from glycolysis or amino acid catabolism) or FAO within the mitochondria can enter the TCA cycle where it is converted to energy molecules such as NADH, GTP, and FADH₂. NADH is shuttled to the mitochondrial respiratory chain which consists of protein complexes (complex I-V) embedded at the inner membrane. The complex I (NADH dehydrogenase) of the mitochondrial respiratory chain converts NADH to NAD⁺, inducing oxidative phosphorylation by the electron transfer chain⁹. The electron transfer along the respiratory chain is regulated by generation of a mitochondrial membrane potential ($\Delta\Psi_m$) through pumping protons (H⁺) from the mitochondrial matrix to the intermembrane space⁷⁰. In the final step of oxidative phosphorylation, ATP is generated via complex V (ATP synthase) phosphorylation of ADP. Changes in the membrane potential caused by cell stress (e.g. oxidative stress or ER stress) results in mitochondrial membrane permeabilization which promotes cell death⁶⁸.

2.2.8. Glucose metabolism

Glucose is the primary carbon source used for energy production by glycolysis and the pentose phosphate pathway. Carbohydrates derived from dietary sources circulate in the bloodstream. Specific transport proteins are required for glucose uptake, export, and trafficking between cell membranes and organelles ^{11,27}. In the liver, hepatocytes take up glucose by the glucose transporter GLUT2 also known as solute carrier family 2, member A2 (SLC2A2) ^{11,71}. Once in the cell, glucose is phosphorylated by GK (Hexokinase IV, HKVI) to generate G6P. In contrast to other cells G6P in hepatocytes can be dephosphorylated by glucose-6-phosphatase to glucose to ensure availability, if required to maintain blood glucose levels ^{11,72}. In fed state, G6P can be stored in form of glycogen by synthesis of glucose 1-phosphate and uridine diphosphate glucose (UDP)–glucose. G6P can also generate NADPH and ribose 5-phosphate via the pentose phosphate pathway. High intracellular glucose levels lead to glucose catabolic processes by glycolysis and synthesis of acetyl-coA from pyruvate in the mitochondria promoting FA *de novo* synthesis. Glucose can be synthesised in hepatocytes by gluconeogenesis where amino acids (alanine), lactate or glycerol can serve as substrate and by glycogen degradation. Generated glucose can be released from the liver and used as energy source by peripheral tissues ^{27,72}. Intermediate substrates from glucose metabolism can be used for protein glycosylation, a post-translational protein and lipid modification that impacts their activity ^{11,73}.

2.2.9. Glucose and fatty acid catabolism

The liver regulates key metabolic processes by responding to nutrients and hormones. The nutritional status regulates hormone secretion and affects anabolic and catabolic processes ¹¹. Metabolic adaptations are necessary to adjust to physiological changes ⁷⁴. In times of nutrient availability, which leads to elevated glucose levels in the blood, insulin secretion is increased, which in turn triggers anabolic processes such as *de novo* lipogenesis and glycogen synthesis. During energy demand, catabolic processes, such as FAO, are induced. FAO induces ketone body synthesis to generate an energy source for the brain during times of energy requirement ^{11,74}.

The PDH complex is critically involved in the accommodation to nutrient demand and supply by regulating FA- and glucose oxidation to maintain blood glucose and ATP levels ^{74,75}. The PDH complex converts pyruvate (CoA and NAD⁺), derived from glycolysis, to acetyl-CoA (NADH and CO₂). Acetyl-CoA can further enter the TCA and can be used as energy source for ATP production or it can be transported into the cytoplasm as substrate for ACC to generate malonyl-CoA for FA synthesis. Thus, PDH complex activity promotes glucose catabolism for

energy generation. PDH function is inhibited by phosphorylation through pyruvate dehydrogenase (PDH) kinases (PDKs) ⁷⁶.

PDKs consist of four PDK isozymes (PDK1-4) and their expression is tissue depended. PDK2 and PDK4 are both expressed in liver ⁷⁷, and PDK4 is located in the mitochondrial matrix and functions as histidine kinase. By PDH phosphorylation, PDK4 interferes with glucose catabolism by reducing the conversion of glucose or pyruvate to acetyl-CoA promoting a metabolic shift from glucose to FA oxidation. A mechanism to preserve pyruvate for gluconeogenesis when glucose is limited ^{76,78}. PDK4 levels are regulated by several mechanisms including starvation ⁷⁹, and activation of PPARs to promote FAO ⁸⁰. Elevated mitochondrial acetyl-CoA levels, NADH from TCA, and ATP from oxidative phosphorylation, positively regulate PDK expression and activity. In contrast, PDK4 expression is downregulated by e.g. insulin and PI3K/Akt signalling activation, and by the presence of pyruvate from glycolysis (or lactate) ^{74,77}.

2.3. Acute and chronic liver inflammation

The liver maintains and restores physiological homeostasis during systemic and local inflammation ⁸¹. Inflammation can be triggered by physiological disturbances induced by pathogens, tissue injury, and tumour growth leading to the activation of immune cells, inflammatory cytokine and chemokine secretion, and inflammatory mediator circulation in the bloodstream ⁸¹⁻⁸⁴. Inflammatory cytokines bind to cytokine receptors on several target cells which can intensify the inflammatory response and impacts immunological and metabolic regulations. Inflammation affects whole body and liver metabolism by decreasing hormone secretion, levels of low and high-density (LDL and HDL), and serum levels of calcium, iron, zinc, and retinol / vitamin A ⁸⁵. Inflammatory cytokines affect gene expression and proteins levels in the liver within hours, leading to increased expression of acute phase proteins including C-reactive protein (CRP), serum amyloid A (SAA), and haptoglobin (Hp) which are released by hepatocytes ^{82,84,86,87}. Inflammation in the liver can be acute or chronic, depending on the persistence of the pro-inflammatory stimulus as well as the efficacy of cellular and molecular mechanisms that actively contribute to the resolution of hepatocyte inflammation ⁸⁸⁻⁹⁰. In general, chronic liver inflammation causes necro-inflammation, constitutive liver regeneration and liver damage ⁸⁸.

2.3.1 NF- κ B pathway

Nuclear factor kappa-light-chain-enhancer of activated B cells (NF- κ B) is a protein family of inducible transcription factors that are essential regulators of inflammation, immune responses, cell survival, apoptosis, proliferation, angiogenesis, cell migration, and invasion^{91,92}. The NF- κ B pathway is a highly conserved pathway that controls the cellular response to pro-inflammatory cytokines (e.g. tumour necrosis factor α (TNF- α), Interleukin 1 β (IL-1 β)), intracellular stress (DNA damage), reactive oxygen species (ROS), ultraviolet (UV) irradiation, and different pathogen derived antigens (lipopolysaccharide (LPS) and bacterial or viral nucleic acids)^{93–95}. The NF- κ B protein family consist of five members, RelA /p65 (RELA), RelB (RELB), c-Rel (REL), p105, precursor of p50 (NF κ B1) and p100, precursor of p52 (NF κ B2) that can form homo- and heterodimers which enables distinct responses to specific stimuli^{91,96,91,96}. Individual dimers show different DNA binding specificity for target gene regulation^{97,98}. All NF- κ B proteins share a conserved domain for DNA binding and dimerization, the Rel homology domain (RHD), and comprise C-terminal activation domains^{99–102}. The activation of NF- κ B transcription factors is tightly controlled by interaction with inhibitory I κ B proteins including I κ B α , I κ B β , I κ B γ , and I κ B ϵ ^{103,104}. I κ B proteins have diverse affinities for distinct NF- κ B dimers. The NF- κ B family precursors p105 and p100 can also serve as I κ B-like proteins, due to their C-terminal domain resembling the structure of inhibitory I κ B proteins^{105,106}.

NF- κ B proteins are part of primary “fast acting” transcription factors. The translocation of NF- κ B proteins into the nucleus is rapid and can take place within minutes after stimulation¹⁰⁷.

In most cells, NF- κ B is present in an inactive state in the cytoplasm bound to inhibitory I κ B proteins¹⁰⁴. There are two prominent pathways leading to the activation of NF- κ B, the canonical (classical) pathway and the non-canonical (alternative) pathway (**Figure 8**)¹⁰⁸. In both pathways NF- κ B activation is regulated by I κ B kinase (IKK) complex. The IKK complex comprises the catalytic kinase subunits IKK α and / or IKK β , and in case of the canonical pathway, the regulatory subunit and the scaffold protein NF- κ B essential modulator (NEMO)¹⁰⁹. Activation of the IKK complex leads to phosphorylation and degradation of inhibitory I κ B proteins, NF- κ B dimer release, translocation into the nucleus, and target gene transcription⁹¹. In the presence of a sustained trigger, the activation of NF- κ B is cyclic and transient, as a result of repeating I κ B protein synthesis and subsequent degradation^{103,110,111}.

The canonical NF- κ B pathway can be induced by diverse stimuli such as inflammatory cytokines, mitogens, growth factors, cellular stress, and microbial components¹⁰⁹. Signalling pathway activation of pattern recognition receptors (PRRs), several cytokine receptors such as tumour necrosis factor-receptors (TNFRs), Toll-like receptor (TLR), T-cell receptor (TCR) and B-cell receptor (BCR), leads to the recruitment of adapter proteins to the cytoplasmic receptor domains (**Figure 8I**)^{94,95,112}. These adapter proteins can subsequently recruit the IKK complex (consisting of IKK α , IKK β , and NEMO) via NEMO K63-ubiquitin binding affinity,

leading to IKK complex activation. The activated IKK complex phosphorylates inhibitory IκBα and results in (K48) ubiquitination, proteasomal degradation, NF-κB protein release and translocation to the nucleus for target gene transcription^{103,109,113,114}. NF-κB members of the canonical pathway are predominantly p50/RelA (or p50/c-Rel) dimers that are sequestered in the cytoplasm bound to the inhibitory IκB protein IκBα^{104,114,115}.

In the non-canonical NF-κβ pathway, the NF-κβ dimers p100/RelB are activated by specific stimuli such as ligands of the TNFR superfamily including lymphotoxin β receptor (LTβR), B-cell activating factor receptor (BAFFR), cluster of differentiation 40 (CD40), and receptor activator of nuclear factor κ B (RANK), that signal via IKK complexes comprising two IKKα subunits (**Figure 8II**)^{116–120}. The activation of the non-canonical pathway is slower, due to the required *de novo* synthesis of NF-κB inducing kinase (NIK)¹²¹. Receptor binding activates NIK that subsequently activates an IKKα complex by phosphorylation. The activated IKKα complex then phosphorylates the IκB domain of p100 which results in partial p100 proteolysis, the release of the p52/RelB dimer, translocation to the nucleus and target gene transcription^{108,120,122}.

NF-κB signalling pathway is associated with several liver diseases including hepatitis, cirrhosis, fibrosis, and hepatocellular carcinoma (HCC)^{96,123}.

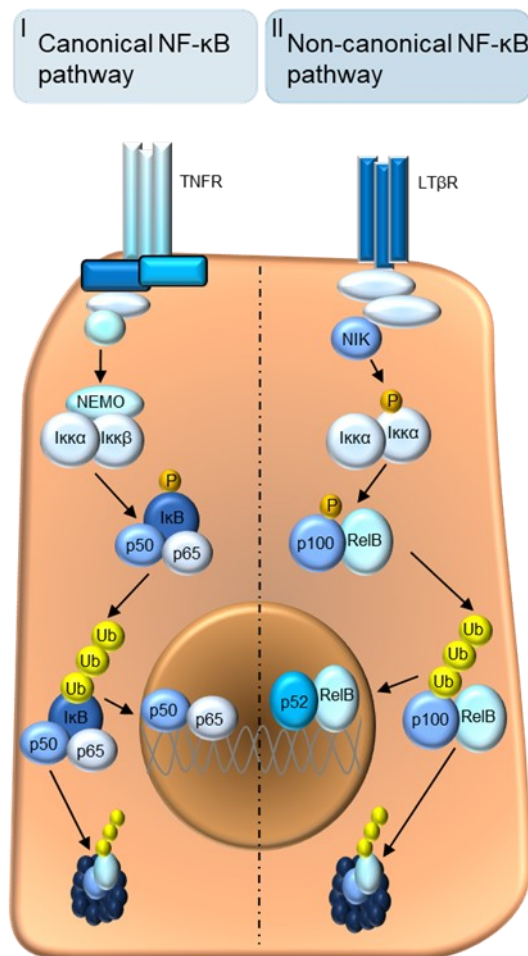


Figure 8: NF-κB signalling pathway

(I) Canonical NF-κB pathway activation via TNFR leads to the recruitment of adapter proteins that subsequently recruit and activate the IKK complex consisting of IKKα, IKKβ, and NEMO. The IKK complex then phosphorylates inhibitory IκB proteins resulting in proteasomal degradation, and NF-κB dimer release consisting of p50/p65. Free NF-κB dimers can translocate into the nucleus where target gene transcription takes place. (II) Non-canonical NF-κB pathway activation through LTβR activates NIK that phosphorylates the IκB domain of p100, leading to partial proteolytic degradation, and NF-κB dimer release consisting of p52/RelB. Released NF-κB dimers translocate into the nucleus leading to target gene transcription.

2.4. Metabolism control and the NF-κB signalling pathway

Inflammatory and metabolic regulation are tightly connected^{124,125}. PDK4 can influence NF-κB signalling by direct interaction with the NF-κB protein RelA/p65. Loss of PDK4 switches NF-κB-driven survival to pro-apoptotic signalling facilitated by the release and subsequent binding of p65 to the TNFR. Apoptotic pathway activation increases the number of dysfunctional mitochondria, reduces glutathione (GSH) levels, and elevates ROS production¹²⁶. High PDK levels are associated with increased cell proliferation in different cancer entities¹²⁷. Cancer cells can control PDK levels on transcriptional and post transcriptional levels to sustain proliferation by inactivation of PDH complex function and mitochondrial oxidation of glucose / pyruvate which stimulates anabolic processes (gluconeogenesis) and promotes cancer cell growth¹²⁸. PPAR-α can affect inflammatory responses in the liver. During inflammation, elevated IL-1β levels promote the secretion of CRP by formation of nuclear CCAAT-box/enhancer-binding protein-β (C/EBP-β)-p50-NF-κB complexes, enhancing CRP promoter activity in hepatocytes. PPAR-α activation decreases CRP secretion by promoting the expression of inhibitory IκBα protein, thus inhibiting the canonical NF-κB pathway by reducing levels of C/EBP-β and p50-NF-κB and interfering with their complex formation¹²⁹. The dihydroxy leukotriene B₄ (LTB₄) is involved in the regulation, initiation, maintenance, and intensity of inflammation. LTB₄ can bind and activate PPAR-α and thereby control inflammatory regulations¹³⁰. Kupffer cell-derived TNF-α or IL-1β can interfere with PPAR-α expression via NF-κB activation, and contributes to TG accumulation in liver¹³¹. In cardiac cells, TNF-α induced NF-κB activation can directly impact FAO by downregulation of peroxisome proliferator activated receptor coactivator 1a (PGC-1a) which elevates glucose oxidation and inhibits FAO. Transcriptional mechanisms are regulated by the interference with DNA-binding activity of PPAR β/δ leading to reduced PDK4 levels¹³². In addition, the NF-κB protein p65 can directly interact with PPARβ/δ which results in a reduction in FAO through decreased PDK4 expression¹³³.

The pro-inflammatory cytokine, Interleukin-17 (IL-17) is critically involved in regulating inflammatory cell response and can activate NF-κB pathway via NF-κB activator 1 (ACT1) and TNFR associated factor 6 (TRAF6)^{134–136}. Increased IL-17A expression, triggered by excess nutrients, increases TG accumulation in the liver by reduction of FAO¹³⁷. Obesity is

associated with elevated IL-17A levels which promotes the development of fatty liver disease
138,139.

2.5. Non-alcoholic fatty liver disease, NAFLD, and non-alcoholic steatohepatitis, NASH

Surplus metabolic energy, due to high caloric intake, in combination with reduced energy expenditure, through a sedentary lifestyle, resulted in a worldwide epidemic of obesity and the metabolic syndrome ¹⁴⁰. In 2016, about 1.9 billion adults were overweight and about 650 million of them were obese (World Health Organization, WHO). Obesity is defined by a body mass index (BMI) greater than 30 kg/m² (weight to height ratio) ¹⁴¹. Obesity and the metabolic syndrome highly increase the risk to develop cardiovascular disease and type 2 diabetes mellitus (T2DM) ^{10,142}.

Obesity is also associated with inflammation ¹⁴³. Nutrient excess and exacerbated lipid storage in adipocytes can lead to immune cell infiltration into WAT and the liver ⁸. Activated immune cells generate an inflammatory environment by secretion of inflammatory cytokines which, in combination with surplus nutrients, is driving metabolic changes ¹⁴⁴. Inflammation can impair insulin signalling and promotes insulin resistance (IR). IR is a pathological condition in which cells are unable to respond to insulin, causes lipolysis in adipocytes, and thereby promotes dysregulation of lipid metabolism (dyslipidaemia) ⁷. Thus, nutrient excess in combination with inflammation triggers increased lipolysis in adipocytes and results in excess FFA release into the bloodstream. Elevated FFAs in the circulation are stored in the liver and promote the development of steatosis and non-alcoholic fatty liver disease (NAFLD) ^{145,146}. NAFLD is the most common chronic liver disease which affects about 25% of the adult population globally ^{147–149}. NAFLD is defined by the development of hepatic steatosis with an alcohol uptake less than 30g per day (for male). In contrast to NAFLD, alcohol fatty liver disease (AFLD) is induced by excess alcohol consumption but displays a similar disease development and progression ^{150,151}. NAFLD is a highly heterogenous disease with distinct clinical manifestations and progression rates, which is dependent on overall metabolism, environmental factors, the microbiome, and genetic risk factors ¹⁰. NAFLD ranges from simple hepatic steatosis (NAFL), characterized by intensified accumulation of lipids in the liver, to steatohepatitis (NASH), associated with exacerbated lipid storage, inflammation, cell stress, hepatocyte damage, apoptosis, and compensatory proliferation. About 3-5% of NAFLD patients can develop NASH which can be associated with fibrosis, cirrhosis, and can lead to NASH-derived HCC ^{10,16,152}. HCC is the fastest rising cancer in Europe and the United States and the third most common cause for cancer related death worldwide ^{153–155}.

Up to date there are no drugs approved for NASH treatment ¹⁵⁶. Thus, weight loss is currently the best “treatment option” for NAFLD and / or NASH by alleviating the risk factors associated with fatty liver disease (American Liver Foundation, <https://liverfoundation.org/>). NAFLD is the

hepatic manifestation of the metabolic syndrome, thus targeting associated metabolic risk factors e.g., T2D and hyperlipidaemia are possible treatment strategies ¹⁵⁷. Metabolic associated treatment options include (i) administration of vitamin A / retinol to reduce oxidative stress caused by inflammation, (ii) targeting nuclear receptors ^{158,159}, such as PPARs by fibrates / PPAR- α agonists that act anti-hyperlipidaemic and anti-inflammatory ^{129,130,160}, thiazolidinediones / PPAR- γ agonists that are insulin sensitising agents and act anti-inflammatory ^{161,162}, and (iii) farnesoid X receptor (FXR) agonists that regulates bile acid, lipid, and glucose metabolism ^{163,164}. Chronic inflammation is a key factor for NAFLD progression and interference with molecular mechanisms driving intrahepatic immune cell infiltration, cytokine secretion, and subsequent intensified steatosis and liver damage provides an attractive therapeutic strategy ¹⁶⁵. Currently, liver biopsy is the clinical standard for diagnosis. Most NASH patients are asymptomatic for decades, only a few patients rapidly progress NASH. The recognition of NAFLD and progression to NASH is critical to prevent, potentially revert and limit disease severity ^{10,166}.

Risk factors for NASH development include the metabolic syndrome which is associated with obesity, T2DM, hypertension, dyslipidaemia, and hyperglycaemia ^{90,167}. The essential step in NAFLD development is the progression from simple steatosis to inflammation-induced steatohepatitis, which is dependent on the response of cells to external stressors and stimuli in the microenvironment ^{10,147,152}. The first and most prominent model describing NAFLD development is the “two hit” hypothesis ¹⁶⁸. In this model, excess lipid accumulation is described as “first hit” which makes hepatocytes susceptible to subsequent stressors, so called “second hits” such as oxidative stress, inflammatory cytokines, xenobiotics, and hypoxia that promotes inflammation and development of NASH ⁸⁸.

Inflammation is critically involved in the NAFLD to NASH transition and NASH-derived HCC development ^{139,144}. A preclinical mouse model demonstrated that immune cell–hepatocyte interaction drives NASH and HCC development. Liver infiltration of metabolic activated immune cells, particularly CD8⁺T cells and NKT cells, induces inflammatory cytokine release and promotes metabolic reprogramming in hepatocytes. The expression of inflammatory cytokines such as tumour necrosis factor superfamily member 14 (TNFSF14 also known as LIGHT) and Lymphotoxin-alpha and beta (LT- α and LT β), which both signal via LT β R, and subsequently non-canonical NF- κ B, is highly increased during NASH. Also, other inflammatory signalling pathways such as the canonical NF- κ B pathway are activated. NASH derived inflammation interferes with lipid metabolism by downregulation of genes involved in mitochondrial β -oxidation (e.g. CPT1, acyl-CoA dehydrogenase family, member 10 (ACAD10), cholesterol metabolism (e.g. ATP-binding cassette transporter (ABCA1)), and triglyceride catabolism (e.g. lipoprotein lipase (LPL), HSL). The inflammatory cytokine LIGHT, mainly

expressed by activated immune cells and natural killer T (NKT) cells, induces intensified lipid storage in hepatocytes and thereby promotes NASH and NASH to HCC progression ¹⁴⁴.

Excess nutrients can induce unconventional prefoldin RPB5 interactor (URI)-dependent DNA damage in hepatocytes which promotes inflammation by T helper 17 (Th17) cell infiltration into the liver. The pro-inflammatory Th17 cells secrete IL-17A, which triggers IR in WAT and leads to FFA release into the blood stream and delivery to the liver. Interference with Th17 cell differentiation or inhibition of IL-17A signalling has been shown to prevent NASH and NASH-induced HCC ¹³⁹.

Cell-cell communication between immune cells, platelets, and hepatocytes is essential for NASH pathology ¹⁶⁵. Platelets are critically involved in inflammation and liver disease by contributing to the activation of the immune system ^{169–171}. The number of activated platelets in the liver is increased in NASH and inhibition of platelet accumulation in the liver results in less immune cell recruitment and inflammatory cytokine secretion, thereby prevents aberrant hepatocyte lipid metabolism ¹⁶⁵. Also Kupffer cells are critically involved in NAFLD development and progression to NASH ^{165,172,173}. TLR4 induced TNF- α secretion by Kupffer cells promotes lipid accumulation and liver injury during NAFLD progression ^{172,172}. Activated Kupffer cells interfere with lipid catabolism by reducing the expression of PPAR- α target genes involved in FAO which results in the upregulation of the NF- κ B pathway in hepatocytes. Inflammatory cytokine induced NF- κ B activation interferes with PPAR- α promoter activity leading to target gene downregulation ¹³¹, displaying the impact of aberrant metabolism induced by inflammation on NAFLD development and progression.

2.5.1. Lipotoxicity

A pre-requisite for NASH development is intensified lipid accumulation in hepatocytes ¹⁶⁸. Elevated lipid storage can induce toxicity in cells also known as lipotoxicity. Lipotoxicity can trigger a cellular stress response, ROS production, inflammasome activation, and affects mitochondria and ER function which in turn induces cell damage and apoptosis by activation of death receptor signalling pathways ¹⁶.

Lipid induced toxic cell response is not only dependent on the lipid amount but also on the lipid species and composition. Specific lipid classes that induce lipotoxicity are not known in detail so far. However, FFAs, free cholesterol (FC), and several other lipids and metabolites have been shown to induce lipotoxicity in hepatocytes ^{10,16}.

One underlying mechanism in hepatocyte lipotoxicity includes elevated ROS generation in the liver, promoted by pro-oxidant lipid classes such as saturated FFAs, palmitic acid, and stearic acid ^{16,174}. FFA storage in form of TGs in LDs was reported as protective mechanism ^{4,175}.

Intensified ROS production affects redox-sensitive signalling pathways and triggers damage of DNA, enzymes, and proteins, which promotes NAFLD pathogenesis ^{176,177}. This mechanism

is partly regulated by oxidative stress induced downregulation of genes involved in lipid catabolic processes, removal of toxic intermediates, oxidative phosphorylation, detoxification, protein and DNA repair mechanisms, and the cellular component recycling mechanisms (i.e. mitophagy and autophagy) ¹⁶. In addition, lipotoxicity promotes expression of inflammatory stress response genes including activator protein 1 (AP-1), nuclear factor erythroid 2–related factor 2 (Nrf2), and NF-κB target genes ^{16,178–180}. Lipotoxicity induced NF-κB activation interferes with mitochondrial morphology and function by promoting mitochondrial fragmentation and reducing mitochondrial respiratory capacity ¹⁸¹.

2.5.2 Mitochondria during NAFLD

Mitochondria are critically involved in NAFLD pathogenesis and their function and activity change during disease development and progression. NASH is associated with mitochondrial dysfunction and impaired FA oxidation ^{182,183}.

Lipid excess constrains the mitochondria to accommodate by increasing FAO which is linked with elevated acetyl-CoA generation. Aberrant acetyl-CoA production can uncouple the TCA from mitochondrial respiration as protective mechanism. Dysregulated TCA increases ROS production and interferes with the function of the electron transport chain and ATP synthesis ^{16,184}. Reduced function of the respiratory chain results in incomplete FAO and thereby promotes generation of toxic lipid intermediates ¹⁸⁵. The accumulation of toxic lipids further affects mitochondrial function, which, in combination with elevated ROS, promotes cellular stress response, lipotoxicity, and cell death ^{186,187}.

Intracellular calcium levels are indicative for cellular energy levels and cellular stress. Energy demand or cellular stress response is leading to increased calcium levels in the cytosol and uptake by a mitochondrial calcium uniporter embedded at the inner mitochondrial membrane ^{68,188}. Elevated calcium in the mitochondrial matrix activates key enzymes of the TCA and ATP-synthase of the respiratory chain for NADH generation, respiration activation, and ATP production. Calcium overload due to oxidative stress interferes with mitochondrial function and morphology and induces apoptotic cell death ^{9,188}. Apoptosis can be activated by two distinct pathways, the intrinsic and the extrinsic pathway. The intrinsic mitochondria linked pathway is induced by cellular stress, ROS, hypoxia, and DNA damaging signals ¹⁸⁹. Apoptotic cell death induced by the intrinsic pathway induces mitochondrial outer membrane permeabilization, associated with decreased membrane potential and release of pro apoptotic factors into the cytosol. In contrast, TNF-α binding to the TNFR can trigger the extrinsic pathway by the activation of cell death effectors such as. pro-caspase 8 and 10 that initiate the apoptotic signalling cascade ¹⁹⁰.

2.6. Hypothesis and Aims of the Thesis

Activated immune cells induce aberrant FA metabolism in hepatocytes by the secretion of pro-inflammatory cytokines and thereby can contribute to NASH and NASH-derived HCC. However, the underlying mechanism remain elusive.

The main aim of this project was to study and understand the impact of proinflammatory cytokines on lipid homeostasis in hepatocytes and to identify underlying mechanisms and signalling pathways in order to identify possible treatment targets for NAFDL and NASH.

My major hypothesis have been:

- Key metabolic processes in hepatocytes such as FA- uptake, *de novo* synthesis, storage, oxidation, and export are directly affected by pro inflammatory cytokines.
- The activation of an inflammatory signalling pathways, such as NF- κ B, in hepatocytes affect major metabolic regulations which induces aberrant lipid metabolism.
- NASH-derived inflammation, caused by proinflammatory cytokines, directly influences the transcriptional and translational machinery of metabolic genes and proteins via activation of inflammatory signalling pathways such as NF- κ B.
- Increased intracellular lipid levels can induce liptotoxicity and affects mitochondrial function, cellular apoptosis, and proliferation.

My major aims have been:

- The establishment of an *in vitro* NASH model to study the impact of proinflammatory cytokines on hepatic lipid metabolism.
- Investigating changes in FA-metabolism pathways by performing experiments with fluorescence and radioactive labelled lipids
- Describing the role of the NF- κ B signalling pathway in inflammation induced altered lipid metabolism by the use of genetically modified cells and specific inhibitors.
- To study the consequence of inflammation and increased lipid accumulation on cellular stress, mitochondrial polarization, cell viability, and proliferation by fluorescence-based assays.
- To address how inflammation influences the lipid concentration and composition in hepatocytes, regulates gene and protein expression and controls signalling pathways by using multi omics approaches including lipidome, transcriptome, proteome, phosphoproteome and protein-based complex analysis.

3. Material and Methods

3.1. Material

Table 1: List of Material and Resources

Product	Company / Supplier	Article Number
Media and Supplements		
William's E Medium, GlutaMAX Supplement-1	Life Technologies	32551087
William's E Medium, w.o. Phenol red,	PAN Biotech	P04-29510S
Fetal Clone II Serum (FCS)	VWR International	HYCLSH30066.03
Penicillin-Streptomycin (10,000 U/mL)	Life Technologies	15140122
Hydrocortison (Pfizer)	Atzelhof Apotheke	PZN1877030
Human Insulin		
PBS	Life Technologies	10010056
Trypsin-EDTA Solution	Sigma Aldrich	T3924
Versene (EDTA)	VWR International	LONZ17-711E
Dimethyl sulfoxide (DMSO)	Sigma Aldrich	D4540
Chemicals, Buffers and Solutions		
Acetic acid	Sigma Aldrich	45731
Sodium acetate	Sigma Aldrich	S2889
EGTA	AppliChem	A0878,0025
CaCl ₂	Sigma Aldrich	C8106
Fetal Bovine Serum (BSA)	Sigma Aldrich	F7524
Trizma® base (Tris)	Sigma Aldrich	T1503
Sodium Chloride (NaCl)	Sigma Aldrich	12781
Perchloric acid	Sigma Aldrich	1090651000
Methanol	Sigma Aldrich	322415
Chloroform	Sigma Aldrich	288306
Roti®-Histofix 4 %	Roth - Carl Roth	P087.3
HBSS	Life Technologies	14175129
Collagenase	Sigma Aldrich	C5138
Collagen, Type I solution from rat tail	Sigma Aldrich	C3867
Ketamin	Atzelhof Apotheke	Ketamin Inresa
Rompun	Bayer	770-081
RIPA Buffer	Cell Signalling Technology	9806S
PhosSTOP™	Sigma Aldrich	4906837001
Pierce BCA Protein Assay Kit	Thermo Fisher Scientific	23225
Whatman filter paper	Sigma Aldrich	WHA1001325

cOmplete™ Protease Inhibitor Cocktail	Sigma Aldrich	11697498001
Clarity™ Western ECL Substrate	Bio Rad	1705060
Precast gels	Bio Rad	3450010
Ethanol absolute	VWR International	20821330
Triton™ X-100	Sigma Aldrich	1086431000
Sodium hydroxide (NaOH)	Sigma Aldrich	S0899
Tween® 20	Sigma Aldrich	P9416
Fatty acids		
Oleic acid	Sigma Aldrich	O1383
Palmitic acid	Sigma Aldrich	P5585
Fluorescence and radioactive labelled fatty acids		
BODIPY™ FL C16	Thermo Fisher Scientific	D3821
R-2-bromopalmitic acid [1-14C] (0.1mCi/ml)	Hartmann Analytic	ARC3623
Acetic acid [1-14C] sodium salt, 50µCi	Hartmann Analytic	ARC0101
Palmitic acid [1-14C], 50µCi	Hartmann Analytic	ARC0172A
Cytokines and inflammatory mediators		
Recombinant Human IL-17A	R&D Systems	317-ILB-050
Recombinant Human TNF-alpha	R&D Systems	210-TA-020
Recombinant Human LIGHT	R&D Systems	664-LI-025
BS1	Genentech	N/A
Recombinant Human IL-4	R&D Systems	204-IL-020
Recombinant Human IFN-γ	Thermo Fisher Scientific	PHC4031
Recombinant Mouse IL-17A	R&D Systems	421-ML-025
Recombinant Mouse TNF-α	R&D Systems	410-MT-010
Recombinant Mouse LIGHT	R&D Systems	1794-LT-025
Inhibitors, Agonists, and Antagonists		
GW6471	Tocris	4618
CP775146	Tocris	4190
TPCA-1	Sigma Aldrich	T1452
Pan Caspase Inhibitor Z-VAD-FMK	R&D Systems	FMK001
N-Acetyl-L-cysteine	Sigma Aldrich	A7250
Primers		
Name	Sequence	Company/Supplier
NFκB2	Fwd: GGGCCGAAAGACCTATCCC Rev: CAGCTCCGAGCATTGCTTG	Sigma Aldrich
PPARA	Fwd: GACAGAAACACACGCGGAA Rev: CCCACCCAGGAGAGAGGTAT	Sigma Aldrich
PDK4	Fwd: CCGTATTTCTACTCGGATGCTG Rev: TGGCTTGGGTTTCCTGTC	Sigma Aldrich
siRNA transfection reagents and siRNAs		

Product		Company / Supplier		Article Number
DharmaFECT4, Transfection Reagent		Horizon Discovery		T-2004-03
Opti-MEM™		Thermo Fisher Scientific		31985062
Silencer Select Negative Control No. 1 siRNA-5 nmol		Invitrogen		4390843
Silencer Select PPARA Pre-Designed siRNA-5 nmol		Invitrogen		AM16708A
Silencer®Select, PDK4		Life Technologies		0007128168
Primary Antibodies				
Western blot antibodies				
Name	Species	Dilution	Company	Article Number
GAPDH	Rabbit	1:1000	Cell Signalling Technology	2118
P-p65	Rabbit	1:1000	Cell Signalling Technology	3033
p65	Rabbit	1:1000	Cell Signalling Technology	8242
p100/p52	Rabbit	1:1000	Cell Signalling Technology	37359
Immunofluorescence antibodies				
PPAR-α	Rabbit	1:500	Abcam	ab227074
PDK4	Rabbit	1:100	Thermo Fisher	PA5-13776
Pyruvate Dehydrogenase E1-alpha subunit (phospho S293)	Rabbit	5 µg/ml	Abcam	ab92696
Cleaved caspase 3	Rabbit	1:400	Cell Signalling Technology	9661
Secondary Antibodies				
IgG(H+L) ReadyProbes™ Alexa Fluor 594	Donkey anti-Rabbit	2 drops / ml	Thermo Fisher Scientific	R37119
IgG (H+L) ReadyProbes™ Alexa Fluor 488	Donkey anti-Rabbit	2 drops / ml	Thermo Fisher Scientific	R37118
IgG (H+L) HRP	Anti-Rabbit	1:5000	Promega	W4011
Staining Solutions and Kits				
Product		Company / Supplier		Article Number
HCS LipidTOX™ Green Neutral Lipid Stain		Thermo Fisher Scientific		H34475
LD540		Dr. Christopher Thiele (Spandl, White, Peychl, & Thiele, 2009)		N/A
Hoechst 33342		Thermo Fisher Scientific		H1399
MitoTracker®Red CMXRos		Cell Signalling Technology		9082
MitoSOX™Red mitochondrial superoxide indicator		Life Technologies		M36008
JC-1 Assay Kit for Flow Cytometry		Life Technologies		M34152

5-Bromo-2'-deoxy-uridine Labeling and Detection Kit I	Sigma Aldrich, Roche	11 296 736 001
PE Annexin V Apoptosis Detection Kit I	BD Pharmingen	559763
Kits and other Material		
Triglyceride Quantification Colorimetric Kit	Sigma Aldrich	MAK266-1KT
Triglyceride Reagent	Sigma Aldrich	T2449
RNeasy Mini Kit	Qiagen	74104
QIAshredder	Qiagen	79656
Mix SYBR® Green PCR Master Mix	Life Technologies	4309155
QuantiTect Rev. Transcription Kit	Qiagen	205314
ChamberSlides, Lab-Tek II, CC2	Thermo Fisher Scientific	10092371
Scintillation vials	Sigma-Aldrich	Z376825
Cell Scraper	Sarstedt	83.1830
Menzel™ Mikroskop-Deckelgläschen (coverslides)	Thermo Fisher Scientific	BBAD02400240
26Gx1/2 Needles	Medsitis	305111
BD Falcon Cell Strainer, 70 µm	BD Bioscience	352350
Fluorescence Mounting Medium	Dako, Cytomation	S302380
Eppendorf tubes	Eppendorf	0030 120.086 0030 120.094
PDVF membrane	Thermo Fisher Scientific	88025
Software		
Software	Manufacturer	Version
GraphPad	GraphPad Prism Software	8.0
QuantStudio™ Real-Time PCR	Applied Biosystem	Software V1.2
Image J / FIJI	64-bit Java	1.8.0_112
Image Lab	Bio Rad	6.0.1
Zen	Carl Zeiss	3.1
FlowJo	BD Bioscience	V8
Hardware and Equipment		
Zeiss Cell Observer motorised, inverted microscope	Carl Zeiss	Observer.Z1
Liquid Scintillation counter	N/A	Packard 1900 TR
SpeedVac™ Vakuumpconcentrator	Thermo Fisher Scientific	SPD120
NanoDrop™ 2000	Thermo Fisher Scientific	ND-2000
ChemiDoc Imaging Systems	Bio Rad	N/A
Heracell 150i CO ₂ Incubator	Thermo Fisher Scientific	51026281
PerkinElmer Plate Reader	Perkin Elmer	N/A
QuantStudio 5 Real-Time-PCR-System	Thermo Fisher Scientific	5

3.2. Methods

3.2.1. Cell culture

Culture Medium, for non-differentiated HepaRG

- Williams E Medium
- 10% FCS
- 1% Penicillin/Streptomycin (10.000 U/ml)
- Human Insulin (5 µg/ml)
- Hydrocortison hemisuccinate (5X10⁻⁵M)

Assay Medium

- Williams E Medium, w.o. Phenole red
- 2%FCS
- 1% Penicillin/Streptomycin (10.000 U/ml)

Culture Medium, for differentiated HepaRG and primary mouse hepatocytes

- Williams E Medium
- 10% FCS
- 1% Penicillin/Streptomycin (10.000 U/ml)
- Human Insulin (5 µg/ml)
- Hydrocortison hemisuccinate (5X10⁻⁵M)
- 1.8% DMSO

3.2.1.1. Cells

Primary mouse hepatocytes were isolated from 8 week old C57BL/6J mice, purchased from Charles River, IKK $\beta^{\Delta\text{hep}}$ mice were obtained from the laboratory of Prof. Mathias Heikenwalder¹⁹¹. HepaRG cells were obtained from Philippe Gripon, PhD¹⁹², and were isolated in the laboratory of Prof.Christian Trepo and Prof Fabien Zoulim. CRISPR-Cas mediated HepaRG cells, HepaRG-sgCtrl, HepaRGsgIKK β , HepaRG-sgNIK and HepaRGsgIKK β +sgNIK were generated in the laboratory of Prof. Mathias Heikenwalder by Tobias Riedl, MSc. All cells were cultured in William E Medium and incubated at 37°C in a humidified atmosphere containing 5% CO₂, in the incubator.

HepaRG cell culture

HepaRG cell culture and differentiation was performed as described previously by Gripon and colleagues¹⁹². In brief, undifferentiated HepaRG were seeded in T.75 flasks and were maintained for 2 weeks in Williams E (culture medium for non-differentiated HepaRG), with a medium change twice a week. For HepaRG differentiation, DMSO (1.8%) was added and cells were cultured in Williams E (culture medium for differentiated HepaRG (dHepaRG)), for another 2 weeks, with a medium change twice a week.

3.2.1.2. Primary mouse hepatocyte isolation

Perfusion buffer

-HBSS (1X)

-EGTA (1 mM)

Digestion buffer

-HBSS (1X)

-CaCl₂ (1 mM)

- Collagenase D (working conc. 0.18 U/mg)

Preparations

For culturing of primary mouse hepatocytes 6 well-plates were coated with collagen I from rat tail, diluted in autoclaved sterile filtered distilled H₂O (dH₂O) to a final concentration of 0,1 mg/ml. 500 µl of the collagen solution was added per well and plates were incubated for 30 min. in the incubator. Then the collagen solution was removed, and wells were washed with PBS. Coated dishes were stored at 4°C in the fridge and were treated with UV light before usage.

All buffers and solutions were freshly prepared and were stored at 4°C until use. The water bath was pre-warmed at 42°C (the digestion buffer should have 37°C during perfusion).

For anaesthesia of mice a Ketamine / Rompun solution (mixed 1:1) was intraperitoneal injected.

Liver perfusion and digestion

Mice were fixed and the abdomen was cut, all organs were moved to access the liver. Then the cannula was inserted into the vena porta, the vena cava was cut (to avoid pressure increase within the liver), and the liver was perfused with the perfusion buffer for 3-5 min. At the beginning of the perfusion the flow rate should be around 8 ml/min and can be increased up to 24 ml/min during perfusion / digestion. To avoid dehydration of the liver perfusion buffer was added on the organ. After perfusion, the liver was digested by digestion buffer for 5-10 min.

Primary hepatocyte cell culture

The digested liver was transferred into a 50 ml tube, containing prewarmed culture medium and by using a tweezer the liver was agitated to liberate the cells. The cell suspension was then transferred, by filtering through a 70 µm strainer, into a new 50 ml tube, filled up to 40 ml with culture medium, and was centrifuged for 3 min. at 300 g. After pelleting the cells, the supernatant was removed, and culture medium was added, and the centrifugation step was repeated. Isolated hepatocytes were counted and 3.5x10⁵ cells were seeded per well of a 6-well plate in culture medium and were incubated in the incubator. After attachment, (after about 4 h) cells were used for further experiments.

3.2.2. Fatty acid metabolism experiments

3.2.2.1. Fatty acid uptake

Radioactive (¹⁴C) labelled bromo-palmitic acid uptake

To quantify FA uptake dHepaRG cells were subjected to ¹⁴C-labelled bromo-palmitic acid. 1.2x10⁵ cells were seeded per well of a 12-well plate in 1 ml assay medium. After attachment, cells were left untreated (as blank control), were treated with FAs, palmitic acid (33 μM) and oleic acid (66 μM) alone, and in combination with inflammatory mediators, including BS1 (0.5 μg/ml), rhLIGHT (500 ng/ml), rhIL-17A (50 ng/ml), and rhTNF-α (50 ng/ml), for 21 h in the incubator. The assay medium was removed and tracer medium was added which contained FAs, palmitic acid (33 μM) and oleic acid (66 μM), and 0.1 μl/ml ¹⁴C R-2-bromopalmitic acid (with an activity of 0.1 mCi/ml) alone, and in combination with inflammatory mediators including BS1 (0.5 μg/ml), rhLIGHT (500 ng/ml), rhIL-17A (50 ng/ml), and rhTNF-α (50 ng/ml). Cells were incubated for 3 h in the incubator. Then the medium was removed, and cells were washed twice with PBS, then they were lysed in radioimmunoprecipitation assay (RIPA) buffer (300 μl per well). Cell lysates were used to determine protein concentration by Bicinchoninic acid (BCA) assay, according to the manufacturer's manual, for normalization. Radioactivity was quantified by using 250 μl of each cell lysate, by scintillation counting.

Fluorescence (BODIPY) labelled palmitic acid uptake

To study FA uptake over time, BODIPY-labelled palmitic acid was used. 1.2x10⁵ cells were seeded per well of a 12-well plate in 1 ml assay medium. After attachment, the assay medium was removed, and cells were left untreated, were treated with FAs, palmitic acid (33 μM), oleic acid (66 μM) and BODIPY-C16 (33 μM) alone, and together with the cytokine combination including BS1 (0.5 μg/ml), rhLIGHT (500 ng/ml), rhIL-17A (50 ng/ml), and rhTNF-α (50 ng/ml), for 1 h, 3 h and 24 h, in the incubator. After incubation, the cells were washed with PBS, were trypsinized and pelleted by centrifugation at 300 g for 3 min. Cell pellets were resuspended in 300 μl of PBS plus 3% FCS. Cells were analysed by flow cytometry, by using BD FACSFortessa, Sony spectral analyser, SP6800, and data were analysed using FlowJo.

3.2.2.2. Fatty acid *de novo* synthesis

De novo synthesis, radioactive (¹⁴C) labelled acetic acid

For FA *de novo* synthesis experiments, 1.2x10⁵ cells were seeded per well of a 12-well plate in 1 ml assay medium. After attachment, the cells were left untreated (as blank control), were treated with FAs, palmitic acid (33 μM) and oleic acid (66 μM) alone, and in combination with

inflammatory mediators, including (BS1 (0.5 µg/ml), rhLIGHT (500 ng/ml), rhIL-17A (50 ng/ml), and rhTNF-α (50 ng/ml), for 21 h in the incubator. Then the assay medium was removed, and tracer medium was added containing 100 µM sodium acetate and 1 µl/ml of acetic acid [¹⁴C] sodium salt alone, and in combination with inflammatory mediators including BS1 (0.5 µg/ml), rhLIGHT (500 ng/ml), rhIL-17A (50 ng/ml), rhTNF-α (50 ng/ml), for 3 h in the incubator. The tracer medium was removed, and cells were washed twice with PBS and were lysed in 300 µl of RIPA buffer per well. 50 µl were stored for determination of the protein concentration by BCA protein assay for normalization, and 200 µl of the cell lysates were used for lipid extraction.

For lipid extraction, 800 µl of chloroform: methanol, in a ratio of 2:1 (533.3 µl chloroform and 266.6 µl methanol) was added per 200 µl of cell lysate (total volume 1 ml) and centrifuged at 14.000 g, for 30 min. The bottom phase (700 µl) was collected and 150 µl of 50% TritonX was added per sample, then samples were SpeedVac dried by a vacuum concentrator, overnight. Cell lipid extracts were resuspended in 700 µl dH₂O, and 600 µl were used for scintillation counting.

3.2.2.3. Fatty acid storage

Neutral lipid stain by LD540 or LipidTOX green, analysed by fluorescence microscopy and flow cytometry

For neutral lipid quantification by LD540 or LipidTOX green fluorescence microscopy, 5.5x10⁴ cells were seeded per well of a 4-well chamber slide in 500 µl of assay medium. After attachment, the cells were left untreated, were treated with FAs, palmitic acid (33 µM) and oleic acid (66 µM) alone, and in combination with inflammatory mediators, including (BS1 (0.5 µg/ml), rhLIGHT (500 ng/ml), rhIL-17A (50 ng/ml), rhTNF-α (50 ng/ml), IL-4 (50 ng/ml), IFN- (3 ng/ml, specific activity: 3.3 x 10⁵ units/mg) and the combination of all cytokines with the same final concentrations, for 24 h in the incubator. In addition to investigate the influence of NF-κB signalling, apoptosis, or ROS production, on neutral lipid accumulation cells were simultaneously stimulated with, the IKKβ inhibitor TPCA-1 (25 nM), with the Pan caspase inhibitor Z-VAD-FMK (100 µM), and the anti ROS agent N-acetyl-cystein (5 mM). After incubation, the assay medium was removed, and cells were washed with PBS and were fixed for 15-20 min in 4% paraformaldehyde. After washing twice with PBS cells were stained with 1µg/ml Hoechst (for nuclear staining) and 0.1 µg/ml with LD540¹⁹³ or LipidTOX green with a final concentration of 1:1000 in PBS, for 30 min. in the dark. After washing twice with PBS, 1 drop of mounting medium per well was added and samples were covered with cover slides. After drying, they were immediately analysed by fluorescence microscopy and analysed by ImageJ. Pictures were taken with an inverted Zeiss Cell Observer microscope.

For neutral lipid quantification by flow cytometry, cells were stained alive in the incubator. Therefore, after 24 h of cell treatment (see above), the assay medium was removed and staining solution was added which contained 0.1 µg/ml LD540 or LipidTOX green with a final concentration of 1:1000 in assay medium, for 30 min. in the incubator. Then the medium was removed and after washing, cells were trypsinized and centrifuged at 300 g for 3 min. for pelleting. Cell pellets were washed once with PBS and then 300 µl of PBS plus 3% FCS was added per sample and cells were immediately analysed by flow cytometry by using BD FACSFortessa, Sony spectral analyser, SP6800, and data were analysed using FlowJo.

3.2.2.4. Fatty acid oxidation (FAO)

Radioactive (¹⁴C) labelled palmitic acid oxidation to CO₂

FAO was determined as previously described in ¹⁹⁴. In brief, 1.2x10⁵ cells were seeded per well of a 12-well plate in 1 ml assay medium. After attachment, the cells were left untreated (as blank control), were treated with FAs, palmitic acid (33 µM) and oleic acid (66 µM) alone, and in combination with inflammatory mediators, including BS1 (0.5 µg/ml), rhLIGHT (500 ng/ml), rhIL-17A (50 ng/ml), and rhTNF-α (50 ng/ml), for 21 h in the incubator. Then the assay medium was removed and the tracer medium was added which contained FAs, palmitic acid (33 µM) and oleic acid (66 µM), and 1 µl/ml of ¹⁴C palmitic acid (with an activity of 0.5 mCi/ml) for 3 h in the incubator. 1.5 ml Eppendorf tubes were prepared for ¹⁴C-CO₂ trapping, therefore round discs of Whatman filter paper were cut and the paper was stuffed inside the cap of an Eppendorf tube. After incubation, cell supernatant was collected (900 µl) and transferred into 1.5 ml Eppendorf tubes. In addition, cells were washed with PBS and lysed by RIPA Buffer for normalization by BCA protein assay, according to manufacturer's protocol. 200 µl of 1 M perchloric acid was added per ¹⁴C-CO₂ trapping Eppendorf tube and 20 µl of 1 M NaOH was added on the paper disc in the cap. Then the cell supernatant was added, and the tube was immediately closed. Samples were incubated at room temperature (RT) for 1 h, then the ¹⁴C-CO₂ trapped paper discs were used for scintillation counting.

3.2.2.5. Fatty acid export

TG determination in cell supernatant

To quantify FA export in form of TGs a TG determination Kit was performed according to the manufacturer's protocol. In brief, 1.2x10⁵ cells were seeded per well of a 12-well plate in 1 ml assay medium. After attachment, the cells were left untreated, were treated with FAs, palmitic acid (33 µM) and oleic acid (66 µM) alone, and in combination with inflammatory mediators, including BS1 (0.5 µg/ml), rhLIGHT (500 ng/ml), rhIL-17A (50 ng/ml), and rhTNF-α (50 ng/ml),

for 24 h in the incubator. Then the assay medium was removed, and cells were washed twice with PBS. Cells were lysed with RIPA buffer, 300 µl per well. A 96-well plate (flat bottom) was used and 100 µl of cell lysate was added per well. Then a solution was added that contained a mixture of Free glycerol (FG) and triglycerides (TG) in a ratio 4:1. As blank control 100 µl RIPA buffer was used, and for TG quantification a glycerol standard was used, therefore 5 µl of glycerol standard (2.5 mg/ml) plus 95 µl H₂O was added per well. After 15 min. at 37°C the colorimetric reaction was measured with a plate reader.

3.2.3. Cell preparation for liquid chromatography mass spectrometry (LC-MS)

For lipidomic analysis, 1×10^6 cells were seeded per 60 mm dish in 2.5 ml of assay medium. After attachment, the cells were left untreated, were treated with rhTNF- α (50 ng/ml) alone, were treated with FAs, palmitic acid (33 µM) and oleic acid (66 µM) alone, and in combination with inflammatory mediators including BS1 (0.5 µl/ml), rhLIGHT (500 ng/ml), rhIL-17A (50 ng/ml) and rhTNF- α (50 ng/ml), for 24 h in the incubator. For lipid extraction, cells were put on ice and were washed one time with ice cold PBS, then 200 µl of ice-cold methanol was added per plate, and cells were scraped and transferred into 1.5 ml Eppendorf tubes. A blank control sample was prepared by performing same procedures without biological sample. The samples were vortexed for protein precipitation and 500 µl of chloroform was added. After vortexing, samples were kept on ice for 10 min., then 200 µl of dH₂O was added for phase separation. Samples were again vortexed and kept on ice for 10 min. and were then centrifuged at 600 rpm for 5 min. The bottom layer (300 µl of chloroform layer) was carefully transferred into a new tube and samples were SpeedVac dried by a vacuum concentrator, overnight. Dried samples were shipped on dry ice for analysis to the EMBL Metabolomics Core Facility (Heidelberg, Germany).

3.2.4. Fluorescence stainings

3.2.4.1. Immunofluorescence staining

For immunofluorescence staining, 5.5×10^4 cells were seeded per well of a 4-well chamber slide in 500 µl of assay medium. After attachment, the cells were left untreated, were treated with FAs, palmitic acid (33 µM) and oleic acid (66 µM) alone, and in combination with all inflammatory mediators including BS1 (0.5 µg/ml), rhLIGHT (500 ng/ml), rhIL-17A (50 ng/ml), and rhTNF- α (50 ng/ml), for 24 h in the incubator. Then the assay medium was removed, and the cells were washed with PBS and were fixed for 15-20 min in 4% paraformaldehyde. Samples were washed with PBS and the primary antibody (see Table 1. Immunofluorescence

antibodies), diluted in PBS, 1% BSA was added either for 1 h at RT, or at 4°C overnight. Then the cells were washed three times with PBS and secondary antibody, diluted in PBS, 1% BSA (see Table 1. secondary antibodies) for 30 min. at RT. After washing with PBS, Hoechst staining solution (1 µg/ml Hoechst in PBS) was added for 15 min. at RT. Samples were washed once with PBS and 1 drop mounting medium was added per well and slides were covered with cover slides. After drying, samples were immediately analysed by fluorescence microscopy and analysed by ImageJ. Pictures were taken with an inverted Zeiss Cell Observer microscope.

3.2.4.2. Mitochondrial staining by MitoTrackerRed

To visualize mitochondria, cells were stained with Mitotracker red staining according to the manufacturer's manual. Briefly, 5.5×10^4 cells were seeded per well of a 4-well chamber slide in 500 µl of assay medium. After attachment, the cells were left untreated, were treated with FAs, palmitic acid (33 µM) and oleic acid (66µ M) alone, and in combination with all inflammatory mediators, including BS1 (0.5 µg/ml), rhLIGHT (500 ng/ml), rhIL-17A (50 ng/ml), and rhTNF-α (50 ng/ml), for 24 h in the incubator. The assay medium was removed and the Mitotracker red staining solution, containing 200 nM MitoTrackerRed in assay media, was added for 30 min. in the incubator. After incubation cells were fixed in ice-cold methanol for 15 min. at -20°C. Then the cells were washed with PBS and mitochondrial staining was analysed by fluorescence microscopy. Pictures were taken with an inverted Zeiss Cell Observer microscope.

3.2.4.3. JC-1 staining to monitor mitochondrial membrane potential

To determine mitochondrial membrane potential cells were stained with JC-1 dye according to manufacturer's protocol. In brief, 1.2×10^5 cells were seeded per well of a 12-well plate in 1 ml assay medium. After attachment, cells were left untreated, were treated with inflammatory mediators, including BS1 (0.5 µg/ml), rhLIGHT (500 ng/ml), rhIL-17A (50 ng/ml), rhTNF-α (50 ng/ml), and the combination of all cytokines alone, were treated with FAs, palmitic acid (33 µM) and oleic acid (66 µM) alone, and in combination with inflammatory mediators, including BS1 (0.5 µg/ml), rhLIGHT (500 ng/ml), rhIL-17A (50 ng/ml), rhTNF-α (50 ng/ml), IL-4 (50 ng/ml) and the combination of all cytokines with the same final concentrations, for 24h in the incubator. In addition, to investigate the influence of NF-κB signalling on mitochondrial polarization, cells were simultaneously stimulated with, the IKKβ inhibitor TPCA-1 (25 nM). After incubation, the assay medium was removed and JC-1 staining solution (10 µl JC-1 in 1 ml Assay Medium, final concentration 2 µM) was added and cells were incubated for 30 min. in the incubator. As

positive control for mitochondrial depolarization 3 μ l of the mitochondrial uncoupler CCCP was added. After staining, cells were washed with PBS, were trypsinized, and centrifuged for 3 min. at 300 g for pelleting. Cell pellets were resuspended in PBS plus 3% FCS and analysed by flow cytometry by using BD FACSFortessa, Sony spectral analyser, SP6800, and data were analysed using FlowJo. The ratio of the JC-1 red to JC-1 green mean area was determined.

3.2.4.4. Mitochondrial superoxide production determination by MitoSOXRed

Mitochondrial superoxide production was visualized by MitoSOXRed staining which was performed according to manufacturer's manual. In brief, 5.5×10^4 cells were seeded per well of a 4-well chamber slide in 500 μ l of assay medium. After attachment, cells were left untreated, were treated with FAs, palmitic acid (33 μ M) and oleic acid (66 μ M) alone, and together with the cytokine combination including BS1 (0.5 μ g/ml), rhLIGHT (500 ng/ml), rhIL-17A (50 ng/ml), and rhTNF- α (50 ng/ml), with and without the IKK β inhibitor TPCA1 (25 nM), for 24 h in the incubator. The assay medium was removed and MitoSOXRed staining solution was added (containing 5 μ M MitoSOX reagent in assay medium) for 10 min. in the incubator. Then cells were washed with assay medium and were imaged alive by fluorescence microscopy. Pictures were taken with an inverted Zeiss Cell Observer microscope.

3.2.4.5. *Immunofluorescence assay for the detection of 5-bromo-2'-deoxy-uridine (BrdU) incorporation into DNA*

To quantify cell proliferation the 5-Bromo-2'-deoxy-uridine Labeling and Detection Kit I was used according to manufacturer's manual. Briefly, for quantification by fluorescence microscopy, 5.5×10^4 cells were seeded per well of a 4-well chamber slide in 500 μ l of assay medium. For analysis by flow cytometry, 1.2×10^5 cells were seeded per well of a 12-well plate in 1 ml assay medium. After attachment, cells were left untreated, were treated with FAs, palmitic acid (33 μ M) and oleic acid (66 μ M) alone, and in combination with all inflammatory mediators, including BS1 (0.5 μ g/ml), rhLIGHT (500 ng/ml), rhIL-17A (50 ng/ml), rhTNF- α (50 ng/ml), for 24 h in the incubator. To investigate the effect of NF- κ B signalling on cell proliferation FA plus IL-17A stimulated cells were additionally treated with the IKK β inhibitor TPCA-1 (25 nM). After incubation, the assay medium was removed and BrdU labelling medium (containing BrdU which can be incorporated into DNA in place of thymidine in proliferating cells) was added and incubated for 1 h in the incubator. For analysis by flow cytometry, cells were washed, trypsinized and pelleted, and all following procedures were performed in 1 ml Eppendorf tubes. The BrdU labelling medium was removed and samples were washed three times with washing buffer, then samples were fixed in ice cold Ethanol fixative (containing 50

mM glycine solution in dH₂O and 70% absolute EtOH, pH 2.0.) for 20 min. at -20°C. Samples were washed again three times with washing buffer and were covered with Anti-BrdU working solution (containing a monoclonal antibody against BrdU) and incubated for 30 min. at 37°C. After washing three times with washing buffer the samples were covered with anti-mouse-Ig-fluorescein working solution (containing fluorochrome-conjugated second antibody) for 30 min. at 37°C. Then samples were washed three times with washing buffer and for evaluation by fluorescence microscope mounting medium was added and samples were covered with cover slides. Pictures were taken with an inverted Zeiss Cell Observer microscope. For analysis by flow cytometry cells were resuspended in PBS plus 3% FCS and were analysed by using BD FACSFortessa, Sony spectral analyser, SP6800, and data were analysed using FlowJo.

3.2.4.6. Determination of apoptosis by Annexin V staining

To quantify cell apoptosis the Annexin V Kit was performed according to manufacturer's manual. In brief, 1.2x10⁵ cells were seeded per well of a 12-well plate in 1 ml assay medium. After attachment, cells were left untreated, were treated with FAs, palmitic acid (33 µM) and oleic acid (66 µM) alone, and in combination with all inflammatory mediators, including BS1 (0.5 µg/ml), rhLIGHT (500 ng/ml), rhIL-17A (50 ng/ml), rhTNF-α (50 ng/ml), in presence and absence of the pan-caspase inhibitor Z-VAD-FMK (100 µM) for 24 h in the incubator. After treatment cells were washed with PBS, were detached by Versene and were pelleted by centrifugation at 300 g for 3 min. Then cells were transferred into 2 ml Eppendorf tubes and were stained in 100 µl of 1x Binding Buffer with 5 µl of PE Annexin and 5 µl of 7-AAD. After mixing, the cells were incubated for 15 min. at in the dark. After incubation, 200 µl of 1x Binding Buffer was added per sample and cells were immediately analysed by flow cytometry, by using BD FACSFortessa, Sony spectral analyser, SP6800, and data were analysed using FlowJo.

3.2.5. siRNA mediated knock down

For si-RNA mediated knock down, 1.2x10⁵ cells were seeded per well of a 12-well plate in 1 ml assay medium. After attachment, the medium was removed and culture medium without antibiotics was added (800 µl per well). Then 5 µl of siRNA (see in Table 1. in siRNA reagents and siRNAs) was added to 95 µl of OptiMEM per transfection, after mixing the solution was incubated for 5 min. at RT. During incubation, 3 µl of Dharmafect and 97 µl of OptiMEM were mixed per sample and incubated for 5 min. at RT. Then 100 µl of the si-RNA OptiMEM solution was added to the Dharmafect OptiMEM solution and were incubated for 20 min. at RT. Then 200 µl of the si-RNA containing solution was added per well, with a final siRNA concentration of 25 nM. After 1 day the medium was changed to culture medium. After 2 days cells were left

untreated, were treated with all inflammatory mediators, including BS1 (0.5 µg/ml), rhLIGHT (500 ng/ml), rhIL-17A (50 ng/ml), rhTNF-α (50 ng/ml) alone, were treated with FAs, palmitic acid (33 µM) and oleic acid (66 µM) alone, and in combination with all inflammatory mediators, including BS1 (0.5 µg/ml), rhLIGHT (500 ng/ml), rhIL-17A (50 ng/ml), for 24 h in the incubator. Then cells were stained with LipidTOX green and neutral lipid accumulation was analysed by flow cytometry (see above).

3.2.6. Immunoblot analysis

Buffers and Solutions

<u>4x Sample buffer</u>	<u>10x SDS running buffer</u>	<u>Semidry transfer buffer</u>
-222.24 mM Tris (pH 6.8)	-30.3 g Tris	-48 mM Tris
-3.52% SDS	-144g Glycine	-39 mM Glycine
-35.2% Glycerol	-10 g SDS	-1.3 mM SDS
-0.016% Bromophenol blue	- ad. 1 L ddH2O	-20 % Methanol
-10% β-mercaptoethanol		-pH 9-9.4

<u>Wash buffer</u>	<u>TBS-T</u>
-1xPBS	-10 mM TRIS
-0.1% Tween20	-0.1% Tween20
	-150 mM NaCl

For immunoblot analysis dHepaRG cells were seeded into 6-well plates in 2 ml assay medium. After attachment, the cells were left untreated, or were treated with FAs, palmitic acid (33 µM) and oleic acid (66 µM) alone, and in combination with inflammatory mediators including BS1 (0.5 µg/ml), rhLIGHT (500 ng/ml), rhIL-17A (50 ng/ml), and rhTNF-α (50 ng/ml), for 24 h in the incubator. For protein extraction cells were put on ice, and were washed with ice cold PBS, for cell lysis 300 µl RIPA buffer supplemented, according to the manufacturer's manual with complete protease inhibitor cocktail and phosphatase inhibitor was added and cells were scraped and transferred into 1.5 ml Eppendorf tubes. Cell lysates were either stored at -80°C or protein concentration was determined by BCA assay, according to the manufacturer's manual. Briefly, 5 µl of cell lysate was added per well of a 96-well plate, flat bottom. As blank control 5 µl of RIPA Buffer was used, and 5 µl of a BSA serial dilution was used for the generation of a standard curve. Copper(II)sulphate and BCA were mixed in a ratio 1:50, and 195 µl of this solution was added per sample. After 5-10min. the protein concentration was measured by a plate reader.

Semidry western blot

For immunoblot analysis 20 µg of protein were diluted in 4X sample buffer, dH₂O and β-Mercaptoethanol. For protein denaturation, samples were boiled at 95°C in the thermomixer for 5 min. Precast gels from BioRad were used and the running chamber was assembled and was filled up with 1x SDS running buffer in the inner and the outer chamber. Then 4 µl of the BioRad Protein marker and 15 µl of the protein samples were loaded per lane. The gels run at 90 V for 60 min. 20% methanol was added to the 1X transfer buffer, and the PDVF membrane was activated for at least 1 min. in 100% methanol. Then the gels were assembled and transferred into a transfer chamber and set at 150 mA for 1 h.

After protein transfer, membranes were blocked in TBS-T plus 5% BSA, for 1 h. After blocking the primary antibody (see in Table 1. Western blot antibodies) was added in TBS-T plus 5% BSA and incubated overnight, at 4°C. On the next day membranes were washed three times in washing buffer for each 10 min. Then the secondary antibody (see in Table 1. Secondary antibodies) was added diluted in TBS-T, and membranes were incubated for 1 h. Then the membranes were washed with TBS-T three times for 10 min. For development, the remaining liquid was removed and ECL substrate was mixed 1:1 and added on the membranes, which were then covered in clingfilm and analyzed by a ChemiDoc imaging system.

3.2.7. RNA isolation for RNA sequencing analysis and reverse transcription into cDNA for RT-PCR

For gene expression analysis, 1.2×10^5 cells were seeded per well of a 12-well plate in 1 ml assay medium. After attachment, cells were left untreated, were treated with inflammatory mediators alone, including BS1 (0.5 µg/ml), rhLIGHT (500 ng/ml), rhIL-17A (50 ng/ml), rhTNF-α (50 ng/ml), and the combination of all cytokines with the same final concentrations, were treated with FAs, palmitic acid (33 µM) and oleic acid (66 µM) alone, and in combination with inflammatory mediators, including (BS1(0.5 µg/ml), rhLIGHT (500 ng/ml), rhIL-17A (50 ng/ml), rhTNF-α (50 ng/ml), and the combination of all cytokines with the same final concentrations, for 24 h in the incubator. To address the effect of NF-κB signalling on cell proliferation FA plus IL-17A stimulated cells were additionally treated with the IKKβ inhibitor TPCA-1 (25 nM). After incubation, the assay medium was removed and cells were washed with PBS, and 300 µl of lysis, RLT Buffer (from RNeasy Kit) was added. Samples were either stored at -80°C or RNA was extracted according to manufacturer's protocol.

In brief, cell lysates were put on ice for 2 min. and were then transferred onto a Qiashreder spin column, which was placed in a 2 ml collection tube, and centrifuged for 2 min, at 14.000 g. 300 µl of 70% EtOH were then added per homogenate into the collection tube and

transferred to a RNeasy Spin Column, which was placed in a 2 ml collection. After centrifugation for 2 min., at 14.000 g, the flow through was discarded and 300 µl of RW1 buffer was added onto the membrane in the RNeasy Spin Column. After centrifugation for 2 min. at 14.000 g, the flow through was discarded and 500 µl of RPE buffer was added, and samples were again centrifuged for 2 min. at 14.000 g, and the flow through was discarded. The last step was repeated once, and the RNeasy Spin Columns were placed into new collection tubes, and for drying the samples they were centrifuged for 2 min, at 14.000 g, to remove any left liquids. The dried RNeasy Spin Columns were then placed into 1.5 ml collection tubes and 20 µl of RNase-free water was added. RNA concentration and quality were determined by Nanodrop analyzer. Isolated RNA was either stored at -80°C or was reverse transcribed for cDNA synthesis.

For RNA sequencing 25 ng RNA (per sample) was delivered to Klinikum rechts der Isar, where RNA sequencing analysis was performed by Dr. Rupert Öllinger, from AG Prof. Roland Rad. For cDNA synthesis the Quantitect Reverse Transcription Kit was used according to the manufacturer's protocol. In brief, all reagents were thawed, and isolated RNA was kept on ice. 12 µl of 500 ng RNA, diluted in RNase-free dH₂O, was used for reverse transcription. To remove genomic DNA, a DNA wipe out step was performed, by adding 2 µl DNA wipe out solution per sample, which were then put on 42°C for 2 min. A master mix (MM) was prepared containing, 4 µl of reverse transcriptase (RT) buffer, 1 µl primers, and 1 µl of RT, thus 6 µl of the MM were added per sample, which were then incubated at 42°C for 20 min for reverse transcription. The reaction was stopped by incubation at 95°C for 3 min. and 180 µl RNase-free H₂O was added and cDNA was stored at -20°C (for long term storage at -80°C).

Real-Time (RT) PCR was performed in triplicates in a 384-well plate using Fast Start SYBR Green Master Rox with custom made primers (see in Table 1. Primers). In brief, a MM was prepared containing, 6 µl of SYBR Mix, 0.06 µl forward and 0.06 µl reverse primer, and 0.88 µl nuclease-free H₂O, then 7 µl of this MM was added per well of a plate and 5 µl of synthesised cDNA was added.

3.2.8. Cell preparation for Proteomics and Phosphoproteomics

For proteomics and phosphoproteomics dHepaRG cells were directly treated in T 75 where they were differentiated. The culture medium was removed and cells were left untreated, were treated with all inflammatory mediators alone, including (BS1(0.5 µg/ml), rhLIGHT (500 ng/ml), rhIL-17A (50 ng/ml) and rhTNF-α (50 ng/ml), were treated with FAs, palmitic acid (33 µM) and oleic acid (66 µM) alone, and in combination with all inflammatory mediators, including (BS1(0.5 µg/ml), rhLIGHT (500 ng/ml), rhIL-17A (50 ng/ml), rhTNF-α (50 ng/ml), for 24 h in the incubator. After incubation, the cells were put on ice, washed once with ice cold PBS, and were

scraped in PBS, transferred into 2 ml Eppendorf tubes, and centrifuged for 3 min. at 300 g. For cell lysis 350 μ l of RIPA Buffer (1 volume pellet: 5 volumes lysis buffer) containing phosphoSTOP phosphatase inhibitors (25X stock in dH₂O) and complete mini EDTA free phosphatase inhibitors (1 tab in 10ml d H₂O) was added. Cells were incubated on ice for 10 min. and were then sonicated with the standard program. After sonication samples were centrifuged for 1 h at 4°C at 14.000 g. The lysates were transferred into a new 1.5 ml Eppendorf tube and protein concentrations were determined by BCA Assay. Samples were delivered to the German Cancer Research Center (DKFZ) MS-Based Protein Analysis Core Facility (GPCF - Protein Analysis Unit (W120) where proteomics and phosphoproteomics analysis was performed.

3.2.9. Cell preparation for Proteome-based complex analysis

For thermal protein profiling dHepaRG cells were directly treated in T75 flasks, used for cell differentiation. At the day before the experiment the culture medium was removed and cells were left untreated, were treated with all inflammatory mediators alone including BS1 (0.5 μ g/ml), rhLIGHT (500 ng/ml), rhIL-17A (50 ng/ml) and rhTNF- α (50 ng/ml), were treated with FAs, palmitic acid (33 μ M) and oleic acid (66 μ M) alone, and in combination with all inflammatory mediators including BS1 (0.5 μ g/ml), rhLIGHT (500 ng/ml), rhIL-17A (50 ng/ml), rhTNF- α (50 ng/ml), for 24h in the incubator. After treatment, cells were delivered to EMBL and experimental procedures were performed by Isabel Becher from the group of Dr. Michael Savitski. Data were analysed by and Mathias Kalxdorf, PhD.

3.2.10. Statistical analysis

Statistical analysis was performed by one-way ANOVA. *: $p < 0.05$; **: $p < 0.01$; ***: $p < 0.001$; ****: $p < 0.001$; ns: not significant. For RNA sequencing based differential expression (DE) analysis, genes were ranked based on their log₂foldchange ($\log_2FC \geq 1$) and adjusted p value ($p_{adj} < 0.05$), and normalized counts of all genes, raw counts (count < 2), were used.

For DE analysis of proteomics, all proteins were ranked by log₂ fold change ($\log_2FC \geq 1$, and p value adjusted ($p_{adj} < 0.05$), for phospho proteomics, phosphoproteins were ranked by p value adjusted ($p_{adj} < 0.1$, with a $\log_2FC > 1$). Graphs were generated using GraphPad Prism8 Software.

4. Results

4.1. Fatty acid metabolism in hepatocytes

4.1.1. *In vitro* experimental set-up to study the influence of inflammatory mediators on hepatic fatty acid metabolism

I developed an *in vitro* NASH model to investigate molecular mechanisms underlying the transition from simple steatosis (NAFLD) to steatohepatitis (NASH). Mouse and human hepatocytes were used to mimic different stages during NAFLD to NASH transition (**Figure 9**). Hepatocytes were either untreated (normal hepatocytes), stimulated with FAs alone (steatotic hepatocytes), and in combination with inflammatory mediators (changed hepatocytes), known to contribute to NASH pathology including LIGHT and IL-17A^{139,144}.

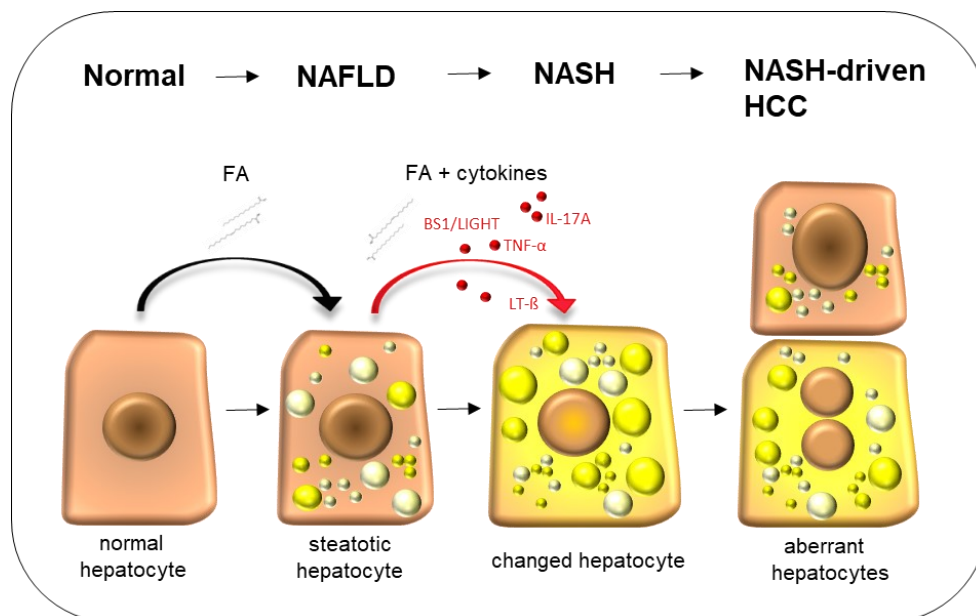


Figure 9: Illustration of the *in vitro* experimental set-up to mimic NAFLD to NASH development in hepatocytes.

FAs induce a steatotic phenotype (LD accumulation, yellow circles) in hepatocytes, to recapitulate NAFLD. FAs together with pro-inflammatory cytokines trigger metabolic changes in hepatocytes and mimic NASH development. NASH can progress towards NASH-derived HCC. As *in vitro* experimental set-up, hepatocytes, dHepaRG cells or primary mouse hepatocytes were, untreated (normal), stimulated with FAs, palmitic and oleic acid, alone, and in combination with inflammatory mediators, LT&R agonist BS1, LIGHT, IL-17A, TNF- α , and a combination of all listed cytokines (Cytokine Combination), (FA + BS1, FA+ LIGHT, FA + IL-17A, FA + TNF- α , FA + Cytokine Combination) for different time points.

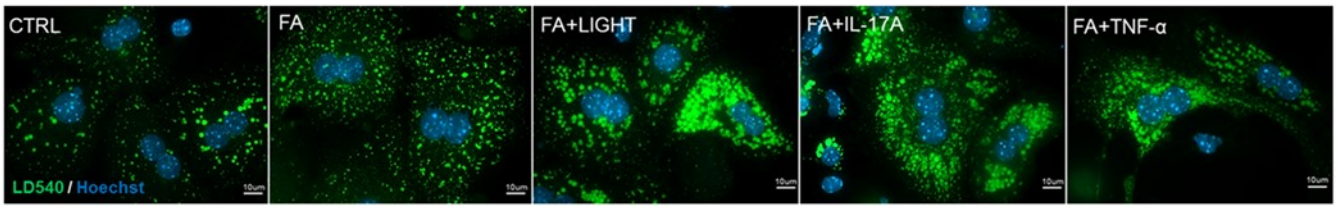
4.1.2. Fatty acid storage into neutral lipids is intensified by NASH-derived inflammatory cytokines

Primary mouse hepatocytes were exposed to FAs alone and in combination with pro-inflammatory cytokines. Consistent with published data ¹⁴⁴, treatment with inflammatory cytokines increased lipid accumulation (**Figure 10A, B**), and promoted the development of macrovesicular steatosis, displayed by an increase of large (1-1.5 μ m) and very large (1.5-2 μ m) LDs (**Figure 10C**). This demonstrated that inflammatory cytokines not only influence LD number but also size in hepatocytes.

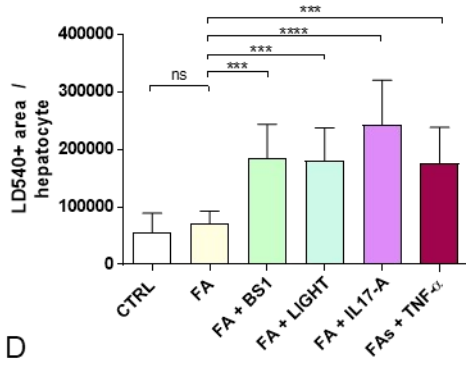
To investigate whether inflammation-induced increased lipid accumulation is a mechanism also affecting human hepatocytes, dHepaRG cells were exposed to FAs and inflammatory mediators. In line with the observations in primary mouse hepatocytes, human dHepaRG cells that were subjected to FAs in combination with inflammatory mediators displayed intensified LD accumulation when compared to FA treated cells (**Figure 10D, E**). The LD number and the LD size were increased in dHepaRG cells that were exposure to an inflammatory, lipid-rich microenvironment (**Figure 10F**). However, the macrovesicular phenotype in dHepaRG cells was less pronounced when compared to primary mouse hepatocytes (**Figure 10C, F**).

Treatment with a combination of all inflammatory mediators (BS1, LIGHT, IL-17A, TNF- α : Cytokine Combination), which more closely recapitulates the inflammatory microenvironment *in vivo*, most significantly increased neutral lipid storage in human hepatocytes (**Figure 10G**). In contrast, hepatocyte stimulation with IL-4 (promoting an anti-inflammatory immune response) or IFN- γ (associated with an anti-viral immune response) did not promote aberrant lipid storage (**Figure 10H, I**), showing that aberrant FA storage is induced by specific pro-inflammatory cytokines.

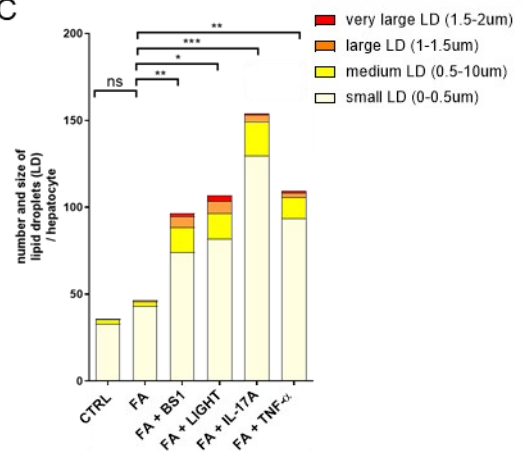
A



B



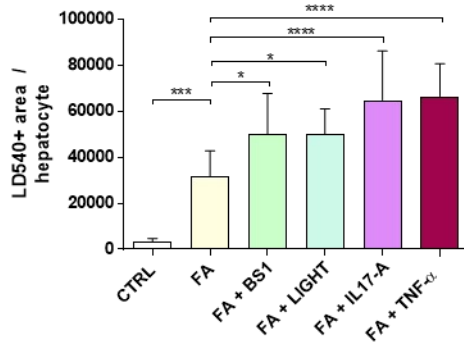
C



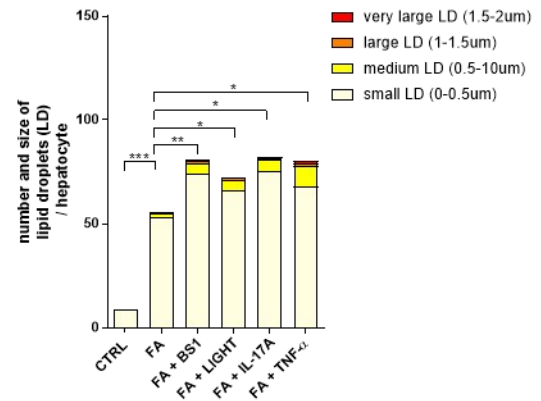
D



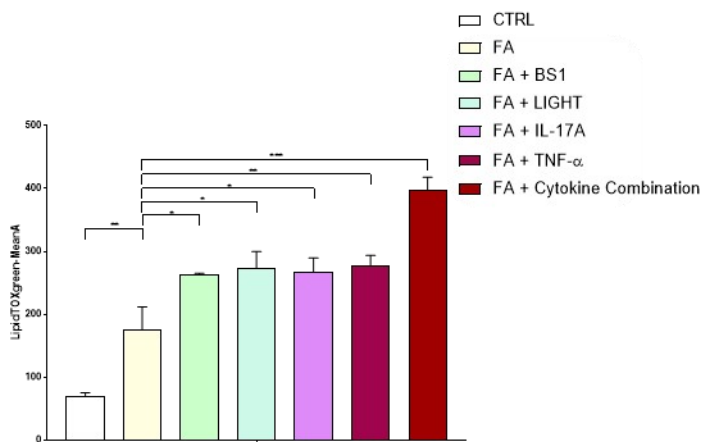
E



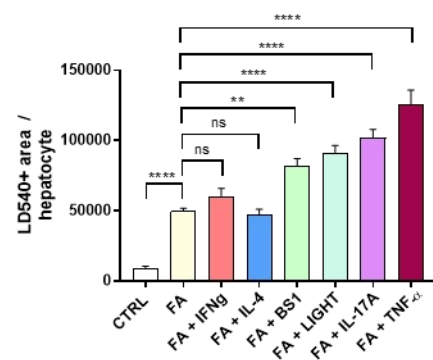
F



G



H



I

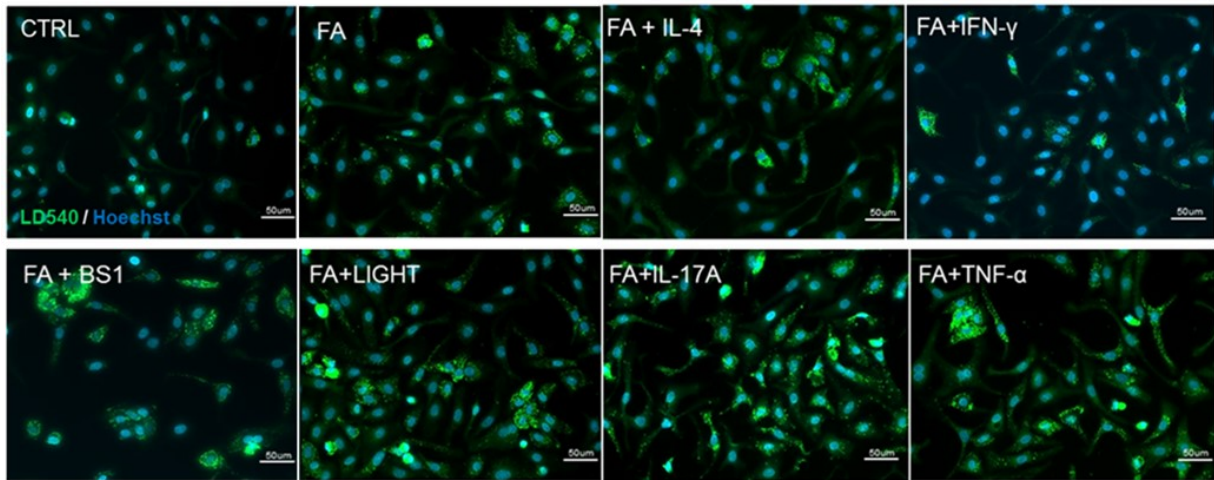


Figure 10: FA storage into neutral lipids in hepatocytes, determined by LD540 / Hoechst and LipidTOX green / Hoechst staining.

(A, B, C) Primary mouse hepatocytes and (D, E, F) dHepaRG cells were left untreated (CTRL), or were treated with FAs and with FAs together with cytokines (FA + LIGHT, FA + IL-17A, FA + TNF- α) for 24h. LDs were visualized by staining with LD540 (neutral lipid stain) and Hoechst (nuclear stain). (A, D) Representative fluorescent pictures. (B, E) Neutral lipid accumulation (pixel area (LD540+area) in microns per hepatocyte), and (C, F) number and size of LDs were analyzed by ImageJ, for (B, C) primary mouse hepatocytes and (E, F) dHepaRG cells. (G-I) dHepaRG cells were left untreated, or were treated with FA alone, and in combination with one or all cytokines (FA + BS1, FA + LIGHT, FA + IL-17A, FA + TNF- α , FA + Cytokine Combination, FA + IL-4, FA + IFN- γ) for 24h. LDs were visualized by staining with LD540 (neutral lipid stain) + Hoechst (nuclear stain). (G) Lipid accumulation of LipidTOX green stained dHepaRG was analyzed by flow cytometry. FA storage was quantified by determination of the LipidTOX green mean area. (H) Neutral lipid droplet accumulation (pixel area (LD540+area) in microns per hepatocyte), was analyzed by ImageJ. (I) Representative fluorescent pictures. Statistical analysis was performed by one-way ANOVA. *: $p < 0.05$; **: $p < 0.01$; ***: $p < 0.001$; ****: $p < 0.0001$; ns: not significant.

4.1.3. Inflammation promotes fatty acid storage in form of triglycerides

Inflammatory cytokines affect intracellular lipid levels, to investigate their influence on lipid composition, the lipidome of dHepaRG cells under normal conditions, in a lipid-rich and inflammatory microenvironment was determined by liquid chromatography mass spectrometry (LC-MS). Several lipid classes were detected including DGs, TG, PLs, and GPLs (**Figure 11A**). FAs were mainly incorporated into TGs, shown by high relative ion intensities (ion counts) when compared to other lipid classes (**Figure 11A, B**). FA storage into TGs was significantly increased by additional inflammatory cytokine stimulation (**Figure 11B, C, D**) including TG(16:0/18:0/18:1), TG(18:0/18:1/18:1), and TG(18:0/18:1/20:2). Only few DGs were identified by lipidomic analysis (**Figure 11A**). FA incorporation into the DGs, including DG (16:0/18:0/0:0) and DG (18:1/18:2/0:0), was significantly elevated by additional inflammatory mediator stimulation (**Figure 11E**). FA storage into PLs was markedly lower (**Figure 11A**),

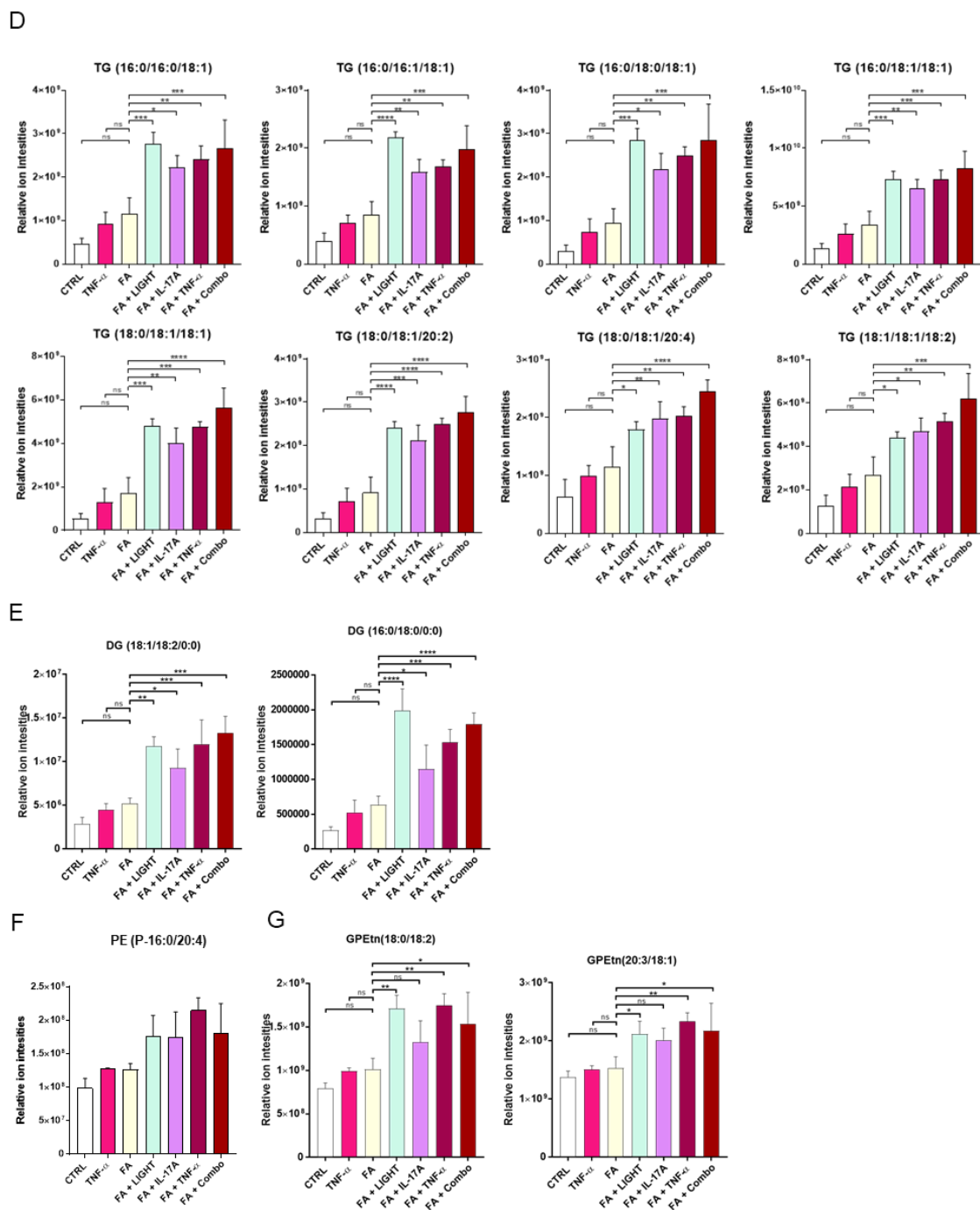


Figure 11: Liquid chromatography-mass spectrometry (LC-MS) analysis of dHepaRG cells under normal conditions, and in an inflammatory microenvironment in presence and absence of lipids.

Lipid composition of dHepaRG cells determined by LC-MS. Cell lipid extracts were analyzed from dHepaRGs that were either untreated, treated with the inflammatory cytokine TNF- α , stimulated with FAs alone and in combination with inflammatory cytokines (FA + BS1, FA + LIGHT, FA + IL-17A, FA + TNF- α , FA + Cytokine Combination) for 24h. (A) Heatmap displays relative ion intensities (ion counts) of detected lipids. (B, C) Relative ion intensities (ion counts) of TGs normalized to CTRL. (D-G) Relative ion intensities (ion counts) of detected lipids, TGs, DGs, PLs, and GPEtn. LC-MS data were not normalized to biological sample amounts. Lipid identification was done by accurate MS1 (< 5 ppm) and in-silico MS/MS match ($> 10\%$ score). Peak area was quantified for 4 replicates per condition. LipidBlast and Waters Library hits from Progenesis was used as Metabolite ID library. Xcalibur Quan

software was used for analysis. The instrument Vanquish-UHPLC_Q-exactive plus_2 was used. Statistical analysis was performed by one-way ANOVA. *: $p < 0.05$; **: $p < 0.01$; ***: $p < 0.001$; ****: $p < 0.0001$; ns: not significant.

4.1.4. Catabolic deficiencies induced by inflammatory mediators promote aberrant lipid storage

To discover metabolic mechanisms of intensified FA storage, upon inflammatory cytokine stimulation, their influence on essential lipid metabolic pathways was determined. Radioactive labelled lipids were used to trace FA- uptake, *de novo* synthesis, and oxidation. To address lipid export, TG concentration was determined in the cell supernatant.

Of note, FA uptake (**Figure 12A**) and FAO (**Figure 12B**) was markedly lower in cells that were exposed to inflammatory cytokines. In contrast, inflammatory mediators showed a negligible effect on FA *de novo* synthesis (**Figure 12C**) and FA / TG export (**Figure 12D**). The molecular regulation of increased FA storage and at the same time reduced FA uptake remained unclear. However, these results showed that downregulation of lipid catabolic processes such as FAO are likely the key mechanism that induces aberrant lipid accumulation in hepatocytes.

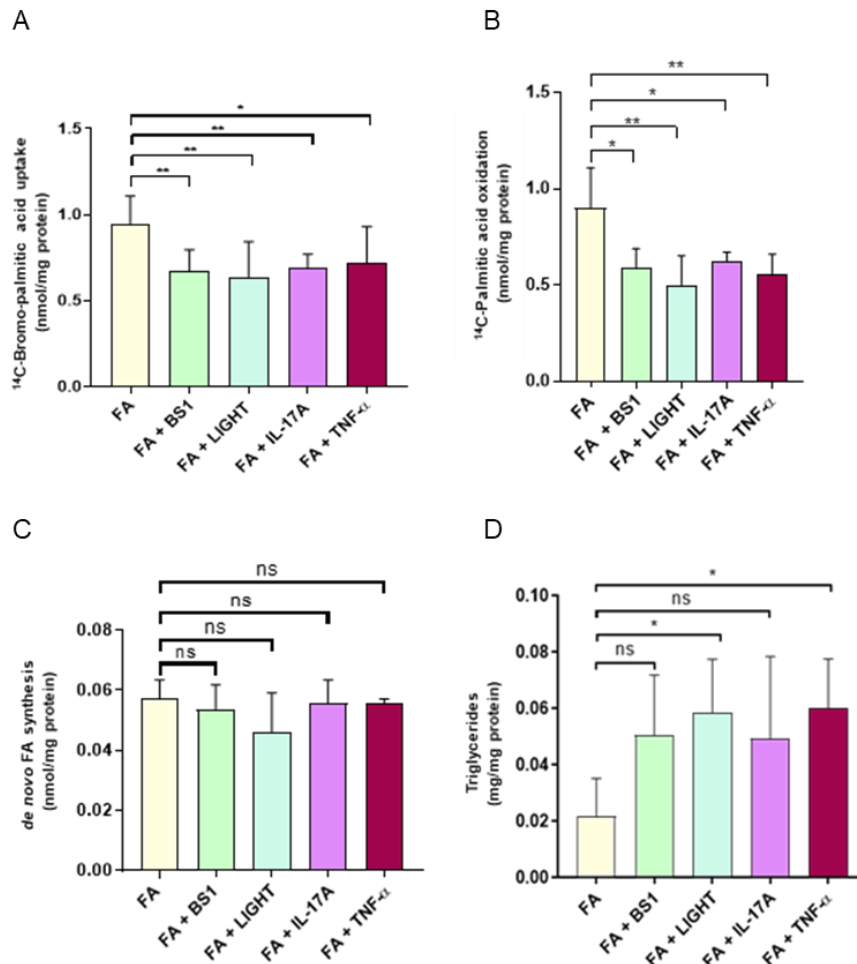


Figure 12: Radioactive labelling of lipids to trace FA- uptake, *de novo* synthesis and oxidation. Lipid export was quantified by secreted TGs.

dHepaRG cells, were treated with FAs alone and in combination with inflammatory cytokines (FA + BS1, FA + LIGHT, FA + IL-17A, FA + TNF- α) for 21h. Radioactive labelled lipids, (A) ^{14}C -Bromo-palmitic acid for FA uptake, (B) ^{14}C -Palmitic acid for FAO, and (C) ^{14}C -Acetic acid (AA) for FA *de novo* synthesis, were additionally added for

another 3h. Radioactivity was measured in (A, C) lipid extracts of cell lysates and (B) cell supernatant by scintillation counting. (D) TG concentration was determined in cell supernatant. All measurements were normalized to biological sample amount, based on the protein concentration, per mg protein. Statistical analysis was performed by one-way ANOVA. *: $p < 0.05$; **: $p < 0.01$; ***: $p < 0.001$; ****: $p < 0.0001$; ns: not significant.

4.1.5. Inflammation rapidly affects fatty acid metabolism in hepatocytes

To further address the influence of inflammatory mediators, known to affect extent and severity of NASH⁸⁸, on FA-uptake, storage, and oxidation over time, dHepaRG cells were subjected to fluorescence (BODIPY) and radioactive labelled (³H) palmitic acid for different time points. FA uptake by hepatocytes was already visible after 1h of treatment. Additional exposure to BS1, IL-17A, TNF- α , and the cytokine combination significantly reduced FA uptake (**Figure 13A**). After 3h of treatment, lipid concentrations were similar between all FA containing conditions without an additional effect induced by inflammatory cytokines. Exposure to inflammatory cytokines decreased FAO after 3h (**Figure 13B**), however not significantly. 24h of treatment with FAs intensified FA concentration which was further increased by simultaneous exposure to the cytokine combination (**Figure 13A**). FAO was significantly reduced after 24h of FA and cytokine stimulation (**Figure 13B**).

These results show that within 1h, a cytokine induced intrahepatic signalling affects / downregulates FA metabolism (FA uptake) in dHepaRG cells. 3h of exposure to lipids and inflammatory mediators showed similar lipid levels, likely due to deficiencies in catabolic processes, such as FAO, which is leading to lipid accumulation. After 24h of inflammatory cytokine treatment, FA storage was further elevated, indicating that intensified catabolic deficiencies over time induce exacerbated lipid accumulation in dHepaRG cells.

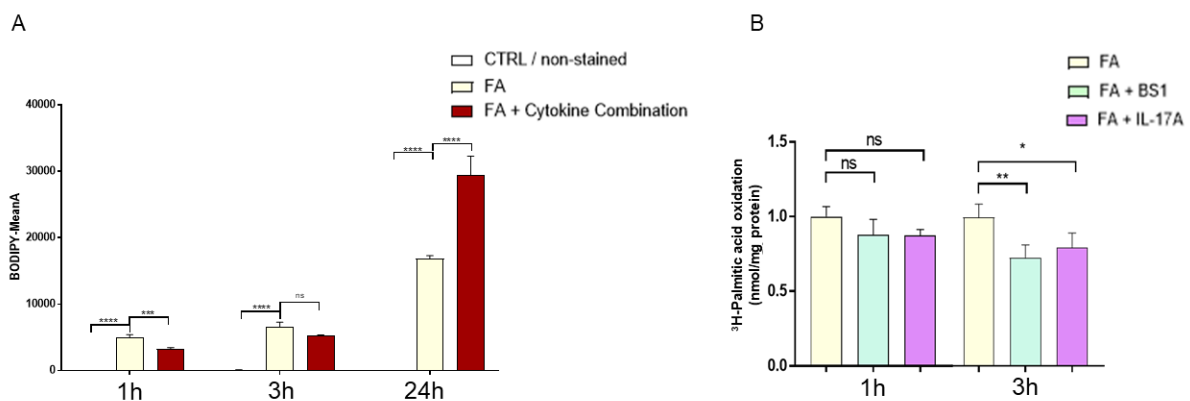


Figure 13: Fluorescence and radioactive labelling of lipids to study FA-uptake, storage, and oxidation in dHepaRG cells.

(A) dHepaRG cells were either untreated, stimulated with FAs plus C₁₆-BODIPY, and with FAs plus C₁₆-BODIPY, together with all cytokines (FA + Cytokine Combination) for 1h, 3h, and 24h. C₁₆-BODIPY uptake and storage was determined by flow cytometry analysis and quantified by BODIPY (fluorescence) mean area. (B) dHepaRG cells were treated with FAs, and with FAs in combination with inflammatory cytokines (FA + LIGHT, FA + IL-17A), and the radioactive labelled FA (³H-palmitic acid), either immediately, for 3h, or after 21h of pre-treatment, with FA, FA

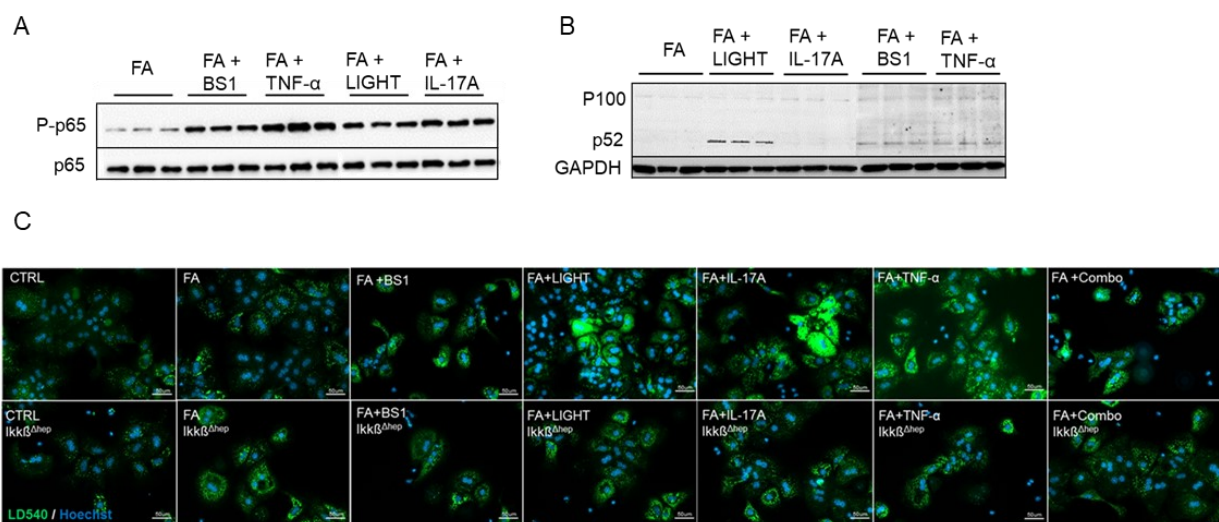
+ LIGHT, and FA + IL-17A), for 3h. Radioactivity was measured in cell supernatant, by scintillation counting. Statistical analysis was performed by one-way ANOVA. *: $p < 0.05$; **: $p < 0.01$; ***: $p < 0.001$; ****: $p < 0.0001$; ns: not significant.

4.1.6. NF- κ B-driven inflammation affects lipid metabolism in dHepaRG cells

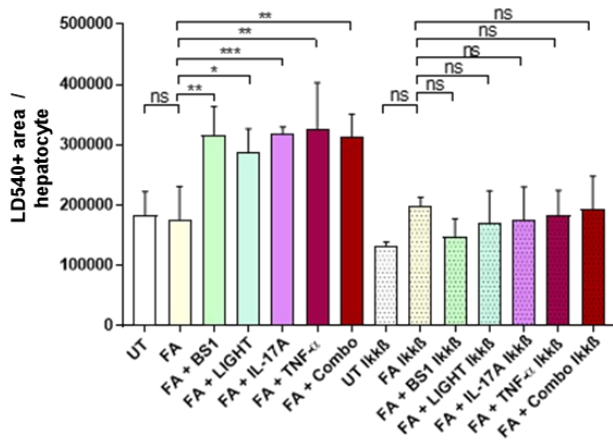
Intensified lipid accumulation was observed upon exposure to pro-inflammatory mediators. Thus, I studied the involved signalling pathways, and how they affect the lipid accumulation in hepatocytes. NASH-derived, pro-inflammatory cytokines, LIGHT, IL-17A, and TNF- α , can activate the canonical (**Figure 14A**) and BS1/LIGHT, TNF- α , the non-canonical NF- κ B signalling (**Figure 14B**). To examine whether increased lipid accumulation was triggered by canonical NF- κ B activation, primary mouse hepatocytes with a hepatocyte specific IKK β knock out (IKK β ^{Δhep}), CRISPR-Cas mediated IKK β knock out (IKK β KO) dHepaRG cells, and dHepRG cells treated with the selective inhibitor of human I κ B kinase-2 (IKK-2/ β), TPCA-1, were used.

In line with previous results, inflammatory cytokine stimulation intensified neutral lipid storage (**Figure 14C, D**). Loss of IKK β in primary mouse hepatocytes and in dHepaRG cells interfered with increased FA storage. Simultaneous exposure to TPCA-1 prevented elevated lipid accumulation induced by inflammatory cytokines (**Figure 14E, F, G**).

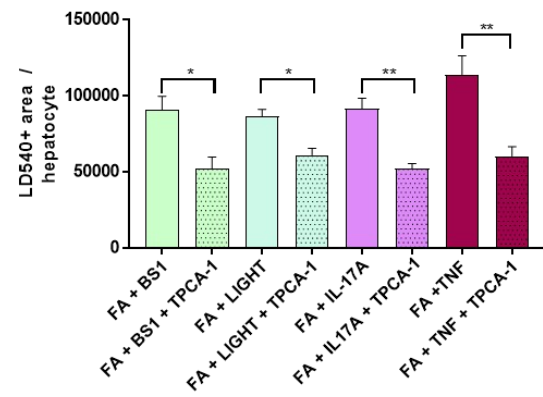
These results clearly demonstrate that canonical NF- κ B signalling affects lipid metabolism in hepatocytes by promoting FA storage into neutral lipids.



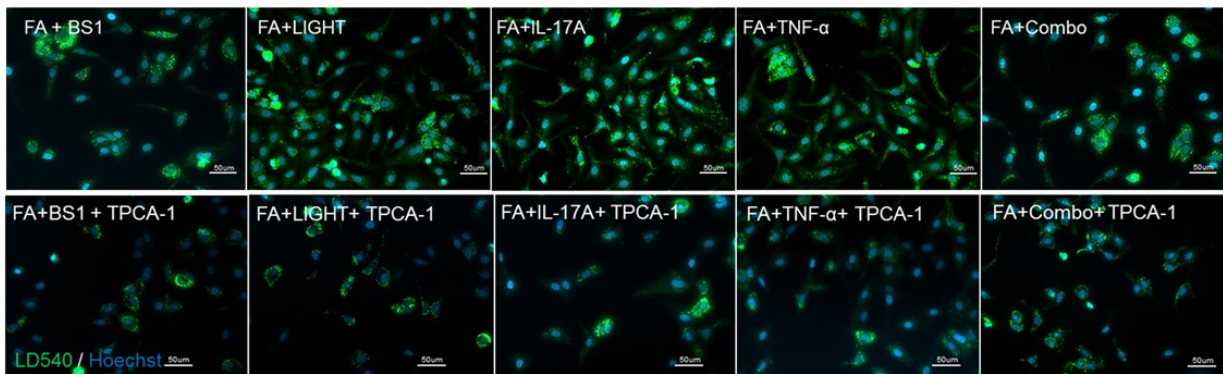
D



F



E



G

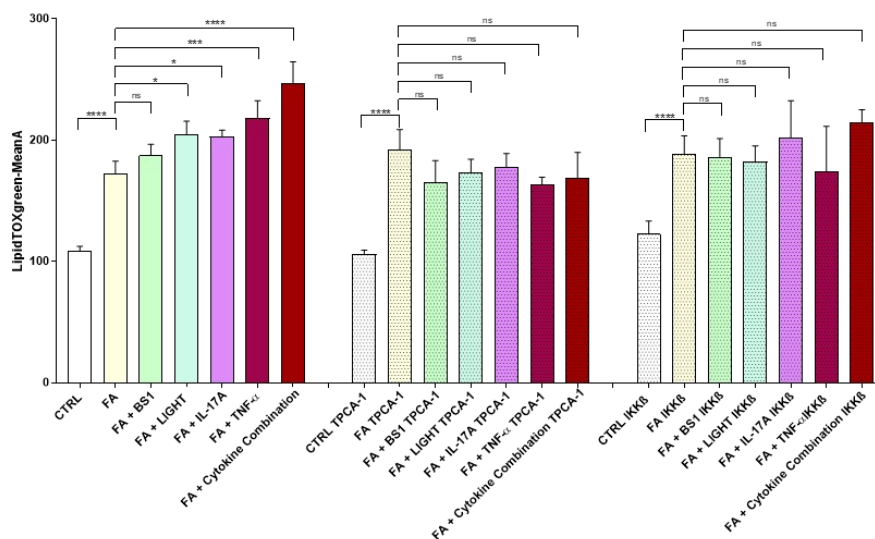


Figure 14: FA storage into neutral lipids in hepatocytes with deficiencies in canonical NF-κB signalling, determined by LD540 / Hoechst and LipidTOX green staining.

dHepaRG cells were either untreated, stimulated with FAs alone and in combination with inflammatory mediators (FA + BS1, FA + LIGHT, FA + TNF-α) for 24h. (A, B) Immunoblot analysis of dHepaRG cells, showing activation of

(A) canonical NF- κ B pathway, by phosphorylation of p65 (P-p65) and (B) non-canonical NF- κ B pathway, by degradation of p100 to p52.

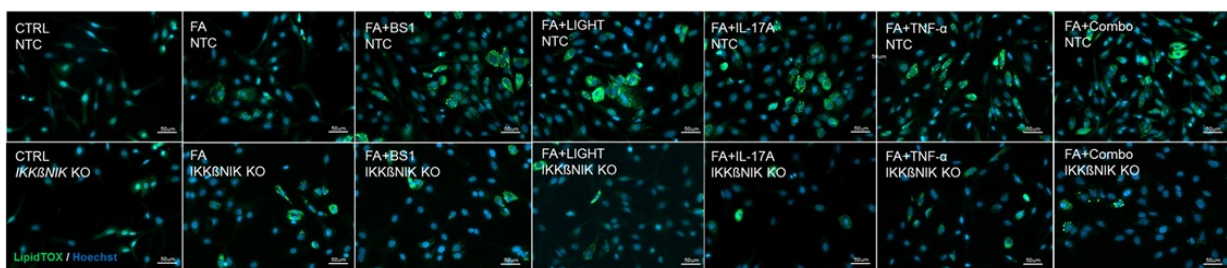
(C, D) Primary mouse hepatocytes, control cells, and cells with a hepatocyte specific IKK β KO (IKK $\beta^{\Delta\text{hep}}$) and (E, F) dHepaRG cells in presence and absence of the IKK β inhibitor, TPCA-1, were left untreated, or were treated with FAs alone and together with cytokines (FA + BS1, FA + LIGHT, FA + IL-17A, FA + TNF- α , FA + Cytokine Combination) for 24h. LDs were visualized by staining with LD540 (neutral lipid stain) + Hoechst (nuclear stain). (C, E) Representative fluorescent pictures. (D, F) Neutral lipid droplet accumulation (pixel area (LD540+area) in microns per hepatocyte), analyzed with Image J. (G) dHepaRG cells in presence and absence of TPCA-1, and CRISPR Cas-mediated IKK β knock out (IKK β KO) dHepaRG cells, were untreated, FA treated and stimulated with FAs plus cytokines (FA + BS1, FA + LIGHT, FA + IL-17A, FA + TNF- α , FA + Cytokine Combination) for 24h. (G) Neutral lipid accumulation, was determined by LipidTOX green staining. LipidTOX green mean area was quantified by flow cytometry analysis. Statistical analysis was performed by one-way ANOVA. *: p < 0.05; **: p < 0.01; ***: p < 0.001; ****: p < 0.0001; ns: not significant.

4.1.7. Activation of the canonical- and non-canonical NF- κ B pathway drives neutral lipid accumulation in hepatocytes

To further investigate the role of canonical and non-canonical NF- κ B signalling on lipid metabolic processes, human hepatocytes with deficiencies in NF- κ B signalling (CRISPR-Cas mediated IKK β KO (canonical) and NIK KO (non-canonical) dHepaRG cells) were generated and used thereafter.

FA treatment induced FA storage into neutral lipids, and additional inflammatory cytokine stimulation further intensified this effect in non-targeting control (NTC) dHepaRG (**Figure 15A, B, C**). Deficiencies in NF- κ B signalling induced by CRISPR-Cas mediated IKK β KO, NIK KO, and IKK β -NIK double KO inhibited intensified FA storage (**Figure 15A, B, C**), revealing that interference with inflammatory cytokine dependent activation of the canonical and non-canonical NF- κ B pathway prevents aberrant lipid accumulation in hepatocytes.

A



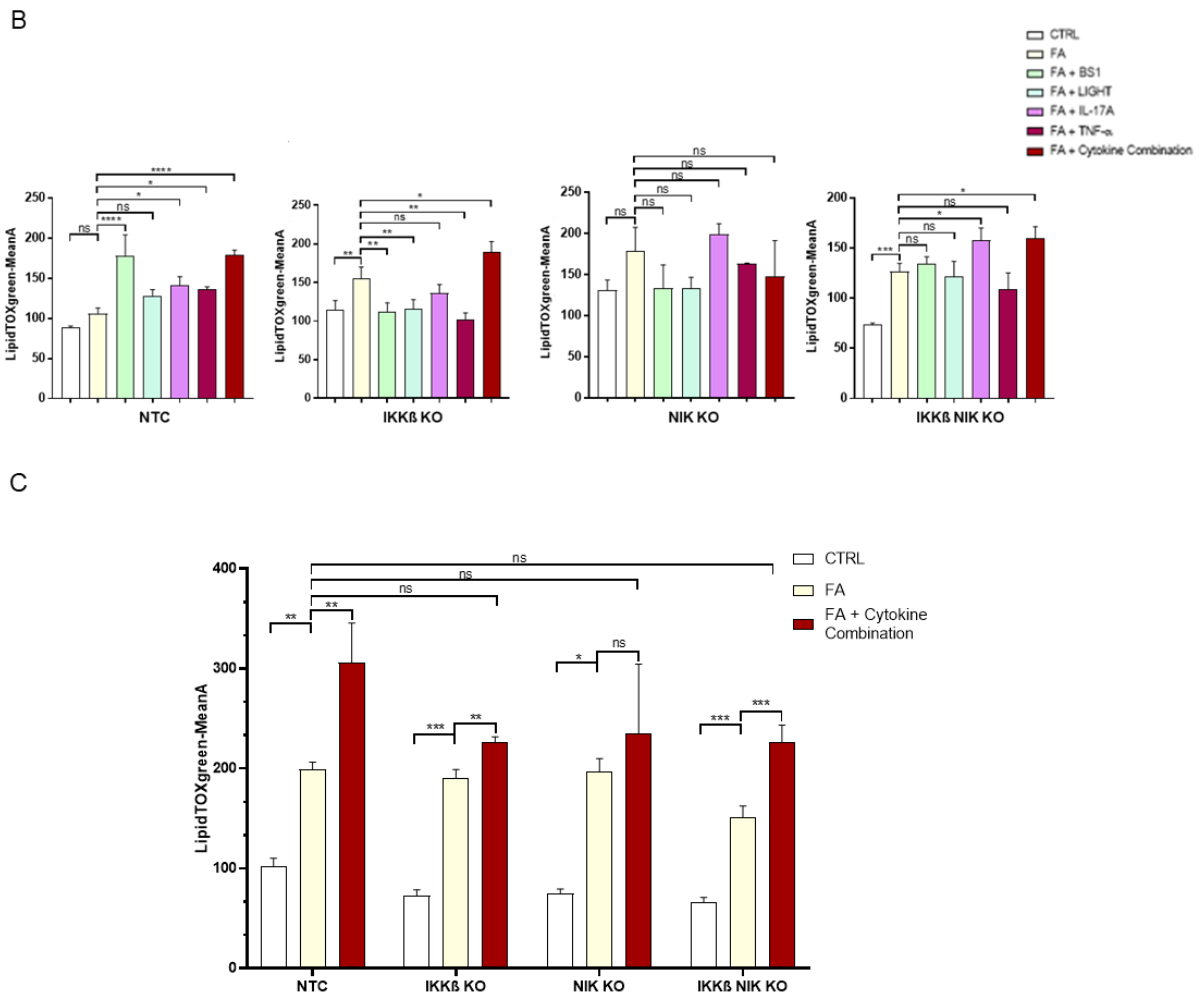


Figure 15: FA storage into neutral lipids in dHepaRG with deficiencies in canonical and non-canonical NF- κ B signalling, determined by LipidTOX green / Hoechst staining.

Non-targeting control (NTC), IKK β knock out (IKK β KO), NIK knock out (NIK KO) and IKK β -NIK double knock out (IKK β NIK KO) dHepaRG cells were, untreated, FA treated and FA plus cytokine treated (FA + BS1, FA + LIGHT, FA + IL-17A, FA + TNF- α , FA + Cytokine Combination) for 24h. (A) Representative fluorescence pictures of LipidTOX green / Hoechst stained dHepaRG cells, to visualize lipid accumulation and (B, C) LipidTOX green mean area was quantified by flow cytometry analysis. Statistical analysis was performed by one-way ANOVA. *: $p < 0.05$; **: $p < 0.01$; ***: $p < 0.001$; ****: $p < 0.0001$; ns: not significant.

4.2. Cellular stress response to inflammation and lipids

4.2.1. Mitochondrial morphology is affected by inflammation in a lipid-rich environment

Mitochondria produce energy (ATP) by oxidative phosphorylation (e.g. by FAO), regulate major metabolic pathways, and are critically involved in cell death control. Mitochondria cannot be formed *de novo*, therefore constant fission and fusion events are taking place. Fission- and fusion-deficiencies promote mitochondrial dysfunction, diminish ATP production, and decrease mitochondrial membrane potential and respiratory chain enzyme activity⁶⁸.

To investigate the involvement of FAs and inflammatory cytokines on mitochondrial morphology, dHepaRG cells were stimulated with lipids and cytokines, and mitochondria were visualized by MitoTrackerRed staining.

Mitochondria of unstimulated and FA stimulated cells showed a similar morphology (**Figure 16**). Cells that were simultaneously treated with lipids and inflammatory cytokines displayed changes in mitochondrial morphology. FA plus BS1 or LIGHT treatment induced a breakup of the mitochondrial network leading to small, independent organelles (presumably induced by mitochondrial fusion deficiency). FA plus IL-17A and TNF- α more likely promoted mitochondrial fusion events which resulted in a highly interconnected network (showing fission-deficiency). Mitochondrial staining showed that inflammatory cytokines affect mitochondrial morphology.

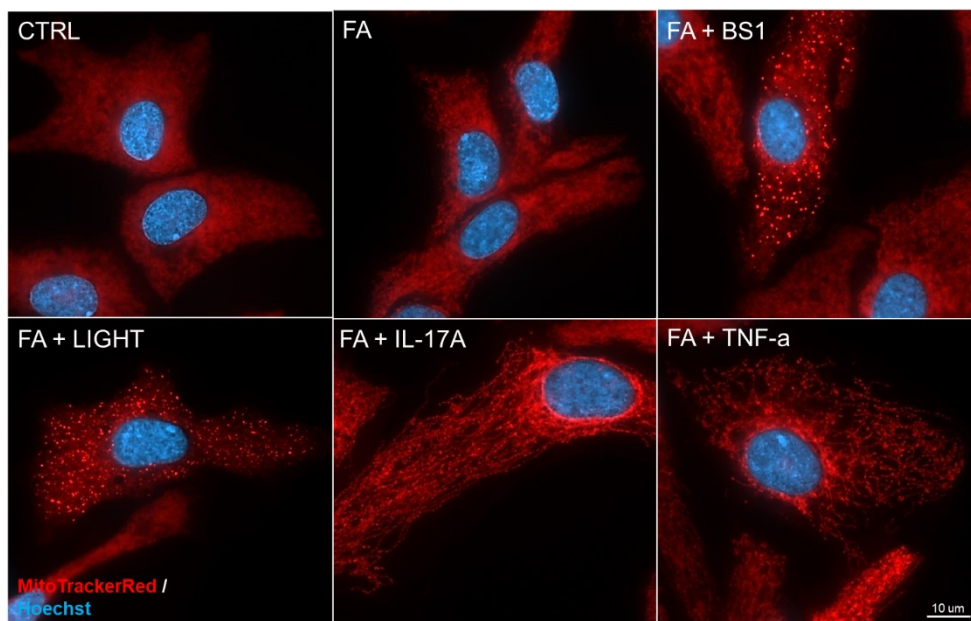


Figure 16: Mitochondrial morphology is affected by inflammation in a lipid-rich environment.

Mitochondrial staining of dHepaRG cells by MitoTracker red.

dHepaRG cells were untreated, stimulated with FAs alone and in combination with inflammatory cytokines (FA + BS1, FA + LIGHT, FA + IL-17A and FA + TNF- α) for 24h. Mitochondria were visualized by MitoTracker Red staining and fluorescence microscopy. Representative images are shown.

4.2.2. Inflammatory cytokines interfere with mitochondrial polarization and function

Mitochondrial ATP synthesis is induced by the generation of an electrochemical gradient where protons (H⁺) are pumped from the mitochondrial matrix to the inner membrane space by oxidative phosphorylation complexes, leading to the formation of a transmembrane potential and ROS. Downregulation of genes that regulate FAO or antioxidation processes promotes mitochondrial depolarization, increases ROS production, and induces functional impairment of mitochondria, by arresting oxidative phosphorylation. In addition, mitochondrial depolarization can interfere with proteins that regulate cellular apoptosis which further increases mitochondrial permeabilization, caspase activation, and cell death. Inflammatory cytokines,

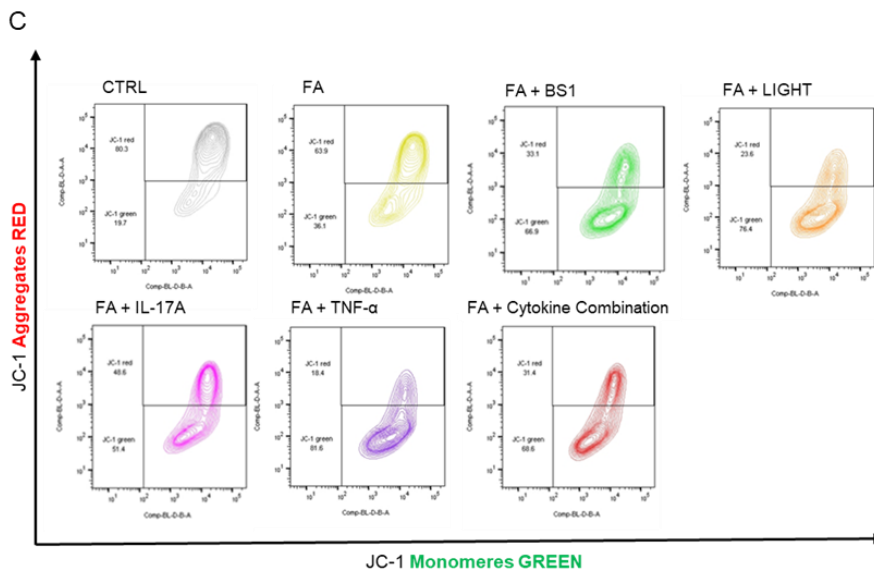
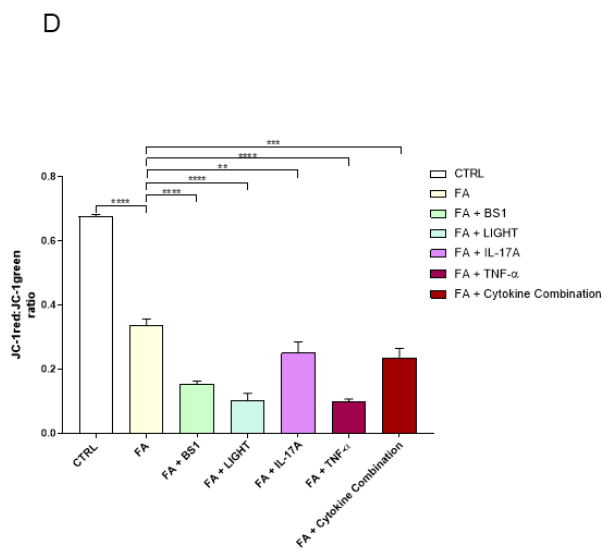
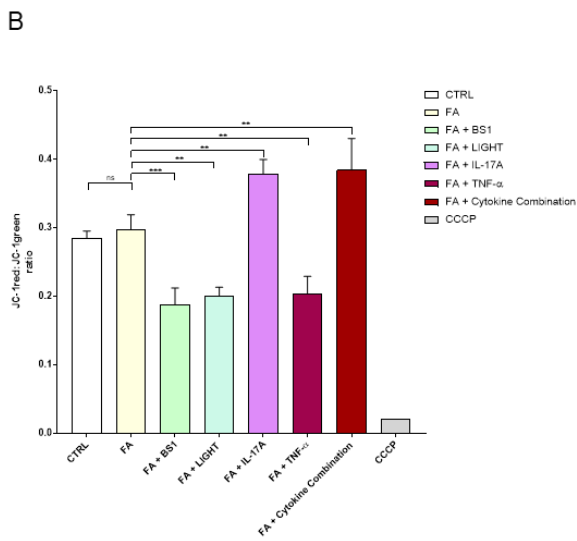
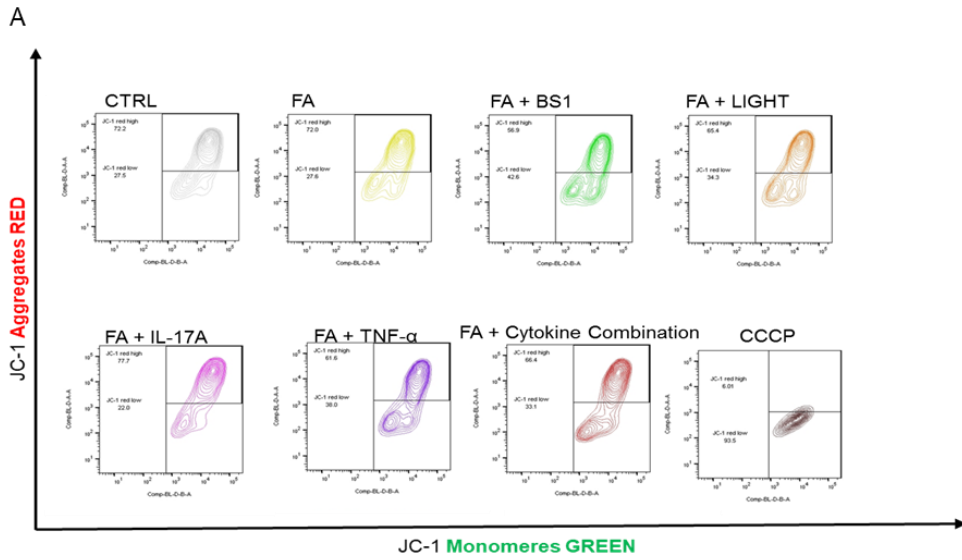
such as TNF- α , can depolarize mitochondrial membranes and can thereby induce mitochondrial dysfunction, however underlying mechanisms are not known in detail yet ¹⁹⁵.

To explore the influence of inflammatory cytokines and FAs on mitochondrial function over time (24h, 48h), cells were stained with the JC-1 dye to monitor mitochondrial membrane potential.

JC-1 accumulation in the mitochondria is shown by a fluorescence emission shift from JC-1 green monomers in the cytoplasm (mitochondrial depolarization, unhealthy) to JC-1 red aggregates (healthy, JC-1 dye trapped in the mitochondria). Pre-apoptotic cells display hyperpolarized mitochondria, whereas apoptotic cells show depolarized mitochondria ¹⁹⁶.

The JC-1 ratio of healthy mitochondria in dHepaRG was determined in untreated control cells (**Figure 17A, B**). As positive control (for mitochondrial depolarization), cells were subjected to the mitochondrial uncoupler, CCCP, which led to a decrease in mitochondrial membrane potential, indicated by a reduced red to green fluorescence ratio when compared to healthy untreated control cells (**Figure 17A, B**). FA treatment did not influence the mitochondrial membrane potential after 24h, shown by a similar JC-1 red to green ratio when compared to unstimulated cells. FA plus BS1, LIGHT, and TNF- α increased the mitochondrial depolarization, indicative for mitochondrial dysfunction and presumably apoptotic cell death. FA stimulation together with IL-17A and the combination of all cytokines induced mitochondrial hyperpolarization, shown by a significant increase in the JC-1 red to green ratio, displaying early-phase of apoptosis (**Figure 17A, B**).

After 48h of stimulation with FAs the JC-1 red to green ratio was decreased, displaying that pro-longed / chronic lipid stimulation reduced mitochondrial polarization, probably by lipotoxicity induced-stress response and ROS production (**Figure 17C, D**). Exposure to FAs plus BS1, LIGHT, IL-17A, TNF- α , and the cytokine combination further intensified mitochondrial depolarization. Cells that were subjected to BS1, LIGHT, TNF- α and the cytokine combination without lipids also displayed mitochondrial depolarization (**Figure 17E, F**). This demonstrates that the activation of inflammatory signalling pathways can induce mitochondrial dysfunction. In contrast, dHepaRG stimulation with the inflammatory cytokine IL-17A alone did not affect mitochondrial functions. These results revealed that inflammatory mediators promoted mitochondrial dysfunction which is dependent on the primary signalling pathway activation and the duration of exposure to the different cytokines and lipids. Inflammation can induce mitochondrial dysfunction and presumably apoptotic cell death either directly (after 24 hours), or induce a pre-apoptotic phenotype which can shift to apoptosis after prolonged treatment for after 48h. Thus, lipid excess in combination with an activated immune signalling in hepatocytes exacerbates mitochondrial dysregulation over time.



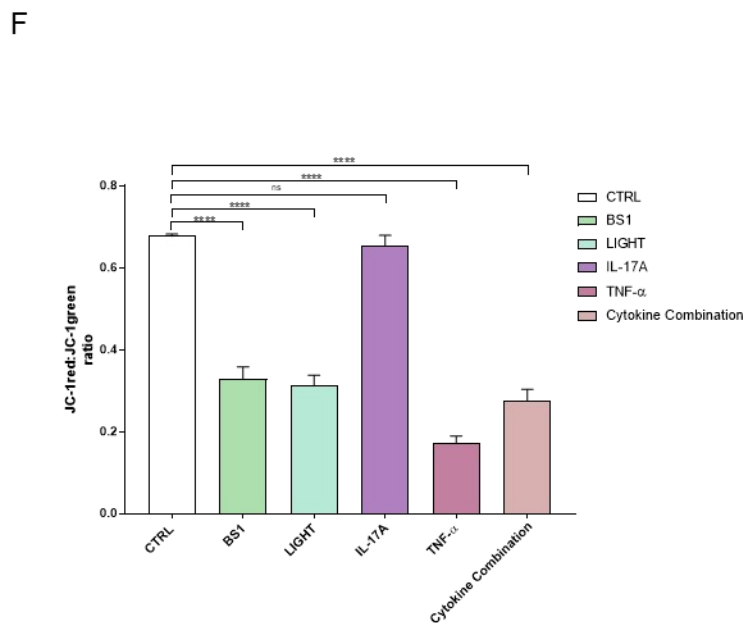
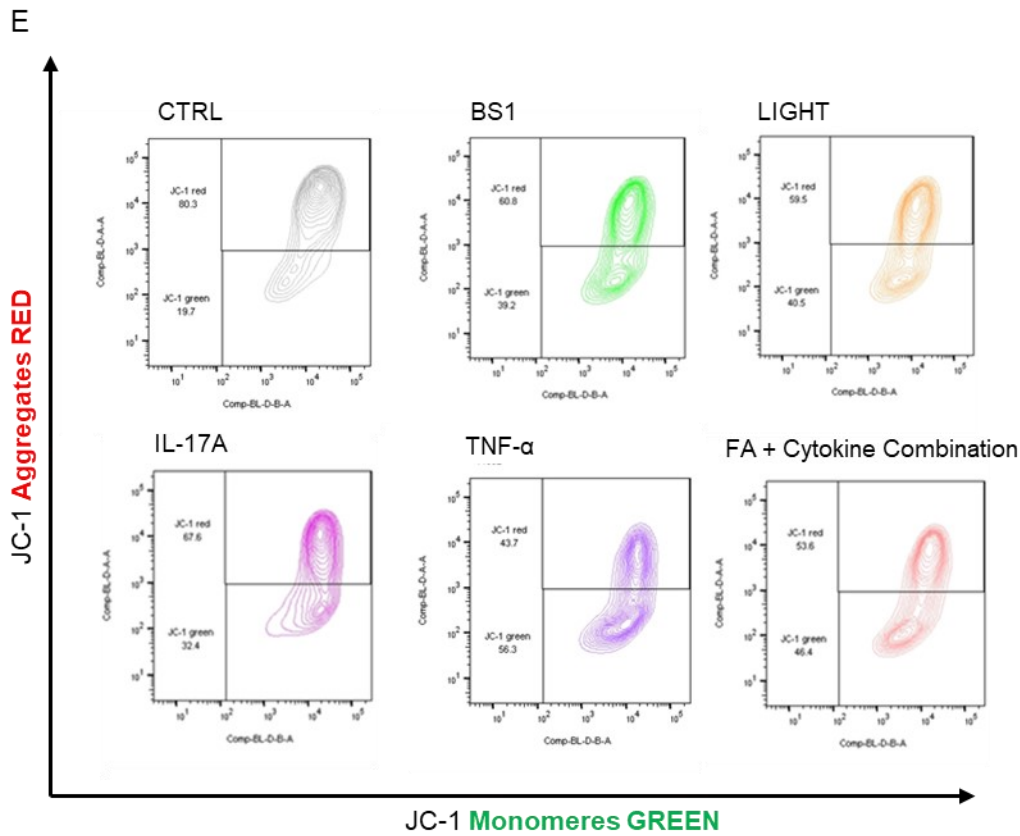


Figure 17: Inflammatory cytokines interfere with mitochondrial morphology and function.

JC-1 staining to monitor mitochondrial membrane potential in dHepaRG cells.

dHepaRG were untreated, were stimulated with inflammatory mediators (BS1, LIGHT, IL-17A, TNF- α , Cytokine Combination) alone, were FA treated, and were treated with FAs plus inflammatory mediators (FA + BS1, FA + LIGHT, FA + TNF- α , FA + Cytokine Combination) for (A, B) 24h and (C-F) 48h. Cells were stained with JC-1 dye to determine mitochondrial polarization, by flow cytometry analysis and quantification of the ratio of the JC-1 red mean area and the JC-1 green mean area. (A, B) As positive control cells were subjected to the mitochondrial uncoupler CCCP. Statistical analysis was performed by one-way ANOVA. *: $p < 0.05$; **: $p < 0.01$; ***: $p < 0.001$; ****: $p < 0.0001$; ns: not significant.

4.2.3. Mitochondrial dysfunction is induced by specific inflammatory cytokines

Exposure to the cytokine IL-4 did not influence FA storage in dHepaRG cells. To study the effect of IL-4 on mitochondrial membrane potential dHepaRG cells were stained with JC-1 dye. FA treatment reduced JC-1 red to green ratio, indicating mitochondrial depolarization. Additional BS1 stimulation further intensified this effect (**Figure 18A, B**). FA plus IL-4 stimulation did not induce mitochondrial dysfunction, as shown by a similar JC1 red to green ratio when compared to the FA condition.

These results demonstrate that only specific inflammatory cytokines promote mitochondrial dysfunction.

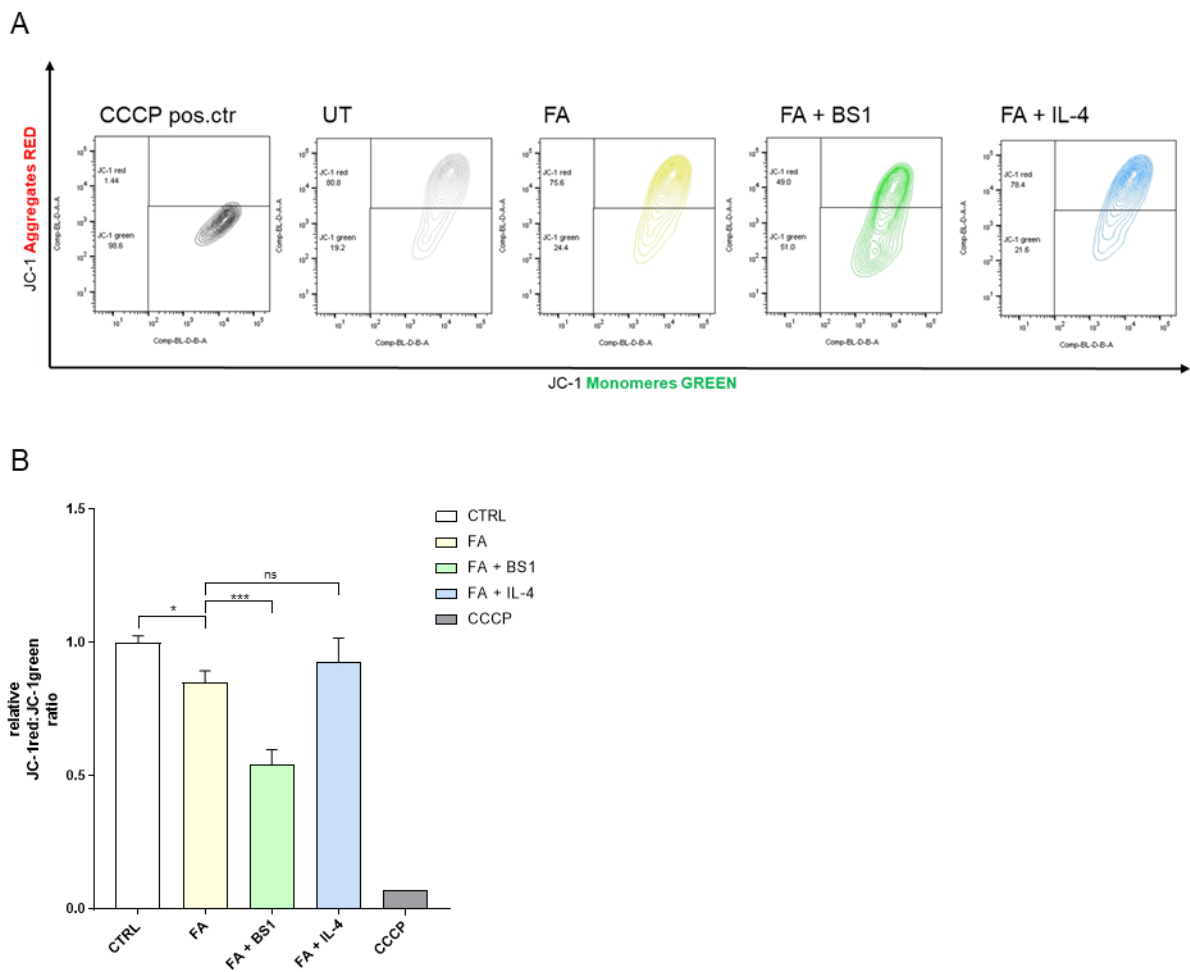


Figure 18: Mitochondrial dysfunction is induced by specific inflammatory cytokines.

JC-1 staining to monitor mitochondrial membrane potential in dHepaRG cells.

(A, B) dHepaRG were, untreated, FA treated, and treated with FAs plus cytokines (FA + BS1, FA + IL4) for 24h. Staining with JC-1 dye to determine mitochondrial polarization by flow cytometry analysis, by quantification of the ratio of JC-1 red mean area and JC-1 green mean area. As positive control cells were additionally treated with the mitochondrial uncoupler, CCCP. Statistical analysis was performed by one-way ANOVA. *: $p < 0.05$; **: $p < 0.01$; ***: $p < 0.001$; ****: $p < 0.001$; ns: not significant.

4.2.4. Inflammatory cytokines affect mitochondrial function via NF- κ B signalling

Inflammatory cytokines can signal via NF- κ B, and interference with the NF- κ B pathway prevented aberrant lipid storage. Thus, to investigate the influence of NF- κ B on inflammation induced mitochondrial dysregulation, cells were treated with the IKK β inhibitor, TPCA-1, and then stained with the JC-1 dye.

FA plus cytokine stimulation decreased mitochondrial membrane potential (**Figure 19A, B**). Simultaneous treatment with the IKK β inhibitor, TPCA-1 prevented the cytokine induced mitochondrial dysfunction (**Figure 19B**). This shows that inhibition of NF- κ B signalling via TPCA-1 prevented mitochondrial depolarization.

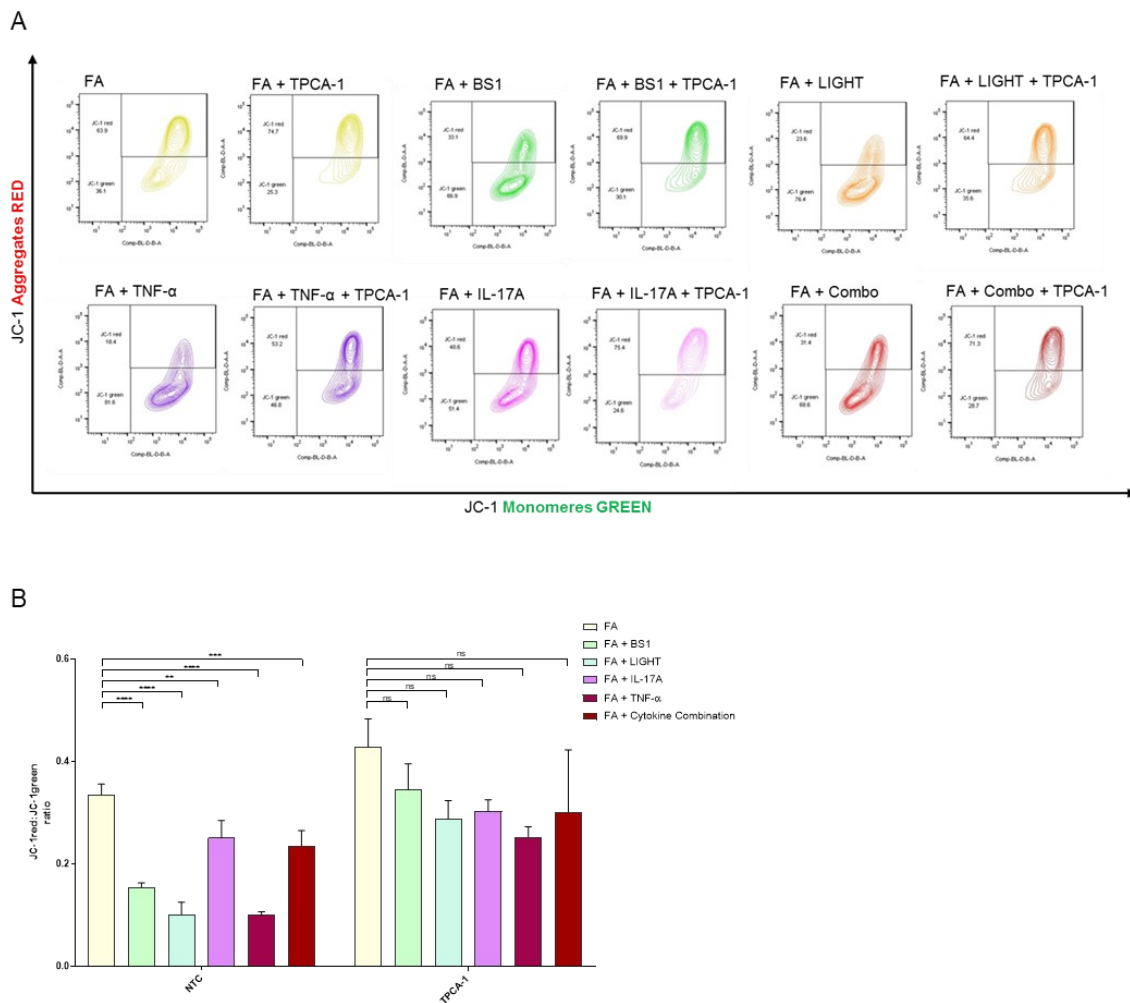


Figure 19: Inflammatory cytokines affect mitochondrial function via NF- κ B signalling.

JC-1 staining to monitor mitochondrial membrane potential in dHepaRG cells.

(A, B) dHepaRG cells, FA treated, and treated with FAs plus inflammatory mediators (FA + BS1, FA + LIGHT, FA + TNF- α , FA + Cytokine Combination), with and without the IKK β inhibitor TPCA-1, for 48h. Staining with JC-1 dye to determine mitochondrial polarization, by flow cytometry analysis, by quantification of the ratio of JC-1 red mean area and JC-1 green mean area. Statistical analysis was performed by one-way ANOVA. *: $p < 0.05$; **: $p < 0.01$; ***: $p < 0.001$; ****: $p < 0.001$; ns: not significant.

4.2.5. Fatty acids and inflammatory cytokines increase reactive oxygen species production, induce cell- apoptosis, proliferation and trigger replication stress and DNA damage

NF- κ B activation by inflammatory cytokines increased lipid accumulation and affected mitochondrial function. To address the effect of inflammation and lipid induced cellular stress response, I determined mitochondrial superoxide production, apoptotic cell death, cell proliferation, and DNA replication dynamics.

FA stimulation induced lipid accumulation and mitochondrial superoxide production, shown by red mitochondrial superoxide staining which correlated with the green lipid staining (**Figure 20A**). This indicates that high intracellular lipid concentrations promoted mitochondrial superoxide generation. Exposure to FAs and the cytokine combination intensified both, ROS production and neutral lipid accumulation, which also correlated with each other. Interference with ROS generation, by additional treatment with N-acetylcysteine, only slightly reduced lipid storage in both, FA, and FA plus inflammatory cytokine stimulated cells (**Figure 20B**). Elevated mitochondrial superoxide generation and intensified lipid accumulation induced by high lipid storage was prevented by simultaneous treatment with the IKK β -inhibitor, TPCA-1 (**Figure 20A, B**). This analysis demonstrates that inflammatory cytokines intensify lipid accumulation and promote, probably as secondary effect, increased ROS production.

To address the influence of inflammation and lipids on apoptosis, cells were stained with cleaved caspase 3 and annexin V antibodies. In the FA stimulated condition, only few cells were positive for red cleaved caspase 3 staining (**Figure 20C**), and the annexin V mean area was increased when compared to untreated cells (**Figure 20D**). FA plus inflammatory cytokine treatment exacerbated the number of red cleaved caspase positive cells and highly increased lipid levels (**Figure 20C**). Inhibition of apoptosis by the pan-caspase inhibitor Z-VAD-FMK, reduced apoptotic cell death in FA and FA plus inflammatory cytokine stimulated cells (**Figure 20D**). Lipid levels were not affected by the inhibition of apoptosis (**Figure 20E**). This revealed that elevated FA storage induced by inflammation intensified apoptotic cells death.

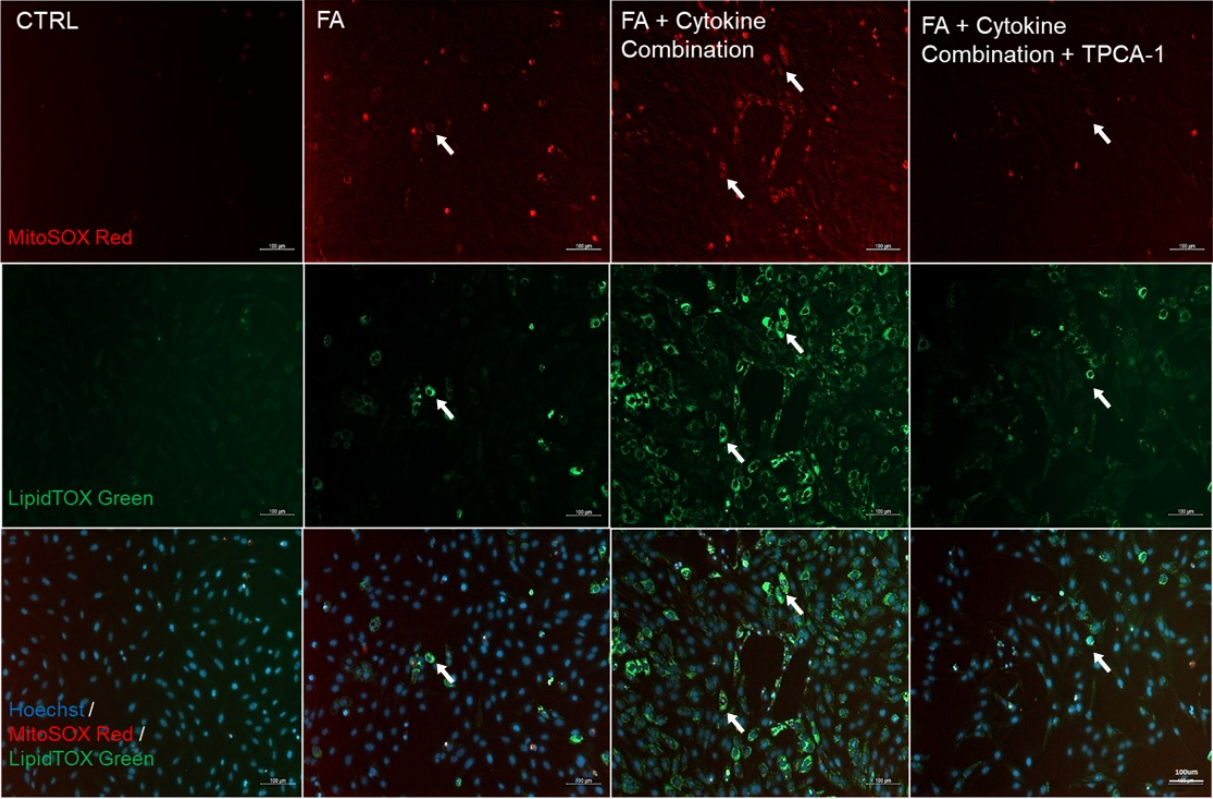
To determine cellular proliferation, cells were treated and stained with bromodeoxyuridine (BrdU). FA treatment mildly induced cell proliferation, shown by positive green nuclear staining, when compared to untreated control cells (**Figure 20F, G**). Additional treatment with inflammatory cytokines further increased the number proliferating cells. Simultaneous exposure to the IKK β inhibitor, TPCA-1 prevented increased cell proliferation (**Figure 20F**), indicating that cell proliferation was promoted by lipid stimulation and intensified by inflammatory NF- κ B-signalling activation.

Inflammatory stress response, apoptosis and compensatory proliferation can affect DNA replication. To study the influence of lipids and inflammatory cytokines on replication stress, protein levels of DNA double strand break markers and replication fork speed was determined. DNA double strand break marker (gH2Ax, 53BP1) levels were elevated by FA treatment and

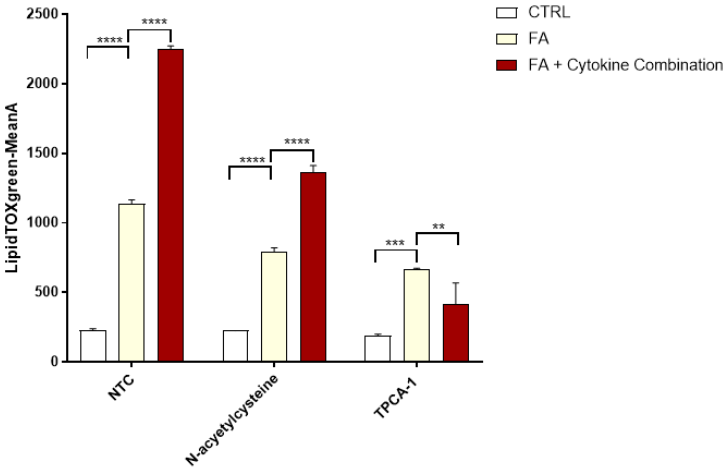
were further increased by additional inflammatory cytokine exposure (**Figure 20H, I**). Replication dynamics by DNA combing demonstrated significant reduced replication fork speed in FA plus inflammatory cytokine stimulated cells when compared to FA treated cells, indicative of replication stress (**Figure 20J**).

This showed that inflammatory cytokines and FAs induce double strand breaks, replication stress and can thereby promote pathogenesis.

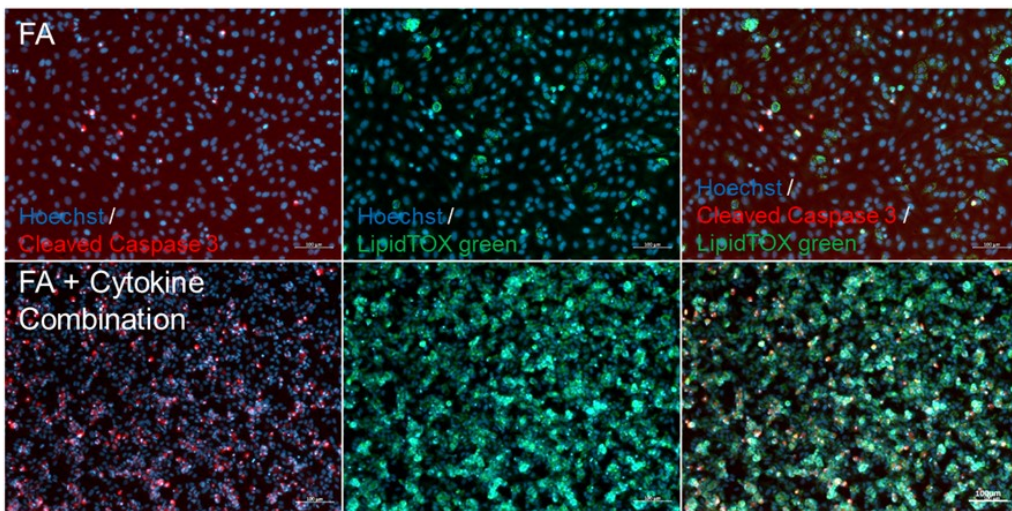
A



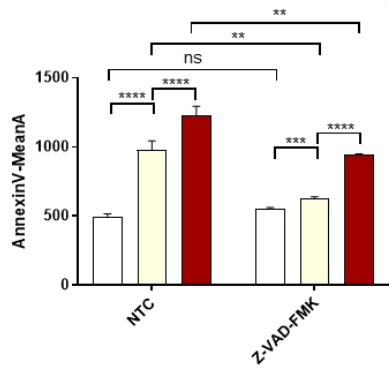
B



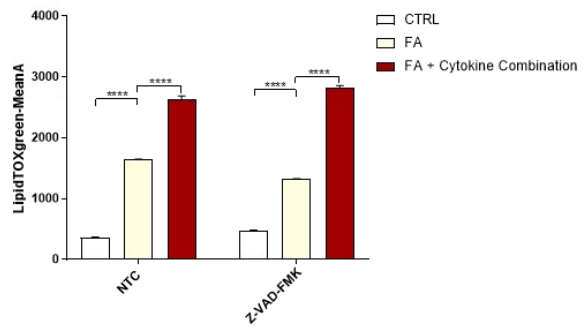
C



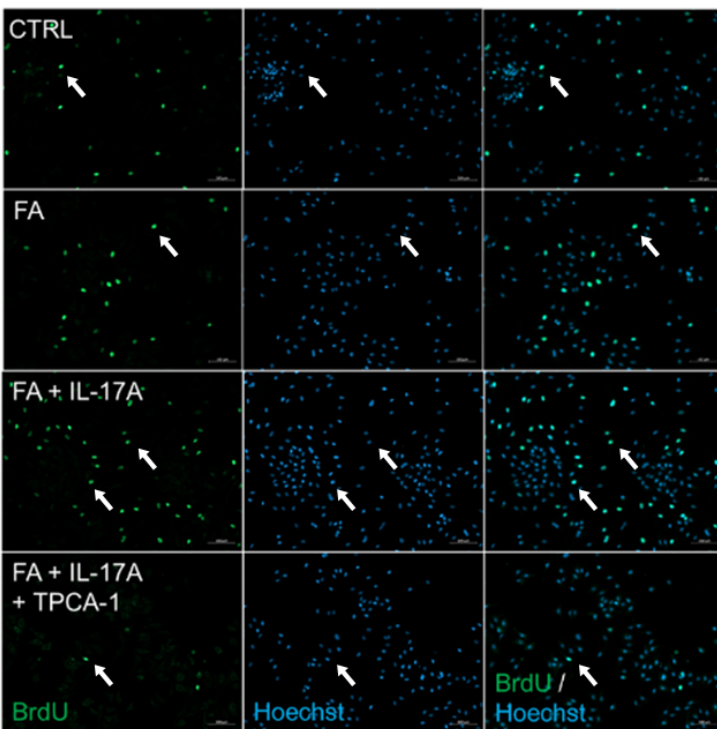
D



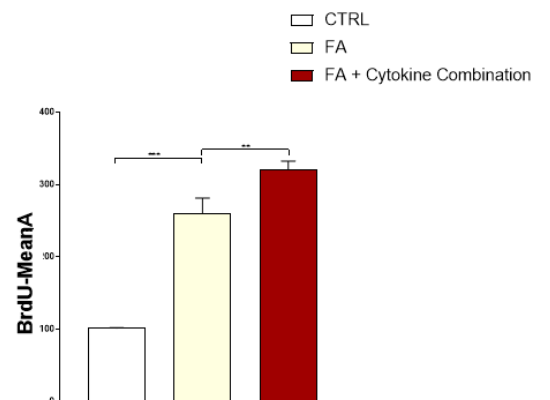
E



F



G



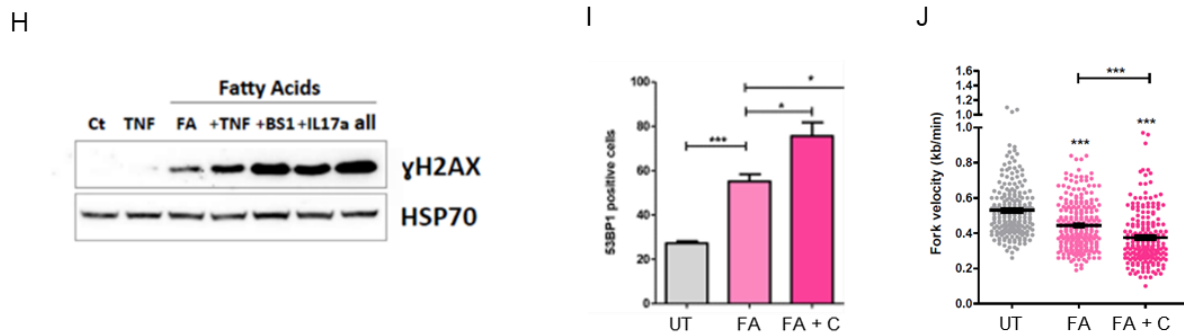


Figure 20: Mitochondrial superoxide production, lipid accumulation, apoptotic cell death, proliferation, and replication stress in dHepaRG cells.

dHepaRG cells were either untreated, treated with FAs alone and in combination with inflammatory cytokines (FA + Cytokine Combination, FA + BS1, FA + LIGHT, FA + IL-17A, FA + TNF- α), with and without the IKK β inhibitor TPCA-1, the ROS inhibitor N-acetylcystein, and the pan-caspase inhibitor Z-VAD-FMK, for 24h. (A) dHepaRG cells were stained with MitoSOX red and LipidTOX green, to visualize mitochondrial superoxide production and neutral lipid accumulation. Representative fluorescence pictures are shown. (B, E) dHepaRG were stained with LipidTOX green to quantify neutral lipid accumulation, analyzed by flow cytometry. Cells were additionally treated with (B) the IKK β inhibitor TPCA-1, the ROS inhibitor N-acetylcystein, and (E) the pan-caspase inhibitor Z-VAD-FMK. (C) Cleaved caspase 3 antibody staining, to quantify apoptotic cell death in combination with LipidTOX green stain, to visualize lipid accumulation by fluorescence microscopy. Representative images are shown. (D) Annexin V staining to quantify cell apoptosis by flow cytometry. Determination of the annexin V mean area (fluorescence). (F, G) Cell proliferation was determined by BrdU staining, by fluorescence microscopy and flow cytometry. (F) Representative pictures of BrdU stained dHepaRG (G) BrdU (fluorescence) mean area was determined by flow cytometry (H) Immunoblot analysis of the DNA damage (double strand break marker), γ H2Ax. (I) quantification of the immunofluorescence staining, of DNA double strand break marker 53BP1, analyzed by imageJ (J) Replication dynamics determination by DNA combing to analyze replication fork speed. (H-J) Immunoblot analysis of γ H2Ax, immunofluorescence analysis of 53BP1, and the determination of replication fork speed assay was performed by Romain Donne, MSc, in a collaboration with Dr. Chantal Desdouets, Statistical analysis was performed by one-way ANOVA. *: $p < 0.05$; **: $p < 0.01$; ***: $p < 0.001$; ****: $p < 0.001$; ns: not significant.

4.3. NF- κ B signalling – PPAR- α signalling

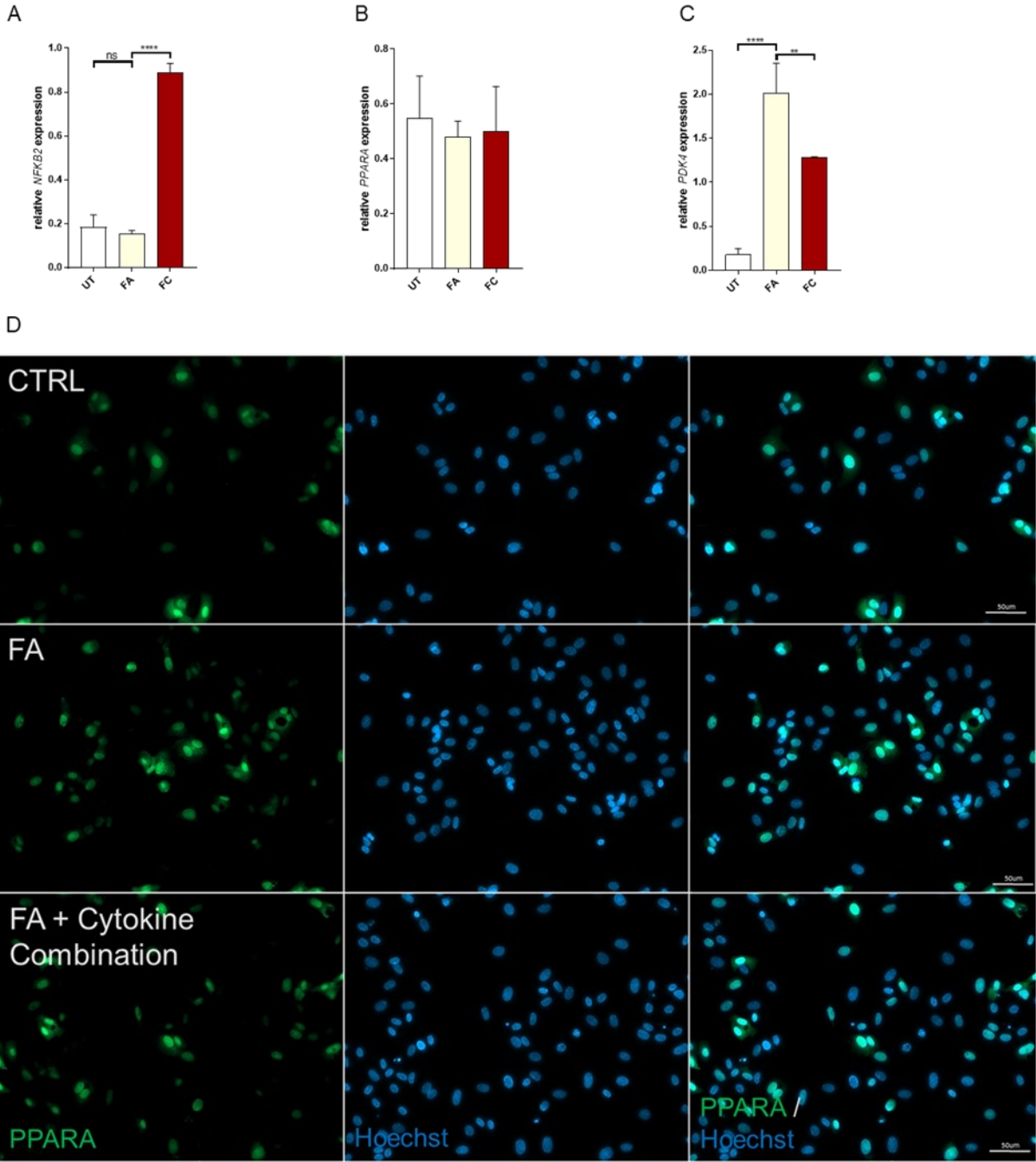
4.3.1. Inflammatory cytokines affect gene and protein levels of PDK4

Aberrant FA storage is induced by inflammation due to lipid catabolic deficiencies. The nuclear hormone receptor, PPARA, regulates major lipid metabolic pathways in hepatocytes including FA- uptake, storage, and oxidation¹⁹⁷. The PPARA target gene PDK4 is critically involved in the regulation of glucose- and FAO by phosphorylation of Pyruvate dehydrogenase complex (PDC)⁷⁴.

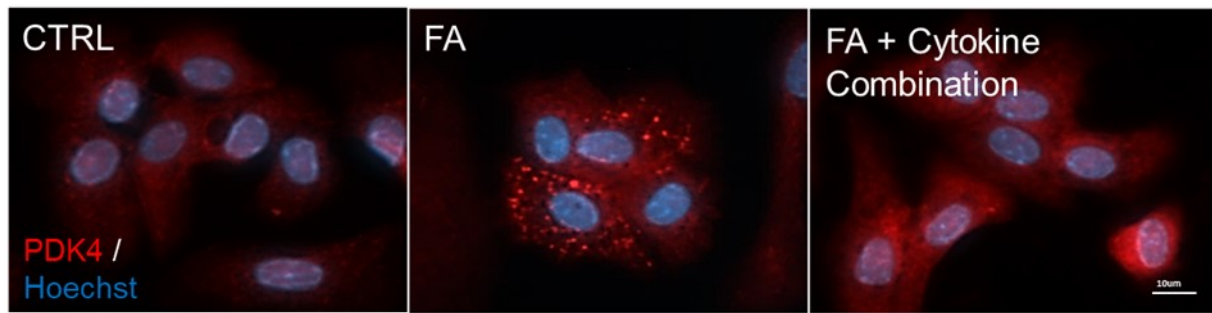
The effect of inflammatory cytokines and lipids on genes and protein levels implicated in NF- κ B- and PPAR- α signalling was determined.

Inflammatory cytokine stimulation upregulated NFKB2 (**Figure 21A**). PPAR- α gene and protein levels remained unchanged by FA, and additional cytokine treatment (**Figure 21B, D**). Lipid stimulation elevated PDK4 levels, additional exposure to inflammatory cytokines

downregulated PDK4 (**Figure 21C, E**). FA stimulation intensified phosphorylation of PDC when compared to untreated and FA plus Cytokine Combination (**Figure 21F**). Showing that increased PDK4 levels correlated with elevated PDC phosphorylation in FA treated cells.



E



F

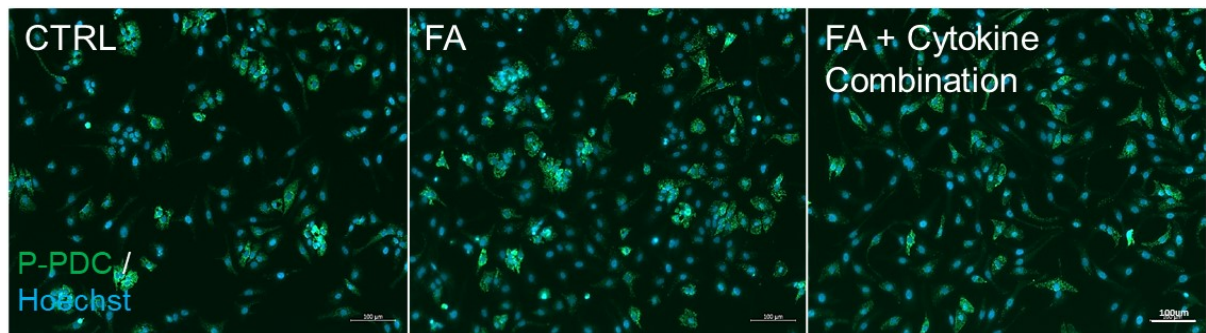


Figure 21: Gene expression analysis and immunofluorescence stainings of dHepaRG cells, stimulated with FAs and cytokines.

dHepaRG cells were, untreated, FA treated, and FA plus inflammatory cytokine (FA + Cytokine Combination) stimulated, for 24h. (A-C) Gene expression analysis of PPAR α , PDK4 and NFKB2, by RT-PCR. Immunofluorescence staining against (D) PPAR α , (E) PDK4, and (F) Phospho-PDC, representative images are shown. Statistical analysis was performed by one-way ANOVA. *: $p < 0.05$; **: $p < 0.01$; ***: $p < 0.001$; ****: $p < 0.0001$; ns: not significant.

4.3.2. PPAR α and PDK4 are not involved in inflammation-triggered elevated lipid accumulation

To investigate the effect of PPAR α and PDK4 on inflammation-mediated downregulation of lipid metabolic processes, si-RNA mediated PPAR α and PDK4 knock down (KD) experiments were performed.

FA treatment induced FA storage into neutral lipids and simultaneous stimulation with inflammatory cytokines further elevated lipid accumulation in NTC cells (**Figure 22A**). Si-RNA mediated PPAR α KD in cells that were exposed to FAs, with and without inflammatory cytokines, revealed comparable lipid levels. Inflammation triggered aberrant lipid accumulation was not affected by loss of PDK4 (**Figure 22A**). Although, gene expression analysis displayed that si-RNA mediated PDK4 KD was efficient (**Figure 22B**).

This showed that increased FA storage upon PPAR α deficiency is an inflammation independent mechanism and that the PPAR α -PDK4 axis is not critical for inflammation triggered aberrant lipid accumulation.

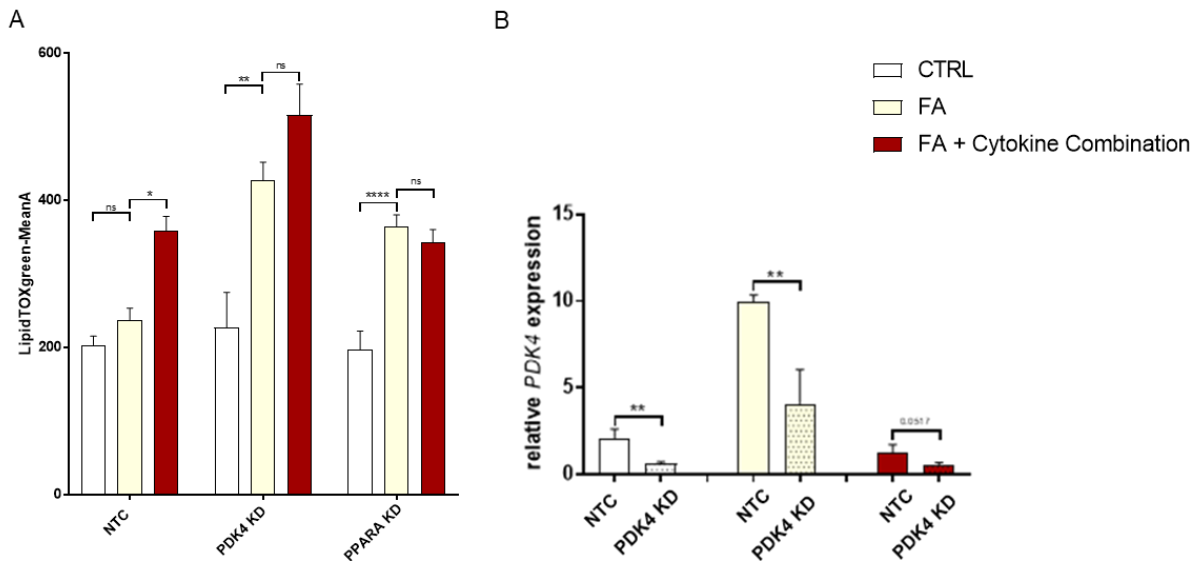


Figure 22: FA storage into neutral lipids in hepatocytes (dHepaRG) determined by LipidTOX green staining.

dHepaRG cells, siRNA-mediated non-targeting control (NTC), PPARA KD and PDK4 KD, cells were untreated, FA treated, and treated with FA in combination with all cytokines (FA + Cytokine Combination) for 24h. Lipid accumulation was quantified by LipidTOX green staining and flow cytometry, by determination of LipidTOX green mean area. Statistical analysis was performed by one-way ANOVA. *: $p < 0.05$; **: $p < 0.01$; ***: $p < 0.001$; ****: $p < 0.001$; ns: not significant.

4.4. Transcriptome profiling by RNA sequencing

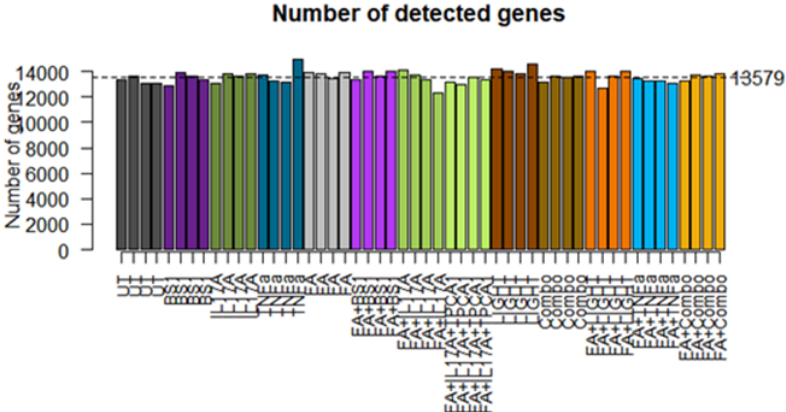
4.4.1. Inflammatory cytokines are the major regulators of overall gene expression in a lipid-rich environment in human dHepaRG cells

Inflammatory mediators induced increased lipid accumulation in hepatocytes, driven by catabolic deficiencies. To explore whether these mechanisms are regulated by gene expression, RNA sequencing analysis was performed to disentangle differences between gene regulations induced by inflammatory mediators, by FAs and by cytokines in combination with FAs.

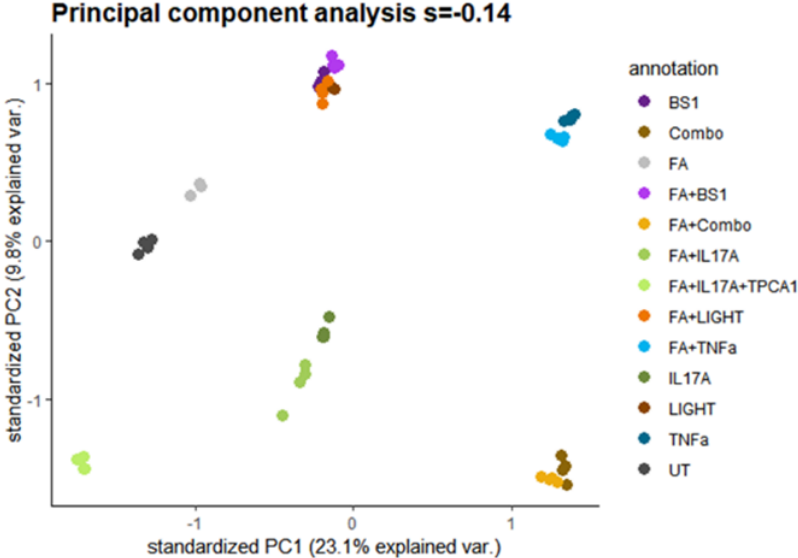
On average, about 13.579 genes were detected per sample (**Figure 23A**). To address similarities and differences between all conditions the samples were clustered by principal component analysis (PCA) (**Figure 23B**) and euclidean distance matrix (tSNE) (**Figure 23C**), using normalized counts of all genes. These results displayed that untreated control cells and FA stimulated cells clustered closely nearby, showing that their gene expression profile is similar. BS1 and LIGHT treated samples with and without FAs were grouping together, revealing a similar gene regulation, induced by $LT\beta R$ signalling activation. In addition, IL-17A stimulated samples in presence and absence of FAs clustered together. Additional stimulation with the $IKK\beta$ inhibitor TPCA-1, of FA and IL-17A treated cells, spatially separated the samples (within the PCA plot) from the other ones, showing that $NF-\kappa B$ inhibition interfered with gene

expression induced by IL-17A. Cells that were stimulated with TNF- α , or the cytokine combination alone and together with FAs, formed groups separately from the other ones. RNA sequencing based sample clustering revealed that inflammatory mediators are the main drivers that induce a specific gene expression profile, whereas the additional effect of FA was marginal.

A



B



C

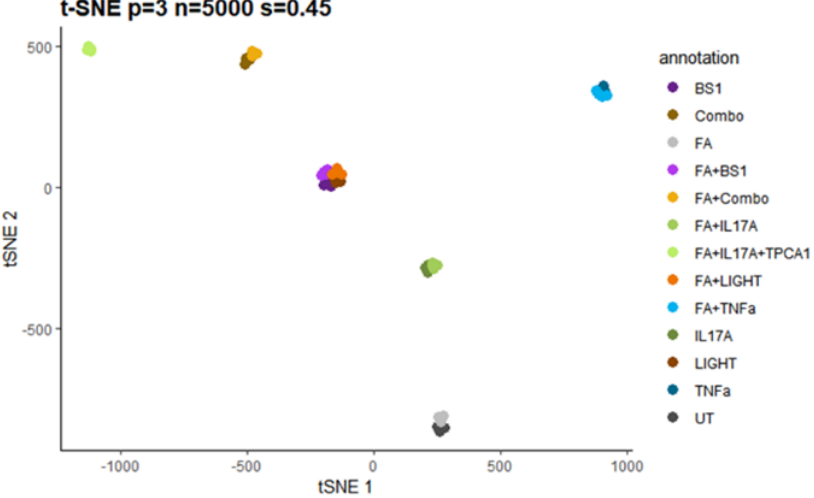


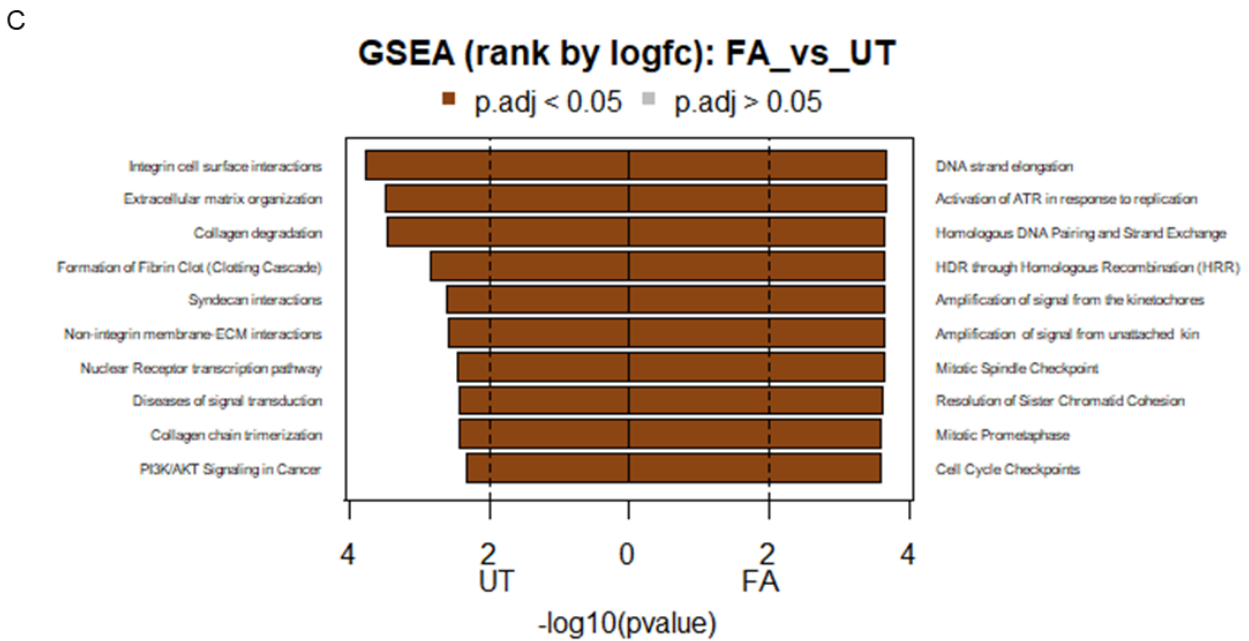
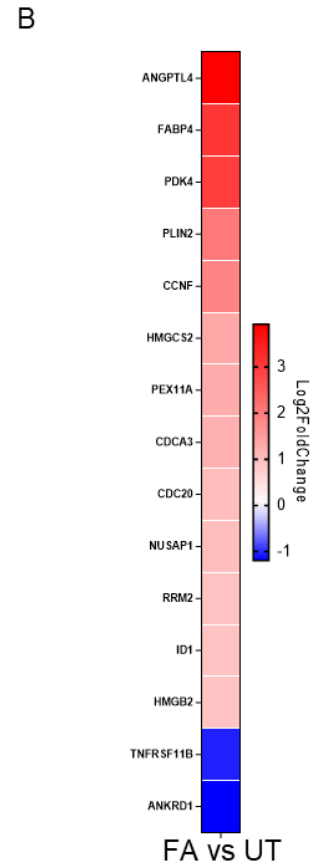
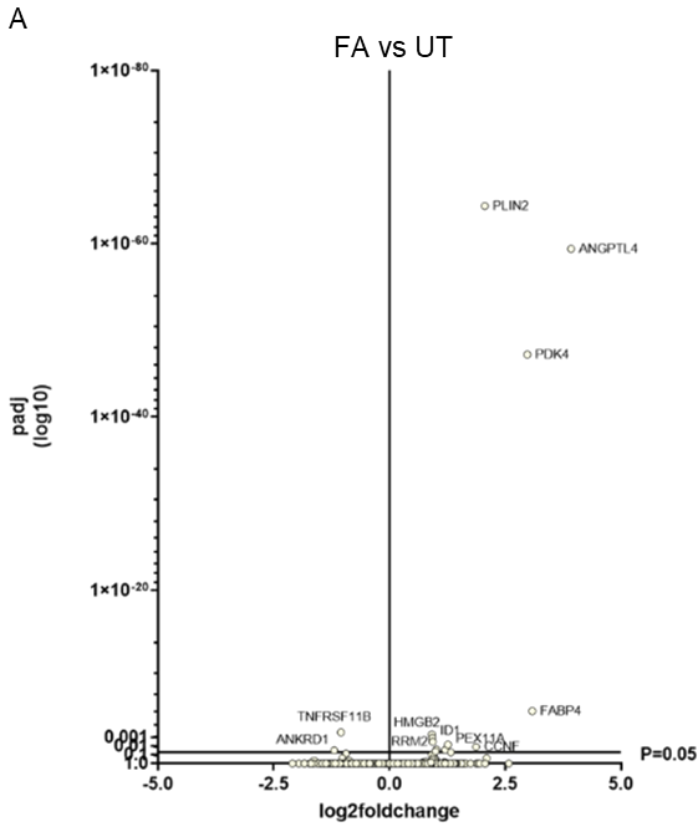
Figure 23: RNA sequencing analysis; general numbers of detected genes, sample clustering by principal component analysis (PCA), and euclidean distance matrix (tSNE).

Human dHepaRG cells were left untreated, were treated with inflammatory mediators (BS1, IL-17A, TNF- α , LIGHT, Cytokine Combination (Combo)) alone, were treated with FAs alone and together with inflammatory mediators (FA + BS1, FA + IL-17A, FA + LIGHT, FA + TNF- α and FA + Combo) for 24h. FA plus IL-17A stimulated cells were additionally treated with the IKK β -inhibitor TPCA-1 (FA + IL-17A + TPCA1). For differential expression (DE) analysis genes were ranked based on their log₂foldchange (log₂FC \geq 1) and adjusted p value (padj $<$ 0.05) and normalized counts of all genes, raw counts (count $<$ 2), were used. (A) Total number of genes detected by RNA sequencing. Sample clustering shown by (B) PCA and (C) tSNE. Genes and proteins were described by using ProteinDomainVisualizer.

4.4.2. Fatty acid stimulation promotes upregulation of genes involved in lipid metabolic processes and proliferation

Differential expression (DE) analysis was performed to discover gene regulations induced by FAs when compared to untreated controls. Lipid stimulation upregulated PPAR- α target genes e.g. ANGPTL4, FABP4, PDK4, FABP1, PLIN2, implicated in lipid uptake-, transport-, storage and catabolism (**Figure 24A, B**). In addition, FA treatment led to elevated expression of genes involved in other metabolic processes such as ketogenesis (HMGCS2) and peroxisomal biosynthesis (PEX11A) and increased levels of genes essential for cell cycle regulation including CCNF (CyclinF, regulates cell cycle transitions), CDCA3 (required for entry into mitosis), DCD20 (essential regulator during cell division, and for activation of anaphase), NUSAP1 (promotes the organization of mitotic spindle microtubules), and RRM2 (involved in biosynthesis of deoxyribonucleotides, thus for DNA synthesis).

Exposure to FAs downregulated genes implicated in the regulation of apoptotic cell death including ANKRD1 (shows increased levels during apoptosis) and TNFRSF11B (can interfere with apoptosis) (**Figure 24A, B**). Gene set enrichment analysis (GSEA) displayed a higher expression of genes involved cell proliferation, including following terms, DNA strand elongation and activation of ATR in response to replication, cell cycle, and M-phase in FA treated cells (**Figure 24C, D**). In untreated cells, expression of genes implicated in extracellular matrix organization, post-translational protein phosphorylation and insulin-like growth factor (IGF) modification was increased. DE analysis showed that FA treatment affected expression of genes involved in lipid metabolic processes, cell proliferation and regulation of apoptosis.



D

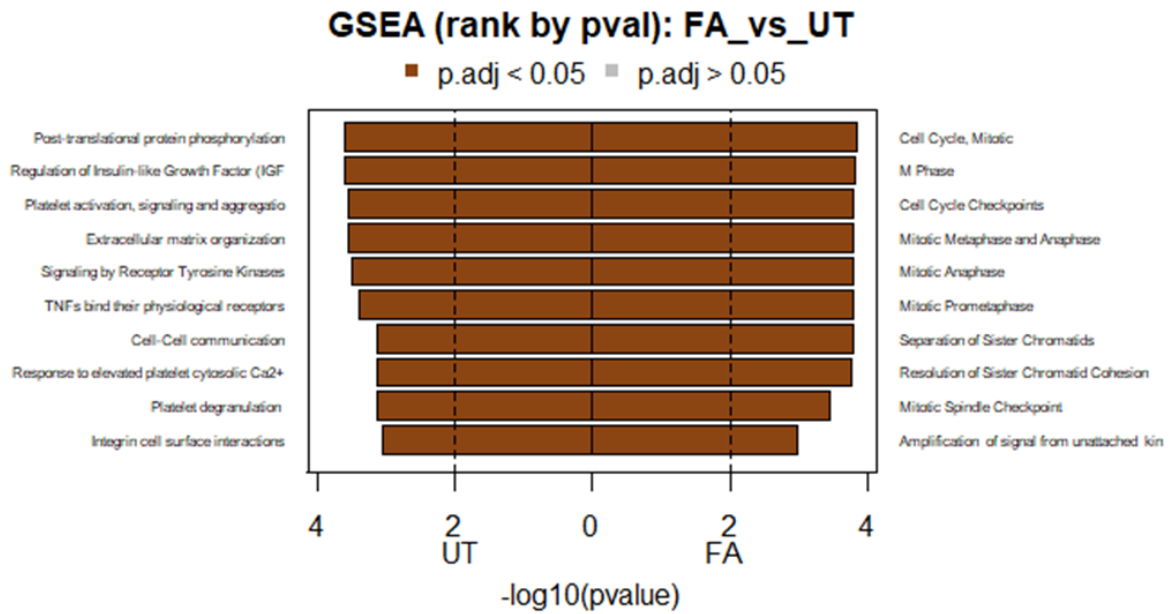


Figure 24: RNA sequencing analysis, volcano plot, heatmap, and gene set enrichment analysis (GSEA), comparing FA treated and untreated dHepaRG cells.

DE analysis (gene ranking based on \log_2 foldchange ($\log_2FC \geq 1$) and adjusted p value ($p_{adj} < 0.05$), (A) Volcano plot (based on DE analysis) illustrates genes that are up- and downregulated by FA stimulation in dHepaRG cells. (B) Heatmap showing significant ($p_{adj} < 0.05$) up- and down regulated genes, ranked by \log_2 foldchange (\log_2FC) (C, D) GSEA ranked by \log_2 fold change with $p_{adj} < 0.05$ or $p_{adj} < 0.05$. Genes and proteins were described by using ProteinDomainVisualizer.

4.4.3. Lymphotoxin β receptor signalling activators affect the expression of genes essential for the regulation of inflammation, proliferation, apoptosis, and metabolic processes

To address the influence of $LT\beta R$ signalling activation on the regulation of the whole gene expression in dHepaRG cells, DE analysis was performed comparing untreated control cells with cells that were exposed to the $LT\beta R$ agonist BS1, or the inflammatory cytokine LIGHT. In addition, FA stimulated cells were compared with FA plus BS1 or LIGHT treated cells.

DE analysis showed that BS1 stimulation in presence and absence of FAs induced a similar gene expression pattern (**Figure 25A, B**). Exposure to BS1 increased levels of genes implicated in the regulation of inflammatory response, cell proliferation and apoptosis. Upregulated genes by BS1 included BIRC3 (regulates apoptotic cell death, inflammatory signalling and cell proliferation), MMP7 and MMP9 (metalloproteases, break down extracellular matrix), TRAF1 and TRAF2 (involved in TNFR signalling, regulate mitogen-activated protein kinase (MAPK), c-Jun N-terminal kinase (JNK), NF- κB signalling, and apoptosis), VCAM1 and ADGRE1 (regulate cell-cell interactions) (**Figure 25A, B**). Downregulated genes by BS1 stimulation included IGFBP5 (can regulate cell growth), KCNJ16 (regulates cellular fluids and

maintains the pH balance), HMGCS2 (catalyses the first reaction of ketogenesis), CA9 (a metalloenzyme, catalyzes the hydration of carbon dioxide), (KRT19 (a biliary cell marker) and GSTA1 (a detoxification enzyme). DE analysis showed that BS1 stimulation in presence and absence of FAs decreased genes involved in the regulation of metabolic processes including enzymes essential for anabolic and catabolic processes, oxidation, and cell differentiation.

GSEA, by Kyoto Encyclopaedia of Genes and Genomes (KEGG), showed elevated enrichment of genes in BS1 stimulated cells, with and without FAs, were involved in cell proliferation and cellular stress response including following KEGG terms DNA Replication, Homologous Recombination Mismatch Repair, Proteasome, Primary Immunodeficiency, Base Excision Repair, Nucleotide Excision Repair, Oocyte Meiosis and Pyrimidine Metabolism **(Figure 25C)**.

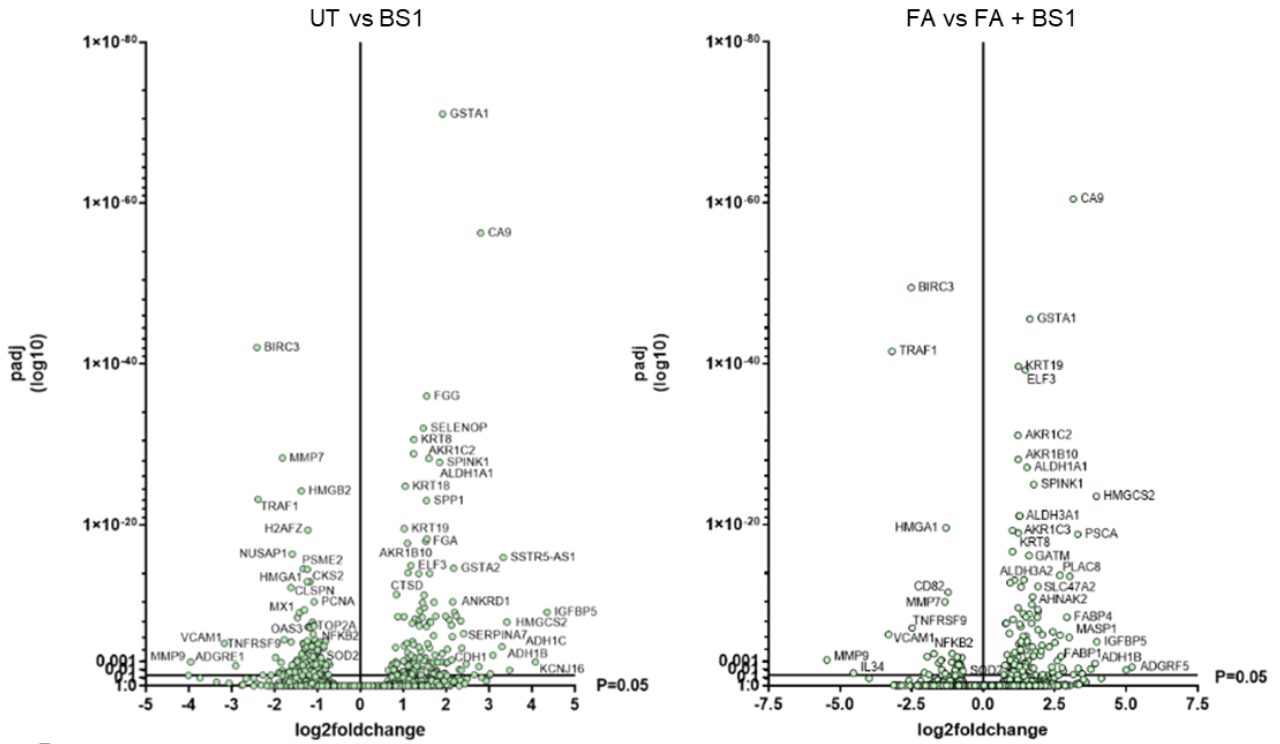
GSEA analysis displayed reduced levels of genes essential for homeostasis of major metabolic processes involved in following KEGG terms, Drug Metabolism - cytochrome P450, (CYPs), Metabolism of Xenobiotics, Complement and Coagulation Cascades, Retinol Metabolism, Steroid Hormone Biosynthesis, Hypertrophic Cardiomyopathy (HCM) and Tight Junction, Type II Diabetes Mellitus, Glycolysis Gluconeogenesis, Peroxisome, Axon Guidance and Calcium Signalling Pathways **(Figure 25C)**.

DE analysis comparing LIGHT with untreated control cells and LIGHT plus FAs with FA treated cells, revealed a similar gene expression profile as BS1 treated cells **(Figure 25D, E)**. Exposure to LIGHT, with and without FAs, increased expression of genes involved in cellular inflammatory stress-response and regulation of proliferation and apoptosis. Upregulated genes comprised e.g. MMP9, IL34 (inflammation), TRAF1, VCAM1, TNFRSF9 (TNFR signalling), and CCNF. Downregulated genes by LIGHT treatment in presence and absence of FAs were implicated in homeostasis of metabolic processes including e.g. IGFBP5, CYP24 (mitochondrial monooxygenase), CA9, GSTA1, KRT19, and HMGCS. KEGG pathway analysis revealed an enrichment of genes implicated in following KEGG terms, DNA replication, Proteasome, Base Excision Repair, Oocyte Meiosis, Progesterone Mediated Oocyte Maturation, and Pyrimidine Metabolism **(Figure 25F)**. Genes involved in several metabolic processes were decreased by LIGHT treatment, included in following terms, Complement and Coagulation Cascades, Drug Metabolism by Cytochrome P450, Metabolism of Xenobiotics by Cytochrome P450, Hypertrophic Cardiomyopathy HCM, Valine Leucine and Isoleucine Degradation, Arrhythmogenic Right Ventricular Cardiomyopathy ARVC, Retinol Metabolism, Steroid Hormone Biosynthesis, ECM Receptor Interaction and Fatty Acid Metabolism **(Figure 25F)**.

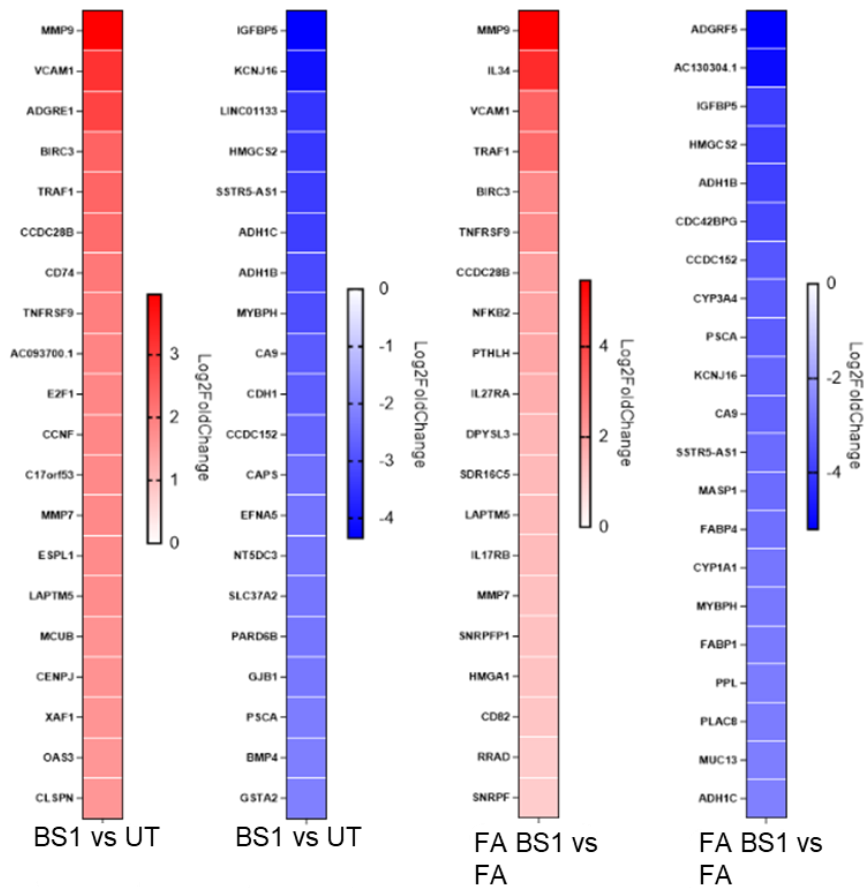
RNA sequencing analysis showed that BS1 and LIGHT treatment induced a cellular inflammatory stress response and interfered with genes essential for several metabolic and oxidative processes. Lipid exposure showed a negligible effect on the whole gene expression

regulation, indicating that an inflammatory microenvironment mainly determines the gene expression profile in presence or absence of FAs.

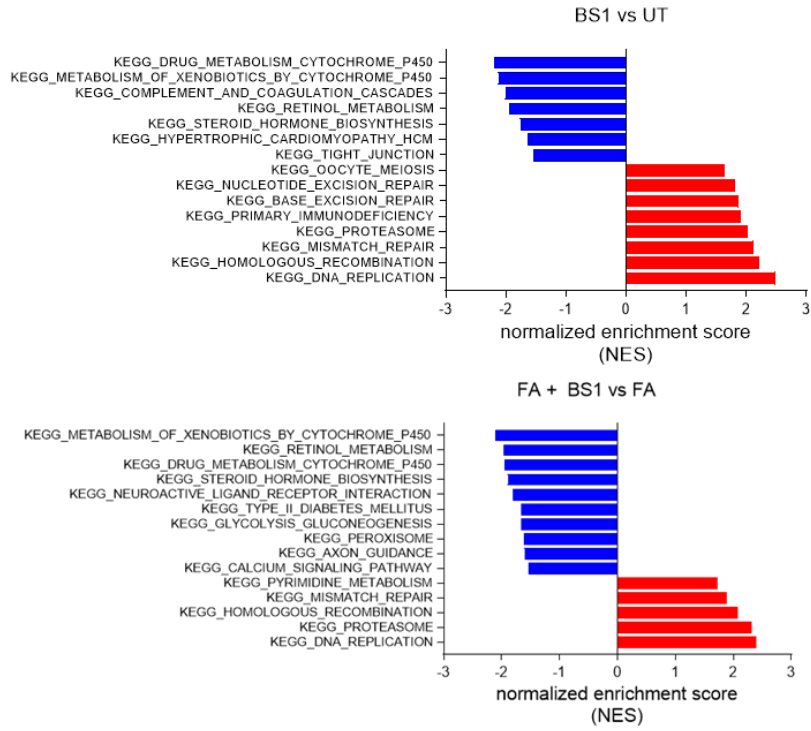
A



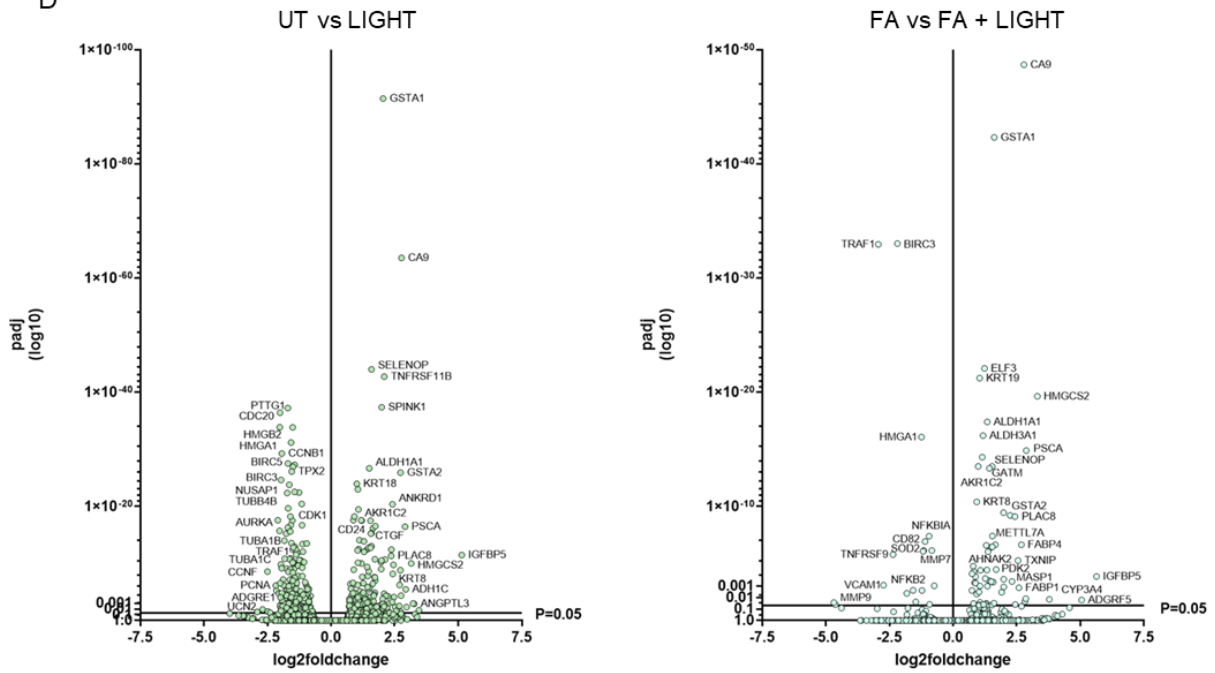
B



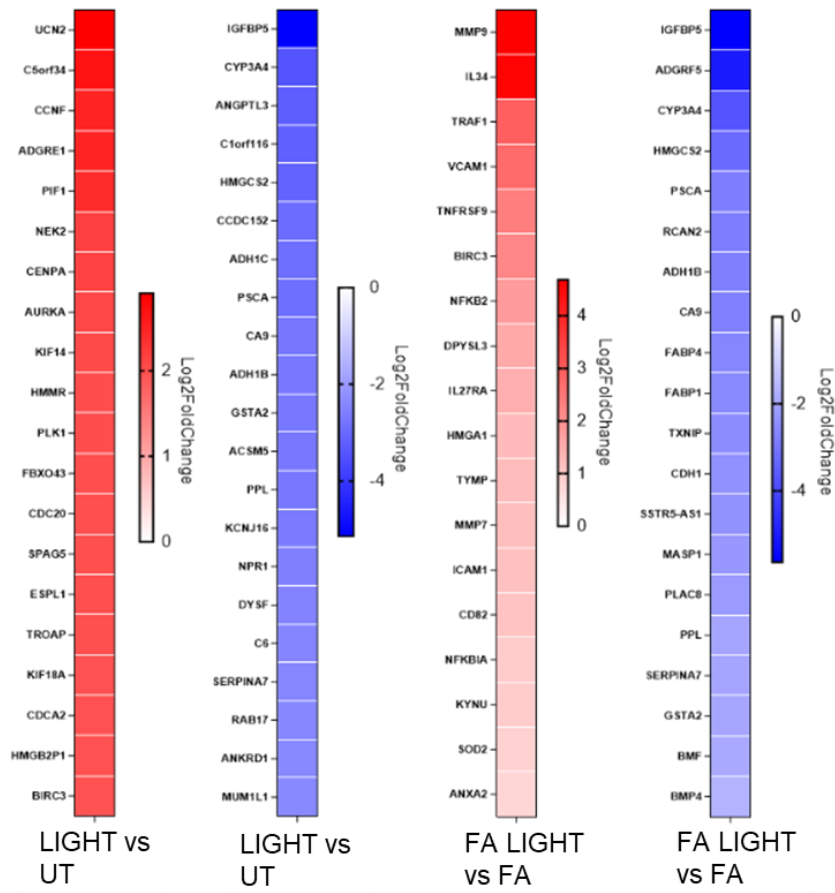
C



D



E



F

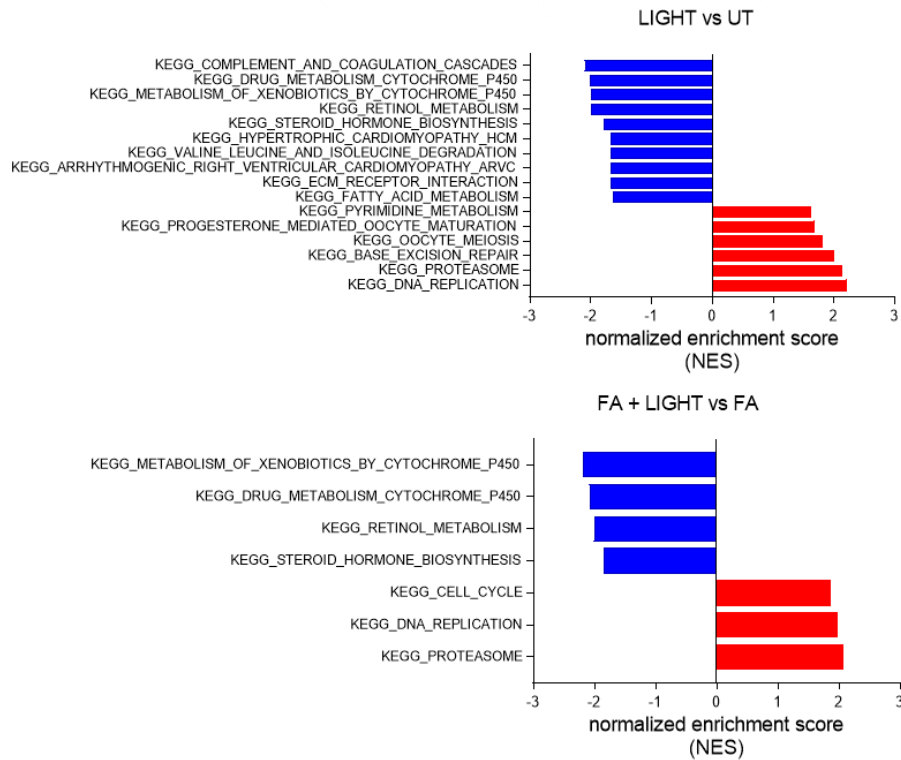


Figure 25: RNA sequencing analysis, volcano plot, heatmap, and gene set enrichment analysis (GSEA), comparing BS1 and LIGHT, with and without FAs, with untreated and FA treated dHepaRG cells.

DE analysis (genes ranked by log₂ fold change (log₂FC≥1) and adjusted p value (padj<0.05)), (A, D) Volcano plot (based on DE analysis) illustrates genes that are up- and downregulated by BS1/LIGHT +/- FA stimulation, when compared to untreated and FA treated cells. (B, E) Up- and downregulated genes, ranked by log₂FC and padj<0.05, (C, F) GSEA, KEGG pathway analysis shows gene enrichment ranked by the normalized enrichment score (NES) and padj<0.05. Genes and proteins were described by using ProteinDomainVisualizer.

4.4.4. IL-17A stimulation elevates the expression of genes involved in the regulation of inflammation and immune response and reduces expression of genes essential for metabolic regulations, NF-κB signalling prevents gene regulations induced by IL-17A

To address the impact of IL-17A on overall gene expression in hepatocytes, DE analysis was performed comparing dHepaRG cells that were treated with IL-17A with untreated control cells and FA plus IL-17A with FA stimulated cells. In line with the results obtained by DE analysis of BS1 and LIGHT, IL-17A treatment primarily regulated gene levels with a minor effect induced by additional FA stimulation (**Figure 26A, B**). Genes that were significantly elevated upon IL-17A stimulation included genes critical for the regulation of inflammatory response, such as chemokines, acute-phase proteins, and pro-inflammatory mediators e.g. LCN2 (sequesters iron, thereby limiting bacterial infections), CXCL1 (chemokine), SOD2 (clears mitochondrial ROS), CRP, SAA4 and LBP (acute-phase proteins), SLC43A2 (amino acid transporter), SERPINB4 (protease inhibitor) and VNN3 (pantetheinase associated with inflammation). Exposure to IL-17A downregulated genes implicated in metabolic, oxidant related processes and biliary cell differentiation markers including GSTA1, KRT19, CA9, CYP3A4 (oxidizes xenobiotics), NAT8 (involved in detoxification), CD36 (FA uptake protein), FABP1 (FA binding protein), HMGCS2, RGS4 (GTPase activating protein), and ATP1A2 (Na⁺/K⁺ ATPase).

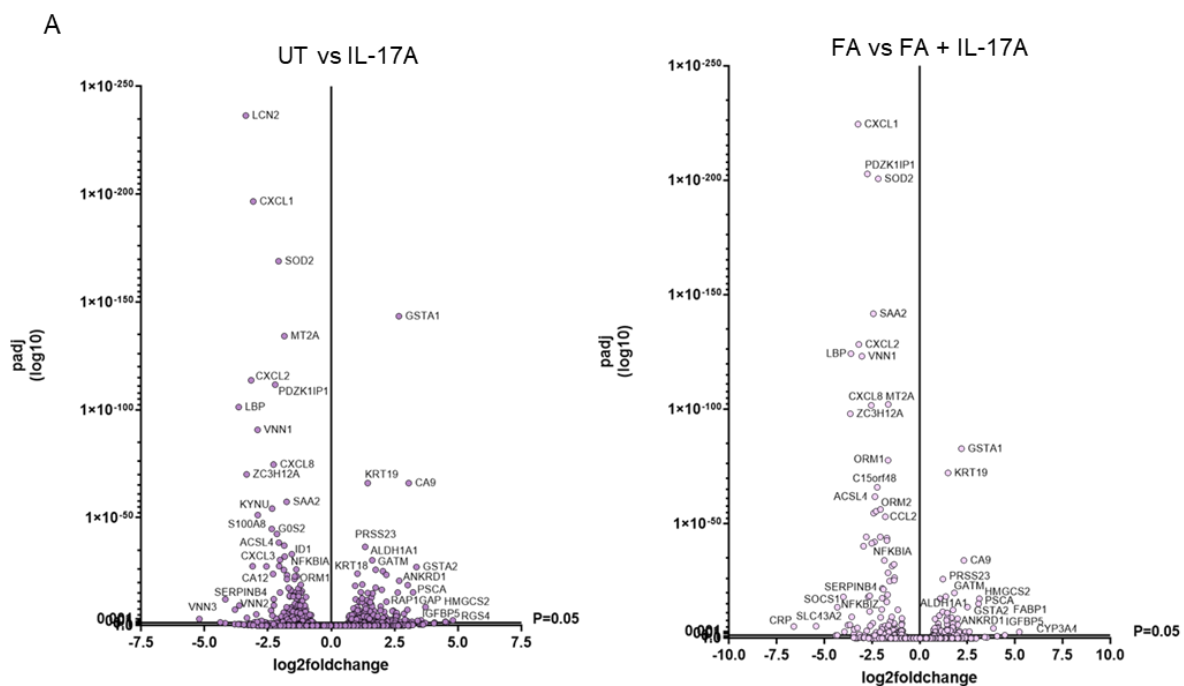
GSEA revealed elevated levels of genes involved in proliferation and inflammation included in following KEGG terms, Cell Cycle, DNA Replication, NOD-like Receptor Signalling Pathway, Oocyte Meiosis and Cytokine-Cytokine Receptor Interaction (**Figure 26C**). IL-17A treatment reduced expression of genes linked to following KEGG terms, Drug Metabolism - Cytochrome P450, Metabolism of Xenobiotics by Cytochrome P450, Extracellular Matrix (ECM) Receptor Interaction, Arrhythmogenic Right Ventricular Cardiomyopathy (ARVC), Dilated Cardiomyopathy, Valine Leucine and Isoleucine Metabolism, Cardiac Muscle Contraction, Complement and Coagulation Cascades, and Tight Junction.

In line with the RNA Sequencing data from BS1 and LIGHT stimulated cells, IL-17A exposure promoted gene expression involved in cellular response to inflammation and downregulated genes essential for the regulation of metabolic processes. IL-17A stimulation induced a specific

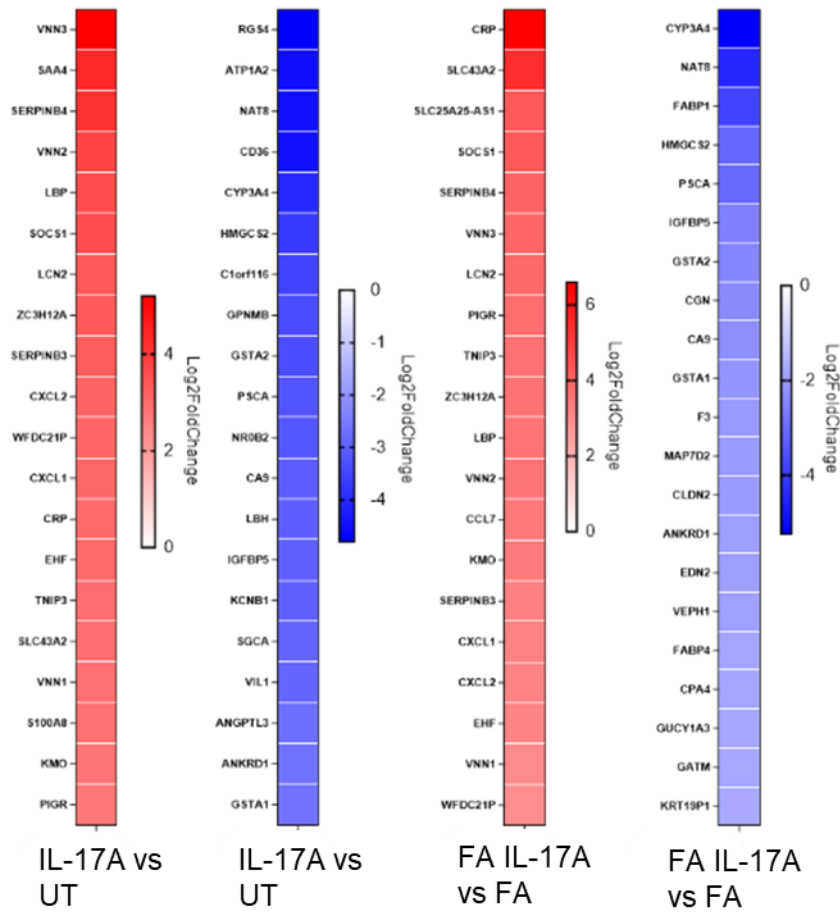
gene expression profile in dHepaRG cells, whereas the effect of additional FA treatment was minor.

Additional TPCA-1 stimulation interfered with the upregulation of genes involved in inflammatory response e.g. CXCL1 and CXCL2, SOD2, SAA, LBP, and VNN (Figure 26D). Simultaneous TPCA-1 treatment did not influence the downregulation of the biliary cell marker KRT19, or CA9, induced by IL-17A, indicating that the downregulation of these enzymes is independent on canonical NF- κ B signalling. FA stimulation with IL-17A plus TPCA-1 upregulated several metabolic associated genes including SEC11 (removes signal peptides from nascent proteins), AFR2 (during regeneration and tumorigenesis), GARS (charge tRNAs with their cognate amino acids), CYP1A1 and CYP1B1. In addition, it downregulated STMN1 (regulates of the cell cytoskeleton), HMGB2 (chromatin-associated non-histone protein involved in transcription, chromatin remodeling and V(D)J recombination), RRM2 (catalyzes the formation of deoxyribonucleotides) (Figure 26D).

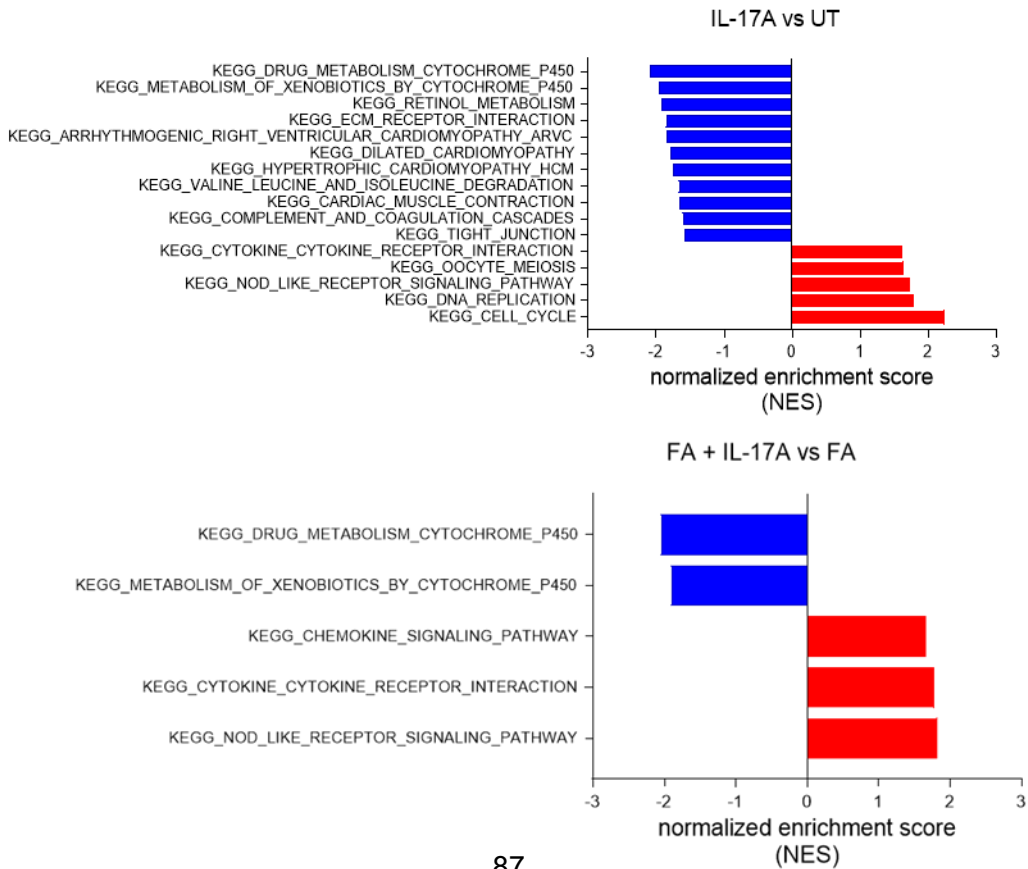
GSEA analysis showed that additional TPCA-1 stimulation upregulated genes involved in metabolic processes included in following KEGG terms Aminoacyl-tRNA Synthesis, Protein Export, Metabolism of Xenobiotics by Cytochrome P450, Retinol Metabolism, Axon Guidance. Downregulated genes were involved in replication included in following KEGG terms, Cell Cycle, DNA Replication, and Oocyte Meiosis. This demonstrated that TPCA-1 prevents inflammatory signalling, induced by IL-17A, and the downregulation of metabolism, showing the critical role of canonical NF- κ B signalling in the regulation of cellular metabolism (Figure 26E).



B



C



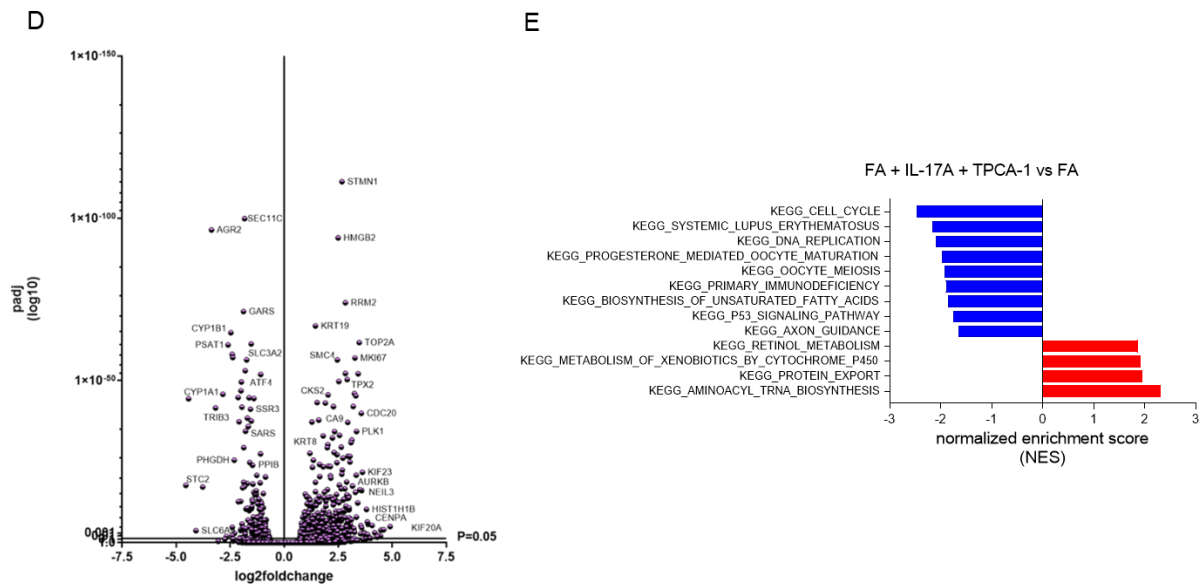


Figure 26: RNA sequencing analysis, volcano plot, heatmap, and gene set enrichment analysis (GSEA), comparing untreated and IL-17A, and FA plus IL-17A (+/- TPCA-1) treated and FA treated HepaRG cells.

DE analysis (genes ranked by log₂ fold change (log₂FC ≥ 1) and adjusted p value (padj < 0.05), (A, D) Volcano plot illustrates genes that are up- and downregulated by (A) IL-17A and FA plus IL-17A (D) and FA plus IL-17A in combination with TPCA-1 vs FA. (B) Up- and downregulated genes, ranked by log₂ fold change (log₂FC) and padj < 0.05 (C, E) GSEA, KEGG pathway analysis shows gene enrichment based on the NES and padj < 0.05. Genes and proteins were described by using ProteinDomainVisualizer.

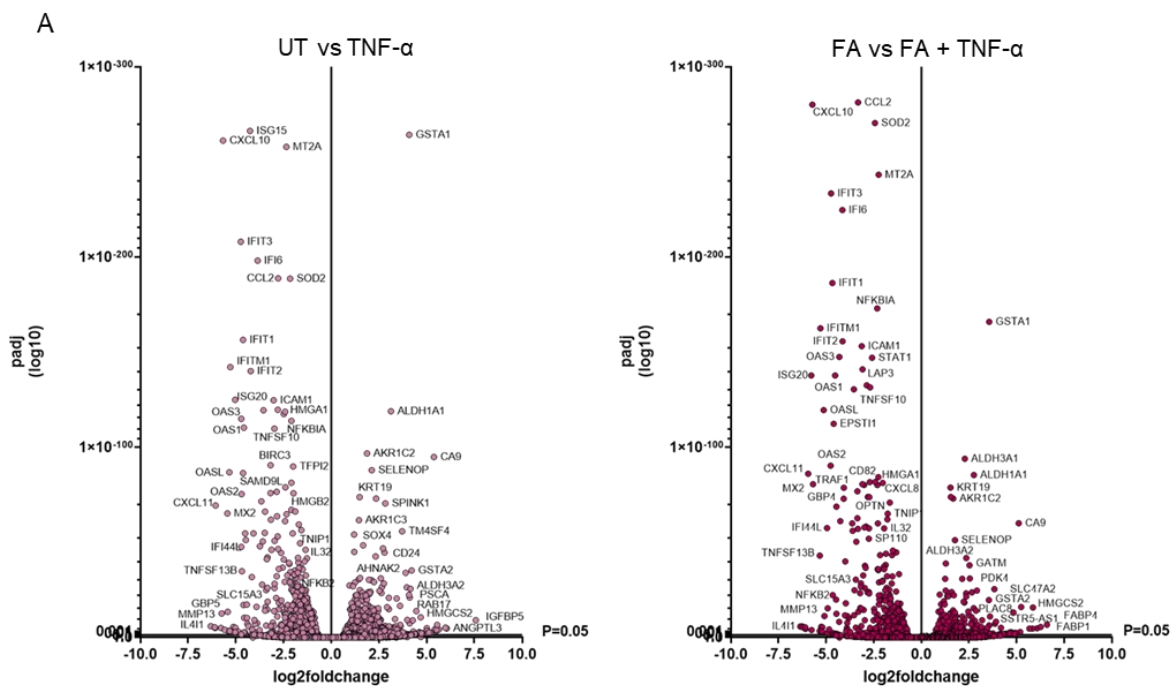
4.4.5. The pro-inflammatory cytokine TNF- α regulates gene expression of various genes critical for inflammation, anti-viral response, and metabolic processes.

To investigate the involvement of TNF- α on the regulation of gene expression in presence and absence of FAs, DE analysis was performed comparing TNF- α with untreated cells and FA plus TNF- α with FA stimulated cells (**Figure 27A**). In line with the DE analysis from the other cytokines (BS1, LIGHT, IL-17A) additional lipid stimulation showed a negligible effect on the whole gene expression regulation induced by TNF- α (**Figure 27A, B**).

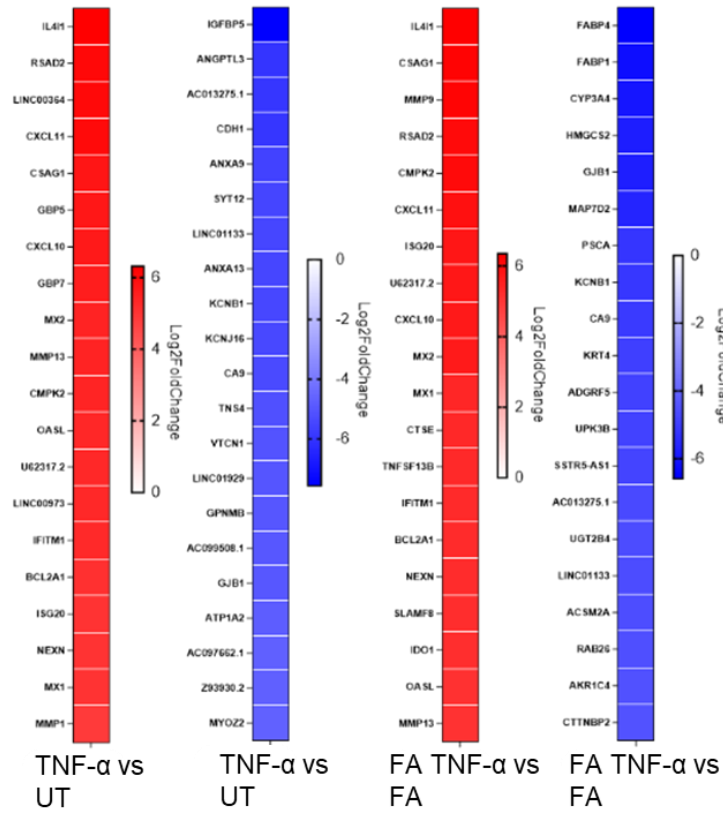
Upregulated genes upon TNF- α treatment included genes involved in regulating immune cell response, anti-viral response, inflammation, proliferation, and apoptosis. e.g. ISG15, IFIT3, IFI6, OAS3 and RSAD2 (associated with type I interferon (IFN) signalling), CXCL10, CXCL11 and CCL2 (chemokines), IL4I1 (L-amino acid oxidase enzyme, having an immunomodulatory function), MMP9, and ICAM (adhesion molecule). Genes that were significantly downregulated by TNF- α treatment included genes involved in several metabolic and oxidant processes, e.g. GSTA1, ALDH1 (aldehyde dehydrogenases), CA9, KRT19, IGFBP5, ANGPTL3 (inhibitor of lipases), CDH1 (regulates cell adhesion), ANXA9 (phospholipid binding protein), FABP4 and FABP1, CYP3A4, and HMGCS2.

GSEA revealed increased enrichment of genes implicated in following KEGG terms, Proteasome, DNA Replication, Cytosolic DNA Sensing Pathway, RIG I Like Receptor Signalling Pathway, NOD Like Receptor Signalling Pathway, Antigen Processing and Presentation, Systemic Lupus Erythematosus, Cytokine-Cytokine Receptor Interaction, Homologous Recombination, Base Excision Repair, Toll Like Receptor Signalling Pathway, Mismatch Repair, Pyrimidine Metabolism, Oocyte Meiosis, RNA Degradation, Apoptosis, Chemokine Signalling Pathway, and Small Cell Lung Cancer (**Figure 27C**). TNF- α treatment reduced the expression of genes included in following KEGG terms, Metabolism of Xenobiotics by Cytochrome P450, Retinol Metabolism, Drug Metabolism Cytochrome P450, Steroid Hormone Biosynthesis, Complement and Coagulation Cascades, Fatty Acid Metabolism Vascular Smooth Muscle Contraction, Glycolysis and Gluconeogenesis, and Butanoate Metabolism (**Figure 27C**).

RNA sequencing based DE analysis showed that TNF- α in presence and absence of lipids upregulated genes involved in regulation of immune cell response, anti-viral response (type I interferon signalling), proliferation, and apoptosis, and downregulated genes critical for oxidation processes and various metabolic pathways.



B



C

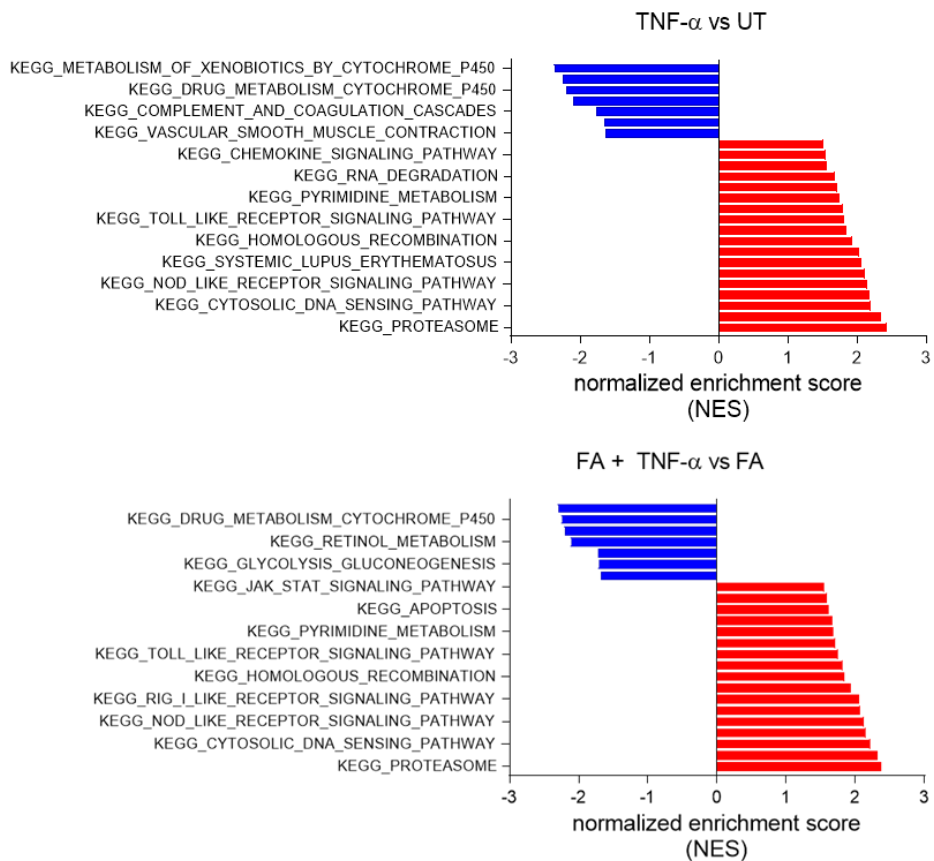


Figure 27: RNA sequencing analysis, volcano plot, heatmap, and gene set enrichment analysis (GSEA), comparing untreated and TNF- α and FA plus TNF- α treated and FA treated HepaRG cells.

DE analysis (genes ranked by log₂ fold change (log₂FC \geq 1) and adjusted p value (padj $<$ 0.05), (A) Volcano plot illustrates genes that are up- and downregulated by TNF- α and FA plus TNF- α . (B) Up- and downregulated genes, ranked by log₂foldchange (log₂FC) and padj $<$ 0.05, (C) GSEA, KEGG pathway analysis shows gene enrichment based on the NES and padj $<$ 0.05. Genes and proteins were described by using ProteinDomainVisualizer.

4.4.6. Inflammatory mediators affect expression levels of genes essential for cellular inflammatory response, proliferation, apoptosis, and regulations of major metabolic processes.

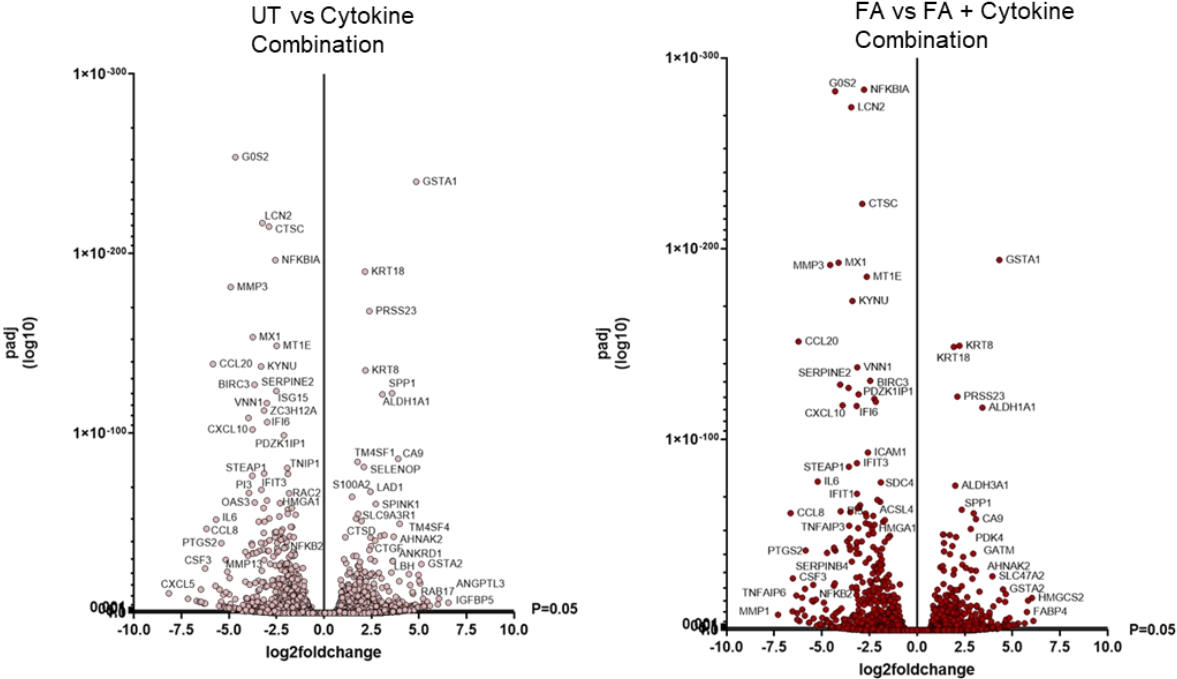
To mimic the *in vivo* situation during NAFLD to NASH progression, human HepaRG cells were stimulated with a combination of inflammatory mediators elevated and known to contribute to NASH development and progression to NASH-derived HCC⁸⁸.

DE analysis revealed that the combination of inflammatory cytokines (BS1/LIGHT, IL-17A and TNF- α) in presence and absence of FAs, increased genes involved in inflammation, immune response, TNF- α target genes and Type I IFN genes (associated with an anti-viral response), comprising G20S (involved in cell cycle regulation), NFKBIA (I κ B α , inhibits NF- κ B pathway activation), BIRC3, IL6 (pro-inflammatory cytokine), IFIT1, TNFAIP6 (a TNF signalling target gene), MMP1 and MMP12, CXCL5, CCL8, and CSF3 (**Figure 28A, B**). In addition, stimulation with the cytokine combination led to downregulation of genes necessary to maintain major metabolic processes and cell differentiation markers, e.g. GSTA1, KRT18 (hepatocyte and biliary cell marker), KRT8 (biliary cell marker), ALDH1A1, ANXA13, IGFBP5, HMGCS2, and FABP4.

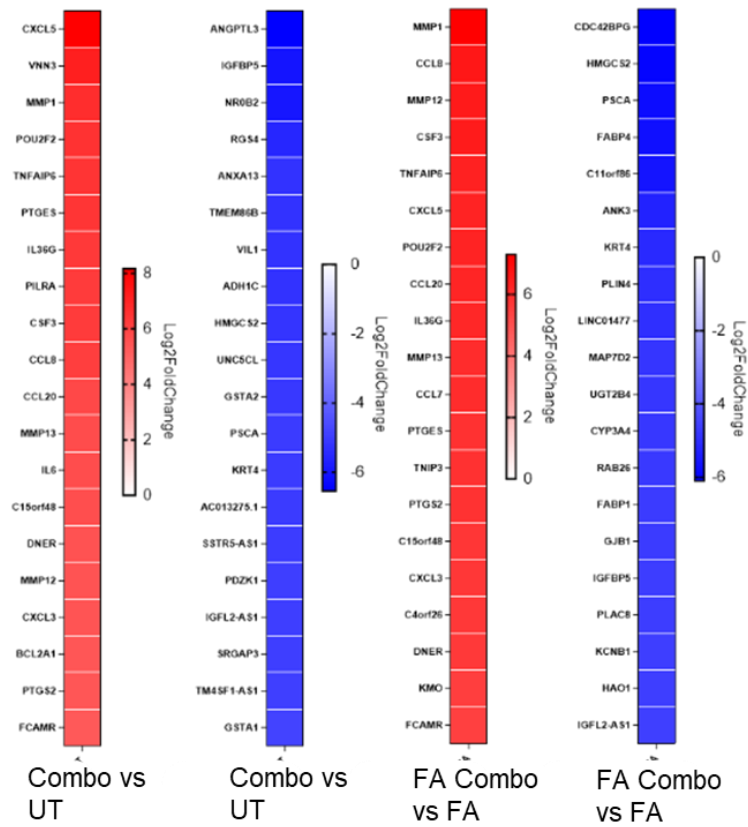
GSEA displayed increased enrichment of genes implicated in inflammation-induced cellular stress response, proliferation, and apoptosis in cells that were treated with the cytokine combination. GSEA included following KEGG terms, Cytokine-Cytokine Receptor Interaction, NOD Like Receptor Signalling Pathway, Proteasome, Chemokine Signalling Pathway, Leishmania Infection, RIG I Like Receptor Signalling Pathway, DNA Replication, Cytosolic DNA Sensing Pathway, JAK STAT Signalling Pathway, Toll-Like Receptor Signalling Pathway, Hematopoietic Cell Lineage, Homologous Recombination, Antigen Processing and Presentation, Systemic Lupus Erythematosus, Intestinal Immune Network For IgA Production, Oocyte Meiosis, Pyrimidine Metabolism, and Apoptosis (**Figure 28C**). Genes involved in overall metabolic processes were decreased by cytokine combination stimulation, included in following KEGG terms, Drug Metabolism Cytochrome P450, Metabolism of Xenobiotics by Cytochrome P450, Retinol Metabolism, Butanoate Metabolism, Histidine Metabolism, Tyrosine Metabolism, Valine Leucine and Isoleucine Metabolism, Dilated Cardiomyopathy, Complement and Coagulation Cascades, Fatty Acid Metabolism, Melanoma, Axon Guidance and Vascular Smooth Muscle Contraction (**Figure 28C**).

This analysis showed that the stimulation with the cytokine combination in presence and absence of lipids highly upregulated genes critically involved in activation of several inflammation-linked pathways and cellular stress response. Several genes essential for the regulation of main metabolic pathways were significantly decreased. RNA sequencing data clearly demonstrated that the whole gene expression profile is primarily driven by presence or absence of an inflammatory mediator inducing similar gene up- and downregulations. Additional FA stimulation only had a negligible effect in all conditions.

A



B



C

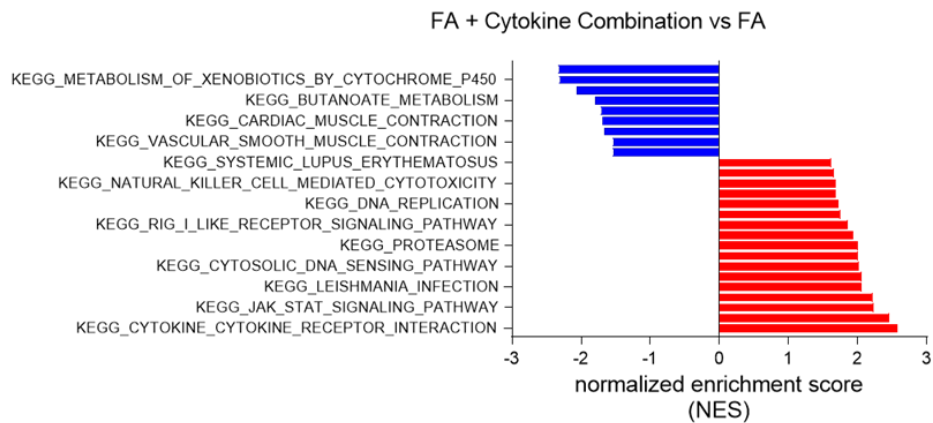
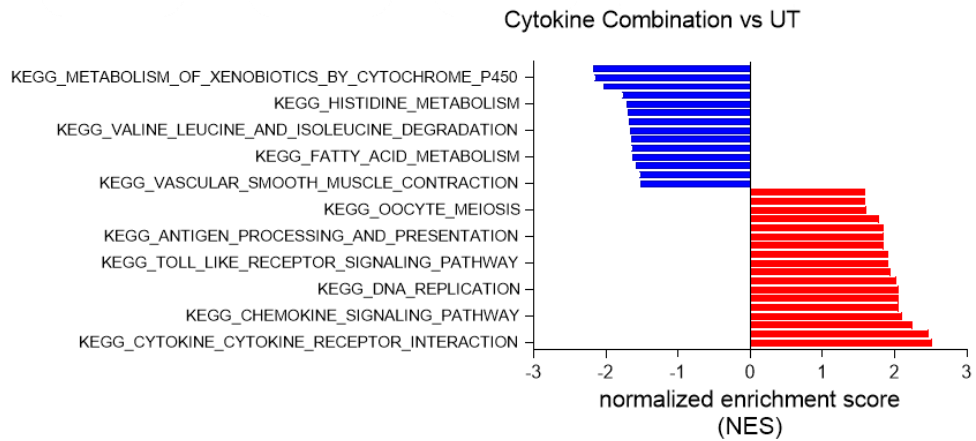


Figure 28: RNA sequencing analysis, volcano plot, heatmap, and gene set enrichment analysis (GSEA), comparing untreated and cytokine combination, and FA plus cytokine combination treated and FA treated HepaRG cells.

DE analysis (genes ranked by log2 fold change ($\log_2FC \geq 1$) and adjusted p value ($padj < 0.05$) (A) Volcano plot illustrates genes that are up- and downregulated by cytokine combination and FAs plus cytokine combination. (B) Up- and downregulated genes, ranked by \log_2FC and $padj < 0.05$, (C) GSEA, KEGG pathway analysis shows gene enrichment based on the NES and $padj < 0.05$. Genes and proteins were described by using ProteinDomainVisualizer.

4.4.7. The overall gene expression is primarily regulated by absence or presence of an inflammatory mediator

DE analysis demonstrated that gene regulation driven by inflammatory mediators (**Figure 29**). The gene expression profile of untreated control cells and cells that were exposed to FAs was similar, displayed by a comparable expression pattern. The gene expression profile of cells stimulated with BS1 or LIGHT with or without FAs more closely resembled the expression profiles of untreated and FA treated cells, whereas IL-17A, TNF- α or cytokine combination stimulated cells showed distinct profiles. The expression pattern of cells treated with IL-17A with and without FAs was distinct compared to the expression profiles induced by the other inflammatory mediators. TPCA-1 treatment prevented up- and down regulation of genes induced by IL-17A, showing that, NF- κ B inhibition prevented gene expression regulations driven by IL-17A. The expression pattern of cells stimulated with TNF- α and the cytokine combination was more similar.

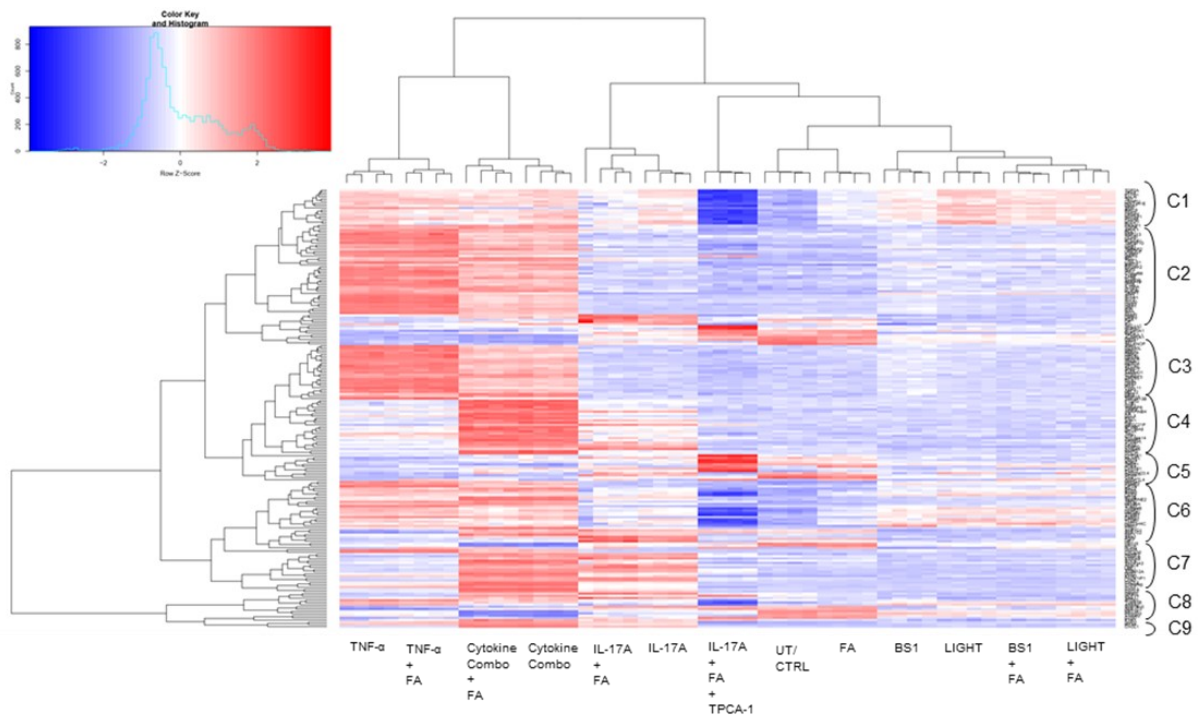


Figure 29: RNA sequencing based differential expression (DE) analysis in dHepaRG cells.

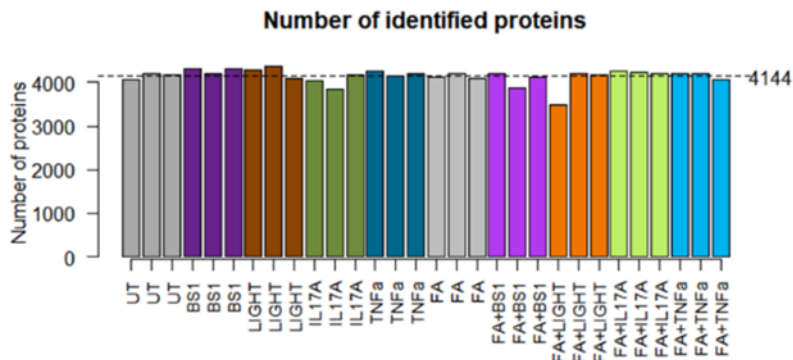
DE analysis (gene ranking based on log₂foldchange (log₂FC≥1) and adjusted p value (padj<0.05)). (A) A heatmap that illustrates genes that are up- and downregulated was divided into subclasses Class 1 (C1) – Class 9 (C9), displaying specific gene set up- and down regulations, in unstimulated, FA stimulated, and inflammatory mediator stimulated cells. Heatmap was separated into different genes classes (C), including following genes **C1**, *TOP2A*, *PLK1*, *CDC20*, *PCLAF*, *NUSAP1*, *CENPF*, *CDK1*, *BIRC5*, *SFN*, *MKI67*, *HIST1H1E*, *CENPU*, *TK1*, *ANLN*, *PTTG1*, *TPX2*, **C2**, *NNMT*, *IFIT3*, *MX1*, *IFI6*, *OAS1*, *OAS3*, *ISG20*, *IFIT2*, *IFITM1*, *IFIT1*, *TRAF1*, *PLAUR*, *ITGA2*, *IL15RA*, *IFI35*, *PARP14*, *SAMD9L*, *NT5E*, *TYMP*, *C19orf66*, *IRF1*, *H1F0*, *EIF2AK2*, *BIRC3*, *LGALS1*, *TNIP1*, *BID*, *WARS*, *ICAM1*, *UBE2L6*, *TNFAIP2*, *CD82*, *CD47*, *TNFSF10*, *PLSCR1*, *LAP3*, *SP100*, *RNF213*, *PML*, *APOL1*, *SQOR*, *PMAIP1*, **C3**, *EBI3*, *HELZ2*, *XAF1*, *CXCL11*, *MX2*, *OAS2*, *OASL*, *EPSTI1*, *TNFAIP3*, *CTSS*, *SAMHD1*, *IFI44*, *SAMD9*, *SP110*, *HERC5*, *IFI44L*, *HERC6*, *DDX58*, *GBP4*, *PARP9*, *GBP1*, *DDX60L*, *IFIH1*, *SELENOP*, **C4**, *CSF1*, *TNC*, *MT1X*, *SLC39A8*, *BPGM*, *WFDC21P*, *PI3*, *SGK1*, *PID1*, *CCL8*, *IL6*, *SERPINB4*, *TNIP3*, *TNFAIP6*, *CSF3*, *IL1B*, *PTGS2*, *TNFSF13B*, *MMP13*, *EBI3*, *HELZ2*, *XAF1*, *CXCL11*, **C5**, *SPINK1*, *AC025423.4*, *PSAT1*, *CYP1B1*, *PDK4*, *THBS1*, *AGR2*, *DDIT4*, **C6**, *TYMS*, *KPNA2*, *PSME1*, *STMN1*, *HMGB2*, *H2AFZ*, *TUBB4B*, *STAT1*, *NFKBIA*, *TFPI2*, *SERPINE2*, *MT1E*, *CKS2*, *RRM2*, *BTG3*, *RAC2*, *OPTN*, *PSME2*, *HMGA1*, *ANGPTL4*, **C7**, *IFITM3*, *SAA1*, *GDF15*, *ORM1*, *CXCL2*, *CXCL3*, *CCL2*, *C15orf48*, *CXCL8*, *LCN2*, *PDZK1IP1*, *KYNU*, *G0S2*, *ZC3H12A*, *VNN1*, *LBP*, *ACSL4*, *SLC43A3*, *SDC4*, *S100A9*, *C9orf16*, *NAMPT*, *CXCL10*, *ISG15*, **C8**, *PLIN2*, *KRT19*, *AKR1C3*, *AKR1B10*, *ANXA2*, *TUBA1B*, **C9**, *MT2A*, *IFITM3*, *SOD2*.

4.5. Proteomics analysis

4.5.1. Inflammatory cytokines affect abundance of proteins implicated in the regulation of inflammation induced cellular stress response and metabolic processes

Whole gene expression analysis, by RNA sequencing, demonstrated that inflammatory mediators induced specific expression profiles in hepatocytes with a minor effect by additional FA stimulation. To investigate the involvement of inflammation, in presence and absence of FAs, on overall protein levels proteomics analysis was performed. About 4.144 proteins were identified per sample (**Figure 30A**). tSNE plot revealed clear differences between the distinct treatment conditions (**Figure 30B**). Proteomics clustering analysis showed similar sample grouping as observed by RNA sequencing clustering analysis. Untreated, and FA treated samples clustered closely together, indicating a similar protein profile. BS1 and LIGHT samples were grouping and FAs plus BS1 and LIGHT formed groups, revealing that these two inflammatory mediators similarly affect protein levels. The formation of the other clusters was induced by IL-17A or TNF- α alone and in combination with FAs, revealing that the induction of a specific proteome was mainly driven by an inflammatory mediator. The additional presence of FA mildly affected protein levels, however more pronounced than observed by whole gene expression analysis.

A



B

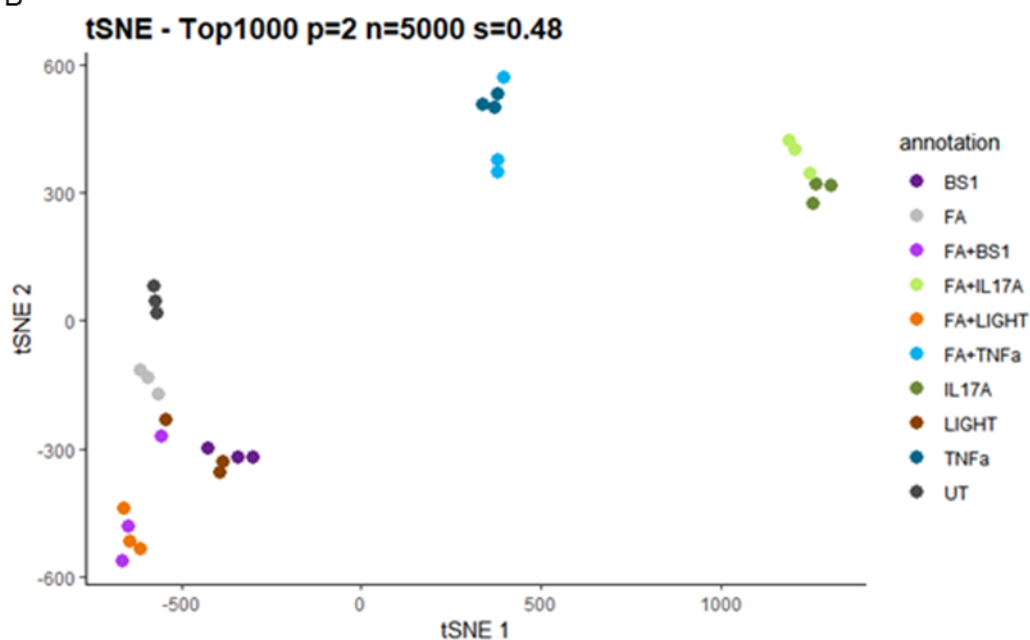


Figure 30: Proteomics analysis of dHepaRG cells stimulated with inflammatory mediators and FAs. Numbers of detected proteins, sample clustering by Euclidean distance matrix (tSNE).

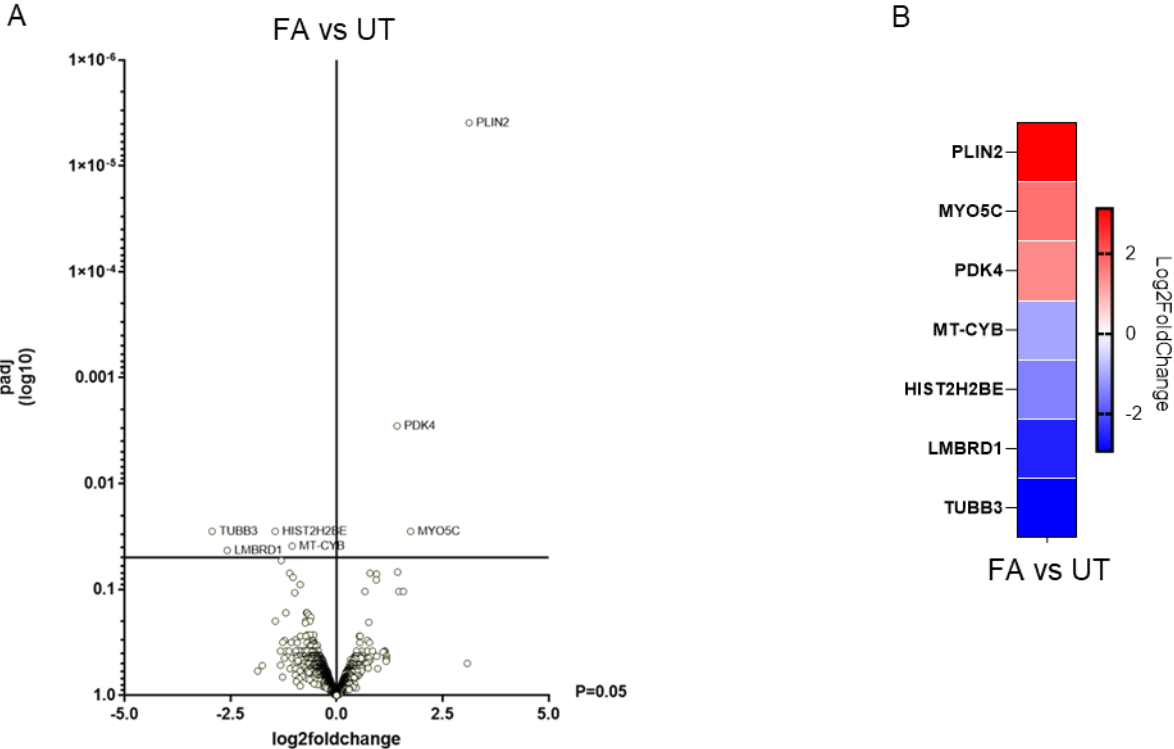
Proteomics analysis of human dHepaRG cells that were left untreated, were treated with inflammatory mediators (BS1, IL-17A, TNF- α , LIGHT), stimulated with FAs, and with FAs in combination with inflammatory mediators (FA + BS1, FA + IL-17A, FA + LIGHT, FA + TNF- α) for 24h. DE analysis (protein ranking based on \log_2 foldchange ($\log_2FC \geq 1$)). (A) On average 4.144 proteins were detected per sample, with at least 2 counts. (B) Normalized counts of proteins were used for sample clustering shown by tSNE. Proteomics analysis filtered data using for at least 2 identified unique peptides.

4.5.2. Fatty acid stimulation leads to elevated levels of proteins implicated in lipid metabolism and proliferation

To examine proteome regulations induced by FAs, inflammatory mediators, and inflammatory mediators in combination with FAs, DE analysis was performed. The regulations driven by FAs were investigated when compared to untreated (UT) control samples (**Figure 31A, B**). In line

with the RNA sequencing DE analysis, lipid stimulation influenced levels of proteins involved in FA metabolism and proliferation. Significantly upregulated proteins included PLIN2 (lipid droplet binding protein that regulates neutral lipid storage), MYO5C (involved in actin-based membrane trafficking) and PDK4 (regulates glucose and fatty acid oxidation). Significant downregulated proteins included TUBB3 (regulates microtubule formation), LMBRD1 (lysosomal cobalamin (Vitamin B12) transporter), HIST2H2BE (core component of nucleosomes, thereby involved in transcription regulation, DNA repair, DNA replication, and chromosomal stability), and MT-CYB (component of the ubiquinol-cytochrome c reductase complex (complex III) of the mitochondrial respiratory chain).

GSEA showed an elevated enrichment of proteins involved in the regulation of proliferation in FA stimulated cells (**Figure 31C**), involved in following KEGG terms, DNA Replication, Protein Export (sec-dependent protein translocation), and Ribosome (including assembly / biogenesis). In addition, proteins essential for cytokine-cytokine receptor signalling (KEGG term, Systemic Lupus Erythematosus) MAPK-, phosphatidylinositol- and calcium signalling (KEGG term, GAP Junctions), and lysosomal mechanisms (KEGG Term Lysosome) were reduced (**Figure 31C**).



C

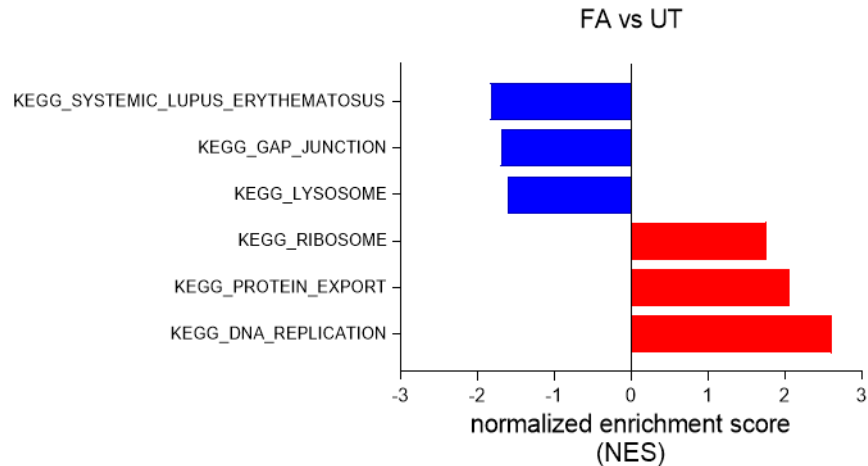


Figure 31: Proteomics analysis, volcano plot, heatmap, gene set enrichment analysis (GSEA), by Kyoto Encyclopedia of Genes and Genomes (KEGG), comparing FA treated and untreated dHepaRG cells.

DE analysis (protein ranking by log2foldchange ($\log_2FC \geq 1$) and adjusted p value ($p_{adj} < 0.05$) displayed by (A) Volcano plot. (B) Heatmap shows up- and downregulated proteins by FA stimulation, ranked by $\log_2FC \geq 1$ with $p_{adj} < 0.05$ (C) GSEA by KEGG (ranked by $NES \geq 1$) with $p_{adj} < 0.05$ (D) GSEA proteins ranked by $p_{adj} < 0.05$. Genes and proteins were described by using ProteinDomainVisualizer.

4.5.3. Exposure to the inflammatory mediators BS1 and LIGHT affects levels of proteins essential for the regulation of inflammation, proliferation, and metabolic processes

To investigate protein regulations induced by BS1 or LIGHT in presence and absence of FAs, DE analysis was performed comparing BS1 or LIGHT stimulated cells with untreated control cells, and FA plus BS1 or LIGHT treated cells with FA treated cells. DE analysis revealed that BS1 and LIGHT stimulation mainly regulated protein levels with a minor effect by additional lipid stimulation (**Figure 32A, B, D, E**). Upregulated proteins by BS1 included GBP4 (hydrolyzes GTP), MX1 (an interferon-induced GTP-binding protein), SAMD9L (regulates cell proliferation and anti-viral response), MCM2, MCM4, and MCM6 (DNA helicases, essential for replication), RRM2 (involved in the generation of deoxyribonucleotides), HMGCS1 (involved in cholesterol synthesis), NFKB2 (NF- κ B p100 precursor of p52), and DPYSL3 (involved in cytoskeleton remodeling). Downregulated proteins included PDK4, CLTB (main component of clathrin coated pits), PLIN2, RAP1GAP (GTPase activating protein), and PTS (involved in folate, vitamin B metabolism).

KEGG pathway revealed enhanced enrichment of proteins implicated in following KEGG terms, DNA Replication, Cell Cycle, Systemic Lupus Erythematosus, and Ribosome (**Figure 32C**). Downregulated proteins by BS1 included proteins and enzymes regulating e.g. endocytosis, autophagy and mechanisms essential for lysosomal processes (KEGG term, Lysosome), calcium signalling (KEGG term, cardiac muscle contraction), and proteins involved

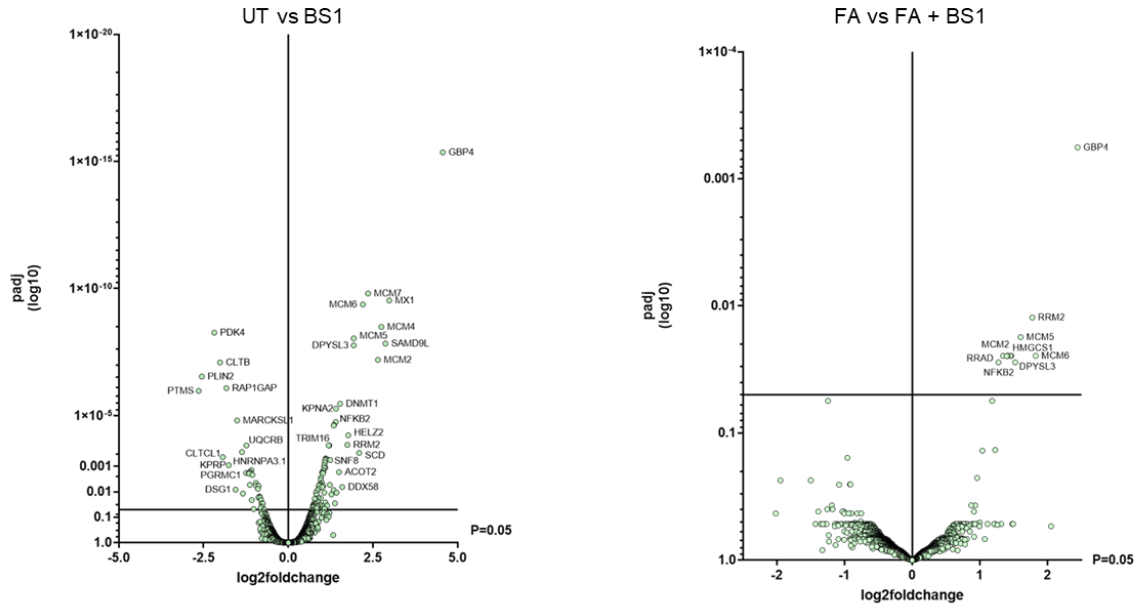
in oxidative phosphorylation (KEGG term oxidative phosphorylation), insulin- and calcium signalling, and Wnt- signalling pathway (KEGG Alzheimer disease), oxidative phosphorylation (KEGG term, Oxidative Phosphorylation), and KEGG Term and Drug Metabolism Cytochrome P450 (**Figure 32C**).

DE analysis comparing LIGHT and LIGHT plus FA stimulated with untreated and FA stimulated cells showed increased proteins levels comprising e.g. MCM4, MCM5 and MCM7 , GBP4, DPYSL3, KPNA2 (nuclear export protein), SAMD9L, HMGCS1, RRM2, and NFKB2 (**Figure 32D, E**). Decreased proteins by LIGHT treatment included PDK4, PLIN2, AHNK2 (nucleoprotein), PDCD4 (localized to the nucleus in proliferating cells), FGG and FGA (form fibrin a matrix, components of blood clots), RAP1GAP, AGT (peptide hormone), and LCN2.

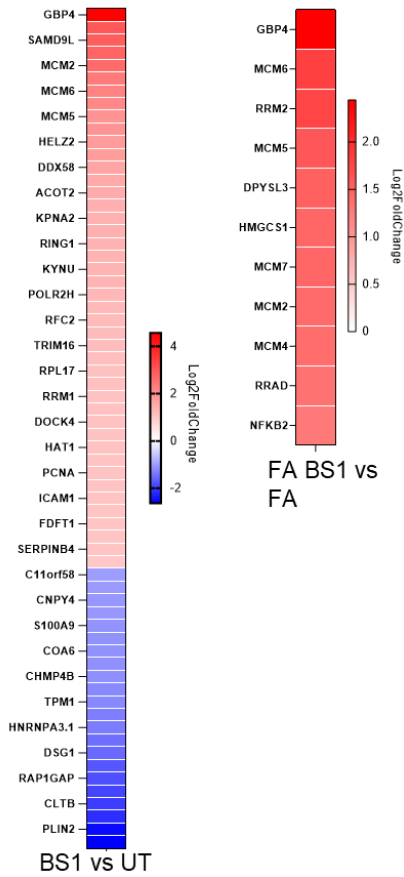
KEGG pathway analysis revealed enhanced protein enrichment implicated in cell proliferation e.g. involved in ribosome assembly / biogenesis (KEGG term, Ribosome), cell cycle regulations, MAPK signalling and DNA biogenesis (KEGG term, Cell Cycle), nucleobase biosynthesis (KEGG term, Pyrimidine Metabolism), DNA replication (KEGG term, DNA Replication), and nucleotide excision repair (KEGG term, Nucleotide Excision Repair) (**Figure 32F**). Downregulated proteins were implicated in e.g. regulation of lysosomal processes (KEGG term, Lysosome), amino acid catabolism (KEGG term, Valine Leucine, and Isoleucine Degradation), fatty acid synthesis and catabolism (KEGG term, Fatty Acid Metabolism), and oxidative phosphorylation (KEGG term, Oxidative Phosphorylation) (**Figure 32F**).

Proteomics analysis showed that protein levels were primarily regulated by absence or presence of an inflammatory mediators (BS1 or LIGHT). In line with the results obtained by RNA sequencing analysis, BS1 and LIGHT exposure increased the abundance of proteins involved in inflammatory stress response and proliferation and reduced levels of proteins involved in several metabolic processes.

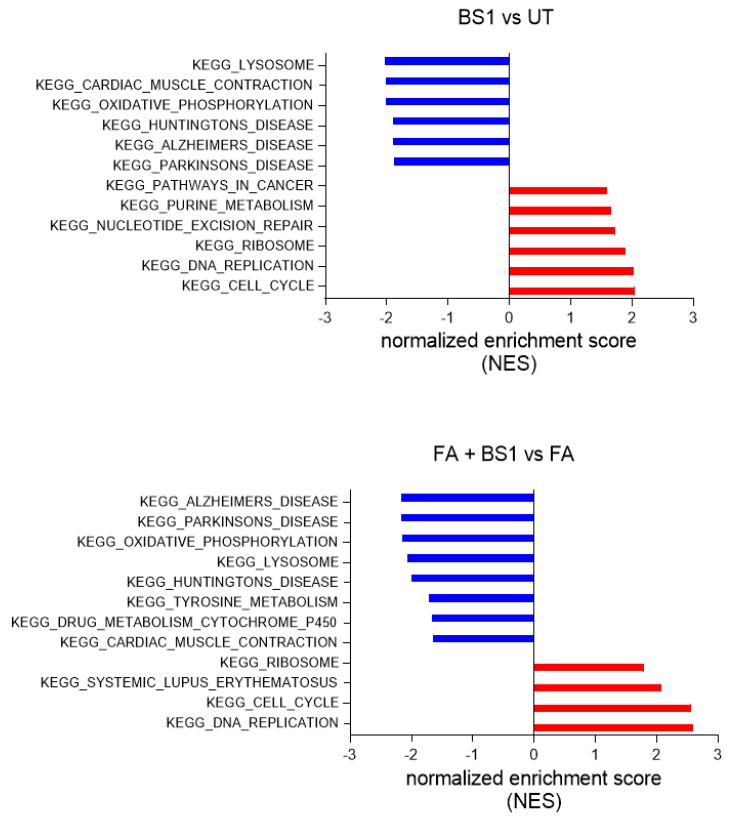
A



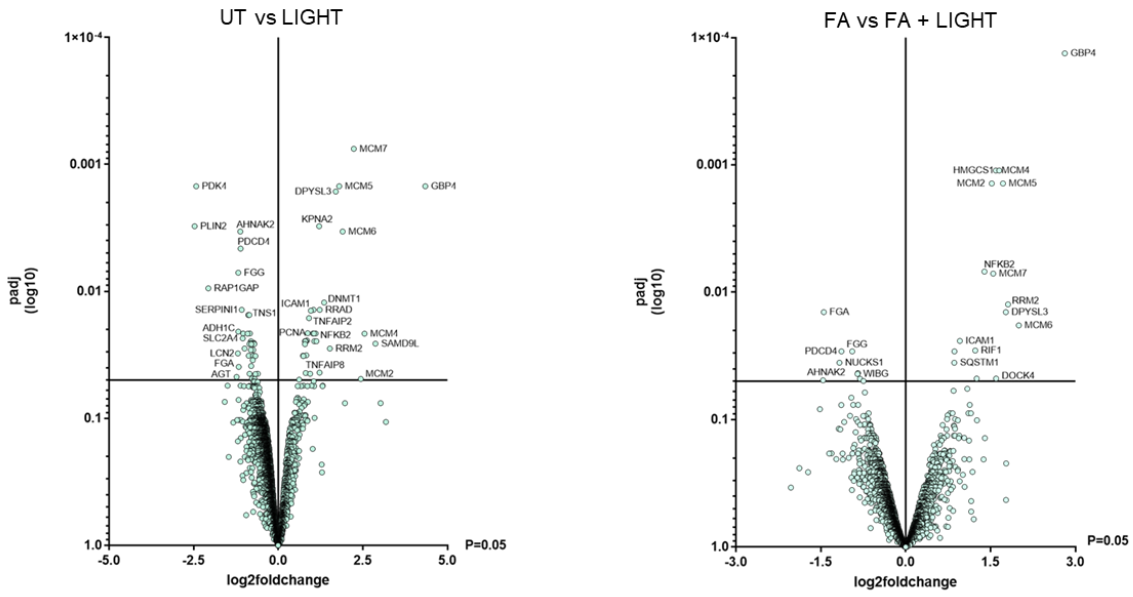
B



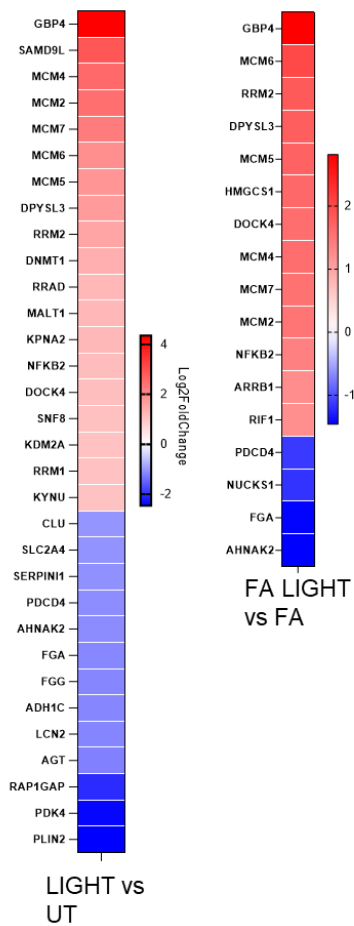
C



D



E



F

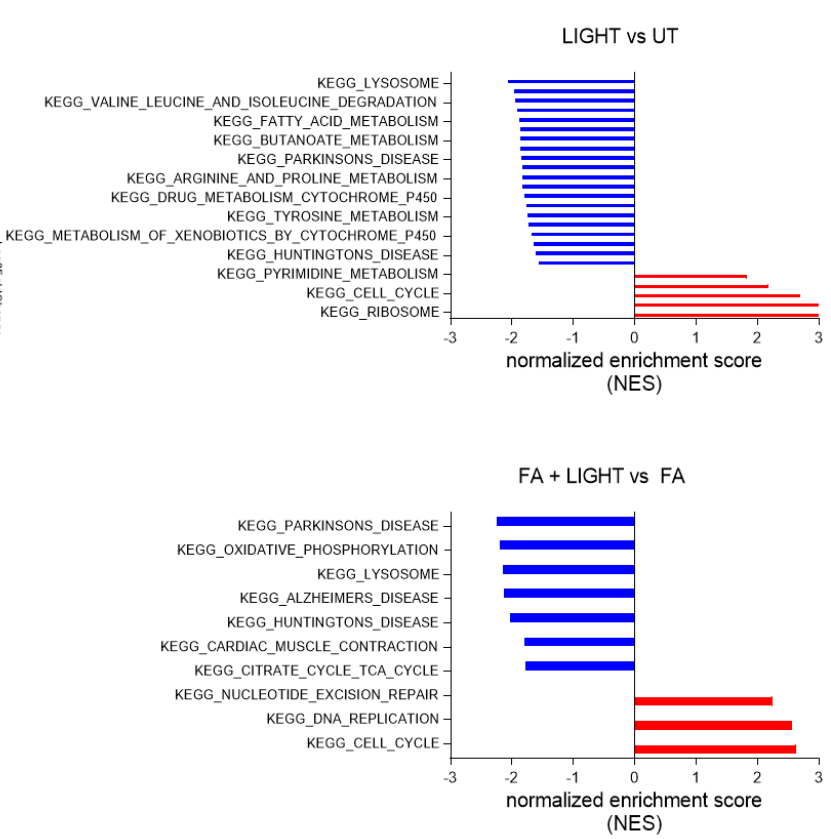


Figure 32: Proteomics analysis, volcano plot, heatmap, gene set enrichment analysis (GSEA), by Kyoto Encyclopedia of Genes and Genomes (KEGG), comparing BS1 or LIGHT and FA plus BS1 or LIGHT with FA and untreated dHepaRG cells.

DE analysis (proteins ranked by log₂ fold change (log₂FC≥1) and p value adjusted (padj<0.05) (A, D) Volcano plot illustrates proteins that are up- and downregulated by FAs and BS1 or LIGHT. (B, E) Up- and down regulated proteins, ranked by log₂FC and padj<0.05. (C, F) GSEA, KEGG pathway analysis shows protein enrichment based on the NES and padj<0.05. Genes and proteins were described by using ProteinDomainVisualizer.

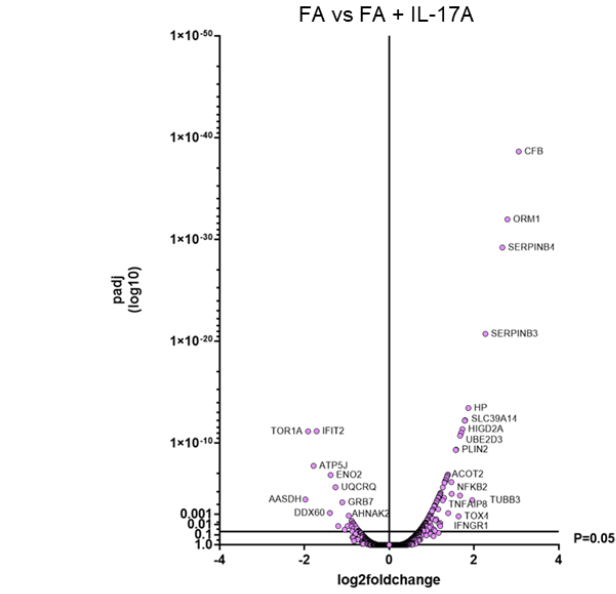
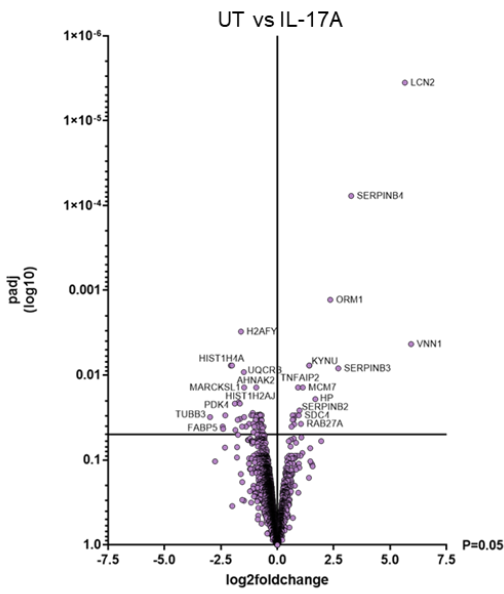
4.5.4. IL-17A stimulation affects abundance of proteins essential for the regulation of inflammation, proliferation, and metabolic processes.

To further address the influence of IL-17A in presence and absence of lipids on overall protein levels, DE analysis was performed comparing IL-17A with untreated and FA plus IL-17A with FA treated cells (**Figure 33A, B**). DE analysis displayed a similar protein regulation as observed by RNA sequencing based DE analysis. Upregulated proteins included LCN2, SERPINB3 and SERPINB4, ORM1, CFB and HP (acute phase proteins), VNN1, and KYNU (kynureninase, associated with inflammation). Down regulated proteins included H2AFY and HIST1H4A (histone proteins), UQCRB (component of mitochondrial complex III subunit), AHNAK2 and MARCKSL1 (calcium signalling and cytoskeleton regulation), TUBB3, FABP5, and PDK4.

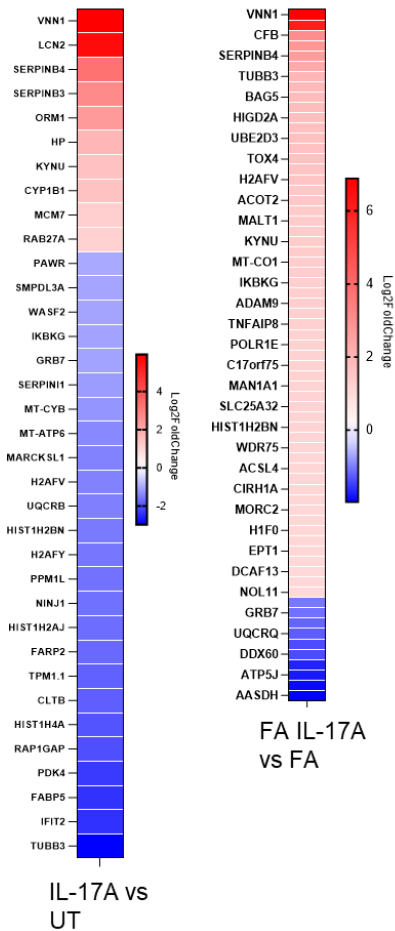
KEGG pathway analysis displayed elevated abundance of proteins in IL-17A treated cells involved in cell proliferation and general inflammatory response including following KEGG terms, DNA Replication, Protein Export and Cytosolic DNA Sensing Pathway (**Figure 33C**). GSEA showed an up regulation of proteins involved in oxidative stress induced senescence, NF-κB associated proteins (e.g. IKBKG, TNFAIP8) and several histone proteins. Downregulated proteins by IL-17A stimulation were implicated in metabolic processes included in following KEGG terms, Beta Alanine Metabolism, Cardiac Muscle Contraction, Valine Leucine Isoleucine Metabolism, Oxidative Phosphorylation, Lysosome, Huntington's Disease, Propanoate Metabolism, Small Cell Lung Cancer, Retinol Metabolism, Butanoate Metabolism and Pyruvate Metabolism (**Figure 33C**).

Overall, cell exposure to IL-17A increased the abundance of proteins involved in inflammatory stress response, proliferation and reduced levels of proteins involved in metabolic processes and histone proteins.

A



B



C

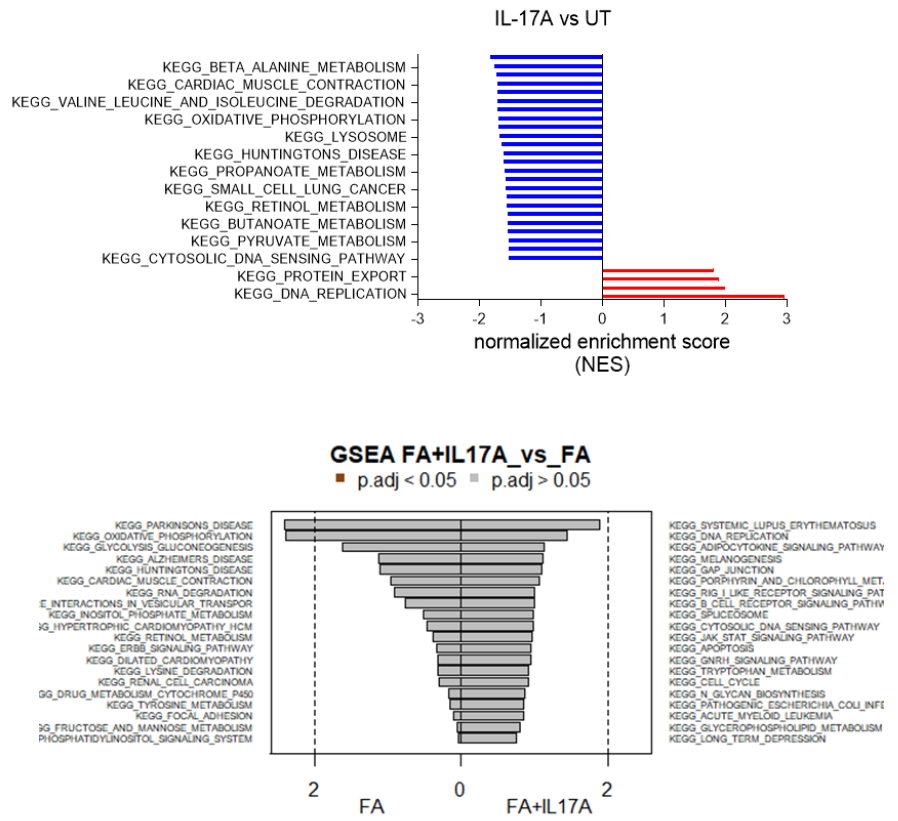


Figure 33: Proteomics analysis, volcano plot, heatmap, gene set enrichment analysis (GSEA), by Kyoto Encyclopedia of Genes and Genomes (KEGG), comparing untreated and IL-17A, and FA plus IL-17A with FA treated dHepaRG cells,

DE analysis (proteins ranked by log₂ fold change (log₂FC≥1) and p value adjusted (padj<0.05) (A) Volcano plot illustrates proteins that are up- and downregulated by FA and IL-17A. (B) Up- and down regulated proteins, ranked by log₂FC and padj<0.05, (C) GSEA, KEGG pathway analysis shows protein enrichment based on the NES and padj<0.05. Genes and proteins were described by using ProteinDomainVisualizer.

4.5.5. TNF- α stimulation increases abundance of proteins critical for the regulation of inflammation and anti-viral response and decreases proteins levels implicated in metabolic processes

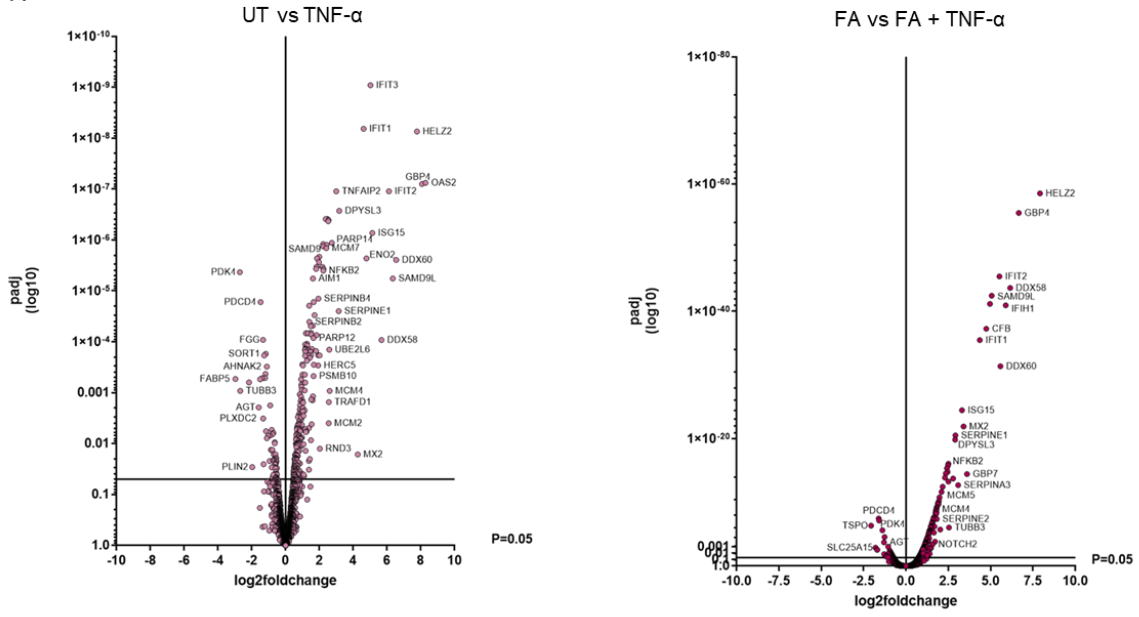
To examine the influence of TNF- α in presence and absence of FAs on overall protein levels DE analysis was performed comparing TNF- α treated with untreated cells, and FA plus TNF- α with FA treated cells (**Figure 34A, B**).

DE analysis showed that TNF- α upregulated e.g. MX, OAS1 and OAS2, HELZ2 (co-activator of PPARA), IFIT3, IFIT1 and IFIT2, GBP4, and DDX58 (involved in anti-viral response).

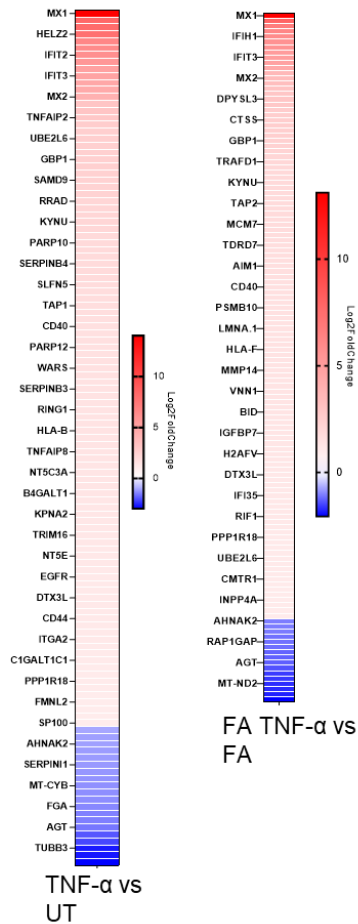
Downregulated proteins included PDK4, PDCD4, FGG, SORT1 (regulates sorting and transport of intracellular proteins), FABP5, and PLIN2. KEGG pathway analysis revealed elevated protein enrichment involved in cell proliferation and inflammation including following KEGG terms, DNA Replication, Antigen Processing and Presentation, Leishmania Infection, Proteasome, Pancreatic Cancer, Cell Adhesion Molecules Cams and Cytosolic DNA Sensing Pathway (**Figure 34C**). In addition, abundance of proteins was reduced that were implicated in regulation of oxidative phosphorylation, vitamin, and drug metabolism, included in following KEGG terms, Oxidative Phosphorylation, Retinol Metabolism and Metabolism of Xenobiotics by Cytochrome P450 and Huntingtons Disease (**Figure 34C**).

Proteomics analysis showed that inflammatory cytokine stimulation increased the abundance of proteins involved in inflammation, immune- and cellular stress response and reduced levels of proteins involved in metabolic processes, similar to RNA sequencing-based gene expression DE analysis.

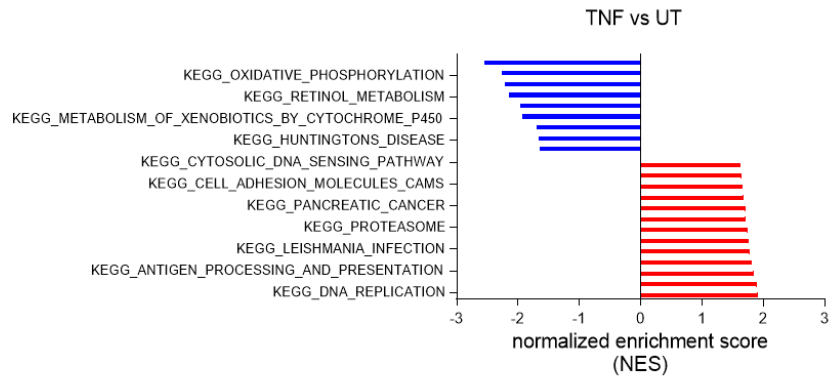
A



B



C



GO-BP: FA+TNFα vs FA

■ p.adj < 0.05 ■ p.adj > 0.05

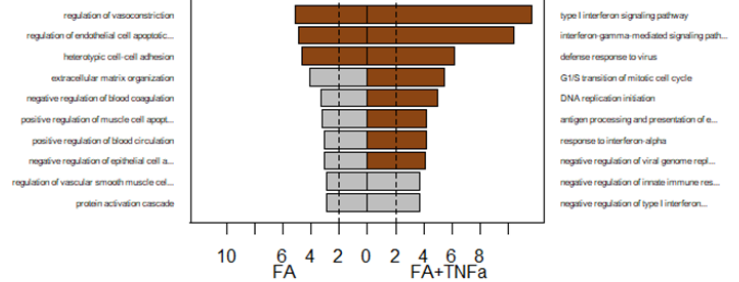


Figure 34: Proteomics analysis, volcano plot, heatmap, gene set enrichment analysis (GSEA), by Kyoto Encyclopedia of Genes and Genomes (KEGG), comparing untreated and TNF- α , and FA plus TNF- α with FA treated dHepaRG cells.

DE analysis (proteins ranked by log₂ fold change ($\log_2FC \geq 1$) and p value adjusted ($padj < 0.05$) (A) Volcano plot illustrates proteins that are up- and downregulated by FAs and TNF- α . (B) Up- and down regulated proteins, ranked by \log_2FC and $padj < 0.05$, (C) GSEA, KEGG pathway analysis shows protein enrichment based on the normalized enrichment score (NES) and $padj < 0.05$ (F)(G) Gene ontology (GO) analysis (DE). Genes and proteins were described by using ProteinDomainVisualizer.

4.6. Phosphoproteomics analysis

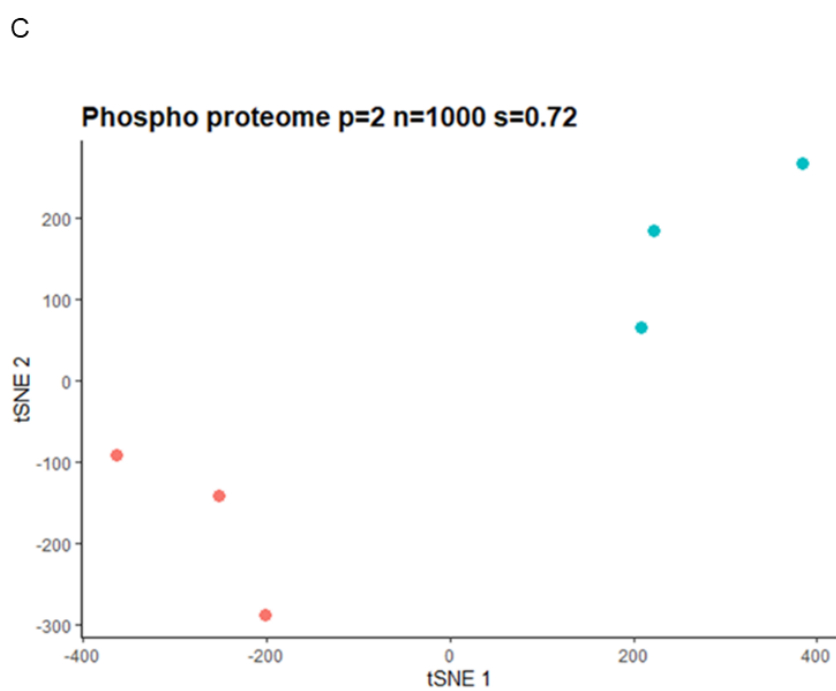
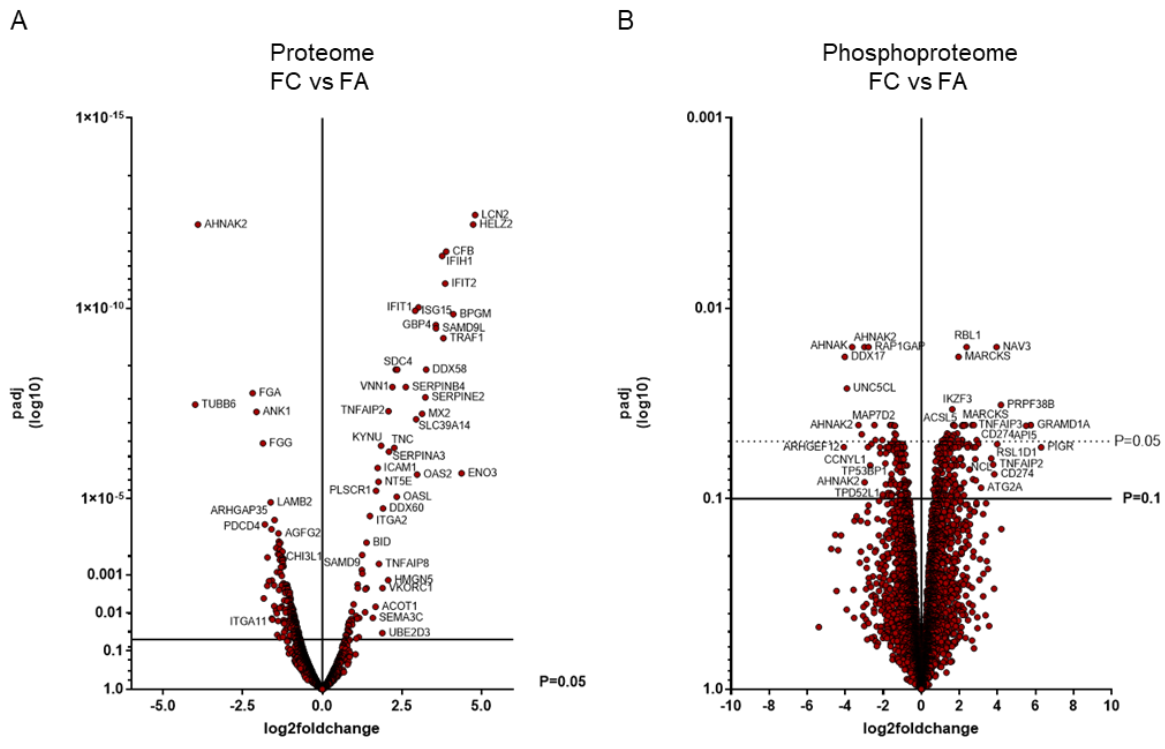
4.6.1. Inflammation affects phosphorylation of proteins involved in the regulation in programmed cell death and DNA damage response

To investigate the effect of inflammation in a lipid rich environment on signalling pathway regulation, phosphoproteomics analysis was performed comparing FA with FA plus inflammatory cytokine treated cells. Previously acquired proteomics data were used to distinguish between regulations in the phosphoproteome and changes in the total proteome (**Figure 35A, B**).

Data were normalized and samples were clustered by tSNE, displaying a clear separation of FA and FA plus cytokine stimulated cells (**Figure 35C**). DE analysis showed several significant different phosphorylation sites in FA plus cytokine treated cells when compared to FA treated cells (**Figure 35B, D**). To determine phospho site changes that are not correlating with abundance changes in the total proteome, DE analysis was performed comparing proteome and phosphoproteome (**Figure 35D**). Proteomics analysis showed elevated levels of proteins in FA and cytokine stimulated cells involved in type I interferon signalling (IFIT1, IFIT2 and IFIT3, ISG15), anti-bacterial response (LCN2), transcriptional co-activator of PPARs (HELZ2), and inflammatory mediators (TNFAIP2 and TNFAIP8). Downregulated protein where involved in blood coagulation (FGA and FGG), and cell migration (AHNAK) (**Figure 35A**).

Several phosphorylation sites were significantly changed independently of total protein abundance (**Figure 35D**). On the phospho-level, an elevated enrichment of proteins involved in apoptotic process regulation, DNA damage response, and inflammation were determined, including following significant increased phospho proteins, ACBD5 (acetyl-CoA binding protein), ACSL5 (acetyl-CoA synthetase, activates long-chain fatty acids and regulates programmed cell death), API5 (antiapoptotic protein), CLIP1 (cytoskeleton protein involved in intracellular vesicle transport), DNMT1 (DNA methyltransferase), EGFR (associated with proliferation and negative regulation of apoptosis), MAP2K4 and MAPK24 (associated with programmed cell death regulation), MARCKS (substrate for protein kinase C, binds calmodulin, actin and synapsin), NCL (regulates endocytosis and is associated with liver regeneration and negative regulation of apoptosis), PALLD (involved in cell migration), RBBP5

(responses to DNA damage), RSL1D1 (involved in the regulation of apoptotic cell death), SMARCA5 (associated with chromatin remodeling and regulation of gene expression), TNKS1BP1 (regulates DNA damage response), and XRCC1 (regulates DNA damage repair). Decreased phosphoproteins included, ARHGEF12 (positive regulator of apoptotic cell death), BIN1 (regulates cell proliferation, lipid tube assembly and positive regulator of apoptotic process), HCFC1 (cell cycle regulator), MYO18A (negative regulator of apoptotic processes), and YAP1 (associated with proliferation, DNA damage and programmed cell death) (**Figure 35D**).



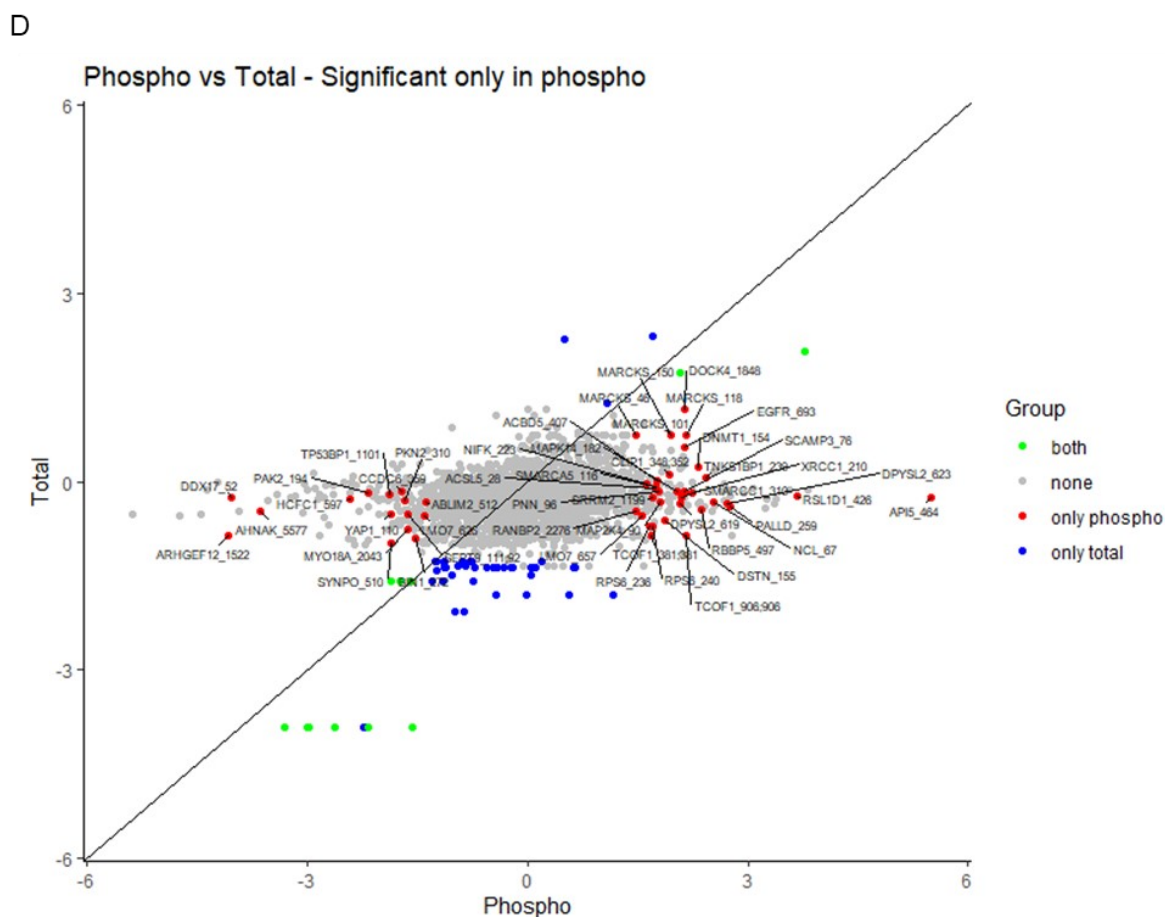


Figure 35: Phosphoproteomics analysis, volcano plot, and tSNE plot, comparing FA with FA plus inflammatory cytokine treated dHepaRG cells.

DE analysis of proteomics, proteins were ranked by log₂ fold change ($\log_2FC \geq 1$, and p value adjusted ($padj < 0.05$), and phospho proteomics, phosphoproteins were ranked by p value adjusted ($padj < 0.1$, with a $\logFC > 1$). (A, B) Volcano plot illustrates proteins / phospho sites that are up- and downregulated by FA and cytokine combination treatment. (C) tSNE based on DE analysis. (D) Total proteome versus phospho proteome. Genes and proteins were described by using ProteinDomainVisualizer.

4.7. Proteome based complex analysis

4.7.1. Inflammatory cytokines downregulate and destabilize proteins that regulate carbohydrate metabolism

To investigate the impact of protein-protein interaction and protein complex formation on the regulation of metabolic and inflammatory processes, protein abundance and protein stability were determined by thermal proteome profiling.

Untreated, cytokine stimulated, FA stimulated, and FA plus inflammatory cytokine stimulated dHepaRG cells were prepared for proteome-based complex analysis. Samples were clustered by tSNE based on abundance scores (**Figure 36A**) and on stability scores (**Figure 36B**). tSNE plot based on protein levels showed a clear group formation according to the different conditions, FA treated samples clustered together and cytokines in presence and absence of

FAs clustered together (**Figure 36A**). In contrast, tSNE plot based on protein stability did not display clear separations between the conditions (**Figure 36B**).

One-sample Limma analysis was performed to compare abundance and stability scores between the different conditions. FA stimulation significantly elevated PLIN2 abundance (**Figure 36C**), whereas protein stability was not significantly affected by FA treatment when compared to untreated control samples (**Figure 36D**). Cytokine stimulation, in absence and presence of FAs, affected protein abundance (**Figure 36E, G**) and thermal stability (**Figure 36F, H**) of several proteins, when compared to control. FAs in combination with inflammatory cytokines influenced protein stability less significantly than cytokine stimulation alone (**Figure 36H**).

To distinguish between regulations that influence protein abundance and stability, induced by FA alone, cytokines alone, and FA plus cytokines, the distinct conditions were compared with each other.

FA treatment alone showed a minor effect as only PLIN2 was significantly upregulated (up on the x-axis) (**Figure 36I**). Inflammatory cytokines affected abundance of various proteins (several up- and down regulated protein along the y-axis). The combination of FA and cytokines further enhanced or diminished the regulations induced by cytokine only (**Figure 36I**). Inflammatory cytokine treatment upregulated several proteins involved in inflammatory response, which was reduced by additional FA stimulation. Protein levels up-regulated by cytokine stimulation (up on y-axis) (FA-diminished cytokine up-regulation (upper left square, $x \leq -1$, $y \geq 1$)) included SERPINB3 (**Figure 36K**) and SERPINB4, MX1, CTSS (protease, regulates adaptive immune response, antigen processing and presentation), IFIT3, ITGA2 (cell adhesion protein), and SAMD9 (**Figure 36I**) (downstream target of TNF- α signalling). Inflammatory cytokine stimulation increased protein levels involved proliferation which was further elevated by simultaneous lipid stimulation, (up on x-axis) (FA-enhanced cytokine up-regulation (upper right square, $x \geq 1$, $y \geq 1$)) included TK1 (**Figure 36L**) (involved in regulation of proliferation, DNA biosynthetic process), TOP2A (DNA topoisomerase, essential during mitosis and meiosis for proper segregation of daughter chromosomes) and MRPL2 (involved in mitochondrial translation). Cytokine treatment downregulated proteins essential for carbohydrate metabolism which was enhanced by simultaneous FA treatment (down on y-axis) (FA-enhanced cytokine down-regulation (lower left square, $x \leq -1$, $y \leq -1$)) included UGT2B15 (**Figure 36M**) (involved in the elimination of xenobiotics and endogenous compounds), SLC2A2 (GLUT-2, glucose transporter), GUSB (involved in carbohydrate metabolic process), DPP4 (induces T-cell proliferation and NF- κ B activation) and HSD17B11 (estradiol dehydrogenase, involved in steroid metabolism). Inflammatory cytokine treatment downregulated protein essential for drug metabolism and glycolysis. Proteins that were decreased (FA-diminished cytokine down-regulation (lower right square, $x \geq 1$, $y \leq -1$))

included CYP2C8 (**Figure 36N**) (drug metabolism process), ALDOB (regulates glycolysis, fructose metabolism), OTC (regulates ammonia homeostasis, arginine biosynthesis, liver development), ADH1B (alcohol dehydrogenase), FABP4 (lipid transport protein), and PKLR (regulates glycolysis).

Several proteins displayed increased or decreased stability induced by inflammatory cytokine stimulation which was further reduced or enhanced by FA plus inflammatory cytokine stimulation (**Figure 36J**).

Increased protein stability induced by FA plus cytokine treatment when compared to FA alone (FA-diminished cytokine up-regulation (upper left square, $x \leq -1$, $y \geq 1$)) included, DNAJC9 (**Figure 36O**) (a co-chaperone of HSP70 family and p53 target), and PRRC2C (**Figure 35J**).

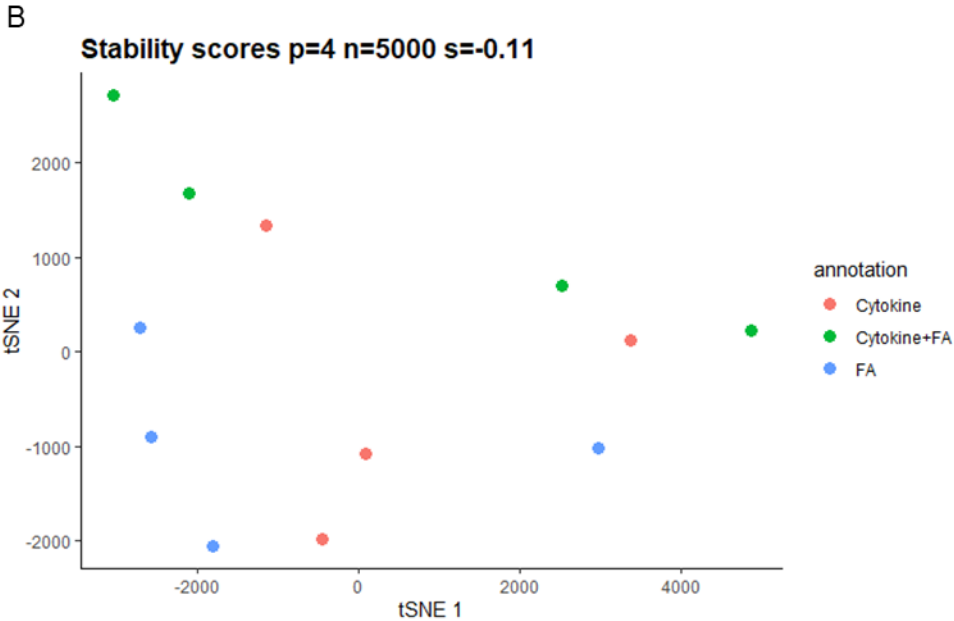
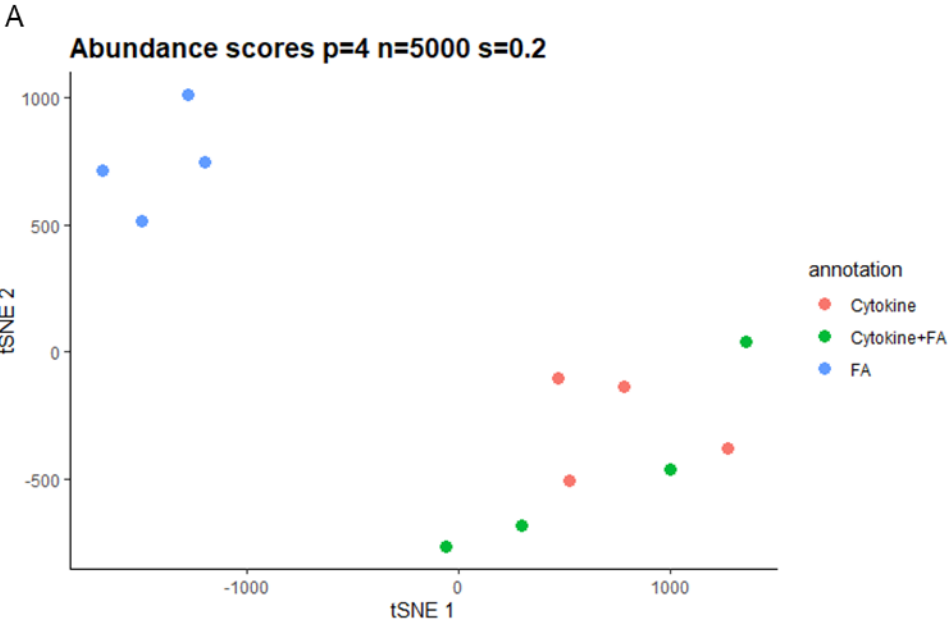
Stability of proteins enhanced in FA conditions and further up-regulated by additional cytokines stimulation (FA-enhanced cytokine up-regulation (upper right square, $x \geq 1$, $y \geq 1$)) included TST (**Figure 36P**) (regulates cyanate catabolic processes), NDUFA9 (NADH dehydrogenase, subunit of complex I of the respiratory chain), NDUFS1 (core subunit of the mitochondrial membrane respiratory chain, NADH dehydrogenase), MYO1B (**Figure 37Q**) (regulates actin filament based movement), GDAP1 (**Figure 36R**) (regulates the mitochondrial network by promoting mitochondrial fission), METTL7B (**Figure 36S**) (methyltransferase), DHRS7 (**Figure 36T**), FMO5 (**Figure 36U**) (drug metabolizing enzyme, a and involved in carbohydrate metabolism), and YKT6 (**Figure 36V**) (implicated in vesicular transport between secretory compartments).

Protein stability that was enhanced by FA stimulation and decreased by cytokines (FA-enhanced cytokine down-regulation (lower left square, $x \leq -1$, $y \leq -1$)) included PGM1 (**Figure 36W**) (catalyzes the transfer of phosphate between the 1 and 6 positions of glucose), CPQ (involved in the hydrolysis of circulating peptides), PSMC1 (26S protease involved in degradation of ubiquitinated proteins), GNAS (**Figure 36X**) (G-protein involved in GPCR signalling), TOLLIP (**Figure 36Y**) (involved in IL-1 β and TLR signalling, affects NF- κ B activation), PARVA (involved in actin cytoskeleton organization and cell adhesion), VBP1 (**Figure 36Z**) (regulates protein folding) and TALDO1 (regulates carbohydrate metabolism).

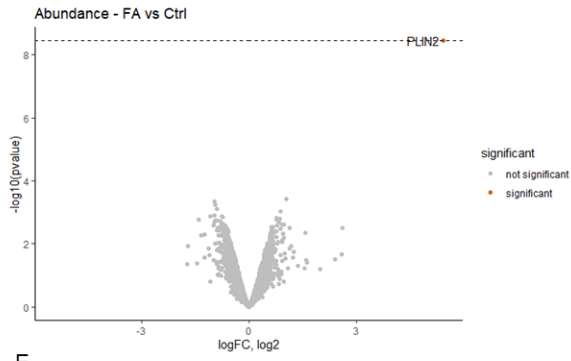
Proteins that were further downregulated by cytokine stimulation (lower right square, $x \geq 1$, $y \leq -1$) included, RPS26 (ribosomal protein), CTPS1 (involved in *de novo* synthesis of cytidine triphosphate CTP, important for phospholipids and nucleic acids biosynthesis), RPL9 (**Figure 36AA**), RPL11, RPL30 and RPL35A (ribosomal proteins), and SPTBN2 (**Figure 36AB**) (regulates actin filaments and antigen processing).

Proteome-based complex analysis showed that inflammatory cytokine treatment upregulated several proteins including proteases, which was reduced by additional FA stimulation. Cytokine stimulation increased protein levels involved in DNA-dependent proliferative processes and stabilized proteins involved in drug metabolism and the regulation of cytoskeleton organization,

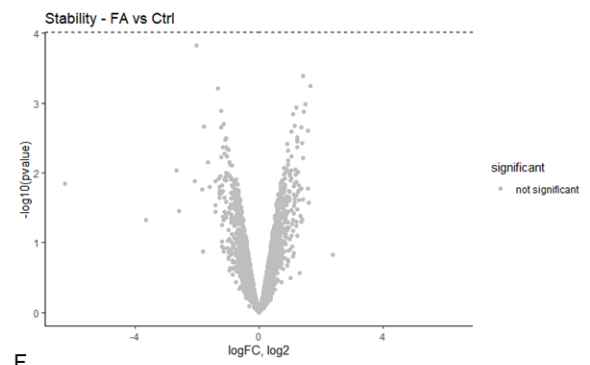
which was further enhanced by additional FA stimulation. Cytokine treatment alone downregulated and destabilized proteins essential for carbohydrate metabolism which was enhanced by simultaneous FA treatment. Inflammatory cytokine treatment downregulated protein essential for drug metabolism and glycolysis and destabilized several ribosomal proteins, which was further diminished by additional FA stimulation.



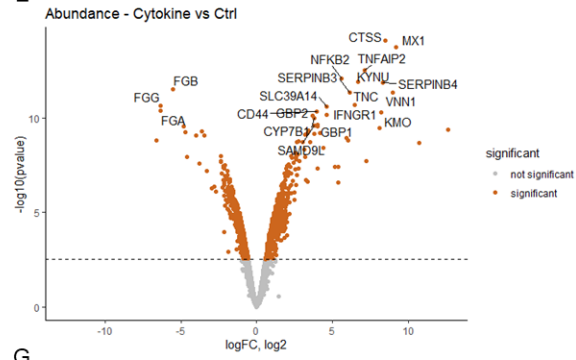
C



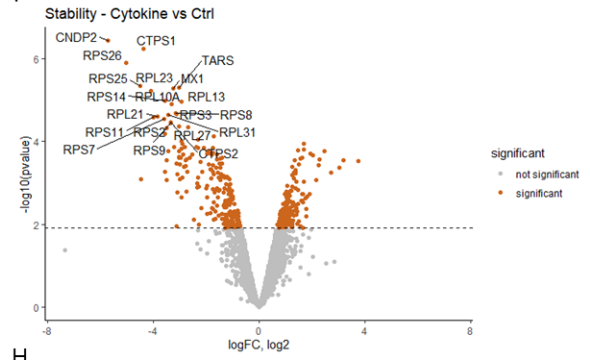
D



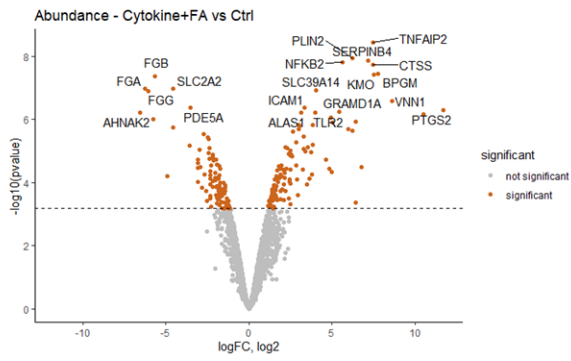
E



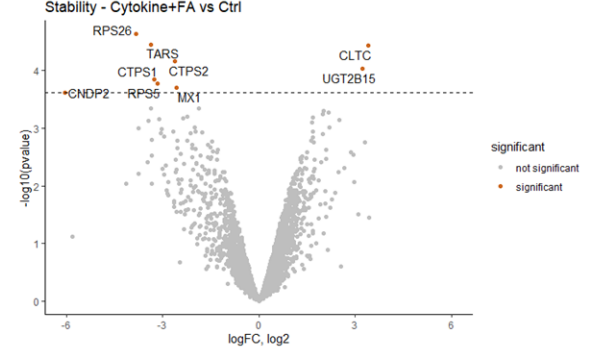
F

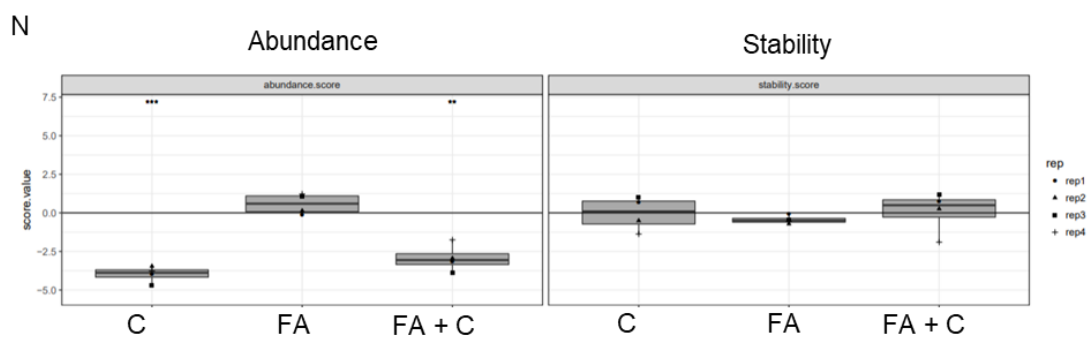
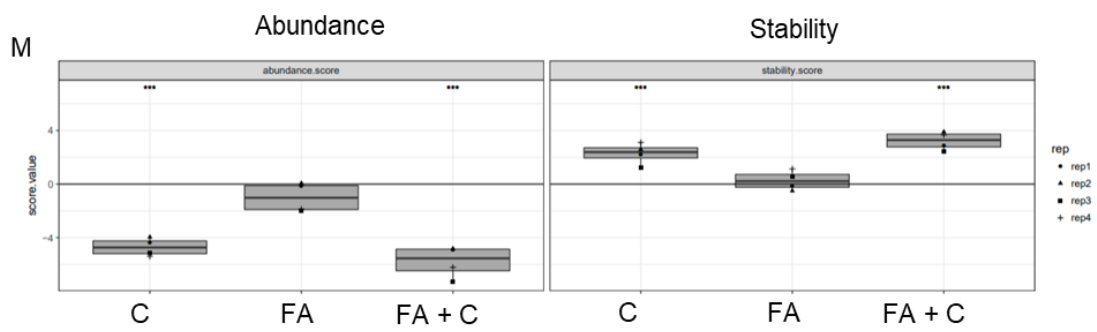
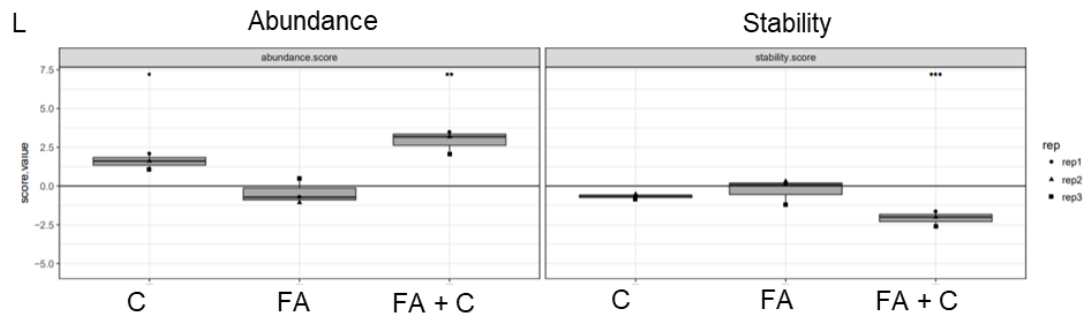
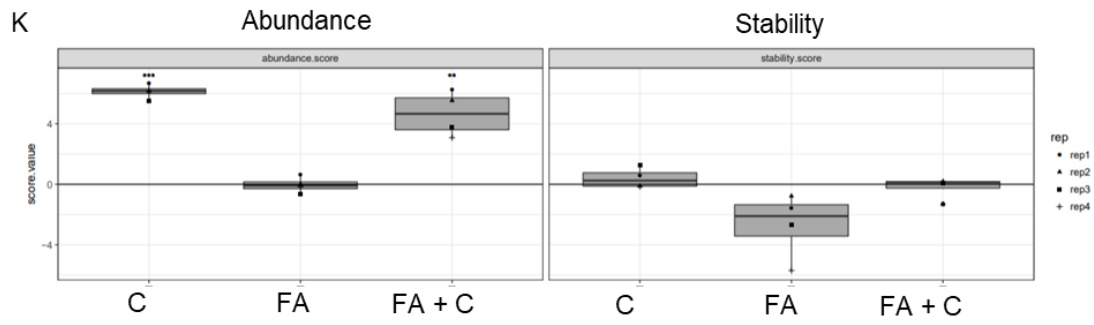


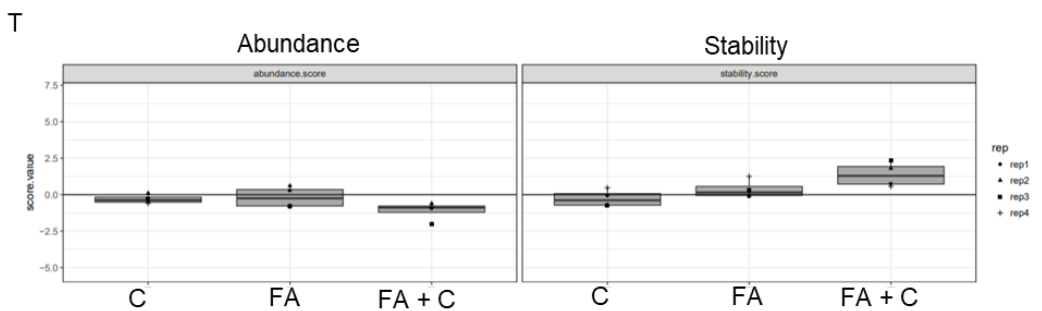
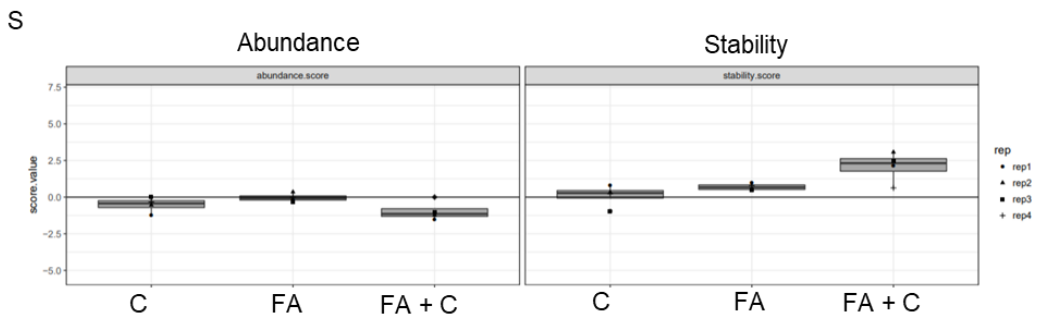
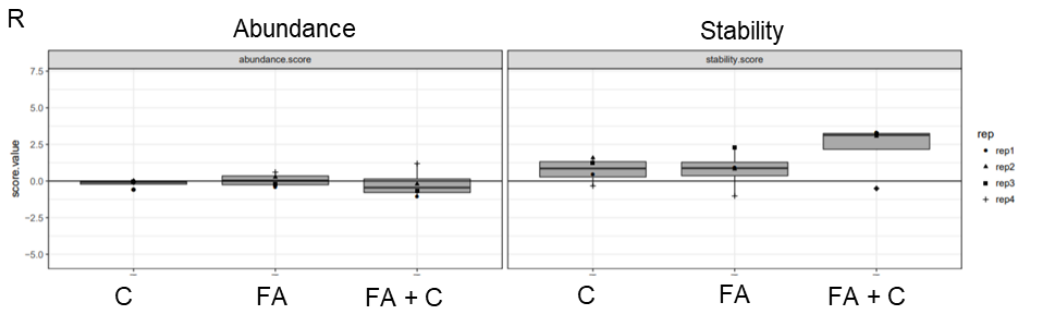
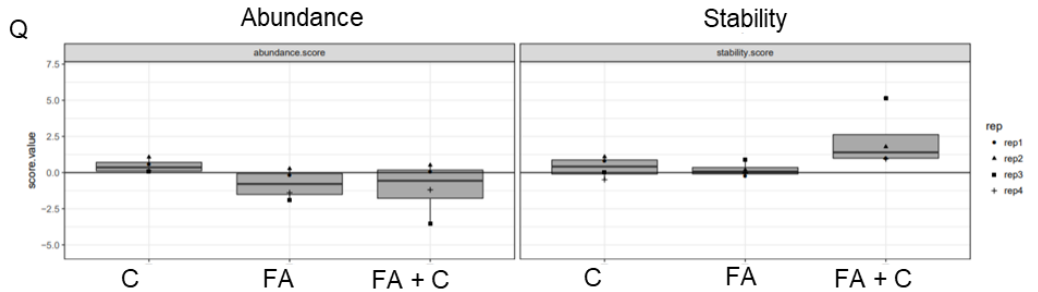
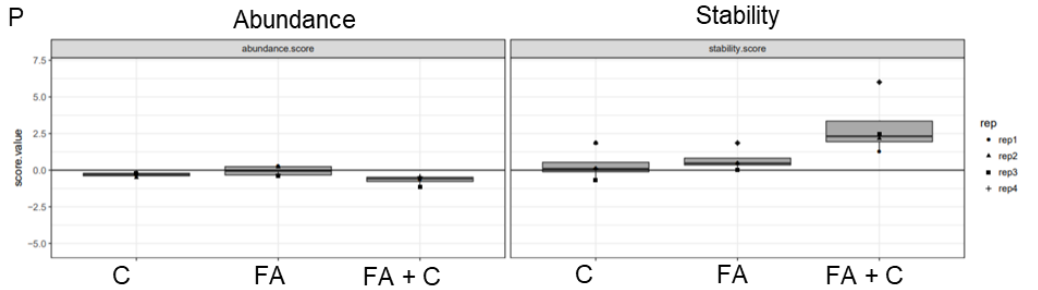
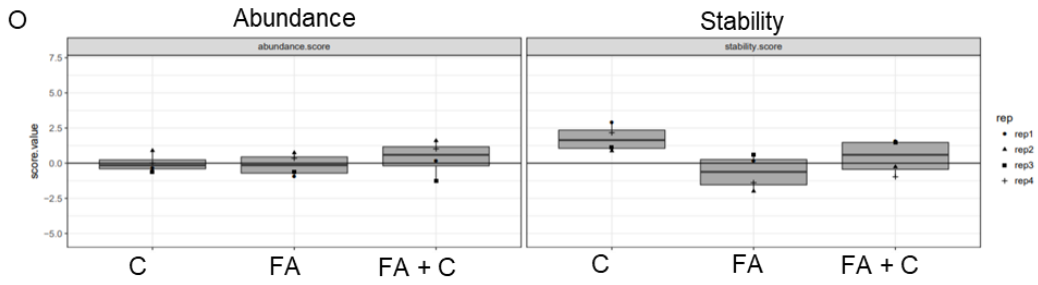
G



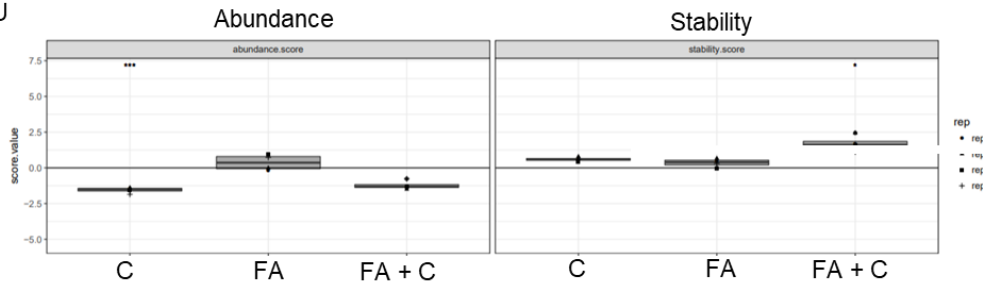
H



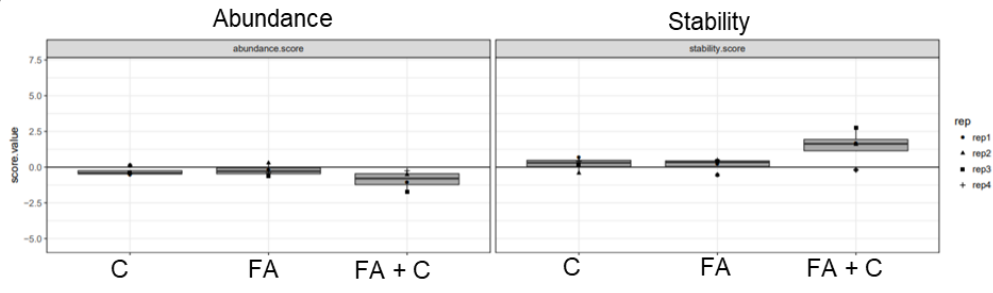




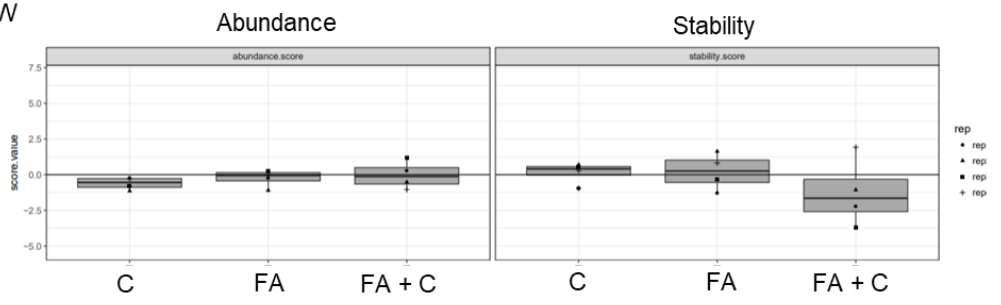
U



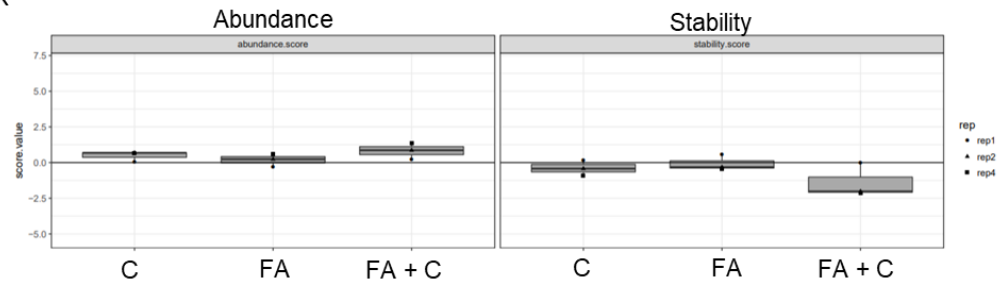
V



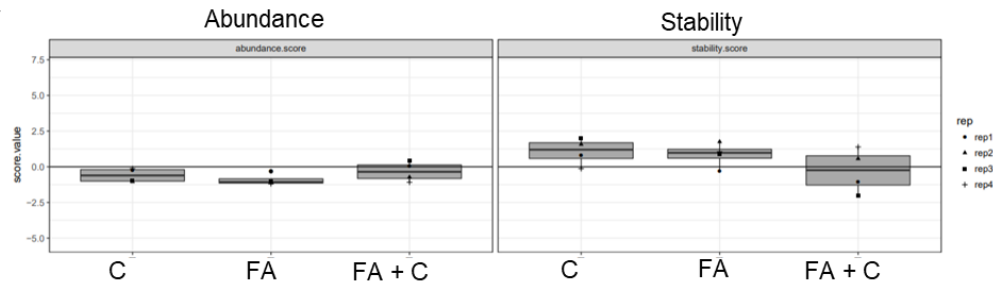
W



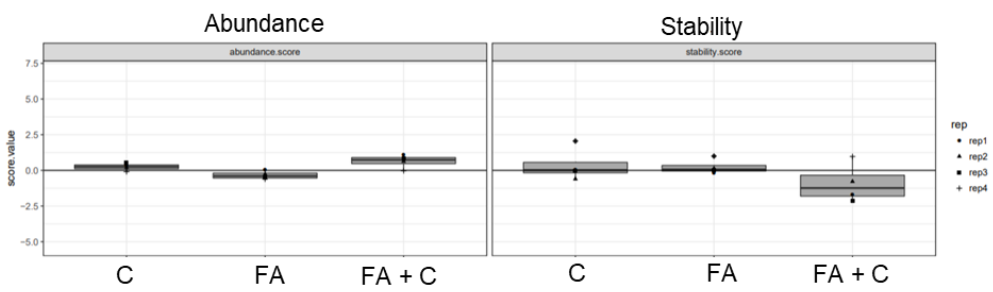
X



Y



Z



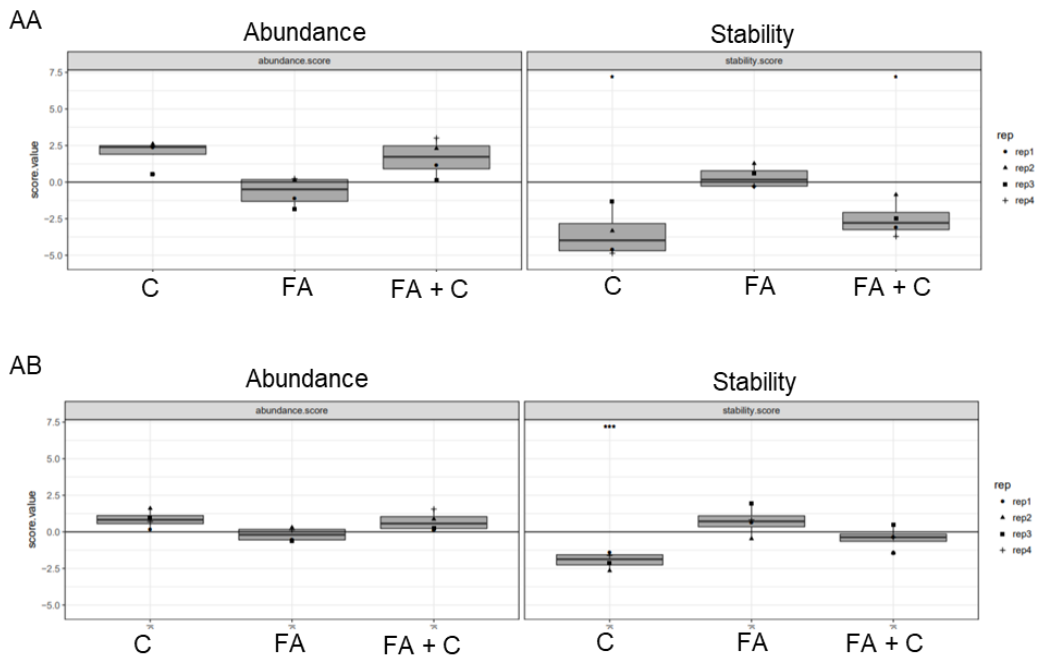


Figure 36: Proteome-based complex analysis of dHepaRG cells stimulated with inflammatory mediators and FAs.

Thermal proteome profiling in human dHepaRG cells which were untreated, treated with inflammatory mediators (BS1, IL-17A, TNF- α , LIGHT), stimulated with FAs and FAs in combination with inflammatory mediators (FA + BS1, FA + IL-17A, FA + LIGHT, FA + TNF- α) for 24h. (A, B) Normalized counts of proteins were used for sample clustering, shown by tSNE, based on (A) protein abundance or (B) protein stability. (C-J) One-sample Limma analysis to compare abundance and stability scores between the different conditions. (K-AB) Abundance and stability score of selected proteins. Genes and proteins were described by using ProteinDomainVisualizer.

5. Discussion

There has been a pandemic rise in the prevalence of obesity and metabolic syndrome, which is associated with an increase in NAFLD, the most common chronic liver disease, affecting about 25% of the population globally ^{10,140}. NAFLD includes a continuum of liver diseases and ranges from hepatic steatosis, a non-alcoholic fatty liver (NAFL), to the more severe form of disease, steatohepatitis, NASH, which can progress to cirrhosis and HCC ^{10,147,152}. Today, we know that not only NASH but the combination of ASH and NASH (BASH) also becomes more and more prevalent ⁸⁸.

Steatotic hepatocytes are in a reversible metabolic state of increased lipid accumulation and additional factors in the microenvironment such as pro-inflammatory cytokines and oxidative stress inducing steatohepatitis. The latter is characterized by exacerbated lipid storage, hepatocyte cell death, and compensatory proliferation, which promotes disease progression ¹⁶⁸. Therefore, the essential step in NAFLD development is the progression from simple steatosis to inflammation-induced steatohepatitis, including high prevalence of necroinflammation, and most likely also DNA damage. Since current treatment options are far from being efficient, the generation of a better understanding of NAFLD development is of high clinical importance.

Thus, I established an *in vitro* NASH model to discover molecular mechanisms underlying the transition from steatosis to steatohepatitis in human hepatocytes, dHepaRG cells.

Using this *in vitro* NASH model, I observed that hepatocytes take up and store FAs in LDs which induced a steatotic phenotype. The stimulation of hepatocytes with FAs and specific inflammatory mediators further increased FA storage, which was leading to intensified accumulation of intracellular LDs. This demonstrated that an inflammatory microenvironment, generated by pro-inflammatory cytokines, affected the lipid metabolic state of hepatocytes.

FA uptake and storage was induced within 1h of treatment, and further continued when stimulation was prolonged. After 24h of cell exposure to FAs, intracellular neutral lipid levels increased about threefold. At the same time FAs were used as energy source by fatty acid oxidation (FAO), observed after 3h and 24h of lipid stimulation. This revealed that FAs are constantly metabolized (FAs are taken up, are stored, and are oxidized) under normal and non-inflammatory conditions.

Further, pro-inflammatory cytokines affected FA uptake and storage immediately after 1h, observed by a significant decrease of intracellular FA levels. After 3h of stimulation the lipid levels were comparable to FA treated cells, presumably due to lipid catabolic deficiencies, determined by reduced FAO. The deficiency of FAO after 24h was further increased, which was reflected by exacerbated lipid accumulation of about six-fold, when compared to the 1h time point. Moreover, the reduced FA uptake, triggered by inflammatory cytokines, sufficed to

promote intensified lipid accumulation, showing that interference with FA catabolic processes is decisive and drives the increased steatotic phenotype in hepatocyte.

In primary mouse hepatocytes, inflammatory mediators not only affected neutral lipid levels but also the size of LDs, observed by an increase of very large (1.5-2 μ m) LDs, which induced a macrovesicular phenotype. In contrast, in dHepaRG cells this macrovesicular phenotype was markedly lower, indicating that freshly isolated primary mouse hepatocytes better recapitulate the *in vivo* situation during NASH, as a differentiated cultured cell line. However, the process of primary hepatocyte isolation and *in vitro* culture can interfere with their function, and their metabolic gene expression profile is not maintained over time, both, in murine and human hepatocytes. Therefore primary hepatocytes are only suitable for short-term metabolic experiments¹⁹⁸. dHepaRG cells were used in several studies as *in vitro* steatosis and drug metabolism model, which showed that their metabolic gene expression profile is stable and maintained, also during long-term experiments comparable to hepatocytes *in vivo*¹⁹⁹⁻²⁰³. These features designate dHepaRG cells as perfect tool to study lipid metabolism in hepatocytes.

FFAs can induce lipotoxicity in cells, thus FA storage in form of TGs in LDs was reported as protective cellular mechanism^{4,175}. It has been suggested that lipotoxicity is not only dependent on intracellular lipid levels but also on the lipid composition¹⁶.

Based on this, I addressed whether inflammatory cytokines induce a distinct lipid metabolic state, not only by increasing lipid levels but also by affecting the lipid composition, when compared to FA stimulated cells.

Lipidomic analysis demonstrated that FAs were mainly stored in TGs, but also in other lipid classes including, DGs, PLs, and GPEtns, which was further intensified, and not changed, by additional exposure to inflammatory mediators. This showed that the lipid concentration, but not the lipid composition, was affected by inflammatory mediators in hepatocytes.

Moreover, only specific, pro-inflammatory cytokines (BS1/LIGHT, IL-17A) that are elevated during NASH^{139,144} indeed induced aberrant lipid accumulation in hepatocytes. Whereas inflammatory mediators that regulate an anti-inflammatory immune response including IL-4, or control anti-viral immune responses, including IFN- γ , did not promote intensified FA storage.

Inflammation contributes to NAFLD development²⁰⁴ and the pro-inflammatory cytokines used in this study activated the canonical (BS1/LIGHT, IL-17A and TNF- α) and non-canonical (BS1/LIGHT, TNF- α) NF- κ B signalling pathway. Therefore, I investigated the influence of inflammatory cytokine induced NF- κ B activation on the lipid metabolic state in hepatocytes. The interference with canonical and non-canonical NF- κ B signalling by treatment with the IKK β inhibitor TPCA-1, or by CRISPR-Cas mediated loss of IKK β or NIK, prevented exacerbated lipid accumulation in hepatocytes and demonstrated that the NF- κ B signalling pathway affects lipid metabolism in hepatocytes by promoting FA storage into neutral lipids. This highlights the

critical role of a pro-inflammatory environment, and activation of inflammatory pathways (NF- κ B) on the development of steatohepatitis (NASH).

Mitochondria are key metabolic organelles for ATP production by oxidization of lipids, through oxidative phosphorylation. During ATP synthesis an electrochemical gradient is generated, resulting in the formation of a transmembrane potential and ROS⁶⁸.

Mitochondria are critically involved in NAFLD development^{182,183}. To adjust to elevated intracellular lipid levels during disease development, mitochondria increase FAO, which is associated with elevated ROS production. Increased ROS decreases respiratory chain function, and ATP-synthesis and is leading to incomplete FAO, which results in accumulation of toxic lipid intermediates, and can induce apoptotic cell death, associated with decreased transmembrane mitochondrial potential¹⁸⁵⁻¹⁸⁷.

Thus, I investigated the influence of FAs and pro-inflammatory cytokines, on mitochondrial morphology, function, and superoxide production.

I demonstrated that FA stimulation alone did not influence mitochondrial morphology when compared to untreated control cells after 24h of stimulation. However, intracellular lipid accumulation in FA treated cells, correlated with elevated mitochondrial superoxide production. In addition, mitochondrial function was influenced by pro-longed (48h) FA stimulation, which was determined by decreased mitochondrial membrane potential. This showed that chronic FA exposure increased lipid levels, FAO, and ROS production, which then affected mitochondrial membrane potential, and induced mitochondrial depolarization.

In addition, the pro-inflammatory cytokines (BS1/LIGHT and TNF- α), without FAs, also reduced mitochondrial membrane potential, revealing that FAs and inflammatory cytokines can independently interfere with mitochondrial function. The impact of FAs is presumably due to increased ROS production, induced by ongoing and elevated FAO, whereas inflammatory cytokines downregulate lipid catabolic genes and antioxidants, observed by gene expression analysis, which can also trigger elevated ROS. Further, pro-inflammatory cytokines (such as TNF- α) might directly induce pro-apoptotic TNFR signalling, which is also reflected by mitochondrial dysfunction.

FAs in combination with inflammatory mediators decreased FAO and changed mitochondrial morphology, shown either by a breakup (BS1/LIGHT), or hyperfusion (IL-17A) of the mitochondrial network. Increased intracellular neutral lipid accumulation promoted mitochondrial superoxide production, which was both intensified by additional inflammatory cytokine stimulation. In addition, the stimulation with FAs and BS1, LIGHT and TNF- α , induced mitochondrial membrane depolarization after 24h and exposure of hepatocytes to FAs and IL-17A or the cytokine combination promoted mitochondrial hyperpolarization. Pro-longed treatment for 48h with all inflammatory mediators promoted mitochondrial depolarization, showing that mitochondrial dysfunction is dependent on the primary signalling pathway

activation and the duration of exposure to the different cytokines and lipids. Thus, inflammation can induce mitochondrial dysfunction either directly (after 24 hours), and presumably apoptotic cell death, or a pre-apoptotic phenotype which can shift to apoptosis at prolonged treatment after 48h²⁰⁵. This demonstrates that FAs and cytokines can independently trigger mitochondrial stress, which is exacerbated by their combination.

In addition, simultaneous anti-ROS treatment did not prevent increased lipid storage, indicating that elevated ROS production is a secondary effect of elevated lipid storage.

Further, only pro-inflammatory cytokines influenced mitochondrial polarization, the anti-inflammatory cytokine IL-4 did not induce mitochondrial dysfunction.

I tested the effect of inflammatory cytokine activated NF- κ B signalling on mitochondrial function, which showed that interference with activation of the canonical NF- κ B pathway prevented mitochondrial depolarization and ROS production.

Mitochondrial dysfunction can trigger apoptotic cell death^{186,187}. Therefore, I studied the effect of FAs and inflammatory cytokines on apoptotic cell death and associated compensatory proliferation. Exacerbated inflammation-induced lipid storage triggered both apoptosis and proliferation, however inhibition of apoptosis by a pan-caspase inhibitor did not influence increased lipid storage.

These data demonstrate that mitochondrial dysfunction, apoptotic cell death and compensatory proliferation are most likely a consequence of increased lipid accumulation, induced by inflammatory cytokines, in a NF- κ B dependent manner. In addition, I determined that this lipid-induced cellular stress response further induced replication stress and increased DNA damage, mimicking NAFLD pathogenesis.

Overall, the data indicate that the essential step in NAFLD development is the pro-inflammatory cytokine-induced exacerbated lipid accumulation, which subsequently affects cellular physiology, metabolic functions, and cell viability. Thus, investigating the underlying molecular mechanisms of inflammation triggered aberrant lipid metabolism in hepatocytes is critical for the identification of potential treatment options.

Therefore, I set out to perform transcriptomics and proteomics analysis to disentangle regulations in hepatocytes that were induced by FAs alone, by inflammatory cytokines, and by FAs in combination with pro-inflammatory cytokines.

Whole gene expression analysis by RNA sequencing and proteomics analysis, demonstrated that FA stimulation regulated the expression of only few genes and proteins, when compared to untreated control cells. This can be partly explained by the fact that lipid metabolic processes are regulated by enzymes and gene or protein abundance is not reflecting the impact of FAs on enzyme function. Thus, the examination of enzyme phosphorylation, interaction with other enzymes or proteins, or quantification of their substrates and final product represents a more sensitive read out.

The expression of genes and proteins that are involved in metabolic processes, mostly PPAR- α targets, including genes and proteins that regulate FA- uptake, transport, storage, oxidation and LD metabolism, was increased by FA stimulation, revealing on-going lipid metabolic processes in hepatocytes. In addition, FA treatment lead to an upregulation of genes and proteins that regulate cell proliferation.

RNA sequencing analysis demonstrated that the overall gene expression was primarily regulated by respective inflammatory mediators (BS1/LIGHT, IL-17A, TNF- α , and the cytokine combination), whereas additional FA stimulation showed a negligible effect.

Omics (transcriptomics and proteomics) analysis showed that all inflammatory cytokines used in this study induced similar gene- and protein up and downregulation. However, some regulations were also distinct and cytokine specific, revealing their primary pathway activation and subsequent target gene transcription.

Heatmap- and sample clustering analysis (by tSNE and PCA) showed that gene regulations induced by BS1 and LIGHT were similar to FA treated and untreated cells. In contrast, the expression profile induced by IL-17A was distinct to the other conditions. TNF- α and cytokine combination treated cells showed a comparable expression profile.

All pro-inflammatory cytokines alone or in combination with FAs induced the expression of genes and proteins involved in cellular stress response, inflammation, immune response, proliferation, and apoptosis.

An analysis comparing transcriptomics and proteomics showed that most proteins which were significantly regulated on proteome level were also significantly regulated on expression level. However, on the transcriptome level, more genes showed significant differential expression. In addition, the up-regulations on proteome and transcriptome were more correlative than the downregulations. This analysis revealed that FA stimulation leads to a significant upregulation of PLIN2 and PDK4 on both, gene and on protein level, whereas all inflammatory cytokines induce the upregulation of NFKB2

Further, the activation of LT β R signalling via BS1/LIGHT highly induced the upregulation of genes involved in inflammation, apoptotic cell death regulation and proliferation including BIRC3, TRAF1, and MMP7. IL-17A stimulation increased the expression of genes involved acute-phase response, including acute-phase proteins, SAA and LBP, in immune response, including chemokines such as CXCL1 and CXCL2, and general inflammatory response such as, VNN1, SOD2, and LCN2. The highest upregulated genes upon TNF- α treatment included genes associated with type I IFN signalling such as ISG15, IFIT3 and IFI6, but also chemokines such as CCL2. The cytokine combination clearly mirrored the gene expression of each single cytokine but also induced a distinct regulation and highly increased genes implicated in cell cycle regulation such as G02S, and regulators of NF- κ B signalling including NFKBI.

I observed that inflammatory cytokine stimulation downregulated genes and proteins induced by FAs, including PPAR- α target genes such as PDK4, showing that inflammatory signalling interferes with lipid metabolic pathways in hepatocytes. Moreover, PPAR- α expression levels were not affected by FA stimulation, indicating that the reduction of PPAR- α target genes is not regulated by decreased levels of the transcription factor itself.

Importantly, inflammatory cytokines not only affected regulations of genes and proteins associated with FA metabolism but also with genes and proteins essential for the regulation of overall metabolic processes, including genes and enzymes of the oxidant system, involved in oxidation of xenobiotics, ketogenesis, amino acid metabolism, vitamin metabolism, cholesterol metabolism, phospholipid metabolism, glucose metabolism and ethanol metabolism. Genes that were significantly downregulated by all cytokines (BS1/LIGHT, IL-17A, TNF- α , and the combination of all cytokines) included KRT19 (a biliary cell marker), GSTA1 (a detoxification enzyme), and CA9 (a metalloenzyme, catalyses the hydration of carbon dioxide).

This demonstrates that proinflammatory cytokines not only decrease the expression of metabolism associated genes and proteins but also of cellular differentiation markers such as keratins (KRT19), revealing that inflammatory cytokines also affect cellular differentiation.

Phosphoproteomics showed an enrichment of phospho-proteins involved in apoptotic process regulation, DNA damage response, and inflammation.

Inflammation influences whole cellular metabolism, and the gene expression of hepatocytes is rapidly changed (within hours) by inflammatory cytokines. After 90 minutes of inflammatory cytokine stimulation, hepatocytes showed elevated expression of inflammation-related genes (NFKB2) and downregulation of metabolic associated genes (PDK4). However, how metabolic genes in FA plus inflammatory cytokine treated cells are regulated, remains elusive.

The overall downregulation of cellular metabolism upon inflammation hints towards a conserved mechanism because it affects several proteins and enzymes essential to maintain hepatic metabolism.

One possible mechanism could be that the activation of the inflammatory pathway (NF- κ B) interferes with the upregulation of metabolic genes, thus their expression levels are kept comparable to untreated cells. Further, the stimulation with inflammatory cytokines alone already decreases gene levels associated with cell metabolic regulations, indicating that downregulation of metabolic genes proteins must be an active mechanism.

Decreased expression of metabolism-associated genes (including FAO, lipolysis and cholesterol metabolism) was also observed in a preclinical NASH mouse model ¹⁴⁴, but the molecular regulations on how inflammation affects cellular metabolism remained unclear.

One hypothesis is that activated inflammatory signalling pathways compete with metabolic signalling pathways. NF- κ B and nuclear receptors such as PPARs are part of the family of primary, rapid acting transcription factors that are present in cells in an inactive state and do

not need to be newly synthesised for activation^{104,206}. This allows for a fast response to distinct stimuli¹⁰⁷. FA stimulation activated PPAR- α , and inflammatory cytokine stimulation activates the NF- κ B pathway, therefore simultaneous activation of both signalling pathways might lead to a competition of e.g. DNA binding sites, co-activators, or co-transcription factors. Due to the ubiquitous presence in cells, primary and rapid acting transcription factors might interact with each other influencing their activation status.

Ligand activated PPAR- α can regulate target gene transcription by direct binding to promoter site of target genes. Other mechanisms include binding to co-transcriptions factor that can activate target gene transcription or by interaction with other proteins that can induce signal transduction and can activate transcription factors that can then bind to target gene promoter sites⁶³. Thus PPAR- α target gene transcription can be influenced by several factors. One possibility is the inhibition of PPAR- α binding to promoter sites by either blocking the target site or by protein-protein interaction or protein complex formation.

Based on this, I performed a protein-based complex analysis with untreated, FA stimulated and FA plus inflammatory cytokine stimulated cells. This protein thermal profiling demonstrated that inflammatory cytokines intensified FA increased stability of proteins involved in mitochondrial respiration and biosynthesis, proteins involved in drug metabolism and the regulation of cytoskeleton organization. In addition, FA-induced increased thermal stability of proteins was reduced by inflammatory cytokines. Cytokine treatment alone downregulated and destabilized proteins essential for carbohydrate metabolism, which was enhanced by simultaneous FA treatment, destabilizing several ribosomal proteins. However, protein interactions can have activating, or inhibitory functions and, thus they can be indicative for positive and negative downstream regulations. Proteome based-complex analysis data showed that there was no transcription factor interaction, however transcription factors are often thermally unstable.

The specific targeting of enzymes critically involved in lipid metabolic processes was inconclusive and will need further detailed experimentation.

For example, the loss of PPAR- α , induced by CRISPR-Cas mediated KO, did not affect lipid accumulation in FA and FA plus inflammatory cytokine stimulated cells (see in Appendix I.I). Interference with PPAR- α activation by additional treatment with an antagonist increased lipid accumulation comparable to FA and cytokine stimulated control cells. Thus, inactivation of PPAR- α promotes a similar lipid metabolic phenotype as induced by inflammatory cytokines. Thus PPAR- α activation status might be affected by inflammatory cytokine stimulation and interference results in downregulation of enzymes essential for FA uptake, transport, and importantly catabolic processes such as FAO. PPAR- α antagonization in FA and cytokine stimulated cells showed no additional effect, indicating that cytokine stimulation already inhibits PPAR- α activation and therefore simultaneous inactivation has no impact. However, PPAR- α

agonization did not prevent increased lipid levels in FA and inflammatory treated cells. Lipid levels in FA stimulated cells remained unchanged, indicating that FAs already activate PPAR- α thus and additional agonization is non effective. This suggests that inflammation induced aberrant lipid storage is not regulated by PPAR- α activation (see in Appendix I.II).

Loss of PPAR- α by si-RNA mediated KD also resulted in increased lipid levels in FA stimulated cells comparable to additional cytokine stimulation. FA plus inflammatory cytokine treated cells displayed comparable lipid levels as the control. PDK4 loss induced elevated neutral lipid accumulation in both FA and FA plus inflammatory cytokines indicating an additional effect.

Omics analysis clearly demonstrated that not only genes and proteins involved in lipid metabolic processes are affected by inflammatory cytokines. Thus, molecular mechanisms that can influence the transcriptional activity of several metabolic genes in response to external and / or internal changes must be involved in this process, such as epigenetic regulations.

The term epigenetics includes heritable changes in gene expression that are not mediated by alterations within the DNA. Changes in the environment can affect epigenetic regulations, and modifications ²⁰⁷. Main epigenetic mechanisms that regulate chromatin accessibility for transcription factors and RNA polymerase, and are associated with gene silencing include, DNA methylation, histone modification and non-coding RNAs ^{208,209}. Inflammatory cytokines can influence epigenetic regulations in cancer ²¹⁰. An inflammatory tumour microenvironment can activate NF- κ B which then interacts with the epigenetic modifier histone deacetylase 1 (HDAC1) to form a gene-silencing complex, affecting gene expression ²¹¹. Metabolic changes in cancer cells can be controlled by epigenetic mechanisms ²¹²

A recent study addressed the transcriptional regulation during liver regeneration, which demonstrated that chromatin accessibility in repopulating hepatocytes was increased in the regulatory regions of genes promoting proliferation and decreased in the regulatory regions of genes involved in metabolism ²¹³.

Thus, the hypothesis is that inflammatory cytokines might regulate gene expression in hepatocytes through epigenetic mechanisms.

Based on this, I performed epigenetic experiments to investigate the influence of inflammatory cytokines on chromatin accessibility by H3K27ac-ChIPSeq analysis and ATAC-sequencing (data not shown). These experiments are ongoing and will pave the way whether epigenetic regulatory mechanisms are key to alter hepatocyte metabolism upon dyslipidemia and inflammation.

In summary, I observed that hepatocytes take up FAs and primarily store them in form of TGs in LDs, and at the same time FAs are used as energy source by FAO. FA stimulation induced upregulation of genes and proteins that are involved in lipid metabolic processes and proliferation. This showed that FA treatment results in ongoing lipid metabolic processes.

In contrast, inflammatory cytokine treatment intensified FA storage by decreasing FA catabolic processes such as FAO, which exacerbated intracellular LD accumulation. Increased lipid accumulation induced lipotoxicity and mitochondrial dysfunction via direct and indirect effects of oxidative stress. The treatment of hepatocytes with inflammatory cytokines activated inflammatory - stress response (NF- κ B signalling), induced cell death, compensatory proliferation, and replication stress and DNA damage and can thereby promote pathogenesis. The most critical finding was that the exposure to inflammatory cytokines alone and in combination with FAs downregulated the expression of genes involved in several metabolic processes, not specific for FA metabolism. Thus, to further study the effect of inflammation on transcriptional dysregulation in hepatocytes and to understanding the transcriptional control of metabolic genes will help to find possible treatment options for NAFLD / NASH.

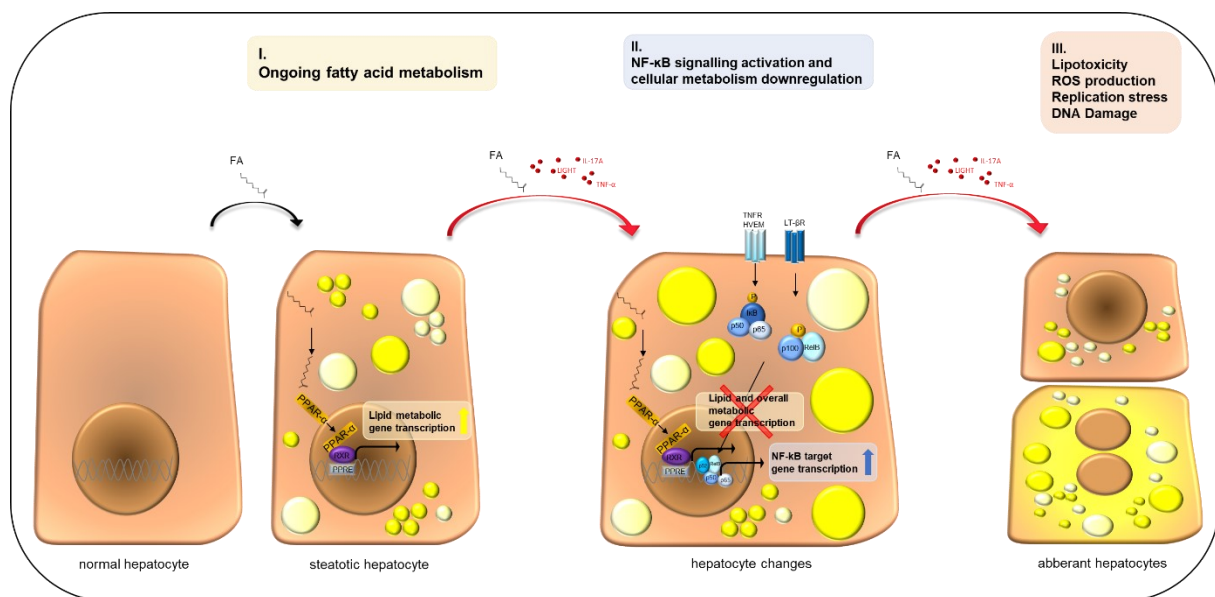


Figure 37: Illustration of molecular mechanisms contributing to NASH development

(I) FA stimulation leads to the activation of PPAR- α , and transcription of genes involved in FA- uptake, transport, storage, and oxidation, and induces a steatotic phenotype (LD accumulation, yellow circles) in hepatocytes. (II) Additional inflammatory cytokine stimulation activates NF- κ B signalling and downregulates genes essential for lipid metabolic processes and overall cellular metabolism. FA stimulation in combination with inflammatory cytokines induce exacerbated LD accumulation and hepatocyte changes and (III) promotes lipotoxicity which is associated with ROS production, and further triggers replication stress and DNA damage.

6. References

1. Wilfling F, Wang H, Haas JT, et al. Triacylglycerol synthesis enzymes mediate lipid droplet growth by relocalizing from the ER to lipid droplets. *Dev Cell*. 2013;24(4):384-399.
2. Houten SM, Wanders RJA. A general introduction to the biochemistry of mitochondrial fatty acid β -oxidation. *J Inherit Metab Dis*. 2010;33(5):469-477.
3. Nguyen P, Leray V, Diez M, et al. Liver lipid metabolism. *J Anim Physiol Anim Nutr (Berl)*. 2008;92(3):272-283.
4. Brasaemle DL, Wolins NE. Packaging of fat: An evolving model of lipid droplet assembly and expansion. *J Biol Chem*. 2012;287(4):2273-2279.
5. Fujimoto T, Parton RG. Not just fat: The structure and function of the lipid droplet. *Cold Spring Harb Perspect Biol*. 2011;3(3):1-17.
6. Bartz R, Li WH, Venables B, et al. Lipidomics reveals that adiposomes store ether lipids and mediate phospholipid traffic. *J Lipid Res*. 2007;48(4):837-847.
7. Schweiger M, Romauch M, Schreiber R, et al. Pharmacological inhibition of adipose triglyceride lipase corrects high-fat diet-induced insulin resistance and hepatosteatosis in mice. *Nat Commun*. 2017;8(May 2016).
8. Shoelson SE, Herrero L, Naaz A. Obesity, Inflammation, and Insulin Resistance. *Gastroenterology*. 2007;132(6):2169-2180.
9. Loeffler G, Petrides PE HP. *Biochemie Und Pathobiochemie*. 9.Auflage. Springer; 2007.
10. Friedman SL, Neuschwander-Tetri BA, Rinella M, Sanyal AJ. *Mechanisms of NAFLD Development and Therapeutic Strategies*. Vol 24.; 2018.
11. Rui L. Energy metabolism in the liver. *Compr Physiol*. 2014;4(1):177-197.
12. Racanelli V, Rehermann B. The liver as an immunological organ. *Hepatology*. 2006;43(2 SUPPL. 1).
13. Wakil SJ, Abu-Elheiga LA. Fatty acid metabolism: Target for metabolic syndrome. *J Lipid Res*. 2009;50(SUPPL.).
14. Furuhashi M, Hotamisligil GS. Fatty acid-binding proteins: role in metabolic diseases and potential as drug targets. *Nat Rev Drug Discov*. 2008;7(6):489-503.
15. Cholewski M, Tomczykowa M, Tomczyk M. *A Comprehensive Review of Chemistry, Sources and Bioavailability of Omega-3 Fatty Acids*. Vol 10.; 2018.
16. Svegliati-Baroni G, Pierantonelli I, Torquato P, et al. Lipidomic biomarkers and mechanisms of lipotoxicity in non-alcoholic fatty liver disease. *Free Radic Biol Med*. 2019;144(May):293-309.
17. Carta G, Murru E, Banni S, Manca C. Palmitic acid: Physiological role, metabolism and nutritional implications. *Front Physiol*. 2017;8(NOV):1-14.
18. Sales-Campos H, Reis de Souza P, Crema Peghini B, Santana da Silva J, Ribeiro Cardoso C. An Overview of the Modulatory Effects of Oleic Acid in Health and Disease. *Mini-Reviews Med Chem*. 2013;13(2):201-210.
19. Schwingshackl L, Hoffmann G. Monounsaturated fatty acids, olive oil and health status: A systematic review and meta-analysis of cohort studies. *Lipids Health Dis*. 2014;13(1).
20. Alves-Bezerra M, Cohen DE. Triglyceride metabolism in the liver. *Compr Physiol*. 2018;8(1):1-22.
21. Nagle CA, Klett EL, Coleman RA. Hepatic triacylglycerol accumulation and insulin resistance. *J Lipid Res*. 2009;50(SUPPL.).
22. Alkhoury N, Dixon LJ, Feldstein AE. Lipotoxicity in nonalcoholic fatty liver disease: Not all lipids are created equal. *Expert Rev Gastroenterol Hepatol*. 2009;3(4):445-451.
23. Hajri T, Abumrad NA. FATTY ACID TRANSPORT ACROSS MEMBRANES: Relevance to Nutrition and Metabolic Pathology. *Annu Rev Nutr*. 2002;22(1):383-415.
24. Kazantzis M, and Stahl A. Fatty Acid transport Proteins, implications in physiology and disease. *Biochim Biophys Acta 2012 May ; 1821(5) 852–857 doi10.1016/j.bbali.2011.09.010*. 2013;1821(5):852-857.
25. Storch J, McDermott L. Structural and functional analysis of fatty acid-binding proteins. *J Lipid Res*. 2009;50(SUPPL.).
26. Foufelle F, Ferré P. New perspectives in the regulation of hepatic glycolytic and lipogenic genes by insulin and glucose: A role for the transcription factor sterol regulatory element binding protein-1c. *Biochem J*. 2002;366(2):377-391.
27. Adeva-Andany MM, Pérez-Felpete N, Fernández-Fernández C, Donapetry-García C, Pazos-García C. Liver glucose metabolism in humans. *Biosci Rep*. 2016;36(6):1-15.
28. Iizuka K. The transcription factor carbohydrate-response element-binding protein (ChREBP): A possible link between metabolic disease and cancer. *Biochim Biophys Acta - Mol Basis Dis*. 2017;1863(2):474-485.

29. Horton JD, Goldstein JL, Brown MS. SREBPs. *J Clin Invest*. 2002;109(9):1125-1131.
30. Sanders FWB, Griffin JL. De novo lipogenesis in the liver in health and disease: More than just a shunting yard for glucose. *Biol Rev*. 2016;91(2):452-468.
31. Beaven SW, Matveyenko A, Wroblewski K, et al. Reciprocal regulation of hepatic and adipose lipogenesis by liver X receptors in obesity and insulin resistance. *Cell Metab*. 2013;18(1):106-117.
32. Kawano Y, Cohen DE. Mechanisms of hepatic triglyceride accumulation in non-alcoholic fatty liver disease. *J Gastroenterol*. 2013;48(4):434-441.
33. Ellis JM, Frahm JL, Li LO, Coleman RA. Acyl-coenzyme A synthetases in metabolic control. *Curr Opin Lipidol*. 2010;21(3):212-217.
34. Takeuchi K, Reue K. Biochemistry, physiology, and genetics of GPAT, AGPAT, and lipin enzymes in triglyceride synthesis. *Am J Physiol - Endocrinol Metab*. 2009;296(6).
35. N.V. B. Electron Transport and Oxidative Phosphorylation. In: BHAGAVAN NVBT-MB (Fourth E, ed. *Medical Biochemistry*. Academic Press; 2002:247-274.
36. Yamashita A, Hayashi Y, Matsumoto N, et al. Glycerophosphate/Acylglycerophosphate acyltransferases. *Biology (Basel)*. 2014;3(4):801-830.
37. Yu Y, Ginsberg H. The role of acyl-CoA:diacylglycerol acyltransferase (DGAT) in energy metabolism. *Ann Med*. 2004;36(4):252-261.
38. Stone SJ, Levin MC, Zhou P, Han J, Walther TC, Farese R V. The endoplasmic reticulum enzyme DGAT2 is found in mitochondria-associated membranes and has a mitochondrial targeting signal that promotes its association with mitochondria. *J Biol Chem*. 2009;284(8):5352-5361.
39. Londos C, Brasaemle DL, Schultz CJ, Segrest JP, Kimmel AR. Perilipins, ADRP, and other proteins that associate with intracellular neutral lipid droplets in animal cells. *Semin Cell Dev Biol*. 1999;10(1):51-58.
40. Kraemer N, Guo Y, Wilfling F, et al. Phosphatidylcholine Synthesis for Lipid Droplet Expansion Is Mediated by Localized Activation of CTP:Phosphocholine Cytidylyltransferase. *Cell Metab*. 2011;14(4):504-515.
41. Martin S, Parton RG. Lipid droplets: a unified view of a dynamic organelle. *Nat Rev Mol Cell Biol*. 2006;7(5):373-378.
42. Murphy S, Martin S, Parton RG. Quantitative analysis of lipid droplet fusion: Inefficient steady state fusion but rapid stimulation by chemical fusogens. *PLoS One*. 2010;5(12).
43. Gong J, Sun Z, Wu L, et al. Fsp27 promotes lipid droplet growth by lipid exchange and transfer at lipid droplet contact sites. *J Cell Biol*. 2011;195(6):953-963.
44. Schott MB, Weller SG, Schulze RJ, et al. Lipid droplet size directs lipolysis and lipophagy catabolism in hepatocytes. *J Cell Biol*. 2019;218(10):3320-3335.
45. Zimmermann R, Strauss JG, Haemmerle G, et al. Fat Mobilization in Adipose Tissue Is Promoted by Adipose Triglyceride Lipase. *Science (80-)*. 2004;306(5700):1383 LP - 1386.
46. Villena JA, Roy S, Sarkadi-Nagy E, Kim KH, Hei SS. Desnutrin, an adipocyte gene encoding a novel patatin domain-containing protein, is induced by fasting and glucocorticoids: Ectopic expression of desnutrin increases triglyceride hydrolysis. *J Biol Chem*. 2004;279(45):47066-47075.
47. Khan SA, Sathyanarayan A, Mashek MT, Ong KT, Wollaston-Hayden EE, Mashek DG. ATGL-catalyzed lipolysis regulates SIRT1 to control PGC-1 α /PPAR- α signaling. *Diabetes*. 2015;64(2):418-426.
48. Ong KT, Mashek MT, Bu SY, Greenberg AS, Mashek DG. Adipose triglyceride lipase is a major hepatic lipase that regulates triacylglycerol turnover and fatty acid signaling and partitioning. *Hepatology*. 2011;53(1):116-126.
49. Kraemer N, Guo Y WF. Phosphatidylcholine Synthesis for Lipid Droplet Expansion Is Mediated by Localized Activation of CTP:Phosphocholine Cytidylyltransferase. *Cell Metab*. 2011;16(8):461-472.
50. Houten SM, Violante S, Ventura F V., Wanders RJA. The Biochemistry and Physiology of Mitochondrial Fatty Acid β -Oxidation and Its Genetic Disorders. *Annu Rev Physiol*. 2016;78(1):23-44.
51. Lee J, Choi J, Scafidi S, Wolfgang MJ. Hepatic Fatty Acid Oxidation Restrains Systemic Catabolism during Starvation. *Cell Rep*. 2016;16(1):201-212.
52. Longo N, Frigeni M, Pasquali M, Biophys B, Author A. CARNITINE TRANSPORT AND FATTY ACID OXIDATION HHS Public Access Author manuscript. *Biochim Biophys Acta*. 2016;1863(10):2422-2435.
53. Preidis GA, Kim KH, Moore DD. Nutrient-sensing nuclear receptors PPAR γ and FXR control liver energy balance. *J Clin Invest*. 2017;127(4):1193-1201.

54. Desvergne B, Michalik L, Wahli W. Transcriptional regulation of metabolism. *Physiol Rev*. 2006;86(2):465-514.
55. Ricote M, Glass CK. PPARs and molecular mechanisms of transrepression. *Biochim Biophys Acta - Mol Cell Biol Lipids*. 2007;1771(8):926-935.
56. Leone TC, Weinheimer CJ, Kelly DP. A critical role for the peroxisome proliferator-activated receptor α (PPAR α) in the cellular fasting response: The PPAR α -null mouse as a model of fatty acid oxidation disorders. *Proc Natl Acad Sci U S A*. 1999;96(13):7473-7478.
57. Muoio DM, MacLean PS, Lang DB, et al. Fatty acid homeostasis and induction of lipid regulatory genes in skeletal muscles of peroxisome proliferator-activated receptor (PPAR) α knock-out mice. Evidence for compensatory regulation by PPAR δ . *J Biol Chem*. 2002;277(29):26089-26097.
58. Reddy JK, Viswakarma N, Jia Y, et al. Coactivators in PPAR-regulated gene expression. *PPAR Res*. Published online 2010.
59. Lee SS, Pineau T, Drago J, et al. Targeted disruption of the alpha isoform of the peroxisome proliferator-activated receptor gene in mice results in abolishment of the pleiotropic effects of peroxisome proliferators. *Mol Cell Biol*. 1995;15(6):3012-3022.
60. Aoyama T, Peters JM, Iritani N, et al. Altered constitutive expression of fatty acid-metabolizing enzymes in mice lacking the peroxisome proliferator-activated receptor α (PPAR α). *J Biol Chem*. 1998;273(10):5678-5684.
61. Kersten S, Rakhshandehroo M, Knoch B, Müller M. Peroxisome proliferator-activated receptor alpha target genes. *PPAR Res*. Published online 2010.
62. Yang X, Fu Y, Hu F, Luo X, Hu J, Wang G. PIK3R3 regulates PPAR α expression to stimulate fatty acid β -oxidation and decrease hepatosteatosis. *Exp Mol Med*. 2018;50(1):e431.
63. McMullen PD, Bhattacharya S, Woods CG, et al. A map of the PPAR α transcription regulatory network for primary human hepatocytes. *Chem Biol Interact*. 2014;209(1):14-24.
64. Martinez-Jimenez CP, Kyrmizi I, Cardot P, Gonzalez FJ, Talianidis I. Hepatocyte Nuclear Factor 4 Coordinates a Transcription Factor Network Regulating Hepatic Fatty Acid Metabolism. *Mol Cell Biol*. 2010;30(3):565-577.
65. Ma X, Wang D, Zhao W, Xu L. Deciphering the roles of PPAR γ in adipocytes via dynamic change of transcription complex. *Front Endocrinol (Lausanne)*. 2018;9(AUG):1-10.
66. Gilde AJ, Fruchart JC, Staels B. Peroxisome Proliferator-Activated Receptors at the Crossroads of Obesity, Diabetes, and Cardiovascular Disease. *J Am Coll Cardiol*. 2006;48(9 SUPPL.):24-32.
67. McGarry JD, Mannaerts GP, Foster DW. A possible role for malonyl CoA in the regulation of hepatic fatty acid oxidation and ketogenesis. *J Clin Invest*. 1977;60(1):265-270.
68. Osellame LD, Blacker TS, Duchon MR. Cellular and molecular mechanisms of mitochondrial function. *Best Pract Res Clin Endocrinol Metab*. 2012;26(6):711-723.
69. Lane N, Martin W. The energetics of genome complexity. *Nature*. 2010;467(7318):929-934.
70. Zorova LD, Popkov VA, Plotnikov EY, et al. Mitochondrial membrane potential. *Anal Biochem*. 2018;552:50-59.
71. Fukumoto H, Seino S, Imura H, et al. Sequence, tissue distribution, and chromosomal localization of mRNA encoding a human glucose transporter-like protein. *Proc Natl Acad Sci U S A*. 1988;85(15):5434-5438.
72. Bechmann LP, Hannivoort RA, Gerken G, Hotamisligil GS, Trauner M, Canbay A. The interaction of hepatic lipid and glucose metabolism in liver diseases. *J Hepatol*. 2012;56(4):952-964.
73. Reilly C, Stewart TJ, Renfrow MB, Novak J. Glycosylation in health and disease. *Nat Rev Nephrol*. 2019;15(6):346-366.
74. Zhang S, Hulver MW, McMillan RP, Cline MA, Gilbert ER. The pivotal role of pyruvate dehydrogenase kinases in metabolic flexibility. *Nutr Metab*. 2014;11(1).
75. Sugden MC, Holness MJ. Interactive regulation of the pyruvate dehydrogenase complex and the carnitine palmitoyltransferase system. *FASEB J*. 1994;8(1):54-61.
76. Sugden MC, Holness MJ. Recent advances in mechanisms regulating glucose oxidation at the level of the pyruvate dehydrogenase complex by PDKs. *Am J Physiol - Endocrinol Metab*. 2003;284(5 47-5):0-7.
77. Jeong JY, Jeoung NH, Park KG, Lee IK. Transcriptional regulation of pyruvate dehydrogenase kinase. *Diabetes Metab J*. 2012;36(5):328-335.
78. Pettersen IK, Tsubira D, Ashrafi H, et al. Upregulated PDK4 expression is a sensitive marker of increased fatty acid oxidation. *Mitochondrion*. 2019;49:97-110.
79. Wu P, Blair P V, Sato J, Jaskiewicz J, Popov KM, Harris RA. Starvation Increases the Amount of Pyruvate Dehydrogenase Kinase in Several Mammalian Tissues. *Arch Biochem Biophys*.

- 2000;381(1):1-7.
80. Song S, Attia RR, Connaughton S, et al. Peroxisome proliferator activated receptor α (PPAR α) and PPAR gamma coactivator (PGC-1 α) induce carnitine palmitoyltransferase IA (CPT-1A) via independent gene elements. *Mol Cell Endocrinol.* 2010;325(1-2):54-63.
 81. Robinson MW, Harmon C, O'Farrelly C. Liver immunology and its role in inflammation and homeostasis. *Cell Mol Immunol.* 2016;13(3):267-276.
 82. Gruys E, Toussaint MJM, Niewold TA, Koopmans SJ. Acute phase reaction and acute phase proteins. *J Zhejiang Univ Sci.* 2005;6 B(11):1045-1056.
 83. Quinton LJ, Jones MR, Robson BE, Mizgerd JP. Mechanisms of the hepatic acute-phase response during bacterial pneumonia. *Infect Immun.* 2009;77(6):2417-2426.
 84. Heinrich PC, Castell J V., Andus T. Interleukin-6 and the acute phase response. *Biochem J.* 1990;265(3):621-636.
 85. Ramadori G, Christ B. Cytokines and the Hepatic Acute-Phase Response. *Semin Liver Dis.* 1999;19(02):141-155.
 86. Moshage H, Groningen. Review Article Cytokines and the Hepatic Acute Phase. 1997;266(September 1996):257-266.
 87. Jain S, Gautam V, Naseem S. Acute-phase proteins: As diagnostic tool. *J Pharm Bioallied Sci.* 2011;3(1):118-127.
 88. Anstee QM, Reeves HL, Kotsiliti E, Govaere O, Heikenwalder M. From NASH to HCC: current concepts and future challenges. *Nat Rev Gastroenterol Hepatol.* 2019;16(7):411-428.
 89. Protzer U, Maini MK, Knolle PA. Living in the liver: hepatic infections. *Nat Rev Immunol.* 2012;12(3):201-213.
 90. Ringelhan M, Pfister D, O'Connor T, Pikarsky E, Heikenwalder M. The immunology of hepatocellular carcinoma review-article. *Nat Immunol.* 2018;19(3):222-232.
 91. Finco, 't TS, Baldwin'tt AS. *Mechanistic Aspects of NF-KB Regulation: The Emerging Role of Phosphorylation and Prote6ly&s.* Vol 3.; 1995.
 92. Karin M, Greten FR. NF- κ B: linking inflammation and immunity to cancer development and progression. *Nat Rev Immunol.* 2005;5(10):749-759.
 93. Taniguchi K, Karin M. NF-B, inflammation, immunity and cancer: Coming of age. *Nat Rev Immunol.* 2018;18(5):309-324.
 94. Siebenlist U. Structure, Regulation, and Function of NF-kappaB. *Annu Rev Cell Dev Biol.* 1994;10(1):405-455.
 95. Baeuerle PA, Henkel T. Function and Activation of. *Annu Rev Med Rev Immunol.* 1994;12.
 96. Luedde T, Schwabe RF. NF-[kappa]B in the liver[mdash]linking injury, fibrosis and hepatocellular carcinoma. *Nat Rev Gastroenterol Hepatol.* 2011;8(2):108-118.
 97. Ghosh G, Duyme G Van, Ghosh S, Sigler PB. Structure of NF- κ B p50 homodimer bound to a κ B site. *Nature.* 1995;373(6512):303-310.
 98. Müller CW, Rey FA, Sodeoka M, Verdine GL, Harrison SC. Structure of the NF- κ B p50 homodimer bound to DNA. *Nature.* 1995;373(6512):311-317.
 99. Ghosh S, Gifford AM, Riviere LR, Tempst P, Nolan GP, Baltimore D. Cloning of the p50 DNA binding subunit of NF- κ B: Homology to rel and dorsal. *Cell.* 1990;62(5):1019-1029.
 100. Kieran M, Blank V, Logeat F, et al. The DNA binding subunit of NF- κ B is identical to factor KBF1 and homologous to the rel oncogene product. *Cell.* 1990;62(5):1007-1018.
 101. Nolan GP, Ghosh S, Liou H-C, Tempst P, Baltimore D. DNA binding and I κ B inhibition of the cloned p65 subunit of NF- κ B, a rel-related polypeptide. *Cell.* 1991;64(5):961-969.
 102. Ruben SM, Dillon PJ, Schreck R, et al. Isolation of a rel-related human cDNA that potentially encodes the 65-kD subunit of NF-kappa B. *Science (80-).* 1991;251(5000):1490 LP - 1493.
 103. Beg A, Jr ASB. The I κ B proteins : multifunctional regulators of Rel / NF-KB transcription actors. Published online 1993:2064-2070.
 104. Baeuerle PA, Baltimore D. I kappa B: a specific inhibitor of the NF-kappa B transcription factor. *Science (80-).* 1988;242(4878):540 LP - 546.
 105. Naumann M, Wulczyn FG, Scheidereit C. The NF-kappa B precursor p105 and the proto-oncogene product Bcl-3 are I kappa B molecules and control nuclear translocation of NF-kappa B. *EMBO J.* 1993;12(1):213-222.
 106. Scheinman RI, Beg AA, Baldwin AS. NF-kappa B p100 (Lyt-10) is a component of H2TF1 and can function as an I kappa B-like molecule. *Mol Cell Biol.* 1993;13(10):6089-6101.
 107. Sen R, Baltimore D. Inducibility of κ immunoglobulin enhancer-binding protein NF- κ B by a posttranslational mechanism. *Cell.* 1986;47(6):921-928.
 108. Bonizzi G, Karin M. The two NF- κ B activation pathways and their role in innate and adaptive immunity. *Trends Immunol.* 2004;25(6):280-288.
 109. Gilmore TD. Introduction to NF- κ B: Players, pathways, perspectives. *Oncogene.*

- 2006;25(51):6680-6684.
110. Brown K, Park S, Kanno T, Franzoso G, Siebenlist U. Mutual regulation of the transcriptional activator NF- κ B and its inhibitor, I κ B- α . *Proc Natl Acad Sci U S A*. 1993;90(6):2532-2536.
 111. Cordle SR, Donald R, Read MA, Hawiger J. Lipopolysaccharide induces phosphorylation of MAD3 and activation of c-Rel and related NF- κ B proteins in human monocytic THP-1 cells. *J Biol Chem*. 1993;268(16):11803-11810.
 112. Zhang D, Lin J, Han J. Receptor-interacting protein (RIP) kinase family. *Cell Mol Immunol*. 2010;7(4):243-249.
 113. Ganchi PA, Sun SC, Greene WC, Ballard DW. I κ B/MAD-3 masks the nuclear localization signal of NF- κ B p65 and requires the transactivation domain to inhibit NF- κ B p65 DNA binding. *Mol Biol Cell*. 1992;3(12):1339-1352.
 114. Zabel U, Henkel T, Silva MS, Baeuerle PA. Nuclear uptake control of NF- κ B by MAD-3, an I κ B protein present in the nucleus. *EMBO J*. 1993;12(1):201-211.
 115. Kawakami K, Scheidereit C, Roeder RG. Identification and purification of a human immunoglobulin-enhancer-binding protein (NF- κ B) that activates transcription from a human immunodeficiency virus type 1 promoter in vitro. *Proc Natl Acad Sci U S A*. 1988;85(13):4700-4704.
 116. Sun SC. The non-canonical NF- κ B pathway in immunity and inflammation. *Nat Rev Immunol*. 2017;17(9):545-558.
 117. Vallabhapurapu S. Non-redundant and complementary functions of adaptor proteins TRAF2 and TRAF3 in a ubiquitination cascade that activates NIK-dependent alternative NF- κ B signaling. *Nat Immunol*. 2008;9(12):594.
 118. Mercurio F, Didonato JA, Rosette C, Karin M. An acute role in NF- κ B-mediated signal transduction. Published online 1993:705-718.
 119. Schmid RM, Perkins ND, Duckett CS, Andrews PC, Nabel GJ. Cloning of an NF- κ B subunit which stimulates HIV transcription in synergy with p65. *Nature*. 1991;352(6337):733-736.
 120. Ryseck RP, Bull P, Takamiya M, et al. RelB, a new Rel family transcription activator that can interact with p50-NF- κ B. *Mol Cell Biol*. 1992;12(2):674-684.
 121. Vallabhapurapu S, Karin M. Regulation and Function of NF- κ B Transcription Factors in the Immune System. *Annu Rev Immunol*. 2009;27(1):693-733.
 122. Bours V, Burd PR, Brown K, et al. A novel mitogen-inducible gene product related to p50/p105-NF- κ B participates in transactivation through a κ B site. *Mol Cell Biol*. 1992;12(2):685-695.
 123. Bettermann K, Vucur M, Haybaeck J, et al. TAK1 Suppresses a NEMO-Dependent but NF- κ B-Independent Pathway to Liver Cancer. *Cancer Cell*. 2010;17(5):481-496.
 124. Gaber T, Strehl C, Buttgerit F. Metabolic regulation of inflammation. *Nat Rev Rheumatol*. 2017;13(5):267-279.
 125. Chauhan P, Saha B. Metabolic regulation of infection and inflammation. *Cytokine*. 2018;112:1-11.
 126. Wu J, Zhao Y, Park YK, et al. Loss of PDK4 switches the hepatic NF- κ B/TNF pathway from pro-survival to pro-apoptosis. *Hepatology*. 2018;68(3):1111-1124.
 127. Stacpoole PW. Therapeutic Targeting of the Pyruvate Dehydrogenase Complex/Pyruvate Dehydrogenase Kinase (PDC/PDK) Axis in Cancer. *J Natl Cancer Inst*. 2017;109(11):1-14.
 128. Woolbright BL, Rajendran G, Harris RA, Taylor JA. Metabolic flexibility in cancer: Targeting the pyruvate dehydrogenase kinase:pyruvate dehydrogenase axis. *Mol Cancer Ther*. 2019;18(10):1673-1681.
 129. Kleemann R, Gervois PP, Verschuren L, Staels B, Princen HMG, Kooistra T. Fibrates down-regulate IL-1-stimulated C-reactive protein gene expression in hepatocytes by reducing nuclear p50-NF κ B-C/EBP- β complex formation. *Blood*. 2003;101(2):545-551.
 130. Devchand PR, Keller H, Peters JM, Vazquez M, Gonzalez FJ, Wahli W. *The PPAR α -Leukotriene 8 4 Pathway to Inflammation Control.*; 1996.
 131. Fang X, Zou S, Zhao Y, et al. Kupffer cells suppress perfluorononanoic acid-induced hepatic peroxisome proliferator-activated receptor α expression by releasing cytokines. *Arch Toxicol*. 2012;86(10):1515-1525.
 132. Palomer X, Álvarez-Guardia D, Rodríguez-Calvo R, et al. TNF- α reduces PGC-1 α expression through NF- κ B and p38 MAPK leading to increased glucose oxidation in a human cardiac cell model. *Cardiovasc Res*. 2009;81(4):703-712.
 133. Planavila A, Laguna JC, Vázquez-Carrera M. Nuclear factor- κ B activation leads to down-regulation of fatty acid oxidation during cardiac hypertrophy. *J Biol Chem*. 2005;280(17):17464-17471.
 134. Xie S, Li J, Wang JH, et al. IL-17 Activates the Canonical NF- κ B Signaling Pathway in

- Autoimmune B Cells of BXD2 Mice To Upregulate the Expression of Regulators of G-Protein Signaling 16. *J Immunol.* 2010;184(5):2289-2296.
135. Seon HC, Park H, Dong C. Act1 adaptor protein is an immediate and essential signaling component of interleukin-17 receptor. *J Biol Chem.* 2006;281(47):35603-35607.
 136. Li X. Act1 modulates autoimmunity through its dual functions in CD40L/BAFF and IL-17 signaling. *Cytokine.* 2008;41(2):105-113.
 137. Shen T, Chen X, Li Y, et al. Interleukin-17A exacerbates high-fat diet-induced hepatic steatosis by inhibiting fatty acid β -oxidation. *Biochim Biophys Acta - Mol Basis Dis.* 2017;1863(6):1510-1518.
 138. Harley ITW, Stankiewicz TE, Giles DA, et al. IL-17 signaling accelerates the progression of nonalcoholic fatty liver disease in mice. *Hepatology.* 2014;59(5):1830-1839.
 139. Gomes AL, Teijeiro A, Burén S, et al. Metabolic Inflammation-Associated IL-17A Causes Non-alcoholic Steatohepatitis and Hepatocellular Carcinoma. *Cancer Cell.* 2016;30(1):161-175.
 140. Swinburn BA, Sacks G, Hall KD, et al. The global obesity pandemic: shaped by global drivers and local environments. *Lancet (London, England).* 2011;378(9793):804—814.
 141. Hurt RT, Kulisek C, Buchanan LA, McClave SA. The obesity epidemic: Challenges, health initiatives, and implications for gastroenterologists. *Gastroenterol Hepatol.* 2010;6(12):780-792.
 142. Lindenmeyer C and MA. The Natural History of Nonalcoholic Fatty Liver Disease - An Evolving View. *Clin Liver Dis.* 2018;176(12):139-148.
 143. Sumarac-Dumanovic M, Stevanovic D, Ljubic A, et al. Increased activity of interleukin-23/interleukin-17 proinflammatory axis in obese women. *Int J Obes.* 2009;33(1):151-156.
 144. Wolf MJ, Adili A, Piotrowitz K, et al. Metabolic activation of intrahepatic CD8+ T cells and NKT cells causes nonalcoholic steatohepatitis and liver cancer via cross-talk with hepatocytes. *Cancer Cell.* 2014;26(4):549-564.
 145. Samuel VT, Shulman GI. Mechanisms for insulin resistance: Common threads and missing links. *Cell.* 2012;148(5):852-871.
 146. Lomonaco R, Ortiz-Lopez C, Orsak B, et al. Effect of adipose tissue insulin resistance on metabolic parameters and liver histology in obese patients with nonalcoholic fatty liver disease. *Hepatology.* 2012;55(5):1389-1397.
 147. Fleet SE, Lavine JE. Current Concepts in Pediatric Nonalcoholic Fatty Liver Disease. *Gastroenterol Clin North Am.* 2017;46(2):217-231.
 148. Younossi Z, Anstee QM, Marietti M, et al. Global burden of NAFLD and NASH: trends, predictions, risk factors and prevention. *Nat Rev Gastroenterol Hepatol.* 2018;15(1):11-20.
 149. Estes C, Razavi H, Loomba R, Younossi Z, Sanyal AJ. Modeling the epidemic of nonalcoholic fatty liver disease demonstrates an exponential increase in burden of disease. *Hepatology.* 2018;67(1):123-133.
 150. Marchesini G, Day CP, Dufour JF, et al. EASL-EASD-EASO Clinical Practice Guidelines for the management of non-alcoholic fatty liver disease. *J Hepatol.* 2016;64(6):1388-1402.
 151. Chalasani N, Younossi Z, Lavine JE, et al. The diagnosis and management of nonalcoholic fatty liver disease: Practice guidance from the American Association for the Study of Liver Diseases. *Hepatology.* 2018;67(1):328-357.
 152. Brunt EM, Wong VW-S, Nobili V, et al. Nonalcoholic fatty liver disease. *Nat Rev Dis Prim.* 2015;1(1):15080.
 153. El-Serag HB, Kanwal F. Epidemiology of hepatocellular carcinoma in the United States: Where are we? Where do we go? *Hepatology.* 2014;60(5):1767-1775.
 154. Torre LA, Bray F, Siegel RL, Ferlay J, Lortet-Tieulent J, Jemal A. Global cancer statistics, 2012. *CA Cancer J Clin.* 2015;65(2):87-108.
 155. Ozakyol A. Global Epidemiology of Hepatocellular Carcinoma (HCC Epidemiology). *J Gastrointest Cancer.* 2017;48(3):238—240.
 156. Oseini AM, Sanyal AJ. Therapies in non-alcoholic steatohepatitis (NASH). *Liver Int.* 2017;37(October 2016):97-103.
 157. Boeckmans J, Natale A, Buyl K, et al. Human-based systems: Mechanistic NASH modelling just around the corner? *Pharmacol Res.* 2018;134(June):257-267.
 158. Kim K, Boo K, Yu YS, et al. ROR α controls hepatic lipid homeostasis via negative regulation of PPAR γ transcriptional network. *Nat Commun.* 2017;8(1).
 159. Cassidy S, Syed BA. Nonalcoholic steatohepatitis (NASH) drugs market. *Nat Rev Drug Discov.* 2016;15(11):745-746.
 160. Boeckmans J, Natale A, Rombaut M, et al. Anti-NASH Drug Development Hitches a Lift on PPAR Agonism. *Cells.* 2019;9(1):37.
 161. Scirpo R, Fiorotto R, Villani A, Amenduni M, Spirli C, Strazzabosco M. Stimulation of nuclear receptor peroxisome proliferator-activated receptor- γ limits NF- κ B-dependent inflammation in

- mouse cystic fibrosis biliary epithelium. *Hepatology*. 2015;62(5):1551-1562.
162. He L, Liu X, Wang L, Yang Z. Thiazolidinediones for nonalcoholic steatohepatitis. *Medicine (Baltimore)*. 2016;95(42):e4947.
 163. El Hadi H, Vettor R, Rossato M. Vitamin E as a treatment for nonalcoholic fatty liver disease: Reality or myth? *Antioxidants*. 2018;7(1).
 164. Han CY. Update on FXR biology: Promising therapeutic target? *Int J Mol Sci*. 2018;19(7).
 165. Malehmir M, Pfister D, Gallage S, et al. Platelet GPIIb/IIIa is a mediator and potential interventional target for NASH and subsequent liver cancer. *Nat Med*. 2019;25(4):641-655.
 166. Ekstedt M, Nasr P, Kechagias S. Natural History of NAFLD / NASH. *Curr Hepatol Rep*. Published online 2017:391-397.
 167. Afshin A, Forouzanfar MH, Reitsma MB, et al. Health effects of overweight and obesity in 195 countries over 25 years. *N Engl J Med*. 2017;377(1):13-27.
 168. Day CP, James OFW. Steatohepatitis: A tale of two "Hits"? *Gastroenterology*. 1998;114(4):842-845.
 169. Chauhan A, Adams DH, Watson SP, Lalor PF. Platelets: No longer bystanders in liver disease. *Hepatology*. 2016;64(5):1774-1784.
 170. Fujita K, Nozaki Y, Wada K, et al. Effectiveness of antiplatelet drugs against experimental non-alcoholic fatty liver disease. *Gut*. 2008;57(11):1583 LP - 1591.
 171. Ramadori P, Klag T, Malek NP, Heikenwalder M. Platelets in chronic liver disease, from bench to bedside. *JHEP Reports*. 2019;1(6):448-459.
 172. Chantal A, Rivera, Patrick Adegboyega, Nico van Rooijen, Arlene Tagalicud, MoniqueAllman and MW. Toll-like receptor-4 signaling and Kupffer cells play pivotal roles in the pathogenesis of non-alcoholic steatohepatitis. *J Hepatol*. 2007;23(1):1-7.
 173. Nakagawa H, Umemura A, Taniguchi K, et al. Article ER Stress Cooperates with Hypernutrition to Trigger TNF-Dependent Spontaneous HCC Development. *Cancer Cell*. 2014;26(3):331-343.
 174. Piccolis M, Bond LM, Kampmann M, et al. Probing the Global Cellular Responses to Lipotoxicity Caused by Saturated Fatty Acids. *Mol Cell*. 2019;74(1):32-44.e8.
 175. Yamaguchi K, Yang L, McCall S, et al. Inhibiting triglyceride synthesis improves hepatic steatosis but exacerbates liver damage and fibrosis in obese mice with nonalcoholic steatohepatitis. *Hepatology*. 2007;45(6):1366-1374.
 176. Bartolini D, Torquato P, Barola C, et al. Nonalcoholic fatty liver disease impairs the cytochrome P-450-dependent metabolism of α -tocopherol (vitamin E). *J Nutr Biochem*. 2017;47:120-131.
 177. Forrester SJ, Kikuchi DS, Hernandez MS, Xu Q, Griendling KK. Reactive oxygen species in metabolic and inflammatory signaling. *Circ Res*. 2018;122(6):877-902.
 178. Takahashi Y, Kobayashi Y, Kawata K, et al. Does Hepatic Oxidative Stress Enhance Activation of Nuclear Factor-E2-Related Factor in Patients with Nonalcoholic Steatohepatitis? *Antioxid Redox Signal*. 2013;20(3):538-543.
 179. Bartolini D, Torquato P, Piroddi M, Galli F. Targeting glutathione S-transferase P and its interactome with selenium compounds in cancer therapy. *Biochim Biophys Acta - Gen Subj*. 2019;1863(1):130-143.
 180. Bartolini D, Dallaglio K, Torquato P, Piroddi M, Galli F. Nrf2-p62 autophagy pathway and its response to oxidative stress in hepatocellular carcinoma. *Transl Res*. 2018;193:54-71.
 181. Nisr RB, Shah DS, Ganley IG, Hundal HS. Proinflammatory NFkB signalling promotes mitochondrial dysfunction in skeletal muscle in response to cellular fuel overloading. *Cell Mol Life Sci*. 2019;76(24):4887-4904.
 182. Sanyal AJ, Campbell-Sargent C, Mirshahi F, et al. Nonalcoholic steatohepatitis: Association of insulin resistance and mitochondrial abnormalities. *Gastroenterology*. 2001;120(5):1183-1192.
 183. Pessayre D, Fromenty B. NASH: a mitochondrial disease. *J Hepatol*. 2005;42(6):928-940.
 184. Sunny NE, Brill F, Cusi K. Mitochondrial Adaptation in Nonalcoholic Fatty Liver Disease: Novel Mechanisms and Treatment Strategies. *Trends Endocrinol Metab*. 2017;28(4):250-260.
 185. Patterson RE, Kalavalapalli S, Williams CM, et al. Lipotoxicity in steatohepatitis occurs despite an increase in tricarboxylic acid cycle activity. *Am J Physiol - Endocrinol Metab*. 2016;310(7):E484-E494.
 186. Gusdon AM, Song KX, Qu S. Nonalcoholic fatty liver disease: Pathogenesis and therapeutics from a mitochondria-centric perspective. *Oxid Med Cell Longev*. 2014;2014.
 187. Koves TR, Ussher JR, Noland RC, et al. Mitochondrial Overload and Incomplete Fatty Acid Oxidation Contribute to Skeletal Muscle Insulin Resistance. *Cell Metab*. 2008;7(1):45-56.
 188. Ermak G, Davies KJA. Calcium and oxidative stress: from cell signaling to cell death. *Mol Immunol*. 2002;38(10):713-721.
 189. Zhang Y, Soto J, Park K, et al. Nuclear Receptor SHP, a Death Receptor That Targets Mitochondria, Induces Apoptosis and Inhibits Tumor Growth. *Mol Cell Biol*. 2010;30(6):1341-

- 1356.
190. Chu W-M. Tumor necrosis factors. *Cancer Lett.* 2013;2(2):105-134.
 191. Namineni S, O'Connor T, Faure-Dupuy S, et al. A dual role for hepatocyte-intrinsic canonical NF- κ B signaling in virus control. *J Hepatol.* 2020;72(5):960-975.
 192. Gripon P, Rumin S, Urban S, et al. Infection of a human hepatoma cell line by hepatitis B virus. *Proc Natl Acad Sci U S A.* 2002;99(24):15655-15660.
 193. Spandl J, White DJ, Peychl J, Thiele C. Live cell multicolor imaging of lipid droplets with a new dye, LD540. *Traffic.* 2009;10(11):1579-1584.
 194. Huynh FK, Green MF, Koves TR, Hirschey MD. Measurement of fatty acid oxidation rates in animal tissues and cell lines. *Methods Enzymol.* 2014;542:391-405.
 195. Kroemer G, Galluzzi L, Brenner C. Mitochondrial Membrane Permeabilization in Cell Death. *Physiol Rev.* 2007;87(1):99-163.
 196. Gergely P, Niland B, Gonchoroff N, Pullmann R, Phillips PE, Perl A. Persistent Mitochondrial Hyperpolarization, Increased Reactive Oxygen Intermediate Production, and Cytoplasmic Alkalinization Characterize Altered IL-10 Signaling in Patients with Systemic Lupus Erythematosus. *J Immunol.* 2002;169(2):1092-1101.
 197. Kersten S, Stienstra R. The role and regulation of the peroxisome proliferator activated receptor alpha in human liver. *Biochimie.* 2017;136:75-84.
 198. Müller FA, Sturla SJ. Human in vitro models of nonalcoholic fatty liver disease. *Curr Opin Toxicol.* 2019;16:9-16.
 199. Belloni L, Di Cocco S, Guerrieri F, et al. Targeting a phospho-STAT3-miRNAs pathway improves vesicular hepatic steatosis in an in vitro and in vivo model. *Sci Rep.* 2018;8(1).
 200. Laurent V, Glaise D, Nübel T, Gilot D, Corlu A, Loyer P. Highly efficient SiRNA and gene transfer into hepatocyte-like HepaRG cells and primary human hepatocytes: New means for drug metabolism and toxicity studies. *Methods Mol Biol.* 2013;987:295-314.
 201. Tanner N, Kubik L, Luckert C, et al. Regulation of drug metabolism by the interplay of inflammatory signaling, steatosis, and xeno-sensing receptors in HepaRG cells. *Drug Metab Dispos.* 2018;46(4):326-335.
 202. Mesnage R, Biserni M, Balu S, et al. Integrated transcriptomics and metabolomics reveal signatures of lipid metabolism dysregulation in HepaRG liver cells exposed to PCB 126. *Arch Toxicol.* 2018;92(8):2533-2547.
 203. Teresa Donato M, Jose Gomez-Lechon M. Drug-induced Liver Steatosis and Phospholipidosis: Cell-Based Assays for Early Screening of Drug Candidates. *Curr Drug Metab.* 2012;13(8):1160-1173.
 204. Anstee QM, Reeves HL, Kotsiliti E, Govaere O, Heikenwalder M. From NASH to HCC: current concepts and future challenges. *Nat Rev Gastroenterol Hepatol.* Published online 2019.
 205. Ibrahim SH, Hirsova P, Gores GJ. Non-alcoholic steatohepatitis pathogenesis: Sublethal hepatocyte injury as a driver of liver inflammation. *Gut.* 2018;67(5):963-972.
 206. Pawlak M, Lefebvre P, Staels B. Molecular mechanism of PPAR α action and its impact on lipid metabolism, inflammation and fibrosis in non-alcoholic fatty liver disease. *J Hepatol.* 2015;62(3):720-733.
 207. Jaenisch R, Bird A. Epigenetic regulation of gene expression: how the genome integrates intrinsic and environmental signals. *Nat Genet.* 2003;33(3):245-254.
 208. Cedar H, Bergman Y. Linking DNA methylation and histone modification: patterns and paradigms. *Nat Rev Genet.* 2009;10(5):295-304.
 209. Holoch D, Moazed D. RNA-mediated epigenetic regulation of gene expression. *Nat Rev Genet.* 2015;16(2):71-84.
 210. Yasmin R, Siraj S, Hassan A, Khan AR, Abbasi R, Ahmad N. Epigenetic Regulation of Inflammatory Cytokines and Associated Genes in Human Malignancies. Pouliot M, ed. *Mediators Inflamm.* 2015;2015:201703.
 211. Kuo PL, Shen KH, Hung SH, Hsu YL. CXCL1/GRO α increases cell migration and invasion of prostate cancer by decreasing fibulin-1 expression through NF- κ B/HDAC1 epigenetic regulation. *Carcinogenesis.* 2012;33(12):2477-2487.
 212. Zhang T, Gong Y, Meng H, Li C, Xue L. Symphony of epigenetic and metabolic regulation - Interaction between the histone methyltransferase EZH2 and metabolism of tumor. *Clin Epigenetics.* 2020;12(1):1-15.
 213. Wang AW, Wang YJ, Zahm AM, Morgan AR, Wangensteen KJ, Kaestner KH. The Dynamic Chromatin Architecture of the Regenerating Liver. *Cmgh.* 2020;9(1):121-143.

7. Acknowledgements

First, I want to thank my supervisor Prof. Mathias Heikenwalder for giving me the opportunity to work in his lab, in this excellent scientific surrounding, for his support, motivation, and knowledge. His guidance helped me during my PhD.

I want to thank my first referee of my thesis and my TAC member, Prof. Dr. Peter Angel, for his support and input during our meetings and for guidance through my PhD.

I want to express my very great appreciation to my TAC member, Prof. Eli Pikarsky for his support and valuable input during our meetings and discussions.

I want to thank Tobias Riedl and Suzanne Faure-Dubuy for their technical and mental support.

I want to thank all the members of our lab, for their team spirit, and technical and scientific support.

My grateful thanks belong to my sister Serena Stadler for her continuous support in general and during my PhD, her valuable scientific input, and scientific discussions. And importantly, I want to thank my parents and my partner for supporting me in my life in general and especially during my time here at the DKFZ in Heidelberg.

I. Appendix

I.I. Inflammation induced increased lipid storage is independent of PPAR- α

To address the role of PPAR- α during inflammation-triggered aberrant FA metabolism CRISPR Cas-mediated HepaRG NTC and PPAR- α KO cells were generated.

FA treatment induced lipid storage which was further increased by additional cytokine stimulation in NTC and in PPAR- α KO cells (**Figure IA**), showing that increased lipid storage induced by inflammatory cytokines was independent on PPAR- α presence. Gene expression analysis showed reduced PPAR- α levels in PPAR- α KO cells when compared to NTC dHepaRG (**Figure IB**). However, PDK4 expression levels in PPAR- α KO cells were similar when compared to NTC dHepaRG (**Figure IC**). This indicates that reduced PPAR- α levels sufficed to induce PDK4 target gene transcription, or that PDK4 transcription was independent on PPAR- α .

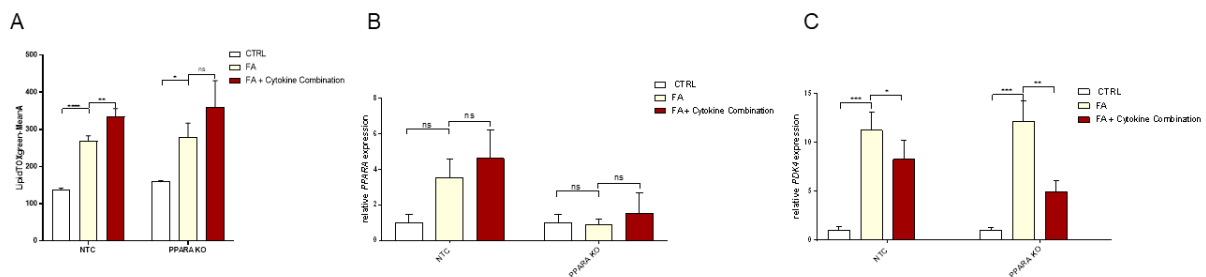


Figure I: Fatty acid storage into neutral lipids in hepatocytes (dHepaRG non-targeting control and PPARA knock out), LipidTOX green / Hoechst staining CRISPR Cas-mediated non-targeting control (NTC) and PPARA knock out (KO) dHepaRG cells, untreated (CTRL), treated FAs, and treated with FAs together with inflammatory cytokines for 24h. (A) neutral lipid stain by LipidTOX Green analysed by flow cytometry (B, C) Gene expression analysis by RT-PCR. Statistical analysis was performed by one-way ANOVA. *: $p < 0.05$; **: $p < 0.01$; ***: $p < 0.001$; ****: $p < 0.0001$; ns: not significant.

I.II. Inflammation driven aberrant lipid accumulation is not regulated by PPAR- α activation

To further study the role of PPAR- α on inflammation driven metabolic alterations, dHepaRG were exposed to the PPAR- α antagonist, GW-6471, and the PPAR- α agonist, WY-14643.

Inflammatory cytokine exposure intensified lipid accumulation in NTC cells as well as in cells that were additionally exposed to the PPAR- α agonist, WY-14643 (**Figure IIA**). PPAR- α antagonization led to elevated lipid levels in FA stimulated cells, however, FA storage in cytokine stimulated cells was not affected (**Figure IIB**), showing that the increased lipid storage in FA stimulated cells is an additional, independent effect. These results show that inflammation driven lipid metabolic downregulation is not linked to the PPAR- α activation status.

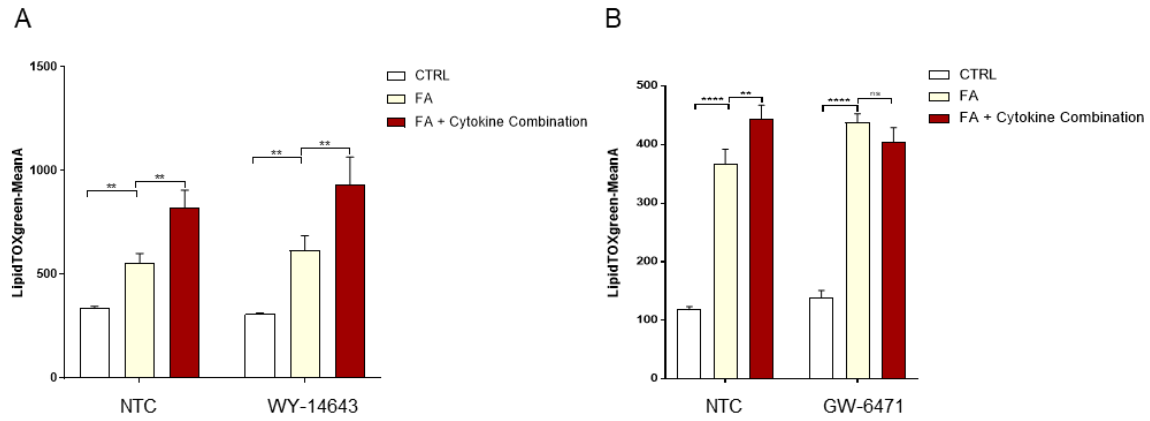


Figure II: Fatty acid storage into neutral lipids in hepatocytes (dHepaRG), LipidTOXgreen staining

dHepaRG cells, untreated (CTRL), FA treated, treated with FAs in combination with cytokines for 24h, in absence and presence of (A) PPARA agonist WY-14643 and (B) PPARA antagonist GW-6471. Lipid accumulation was quantified by LipidTOX Green staining and flow cytometry. Statistical analysis was performed by one-way ANOVA.

*: $p < 0.05$; **: $p < 0.01$; ***: $p < 0.001$; ****: $p < 0.001$; ns: not significant.